CAPACI OCCASIO
FOUNDED 1894

SAIMM

JOURNAL OF THE SOUTHERN AFRICAN INSTITUTE OF MINING AND METALLURGY

VOLUME 117 NO. 11 NOVEMBER 2017

ELBROC
MINING PRODUCTS (PTY) LTD

TH ARCH SUPPORT SYSTEMS



APPLICATIONS

- Tunnel junctions
- Over and under ore passes
- Haulage
- Incline shaft portals
- Active support through bad ground conditions, dykes, faults, friable ground

BENEFITS

- Simple and fast installation
- High load carrying capacity
- Long operational life
- Suitable for tunnels from 4.15m to 5.5m wide
- Upright support beams cater for tunnel heights from 3.1 to 6.5m
- Cost effective
- Dimensional and design flexibility

PROFILE SETS

Ring Set

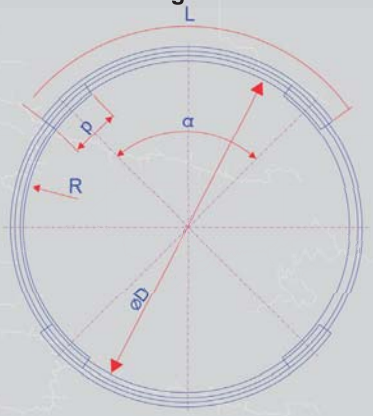

Semi Arch Set

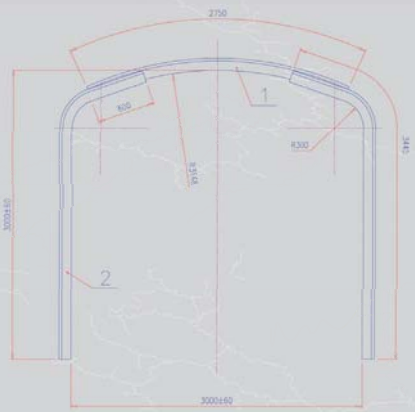

Half Arch Set

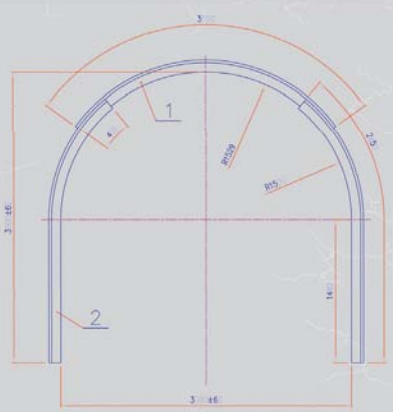

Production capabilities:

- Standard arch lengths from 1.8m to 5.5m
- Minimal curvature R 1000mm, at R 1200mm at R 1600mm

SABS ISO 9001

FOR OUR FULL PRODUCT RANGE
PLEASE VISIT OUR WEBPAGE

a member of the rbh royal bafokeng holdings

Tel: 011 974 8013 • Fax: 011 974 2019 • sales@elbroc.co.za

www.elbroc.co.za

mogs

We strive to offer you the lowest cost of ownership

Weir Minerals is a leading designer and manufacturer of mine dewatering solutions, slurry pumps, hydrocyclones, valves, screens, centrifuges, crushers, feeders, washers, conveyers, rubber lining, hoses and wear-resistant linings for the global mining and minerals processing, sand and aggregate, and power and general industrial sectors.

For more information contact us on +27 11 9292600

WEIR

Minerals
www.minerals.weir
www.weirafricastore.com

OFFICE BEARERS AND COUNCIL FOR THE 2017/2018 SESSION

Honorary President
Mxolis Donald Mbuyisa Mgojo
President, Chamber of Mines of South Africa

Honorary Vice-Presidents
Mosebenzi Joseph Zwane
Minister of Mineral Resources, South Africa

Rob Davies
Minister of Trade and Industry, South Africa

Naledi Pandor
Minister of Science and Technology, South Africa

President
S. Ndlovu

President Elect
A.S. Macfarlane

Senior Vice-President
M.I. Mthenjane

Junior Vice-President
Z. Botha

Immediate Past President
C. Musingwini

Honorary Treasurer
J.L. Porter

Ordinary Members on Council

V.G. Duke
I.J. Geldenhuys
M.F. Handley
W.C. Joughin
E. Matinde
M. Motuku
D.D. Munro
G. Njowa
S.M Rupprecht
A.G. Smith
M.H. Solomon
D. Tudor
D.J. van Niekerk
A.T. van Zyl

Past Presidents Serving on Council

N.A. Barcza
R.D. Beck
J.R. Dixon
M. Dworzanowski
H.E. James
R.T. Jones
G.V.R. Landman
R.G.B. Pickering
S.J. Ramokgopa
M.H. Rogers
D.A.J. Ross-Watt
G.L. Smith
W.H. van Niekerk
R.P.H. Willis

G.R. Lane–TPC Mining Chairperson
Z. Botha–TPC Metallurgy Chairperson

A.S. Nhleko–YPC Chairperson
K.M. Letsoalo–YPC Vice-Chairperson

Branch Chairpersons

Botswana	L.E. Dimbungu
DRC	S. Maleba
Johannesburg	J.A. Luckmann
Namibia	N.M. Namate
Northern Cape	W.J. Mans
Pretoria	R.J. Mostert
Western Cape	R.D. Beck
Zambia	D. Muma
Zimbabwe	S. Matutu
Zululand	C.W. Mienie

Corresponding Members of Council

Australia:	I.J. Corrans, R.J. Dippenaar, A. Croll, C. Workman-Davies
Austria:	H. Wagner
Botswana:	S.D. Williams
United Kingdom:	J.J.L. Cilliers, N.A. Barcza
USA:	J-M.M. Rendu, P.C. Pistorius

PAST PRESIDENTS

*Deceased

* W. Bettel (1894–1895)
* A.F. Crosse (1895–1896)
* W.R. Feldtmann (1896–1897)
* C. Butters (1897–1898)
* J. Loevy (1898–1899)
* J.R. Williams (1899–1903)
* S.H. Pearce (1903–1904)
* W.A. Caldecott (1904–1905)
* W. Cullen (1905–1906)
* E.H. Johnson (1906–1907)
* J. Yates (1907–1908)
* R.G. Bevington (1908–1909)
* A. McA. Johnston (1909–1910)
* J. Moir (1910–1911)
* C.B. Saner (1911–1912)
* W.R. Dowling (1912–1913)
* A. Richardson (1913–1914)
* G.H. Stanley (1914–1915)
* J.E. Thomas (1915–1916)
* J.A. Wilkinson (1916–1917)
* G. Hildick-Smith (1917–1918)
* H.S. Meyer (1918–1919)
* J. Gray (1919–1920)
* J. Chilton (1920–1921)
* F. Wartenweiler (1921–1922)
* G.A. Watermeyer (1922–1923)
* F.W. Watson (1923–1924)
* C.J. Gray (1924–1925)
* H.A. White (1925–1926)
* H.R. Adam (1926–1927)
* Sir Robert Kotze (1927–1928)
* J.A. Woodburn (1928–1929)
* H. Pirow (1929–1930)
* J. Henderson (1930–1931)
* A. King (1931–1932)
* V. Nimmo-Dewar (1932–1933)
* P.N. Lategan (1933–1934)
* E.C. Ranson (1934–1935)
* R.A. Flugge-De-Smidt (1935–1936)
* T.K. Prentice (1936–1937)
* R.S.G. Stokes (1937–1938)
* P.E. Hall (1938–1939)
* E.H.A. Joseph (1939–1940)
* J.H. Dobson (1940–1941)
* Theo Meyer (1941–1942)
* John V. Muller (1942–1943)
* C. Biccard Jeppe (1943–1944)
* P.J. Louis Bok (1944–1945)
* J.T. McIntyre (1945–1946)
* M. Falcon (1946–1947)
* A. Clemens (1947–1948)
* F.G. Hill (1948–1949)
* O.A.E. Jackson (1949–1950)
* W.E. Gooday (1950–1951)
* C.J. Irving (1951–1952)
* D.D. Stitt (1952–1953)
* M.C.G. Meyer (1953–1954)
* L.A. Bushell (1954–1955)
* H. Britten (1955–1956)
* Wm. Bleloch (1956–1957)
* H. Simon (1957–1958)
* M. Barcza (1958–1959)
* R.J. Adamson (1959–1960)
* W.S. Findlay (1960–1961)
* D.G. Maxwell (1961–1962)
* J. de V. Lambrechts (1962–1963)
* J.F. Reid (1963–1964)
* D.M. Jamieson (1964–1965)
* H.E. Cross (1965–1966)
* D. Gordon Jones (1966–1967)
* P. Lambooy (1967–1968)
* R.C.J. Goode (1968–1969)
* J.K.E. Douglas (1969–1970)
* V.C. Robinson (1970–1971)
* D.D. Howat (1971–1972)
* J.P. Hugo (1972–1973)
* P.W.J. van Rensburg (1973–1974)
* R.P. Plewman (1974–1975)
* R.E. Robinson (1975–1976)
* M.D.G. Salamon (1976–1977)
* P.A. Von Wielligh (1977–1978)
* M.G. Atmore (1978–1979)
* D.A. Viljoen (1979–1980)
* P.R. Jochens (1980–1981)

G.Y. Nisbet (1981–1982)
A.N. Brown (1982–1983)

* R.P. King (1983–1984)

J.D. Austin (1984–1985)
H.E. James (1985–1986)
H. Wagner (1986–1987)

* B.C. Alberts (1987–1988)

C.E. Fivaz (1988–1989)
O.K.H. Steffen (1989–1990)

* H.G. Mosenthal (1990–1991)

R.D. Beck (1991–1992)

* J.P. Hoffman (1992–1993)
* H. Scott-Russell (1993–1994)

J.A. Cruise (1994–1995)
D.A.J. Ross-Watt (1995–1996)
N.A. Barcza (1996–1997)

* R.P. Mohring (1997–1998)

J.R. Dixon (1998–1999)
M.H. Rogers (1999–2000)
L.A. Cramer (2000–2001)

* A.A.B. Douglas (2001–2002)

S.J. Ramokgopa (2002-2003)
T.R. Stacey (2003–2004)
F.M.G. Egerton (2004–2005)
W.H. van Niekerk (2005–2006)
R.P.H. Willis (2006–2007)
R.G.B. Pickering (2007–2008)
A.M. Garbers-Craig (2008–2009)
J.C. Ngoma (2009–2010)
G.V.R. Landman (2010–2011)
J.N. van der Merwe (2011–2012)
G.L. Smith (2012–2013)
M. Dworzanowski (2013–2014)
J.L. Porter (2014–2015)
R.T. Jones (2015–2016)
C. Musingwini (2016–2017)

Honorary Legal Advisers
Scop Incorporated

Auditors
Genesis Chartered Accountants

Secretaries
The Southern African Institute of Mining and Metallurgy
Fifth Floor, Chamber of Mines Building
5 Hollard Street, Johannesburg 2001 • P.O. Box 61127, Marshalltown 2107
Telephone (011) 834-1273/7 • Fax (011) 838-5923 or (011) 833-8156
E-mail: journal@saimm.co.za

Typeset and Published by
The Southern African Institute of Mining and Metallurgy
P.O. Box 61127
Marshalltown 2107
Telephone (011) 834-1273/7
Fax (011) 838-5923
E-mail: journal@saimm.co.za

Printed by
Camera Press, Johannesburg

Advertising Representative
Barbara Spence
Avenue Advertising
Telephone (011) 463-7940
E-mail: barbara@avenue.co.za

The Secretariat
The Southern African Institute of Mining and Metallurgy

ISSN 2225-6253 (print)
ISSN 2411-9717 (online)

SAIMM
JOURNAL OF THE SOUTHERN AFRICAN INSTITUTE OF MINING AND METALLURGY
FOUNDED 1894

VOLUME 117 NO. 11 NOVEMBER 2017

Contents

SULPHURIC ACID CONFERENCE

SAIMM
JOURNAL OF THE SOUTHERN AFRICAN INSTITUTE OF MINING AND METALLURGY
VOLUME 117 NO. 11 NOVEMBER 2017

Contents *(continued)*

SULPHURIC ACID CONFERENCE

PAPERS OF GENERAL INTEREST

The 6th Sulphur and Sulphuric Acid Conference

The 6th biennial Sulphuric Acid Conference and Workshop was held in Cape Town between 9 and 11 May 2017.

Approximately 90 delegates attended with regional representation from South Africa, Namibia, Zimbabwe, and the DRC and from further afield with delegates from Germany, the USA, UK, The Netherlands, Canada, and Denmark. Delegates representing plant operations management, technical experts, traders, transporters, and vendors were all present.

The conference began with a workshop on the care of sulphuric acid catalyst using a host of case studies, which was sponsored by Haldor Topsoe.

The main conference had three keynote speakers

- The 'Big Cat Guy' gave an enthralling talk on how the big cats behave and how this is similar to what we have to do in business – teamwork, competition, motivation and focus
- Ms Freda Gordon gave a talk on the global sulphur and sulphuric acid markets – supply and demand, and the current picture plus future outlook
- Ms P. Gwaze from the Department of Environmental Affairs spoke on the NAEIS emissions reporting system and the new regulations that will be introduced.

Sixteen Technical papers were presented, covering plant uprating case studies, technical improvements, sulphur melting, water saving methodologies, and recovery and processing of smelter off-gases.

A social programme also included a cocktail party and a whiskey pairing dinner.

Feedback from delegates indicated that the conference was well received and gave opportunities for people with common issues a platform to engage, share ideas, and 'network'.

The next Sulphur and Sulphuric Acid Conference conference is still being planned but is scheduled for 2019.

S. Sackett
on behalf of the Organizing Committee

Summer is finally here and Christmas is around the corner. I do hope that you are all enjoying the warm weather that is prevalent in Southern Africa at this time of the year and, at the same time, have started shopping for those elusive but perfect Christmas gifts for friends and families.

Since taking over the reins as the President of the SAIMM, I have been invited to a number of events and meetings in the past few months. I have interacted with a lot of professionals and held discussions on a number of diverse and relevant (and even sometimes irrelevant) topics pertinent to the mining and minerals industry. The controversial new Mining Charter, low metal prices, ECSA, state capture, the ANC leadership race, water restrictions in the Western Cape, and of course the weather, have all been fodder for conversations at various events. However, one topic that never fails to come up, and for obvious reasons, is women in the mining and minerals industry. As such, it would be remiss of me not to take the opportunity to celebrate the valuable contribution that women make in the mining and minerals sector. Similarly, it would be imprudent to overlook the challenges that women continuously face as they contribute to the country's economy. For the above reasons, I would like to focus on this relevant and important subject this month.

In the past, the majority of the workforce at the forefront of the operational aspects of the mining and minerals industry was male. Females were mostly confined to administrative roles. Before 1990, mining companies were legally prohibited from employing women for underground mining activities. However, change has occurred over the years; women now play a prominent role in all aspects of mining activities, from entry to board level and at both administrative and operations levels. This is largely attributed to women's ability to organize and solve tough problems. In addition, women also usually possess a multi-skills set that brings in strength and diversity to a company's operations. They contribute a much-needed fresh perspective to an industry that is in significant need of innovative solutions to ever-growing challenges. Notably, research has shown that companies that have more women at board and senior management levels tend to perform much better than those without. Gender diversity is, therefore, good for the sector.

However, even with the significant contributions that gender diversity brings to a company's operations, women still face a lot of challenges in the mining and minerals industry. This well-established industry has been male-dominated for a long time, and furthermore, with Africa being predominantly a patriarchal society, many employees have well-defined views on the nature and environment of the workforce as well as the role of women in it. Issues such as paternalism, ethnic traditions, different standards for judging men and women, work-life balance, different styles of communication, sexual harassment, and different needs in terms of health and hygiene as well as PPE-related issues, can create an uncomfortable working environment for women. In addition, generally the male is still considered as the breadwinner of the family, which can lead to training, skills development, and promotion opportunities being preferentially offered to males rather than females. Such attitudes and prejudices can have a severe impact and bearing on the women's mental wellbeing, productivity, and performance. Ultimately, this can affect women's retention and progression in the mining and minerals sector. As a result, the overall effect of such challenges has understandably resulted in most women changing their career paths.

Both the mining companies and women themselves have a significant role to play in overcoming some of the challenges found in the industry. Firstly, women need to shift their mind-set from 'victim' to empowerment. Women also need to understand the company culture and the environment in which they work. It is only through having an understanding of their working environment that they can become agents to effect change. They can be able to propose a culture, structures, and policies as well as cultivate an environment that can empower and accommodate them. A supportive network through involvement in professional voluntary organizations and participation in professional panels is also vital. Women also need to find strong and capable mentors that can guide and nurture them at different stages of their career. Importantly, women should also serve as mentors to the next generation of women that enter the industry.

Companies, on the other hand, must be committed to gender equality and diversity management and to providing a safe and supportive environment. Although subtle aspects of male-oriented culture that are hostile to women can be extremely hard to manage because they are deeply ingrained and because their impact is sometimes difficult to demonstrate, management attitude is vital to effecting changes in the sector. This attitude or outlook can be passed down to the rest of the workforce. Notably, in some instances there is a gap in perception of the existence of these problems. Management must, therefore, recognize that barriers exists and foster a work culture that promotes the success of both genders.

The SAIMM had its first female member in 1977. Currently the Institute has about 18.4% female membership and is on a drive not only to grow the female membership, but to also engage with this group on pertinent issues that affect them at the professional level. The Institute also needs to engage the mining sector leadership in promoting an environment that fosters the retention and growth of women in the mining sector. I am happy to see changes coming through our Institute in this regard. I challenge all of us as members of SAIMM to play our part, wherever we are, in helping to change the attitude of the industry towards its female workforce.

S. Ndlovu
President, SAIMM

http://dx.doi.org/10.17159/2411-9717/2017/v117n11a1

Tenke Fungurume Mining – an update

by H. Lee* and J. Wellington†

Synopsis

With the successful commissioning of a 600 t/d sulphuric acid plant as part of the new metallurgical complex in Lualaba Province in the DRC, Tenke Fungurme Mining (TFM) continues to develop this site and increase copper production using a systematic approach. This paper outlines the key challenges encountered and solutions adopted to reliably increase acid production in a remote location. Development of acid plants no. 1 and no. 2, including debottlenecking and environmental upgrades, is described.

Keywords
sulphuric acid plant, debottenecking, capacity expansion.

Introduction

With the successful commissioning of the 600 t/d sulphuric acid plant as part of the new metallurgical complex in Lualaba (formerly Katanga) Province in the DRC, Tenke Fungurume Mining (TFM) continues to develop this site and increase copper production using a systematic approach (Hayward, 2016). As of 2016, the facility produced 205 kt copper and 16 kt cobalt per annum. As the metal production capacity increases, the demand for sulphuric acid also continues to increase. It became apparent that the acid demand within the complex would continually exceed the existing acid plant (AP1) capacity, even with the plant being able to consistently operate at 660 t/d. Therefore, TFM has taken a staged approach to increase acid availability on site, with the first stage involving debottlenecking of AP1 and the second stage building a new acid plant (AP2) to complement the existing AP1.

Capacity expansion of AP1

In 2011 TFM engaged the services of Chemetics to study the potential for capacity increases in AP1. To ensure the expansion project would be executed with cost and technical certainty, the study was conducted in two phases:

Phase 1—A high-level study to identify capacity constraints of existing equipment, including a review of any areas of concern at current operating rates, and evaluation of two capacity increase options: a lower increase that could be implemented with limited change and capital, and a maximum capacity case considering additions to and replacement of equipment.

Phase 2—A detailed study that lists all the changes required to enable the plant to reach the capacity increase selected in phase 1 of the study. The scope included preparing PFDs and P&IDs for current and future operating cases, and a site visit to review the current operation and identify any operational constraints that could prevent the plant from reaching the new target in acid production.

For any sulphuric acid plant production increase, the key considerations that must be taken into account are as follows:

- SO_2 gas concentration and conversion
- Plant volumetric flow rate
- Gas side pressure drop across the system
- Additional heat load.

The SO_2 conversion and resultant gas concentration in the stack that must be achieved by the plant is usually as per statutory (permit) requirements and cannot be relaxed at any operating rates. Therefore, it becomes one of the main considerations in any capacity increase. In sulphur-burning applications, SO_2 gas concentrations of up to 12% by volume to bed 1 of the converter can now be achieved in new plant designs. For existing plants where higher throughput is desired, an increase in SO_2 gas concentration

* *Chemetics Inc. a Jacobs Company, DRC.*
† *Tenke Fungurume Mining, Freeport-McMoRan Copper & Gold Inc, Canada.*

 ISSN 2225-6253. This paper was first presented at the 6th Sulphuric Acid 2017 Conference', *9–12 May 2017, Southern Sun Cape Sun, Cape Town.*

is a normal and often-used approach. Special care must be taken to address the lower oxygen to sulphur dioxide ratio that will be present for conversion.

Plant volumetric flow is a function of production rate and the design SO_2 gas concentration. The optimum plant design minimizes flow by increasing the SO_2 gas concentration while still meeting emission requirements.

Increases in flow will raise the overall gas side pressure drop by approximately a square ratio. The capacity of the main blower then typically becomes the plant limitation to further increases. Other large equipment such as the strong acid towers may also have hydraulic limitations that must be addressed.

Heat is generated from the combustion of sulphur, the oxidation of SO_2 to SO_3, and finally the absorption of SO_3 into strong acid and its subsequent dilution. The heat generated in each of these process steps is in direct proportion to the production rate. The heat produced by the combustion of sulphur is removed in the waste heat boiler, that from SO_2 oxidation by steam superheaters and economizers located between converter passes, and the heat from absorption of SO_3 and acid dilution by the strong acid coolers.

For phase 1 of the expansion study, the following key assumptions/design decisions were made:

- SO_2 emissions to atmosphere would not exceed the original design basis
- Converter with internal superheater and reheat exchanger would not be modified
- Blowers would not be replaced
- Strong acid towers would not be replaced or significantly modified
- Steam equipment would not be replaced
- Cold reheat exchanger would not be replaced
- Turbine generator set and dump condenser not to be limiting to any capacity increases
- The two capacities identified and evaluated were:
  - Option 1 - 750 t/d as 100% H_2SO_4
  - Option 2 - 825 t/d as 100% H_2SO_4.

This study resulted in the following key limitations to further production increases above current rates being identified:

- SO_2 conversion and emissions
- Inter-tower hydraulics
- Strong acid circulation and cooling.

At capacities above 825 t/d several equipment items, including the blowers, inter-tower, and mist eliminators reach their ultimate capacity limit and require replacement or significant modification.

One possibility to increase capacity was by raising SO_2 concentration at the furnace and boiler system to the original 14% SO_2 by volume design. However, raising the furnace temperature would potentially impact on materials and equipment maintenance requirements. After reviewing with TFM, it was decided that furnace operation SO_2 concentration would be increased to 12% SO_2 by volume in order to minimize volumetric flows downstream and keep the plant pressure profile and system hydraulics within acceptable ranges.

To improve inter-tower hydraulics and reduce pressure drop, low pressure-drop packing was used. This packing had more open area than conventional saddles while maintaining good SO_3 absorption efficiency. With the increase in plant rate the inter-tower acid outlet temperature will also increase, therefore an increase in acid circulation rate is also required to ensure that the acid outlet temperature is below the safe operating temperature of the SARAMET™ alloy tower.

The findings and recommendations of the phase 1 study were reviewed with TFM, which resulted in TFM engaging Chemetics to proceed with phase 2 of the expansion study with the selected target of 825 t/d acid production. The following tasks were completed.

- Develop PFDs for the current (650 t/d) and future (825 t/d) operation
- Review the BFW, deaerator, and LP steam system during a site visit to identify and solve bottlenecks
- Review cooling water system during site visit to ensure sufficient cooling water is available to handle the extra heat load after the expansion
- Review plant operation during site visit to identify any other operational constraints that would prevent the plant from reaching 825 t/d capacity
- Rate the existing boiler for expanded capacity using the observed in-service heat transfer coefficients during operation at 1200°C furnace temperature
- Summarize all plant changes required to enable TFM to execute the project.

As a starting point, the current plant operation was reviewed to develop an as-is flow sheet. From this starting point, the flow sheet for the expanded plant was developed. The combination of current plant operating data and the calculated requirements after expansion allowed for a detailed analysis of the critical equipment and verification of the recommended modifications identified in the phase I study.

At the conclusion of the phase 2 study, it was determined that the following items should be completed in order to reach the 825 t/d expansion target:

(a) Install new packing in the inter- and final towers
(b) Install new catalyst in the converter
(c) Replace underperforming inter economizer
(d) Modify the deaerator system to allow operation at higher temperature
(e) Install a new, larger acid cooler to increase acid cooling capacity
(f) Install a larger acid supply pipe to inter-tower and new distributor to inter-tower to allow inter-tower acid circulation rate to increase.

As with most plant expansion projects, the modifications were implemented during a planned plant turnaround. It was critical that the turnaround was completed on time as acid production was halted during this period, so any delays in the plant restart would have a significant impact on copper production. As part of the phase 2 study work, Chemetics provided a detailed procurement plan and shutdown works schedule to allow TFM's project team to implement all the changes in an organized, efficient, and safe manner. Furthermore, TFM engaged the services of Chemetics to provide site technical advisory services to support the

September 2012 maintenance turnaround of the sulphuric acid plant. The main scope of services included performing internal visual inspections to assess the condition of the equipment and provision of technical assistance during the plant modifications. After the plant turnaround, the plant was restarted and proved able to consistently produce 825 t/d.

Development of second acid plant (AP2)

After successful completion of the AP1 expansion project, planning began for the second sulphuric acid plant (AP2). While AP1 was a successful project for TFM, nevertheless, TFM's project team, operations team, and technology provider (Chemetics) were brought together to conduct a formal 'lessons learned' session during the feasibility study stage for AP2. Key project team members from all three parties met to review all aspects of the design and generate ideas on what could be done to make AP2 better than AP1. The following recommendations were identified and implemented in the AP2 project:

- Larger platforms around the front end of the sulphur furnace to allow better access to sulphur gun changes
- Revamp DCS operator interface to improve usability; the number of screens was revamped to allow operators to see the 'core' of the acid in only two screens
- Addition of a continuously operating caustic scrubber to reduce SO_2 emissions to below 20 ppm, well within World Bank recommended emission guidelines.

Chemetics innovations

In addition to the above design changes to improve usability, Chemetics continues to build on their successful experience in AP1 and work with TFM operations to improve on the 'best in class' technology slated for the AP2 project. Although infrastructure in the DRC has been significantly improved since the first project, executing a large complex project in the country remains a challenge. Limited port access, long distances from ports to site, poor infrastructure and road conditions, and shortage of skilled labour within the country remain the top issues. In addition, the plant capacity in AP2 is more than double the original AP1 capacity, which results in larger equipment sizes and pushes the shipping constraints to the limits.

To address these challenges, the following strategies were developed in designing key equipment in the acid plant:

- Use of proven designs for critical process equipment
- Minimize field fabrication/installation
- Maximize off-site prefabrication
- Provide complete assembled equipment if deemed suitable for road transportation.

SARAMET™ acid towers, piping and ISOFLOW™ distributor

For the AP2 project, TFM has continued to use SARAMET™ acid towers in preference to conventional brick-lined towers after considering the advantages of prefabricating the entire tower, including internals, off-site. The general dimensions of the dry, inter-, and final towers are shown in Table I. The overall dimensions of these towers are within the shipping capability of ground transportation, thus the towers could be shipped to site in a single piece without further field assembly. Once the towers are lifted into position the tower packing and acid distributors can be installed immediately (Figures 1 and 2). This eliminates the cost premium required to bring in specialist contractors to complete the acid bricking installation on-site.

For the acid distributors, the newest generation of ISO-FLOW™ trough distributors were installed in AP2. In this innovative design, acid flows from the main header to the bottom of the trough, and then upwards via a series of calming plates which also filter out debris. Choking of flow orifices through downcomers is essentially eliminated (Figure 3). This innovation also reduces the number of parts, which reduces overall cost and simplifies installation and maintenance.

Table I

General dimensions for the Tenke acid towers (AP2)

Application	Diameter (m)	Overall height (m)
Dry tower	5.2	14.3
Inter-tower	5.6	18.3
Final tower	5.6	18.3

Figure 1—Completed SARAMET™ acid towers arrive at TFM site

Figure 2—SARAMET™ acid towers in installed position

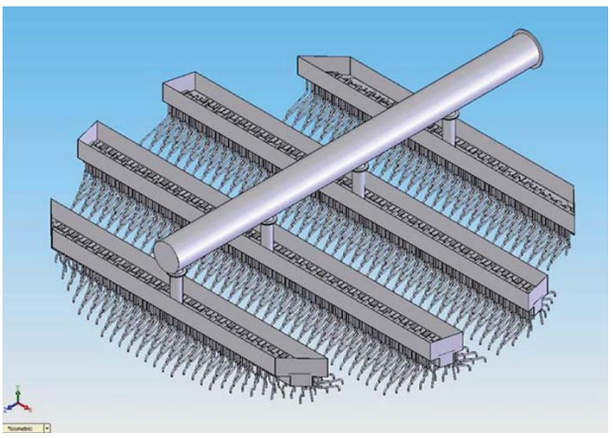

Figure 3—ISO-FLOW™ trough distributor

Figure 4—Sulphur furnace shell delivered to site

Prefabricated sulphur furnace

The sulphur furnace is a critical component for reliable acid plant operation. The furnace incorporates Chemetics' proprietary design features such as individual combustion air control to each sulphur gun for optimal air-sulphur mixing, no internal baffles or checker walls, insulated shell designed to ensure optimum shell temperature, and dual saddle support to minimize stress on the shell and refractory.

The furnace shell was fabricated off-site and shipped to site in a single vessel, followed by refractory installation and curing on-site under the supervision of the refractory supplier (Figures 4 and 5).

Figure 5—Sulphur furnace internals

Internal heat exchangers and modular converter

The converter is the focal point of the sulphuric acid process. This vessel contains the series of catalyst beds that convert the sulphur dioxide gas to sulphur trioxide. The gas flows in series through these beds with intermediate cooling between each bed. The converter at Tenke AP2 is similar to that at AP1, which features Chemetics' patented all-stainless design. The Chemetics design incorporated an internal superheater inside the core of the converter, which eliminates the hot gas ducting between beds 1 and 2, which is well known to be a continual maintenance problem on many plants owing to the very high gas and metal temperatures (Figure 6).

To minimize field construction the converter was constructed using a modular approach. The converter was shipped to site as prefabricated modules and assembled on-site. This method greatly reduces construction time from 2 to 3 months for a conventional 'knock-down' build to less than 1 month. This unique approach also improved the overall quality of the construction, since the majority of the fabrication was completed off-site in a fabrication shop under ideal conditions (Figures 7 and 8).

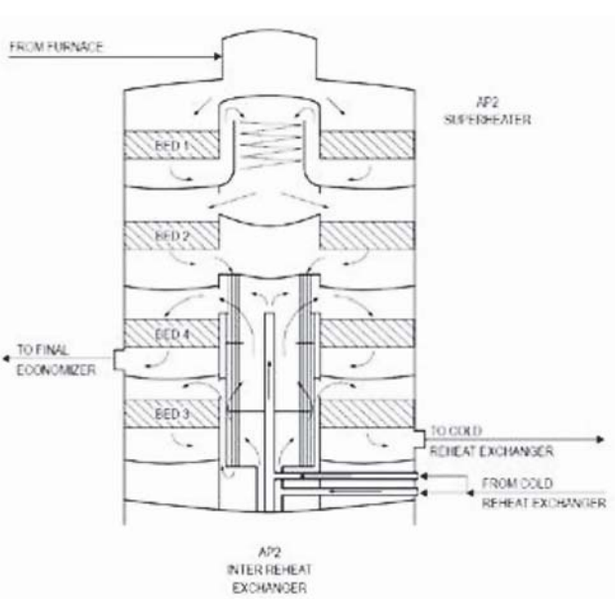

Figure 6—Tenke AP2 converter – process gas flow schematic

Commissioning and operation

Although the basic design of AP2 is the same as of AP1, nevertheless the design went through a detailed hazard and operability (HAZOP) study, with particular emphasis on the impact of all changes that were implemented in the AP2 project.

Figure 7—Prefabricated converter modules

Figure 8—Converter modules assembly on site

Before commissioning, TFM, Hatch GOBA, and Chemetics developed a joint commissioning plan with all teams actively participating in the development and execution of the plant startup plan. The startup plan was structured to meet a systems-based approach whereby the plant was broken down into systems. For each system, the individual tasks required to bring the status of the system from mechanical completion to commissioning were identified.

The sequence of steps to be taken for distinct tasks within each system was jointly developed between Chemetics' commissioning specialists and TFM's commissioning team and approved by TFM's Commissioning Manager prior to starting of the task. The integrated commissioning team also worked with commissioning/operations personnel where specific safety procedures such as confined space entry permits, lockout/tagout, line, and flange break permits were to be issued prior to start of commissioning.

During commissioning, daily meetings were held at TFM's site office to plan and coordinate tasks to ensure everyone was aware of what other teams were working on at the site.

Before commissioning a new process area or a piece of equipment, all Chemetics commissioning team members were required to complete a Safe Plan of Action (SPA). SPA is a safety system designed to systematically review all the potential hazards prior to the start of work in the field (Figure 9). This ensured that every team member involved in the task understood the work and all identified hazards were mitigated by appropriate control measures. The SPA system was designed to integrate with Tenke Fungurme's lockout/tagout procedures to ensure all commissioning tasks could be done safely.

With a detailed systematic plan in place, the integrated startup team worked with the construction team to prioritize resources to complete critical path items according to the commissioning schedule. The acid plant reached mechanical completion status in January 2016 and first acid production in early February. The plant has exceeded nameplate capacity of 1400 t/d since three weeks after the first acid production.

Summary

Increasing sulphuric acid production at Tenke Fungurume Mining while maintaining copper production presented some unique challenges. The staged strategy of first expanding the capacity of AP1 using a systematic approach, followed by execution of AP2 project using proven AP1 execution strategies as well as incorporating lessons learned from the first acid plant project, has proven to be a success. With the successful debottlenecking of AP1 and safe startup of AP2, TFM is able to increase copper and cobalt production as well as reduce overall production costs as reliable on-site acid production eliminates the need to import acid.

Reference

Hayward, K. 2016. Tenke Fungurume looks to the future with second acid plant. Sulphuric Acid Today, Spring/Summer 2016. ◆

Safe Plan of Action

CHEMETICS®

Review checklist while completing the SPA table. Check all that apply.

A new SPA is required if the job scope or work conditions change.

Required Permits	Hazards	Safe Plan
☐ Confined Space	☐ Overhead Utilities	☐ Power de-energization required ☐ Insulation blankets required ☐ Wire watcher required ☐ Required clearance distance = _____Ft. ☐ Safe work zone marked
☐ Critical Lift	☐ Crane or other Lifting Equipment	☐ Signalman assigned ☐ Tag lines in use ☐ Area around crane barricaded ☐ Lifting equipment inspected ☐ Personnel protected from overhead load
☐ Hot Work	☐ Underground Utilities	☐ Reviewed as-builts ☐ Subsurface surveys ☐ Received dig permit ☐ Required clearance distance = _____ Ft. ☐ Safe work zone Marked
☐ Lock Out/Tag Out	☐ Electrical	☐ Lock Out/Tag Out/Try Out ☐ Permit required? ☐ Confirm that equipment is de-energized ☐ Reviewed electrical safety procedures
☐ Soil Disturbance (Over 12")	☐ Excavations	☐ Permits ☐ Inspected prior to entering ☐ Proper sloping/shoring ☐ Barricades provided ☐ Access/egress provided ☐ Protection from accumulated water
☐ Utility Clearance	☐ Fire Hazard	☐ Hot Work Permit ☐ Fire Extinguishers ☐ Fire watch ☐ Adjacent area protected ☐ Unnecessary flammable material removed
Required PPE	☐ Vehicular Traffic or Heavy Equipment	☐ Traffic Barricades ☐ Cones ☐ Signs ☐ Flagmen ☐ Lane closure ☐ Communication with equipment operator
☒ Hard Hat, Class C	☐ Noise >85 dB	Hearing protection is required: ☐ Ear plugs ☐ Ear Muffs ☐ Both
☐ Hard Hat, Class E *(Elect. Protect)*	☐ Hand & Power Tools:	☐ Inspect general cond. ☐ GFCI in use ☐ Identified PPE required for each tool ☐ Reviewed safety requirements in operators manual(s) ☐ Guarding OK
☐ Ear Plugs/Ear Muffs	☐ Hand Hazards	List sharp tools, material, equipment: _____ ☐ PPE gloves, etc. ☐ Protected sharp edges as necessary
Eye Protection:	☐ Manual Lifting	☐ Reviewed proper lifting tech. ☐ Identified material requiring lifting equipment ☐ Hand protection required ☐ Back support belts
☒ Safety Glasses	☒ Ladders	☐ Inspect general cond. before use ☐ Ladder inspected with in last quarter ☐ Ladder tied off or held ☐ Proper angle and placement ☐ Reviewed ladder safety
☐ Face Shield	☒ Scaffolds	☐ Inspect general condition before use ☐ Tags in place ☐ Properly secured ☐ Toe boards used ☐ Footings adequate ☐ Materials properly stored on scaffold
☐ Chemical Goggles	☒ Slips, Trips Falls	☐ Inspect for trip hazards ☐ Hazards marked ☐ Tools & material properly stored ☐ Extension cords properly secured ☐ Work zone free of debris
☐ Welding Hood	☒ Pinch Points	List potential pinch points: _____ ☐ Working near operating equipment ☐ Hand/Body positioning
Hand Protection:	☐ Working w/ Chemicals	☐ List specific chemicals involved and list hazards and precaution on front side. ☐ Reviewed MSDS ☐ Exposure Monitoring required ☐ Have proper containers and labels. ☐ Identified proper PPE (respirators, clothing, gloves, etc.)
☒ Cut Resistant Gloves	☐ Asbestos or Lead Paint Potential	☐ Areas to be worked may contain asbestos or lead paint ☐ Asbestos controls incorporated ☐ Lead based point controls in place ☐ Exposure monitoring conducted.
☐ Welders Gloves	☒ Heat Stress Potential	☐ Heat stress monitoring (>85°) ☐ Liquids available ☐ Cool down periods ☐ Sun Screen ☐ Reviewed Heat Stress symptoms
☐ Nitrile Gloves	☐ Cold Stress Potential	☐ Proper clothing (i.e.. gloves, coat, coveralls) ☐ Wind chill <32° ☐ Reviewed Cold Stress symptoms ☐ Warm up periods
☐ Surgical Gloves	☒ Environmental	☐ Air emissions ☐ Water discharge ☐ Hazardous wastes ☐ Other wastes ☐ Pollution prevention ☐ Waste minimization
☐ Rubber Gloves	☒ Natural or Site Hazards	☐ Weather ☐ Terrain ☐ Adjacent operations or processes ☐ Biological hazards ☐ Animals/reptiles/insects hazards
☐ Elect. Insulated Gloves	☐ Adjacent Work/Processes	☐ Notified them of our presence ☐ Other workers adjacent, above, or below. ☐ Coordinated with adjacent supervisor/customer/operator ☐ Need barriers between.
☐ Arm Sleeves	☒ Barricades/covers	☐ Caution barricade tape required ☐ Danger barricade tape required ☐ Rigid railing required ☐ Covers over opening ☐ Warning signs required
Foot Protection:		
☐ Sturdy Work Boots		
☒ Safety Toe Boots		
☐ Rubber Boots		
☐ Rubber Boot Covers		
☐ Dielectric Footwear		
Respiratory Protection:		
☐ Dust Mask		
☐ Air Purifying Respirator		
☐ Supplied Air Respirator		
☐ SCBA		
☐ Emergency Escape Respirator		
Special Clothing:		
☐ Tyvek ®		
☐ Poly Coated Tyvek ®		
☐ Fire Resistant Coveralls		
☐ Rain Suit		
☒ Safety Vest		
Fall Protection:		
☒ Harness	Additional Information:	
☐ Double Lanyard Required		
☐ Anchorage Point Available		
☐ Additional Anchorage Connector Needed e.g. Cross Arm Strap, etc.		
☐ Retractable Device Needed		
☐ Horizontal Life Line System Req'd.		
☐ Fall Clearance Distance Adequate		
☐ Fall Rescue/Retrieval Plan Set Up		

0-FRM-8268-R1 SPA – Field Visit

Figure 9—Safe Plan of Action form (partial sample)

http://dx.doi.org/10.17159/2411-9717/2017/v117n11a2

Economical abatement of high-strength SO_2 off-gas from a smelter

by R. Dijkstra, B. Senyard, U. Shah, and H. Lee

Synopsis

With increasing use of oxygen enrichment and advances in smelting technology, SO_2 concentrations in smelter off-gases are increasing, which necessitates larger acid plant equipment and increases in capital and operating. To counteract the shortcomings in conventional acid plants, Chemetics provides two unique solutions: the Chemetics High Strength (CHS™) process and the Chemetics Pseudo-Isothermal process utilizing the CORE™ reactor technology. In this paper we present a general outline of these two solutions and how they can be implemented in new or existing acid plants.

Keywords
smelter off-gas, high-strength SO_2, pseudo-isothermal process.

Introduction

Most non-ferrous smelter operations are coupled with a metallurgical sulphuric acid plant to treat SO_2-containing off-gases before discharge to the atmosphere. With the increasing use of oxygen enrichment to increase production in existing smelters, and due to advances in smelting technology, more and more smelting operations are producing off-gases with SO_2 concentrations well above 30 vol%. The concentrated gases may be mixed with lower concentration off-gases from secondary processing or other emission sources before entering the off-gas cleaning and acid plant.

As smelter off-gases are generally deficient in oxygen, it is necessary to add oxygen, typically using ambient air, to the gas prior to the drying tower in the acid plant. The resulting SO_2 concentration in the process gas after this O_2:SO_2 ratio adjustment is typically between 15 and 25 vol% SO_2 at the acid plant converter. However, the conventional sulphuric acid plant (double contact – double absorption) is limited to no more than 13 vol% SO_2 at the converter inlet in order to keep the gas temperature leaving the first catalytic stage below the thermal stability limit (approx. 630°C) of the vanadium-based catalyst.

Air addition in excess of the amount required for adjusting the oxygen content increases the gas volume processed through the acid plant and consequently the equipment size, and capital and operating costs. Higher gas throughput also increases the heat loss to the acid circuit, thereby reducing energy recovery from the gas contact section and increasing cooling water demand. With newly built and future smelter operations designed to produce high-concentration SO_2 gas at increasing throughputs, ever more air dilution is required to keep within the limits of conventional acid plants. In some cases, gas volumes exceed the design limit of single-train acid plants (currently around 5000 t/d), which forces designers to resort to multiple train contact plants, thus further increasing plant footprint and CAPEX/OPEX.

To counteract these shortcomings of the conventional acid plant, Chemetics Inc., with more than 50 years of experience in sulphuric acid technology, now offers two solutions: The Chemetics High Strength (CHS™) process and the Chemetics Pseudo-Isothermal process utilizing the CORE™ reactor technology.

Chemetics High Strength (CHS™) process

The CHS™ process is designed for two typical situations:

- Locations where the gas received from the smelter is high in SO_2 but deficient in oxygen, such that dilution air or oxygen is required to achieve the required O_2:SO_2 ratio for the conversion
- Locations with multiple SO_2 off-gas sources (such as a flash furnace coupled with Peirce-Smith converters) that have different SO_2 concentrations but are not necessarily deficient in oxygen when

* *Chemetics In. Canada.*
 ISSN 2225-6253. This paper was first presented at the 6th Sulphuric Acid 2017 Conference', *9–12 May 2017, Southern Sun Cape Sun, Cape Town.*

mixed together, and where the client is considering installing separate gas-cleaning systems for these gas sources for operational (reliability) or process (*e.g.* different gas cleaning requirements) reasons.

The CHS™ process capitalizes on the difference in the SO_2 concentrations of the feed streams, resulting in the ability to process gases containing up to approximately 18% SO_2.

Process description

The CHS™ design (Figure 1) processes the two gas streams (high and low SO_2 concentrations) by reconfiguring the contact section. A separate drying tower (with a common acid system) and blower is used for each stream. After drying, the weak gas (which also includes all required dilution air to maintain the correct O_2:SO_2 ratio) is mixed with part of the strong gas to provide a gas containing approximately 13% SO_2 at the inlet of the first catalyst bed. After part of the SO_2 is converted to SO_3, the now SO_3-rich gas from bed 1 is combined with the remaining strong SO_2 gas and processed in a further four catalyst beds. The overall arrangement is a 4+1 DCDA configuration. Energy recovery from the hot gas leaving beds 3, 4, and 5 enables the production of high-pressure steam.

Taking full advantage of Chemetics' experience and expertise in acid plant equipment design, the converter used for the CHS™ process is a single stainless-steel five-bed converter with two internal heat exchangers (see Figure 2). The advantages of the Chemetics stainless steel converter design are well known and include all-welded construction, rapid heat-up time, improved reliability, excellent gas distribution, and less external hot gas ducting.

CHS™ *vs.* conventional plant – case study

For comparison between the CHS™ and a conventional acid plant, the off-gas sources from a recent study are considered (Table I).

In a conventional acid plant, these sources would be blended and delivered to the drying tower as a single feed stream. Additional dilution air, required to control the first-pass converter bed temperature, results in about 27% increase in the gas throughput. The CHS™ design receives these streams separately and requires no further dilution air. Gas flow through any of the CHS™ converter passes is no more than the total feed gas flow rate. This flow reduction, effectively 25% lower in the study case, translates to capex and opex savings in addition to approximately 20% improvement in energy recovery.

Compared with competitor technology, which recycles hot SO_3-rich gas from bed 3 to suppress the temperature rise in the first pass, the CHSTM design offers many benefits (Table II). These include a significantly lower gas flow rate

Figure 2—Chemetics five-pass converter with two internal heat exchangers

Table I

Case study gas feeds

	Strong SO_2 gas	Weak SO_2 gas	Combined SO_2 gas
SO_2 concentration	25	8	16.5
O_2/SO_2 ratio	0.5	2	0.86
% of total feed	50	50	100

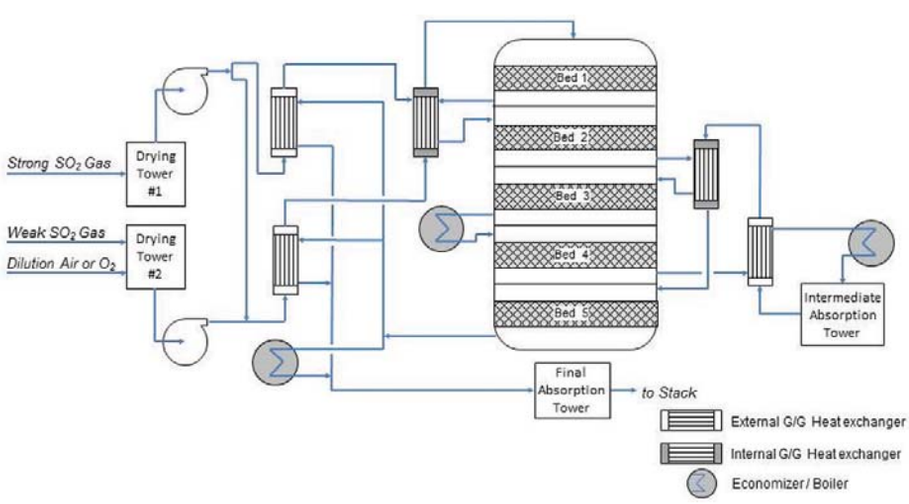

Figure 1—CHS™ generic process flow diagram

Table III

Case study results

Parameter	CHS™	Conventional
Gas throughput		
Bed 1		
Vol% SO_2	13%	13%
Gas flow (% of total feed)	80	127
Bed 2		
Vol% SO_2	9.2%	4.5%
Gas flow (% of total feed)	96	122
Energy efficiency		
Blower power	88	100
Energy recovery	120	100

through the converter beds and the heat exchangers upstream of the intermediate absorption tower, higher equilibrium conversion prior to intermediate absorption, reduced power consumption, and fewer reliability concerns associated with a hot SO_3 gas recycle fan.

Pseudo-isothermal converter – Chemetics Core™

In August 2016 Chemetics acquired all patents and know-how for the BAYQIK® converter technology from Bayer AG. This converter technology, now marketed under the CORE™ name, is a proven pseudo-isothermal reactor system capable of converting high-strength SO_2 gas without diluting the gas with air or recycled process gas. The first commercial installation in Germany (see Figure 3) has been operating continuously for more than 8 years, processing gas with up to 21 vol% SO_2. A second plant was commissioned in January 2017 and is processing gas up to 15 vol% SO_2. The technology is most valuable in treating a single strong gas source, but can also be an economical pre-converter for a plant with multiple off-gas sources

Process description

The Chemetics CORE™ converter is the only commercially available isothermal converter system for SO_2 oxidation. Continuous removal of the reaction heat using air or molten salt allows the process temperature to be controlled within the operating limit of the catalyst.

In addition to the ability to convert high-concentration SO_2 gas, the pseudo-isothermal process also operates farther from the equilibrium curve than the conventional multi-pass adiabatic process, as shown in Figure 4. This translates into lower overall catalyst loading and significantly higher conversion in a single pass.

The pseudo-isothermal process is carried out in a patented tubular converter (see Figure 5). The SO_2 process gas flows through the tubes, which are filled with a carefully selected mixture of vanadium-based catalyst. A cooling medium (air or molten salt, depending on the reactor size) is introduced on the shell side to remove the reaction heat. Heat transfer is optimized in the design of the reactor. Energy recovered from the circulating cooling medium can be used for preheating the process gas and for generating high-pressure steam. CORE™ reactors designs for capacities up to 100 000 Nm³/h (equivalent to approx. 2000 t/d acid production) are currently available, with higher capacity designs under development.

There are several approaches to using the Chemetics CORE™ technology in handling high-strength SO_2 gas.

In-line Chemetics CORE™

In an in-line configuration, the CORE™ reactor can simply replace the primary contact plant, which typically includes beds 1 through 3 and intercooling gas exchangers in an adiabatic design. As a result, the in-line Chemetics CORE™ design reduces not only the gas flow through the plant but also the number of major equipment items and the overall plant pressure drop.

This significant reduction in plant size is demonstrated in the following comparison between the various technologies using a baseline case of 25 vol% SO_2 off-gas with adequate oxygen content (O_2/SO_2 ratio ≥ 0.8). In a conventional design, air addition required to reduce the SO_2 concentration to 13 vol% results in near-doubling of the gas flow through the contact plant. The CHS™ design can reduce the dilution air requirement by adjusting about half of the feed gas to 13 vol% prior to bed 1. The resulting gas flow through the acid plant is reduced to 75% of that in the conventional design, but is still elevated at 150% of the feed gas flow. If the hot SO_3 recycle approach is used, the gas flow rate to bed 1 will be reduced to about 140% of feed gas flow (or approximately 70% of the gas flow for a conventional

Figure 3—CORE™ installation processing gas up to 21 vol% SO_2 and operating since 2009

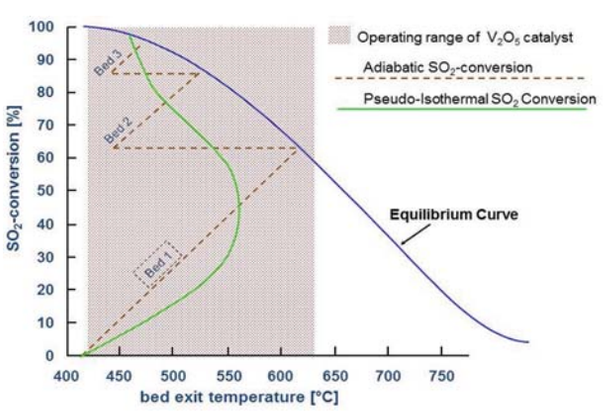

Figure 4—SO_2 conversion curve of conventional adiabatic process *vs* pseudo-isothermal process

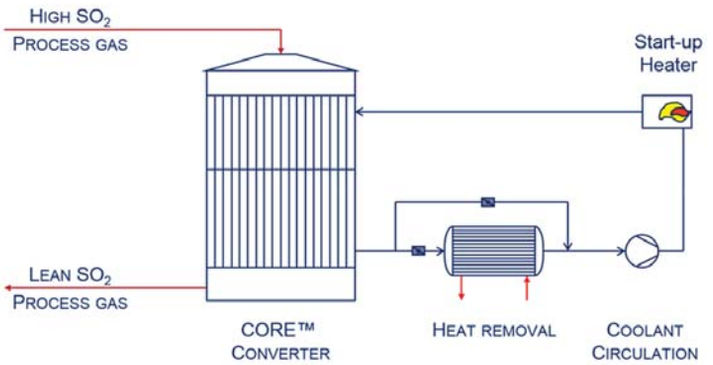

Figure 5—Standalone Chemetics CORE™ system

design). However, in the absence of dilution air, the number of adiabatic passes must increase to achieve the same SO_2 emission allowance. This results in a contact plant with up to six passes and three absorption towers. Finally with the Chemetics in-line design using a CORE™ reactor coupled with secondary contact, the gas flow to bed 1 is not only the lowest but also the number of reaction stages is minimized (see Figure 6).

Since SO_2 conversion in excess of 90% can be achieved using a single Chemetics CORE™ reactor, the downstream secondary contact section can be customized based on the client's specific needs. This second SO_2 abatement process can be (i) a conventional single or dual adiabatic design, (ii) another single-pass CORE™ reactor, or (iii) a regenerative SO_2 tail-gas treatment unit. For instance, if a client desires the smallest plant footprint and the flexibility of equipment modularization, a Chemetics CORE™ reactor coupled with a regenerative tail-gas unit would be the preferred solution, at the expense of steam consumption in the tail-gas unit. This combination is especially suitable for smaller capacities or locations where a regenerative scrubbing system is already required to capture the SO_2 gases prior to conversion to acid.

Chemetics CORE™ pre-converter

Another application of the technology is to treat only a portion of the strong SO_2 feed gas, with the SO_3-rich gas leaving the isothermal pre-converter directly mixed with rest of the strong feed gas and processed through a standard adiabatic contact plant. This configuration may be attractive for large-capacity new plants, where the benefits of directly treating a strong feed gas are fully realized with a smaller CORE™ reactor and cooling system. This same concept also highlights the value of the reactor technology for brownfield plant expansion, where a planned upgrade in the smelter operation would increase the SO_2 gas concentration going to an existing acid plant. The conventional design would require diluting the strong gas with air, resulting in a gas flow rate beyond the capacity of the existing acid plant. In many cases, a new double-contact acid plant or a costly debottlenecking of the existing contact plant would be required. In such applications, an add-on Chemetics CORE™ module is a more economical solution. The CORE™ module converts and removes the extra SO_2, resulting in a gas to the existing acid plant that is the same volume and concentration as before the

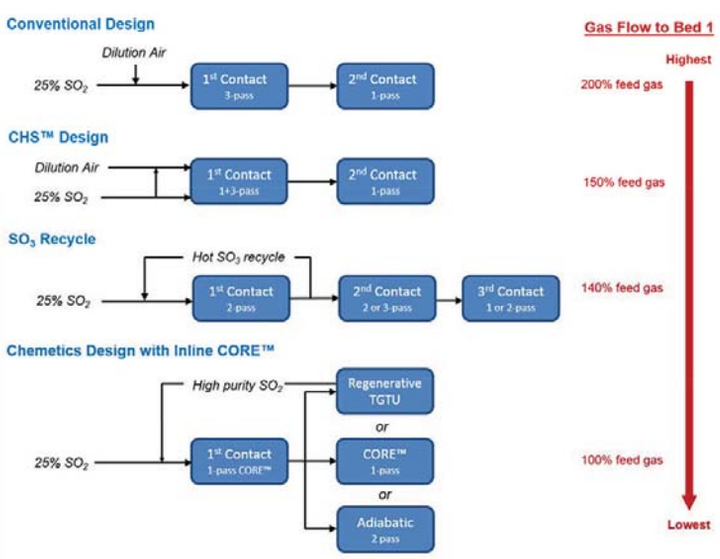

Figure 6—Technologies for treating a single high-strength SO_2 source

smelter expansion. This solution thus offers a compact design, smaller footprint, and improved energy efficiency at lower capital and operating cost.

An example of the pre-converter line-up is shown in Figure 7. Optional add-ons such as a dedicated SO_2 booster fan and intermediate absorption tower are offered, depending on the project requirement. Acid produced in the intermediate absorption tower is of high quality as any remaining impurities in the process gas have already been washed out in the drying tower. In some cases this premium quality acid can be sold at significantly higher prices, improving profitability.

The Chemetics CORE™ converter operation can be adjusted by controlling the temperature of the cooling medium (controlling conversion) or by adjusting the gas flow through the reactor. If the SO_2 concentration from the smelter is low, the unit can be taken off-line into 'hot standby' and can stay in this mode for any length of time while maintaining optimum catalyst temperature for immediate restart. From hot-standby mode the plant can be switched to on-line by simply restarting the gas flow. This operational flexibility maintains a steady gas concentration to the downstream acid plant despite variability in feed gas, and thereby improves the acid plant reliability.

The versatility of the Chemetics CORE™ technology, with its ability to handle high-strength SO_2 gas and fluctuating process conditions, makes it a powerful solution for metallurgical SO_2 off-gas abatement which also allows for increased steam production. When used in smelter expansions to accept higher concentration gas, the CORE™ technology is by far the most cost-effective solution.

Summary and Conclusions

Chemetics offers several solutions for treating high-strength SO_2 off-gas without requiring excess dilution air or recycling of hot process gas. While CHS™ is best suited for applications with multiple large SO_2 gas streams, process designs integrating the Chemetics CORE™ reactor can directly treat concentrated gas streams as high as 50 vol% SO_2. Both approaches use proven equipment and catalyst and simple controls. Their advantages over the conventional acid plant design are summarized in Table III. Chemetics' success in the sulphuric acid industry has been built on focusing on the client's needs. With the evolution of increasingly high-concentration SO_2 off-gases, Chemetics is able to offer customized solutions for any conditions by selecting the appropriate process. The optimized solution is reached by closely working together with our clients to ensure that their needs are fully realized.

Table III

Summary of advantages of CHS™ and CORE™

	Chemetics High Strength (CHS™)	Chemetics CORE™
Capital improvement		
Reduced plant size - No air dilution beyond O_2: SO_2 ratio adjustment, - No process gas recycle	✓	✓
Reduced footprint	✓	✓
Ease of integration	✓	✓
Reduced reaction stages		✓
Operating Improvement		
Lower utility consumption (power, cooling water)	✓	✓
Improved energy recovery and steam production	✓	✓
Improved acid plant availability	✓	✓
Increased catalyst life (reduced thermal stress)		✓
Higher purity product acid		✓

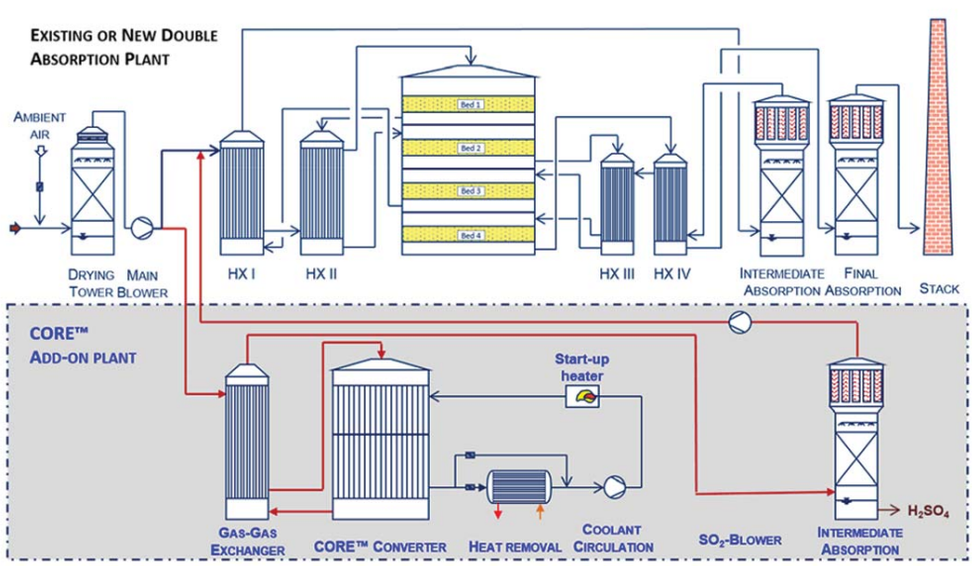

Figure 7—Example of the pre-converter line-up

CM solutions

metallurgical consultancy & laboratories

maximizing metallurgy

Our four-in-one solution.
We do your test work,
interpret it,
model it
and integrate the results
in metallurgical designs.

Our laboratory areas of expertise

- Mineral processing
- Hydrometallurgy
- Chemical analysis
- Process development
- Solid liquid separation
- Pyrometallurgy

CM SOLUTIONS IS AN
ISO 9001:2008
ACCREDITED COMPANY
Certificate 91215729,
audited by DEKRA GmbH, Stuttgart

T 011 608 0019
F 011 608 4067
C 082 441 2788
E consultants@cm-solutions.co.za

Pinelands Office Park
Unit T5, 1 Ardeer Road
Modderfontein, 1609
South Africa

Find us on www.cm-solutions.co.za

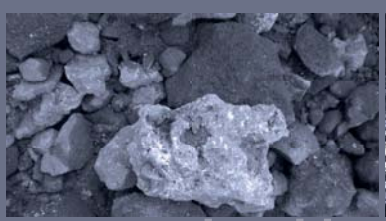


conductivity **leaching** test rig calcining wet chemistry sulfides shaking agitation electrowinning filtration furnace ion exchange **open tanks** roasting solvent extraction batch tests milling DMS pressure oxidation TCLP cyclone Isotherms PSD pilot plant cathode kinetics **cell design** flocculant screening **flotation** crushing ICP-OES crushing pyrometallurgy cyanidation attritioning **water analysis** thickening pressure **oxidation** heap pH control solid liquid separation

http://dx.doi.org/10.17159/2411-9717/2017/v117n11a3

Protect your catalyst by improving your sulphur filtration process

by J. Hermans

Synopsis

Downtime of a sulphuric acid plant is costly. Poor catalyst screening due to loss of high pressure on the catalyst bed is one of the major reasons for downtime. Sulphurnet has developed a technology that improves the efficiency of the liquid sulphur filtration process. Less ash is transferred to the catalyst. This enables acid plants to run for 28 to 30 months without catalyst screening. Other advantages of the process are reduced losses of liquid sulphur in the filter cake, and lower maintenance costs due to the longer lifetime of filter leafs. Finally, we address some environmental issues to reduce emissions and the losses of the sulphur in various areas.

Keywords
sulphuric acid plant, catalyst pollution, liquid sulphur filtration.

Introduction

Downtime of a sulphuric acid plant is costly. High pressure drop in the first catalyst bed is the main cause of downtime. The pressure drop requires catalyst screening, replacement of the catalyst, as well as preheating the system. Downtime or losses of production are therefore only one aspect of the problem – additional costs are incurred in the replacement of catalyst and the fuel consumption for preheating the plant. Catalyst pollution is mainly due to ash and other impurities in the liquid sulphur. In this article we explain how this pollution can be prevented.

Prevention of pollution

There are two methods of preventing ashes from entering the catalyst bed:

- Hot gas filters
- Liquid sulphur purification by filtration.

Hot gas filter

The hot gas filter is one of the oldest technologies in the market. The filter consists of a tank filled with glass beads or volcanic rock particles, which provides a deep bed filtration system that removes dust particles. The increasing volume of fine solids in the filter contributes to the pressure drop, which affects the main blower and the plant efficiency. This is one reason why the hot gas filter is losing acceptance. Furthermore, the filter needs manual cleaning and the glass beads or volcanic rock particles require sieving before they can be re-used.

Liquid sulphur filtration

Liquid sulphur filter systems are the predominant filtration systems used in the sulphuric acid industry. In the 1940s the RP Adams company introduced the liquid sulphur candle filter, a system with ceramic candles making use of pre-coating. This technology was patented by E.I. Dupont De Nemours in 1942. The most popular technology nowadays is the pressure leaf liquid sulphur filter, which is fully steam-jacketed to prevent solidification of sulphur (Figure 1). The filter leafs are made of stainless steel. This is a modern update of a technology that was introduced in the 1930s.

Donovan and Barnett (1959) compared the candle and pressure-leaf filter technologies. They described tests with various grades of precoat and additions of body feed, and presented a table of recommended conditions for plant filtration of sulphur. The flow rates given in this article from 1959 are outdated but are unfortunately still being used to design today's liquid sulphur filters. The result is not only oversized filter systems (inflated CAPEX), but the operational characteristics and performance of these filters are disappointing, with high losses of liquid sulphur in the filter cake, difficulties when cleaning the filter, and a high ash content passing the filter (OPEX). The liquid sulphur filters are blamed for these shortcomings. A solution would be to add a polishing filter, which would entail additional CAPEX and OPEX.

Two important developments in todays' technology stem from the findings from Donovan and Barnett. The first is the quality of the liquid sulphur. Whereas in 1959 Frasch

* *Sulphurnet, Netherlands.*
 ISSN 2225-6253. This paper was first presented at the 6th Sulphuric Acid 2017 Conference', *9–12 May 2017, Southern Sun Cape Sun, Cape Town.*

Protect your catalyst by improving your sulphur filtration process

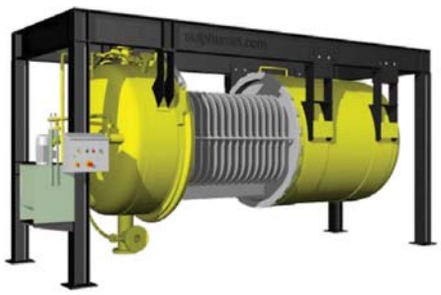

Figure 1—Liquid sulphur pressure-leaf filter

sulphur was the main source of sulphur, in 2017 liquid sulphur is sourced mainly from the refineries. The sulphur direct from the refinery contains < 200 ppm ash and the organic content is minimal. The main problem with today's sulphur is contamination during transportation, and the formation of sulphuric acid due to the presence of the *Thiobacillus* bacterium. Neutralization of the acid with lime or quicklime results in a much higher solid content than the original ash content in the sulphur. To prevent acid formation, dry storage is recommended. The second development is precise and reliable process instrumentation and automation. This is beneficial for the operation, since it enables control from a distance and, more importantly, optimization of the filtration process. The liquid sulphur filter requires a driving force to create a flow that can overcome the resistance of the filter cake build-up during the filtration cycle.

The other important piece of process equipment providing the driving force is the liquid sulphur pump. Efficient pumps can reduce operational cost. Successful sulphur filtration begins with understanding the process. In the sulphur pumping system, the objective is to transfer the liquid sulphur from a dirty sulphur pit or tank via the filter system to a destination, *e.g.* a clean liquid sulphur storage tank or pumping pit. The flow rate is equal to the driving force divided by the resistance, the driving force being the total pressure drop required to achieve a liquid flow.

The resistance is the sum of various energy losses in the system. These head losses are of three types:

- *Static pressure*—The height of the filter system and storage system. This is a constant value
- *Pressure differential of the filter*—Losses caused by the resistance of the filter cake. This is variable over the filtration cycle.
- *Friction head*—The friction loss is due to the liquid being moved in pipes and valves. This is a constant value.

Filtration efficiency is affected by three variables as shown in Figure 2. These are the actual pump curve, the increasing cake thickness, and the flow rate.

Since a centrifugal pump is used, after the precoating cycle there is a small head loss through the filter but only a 3 mm cake thickness. The pump will therefore run out on its performance curve to a flow rate corresponding to the resistance head of the system (this can be 30% higher than the design flow rate). As the filter cake increases in thickness and the resistance head in the filter increases, the pump moves back toward the left side of its performance curve and

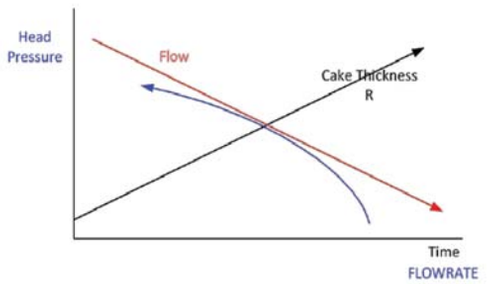

Figure 2—Variables affecting the filtration process

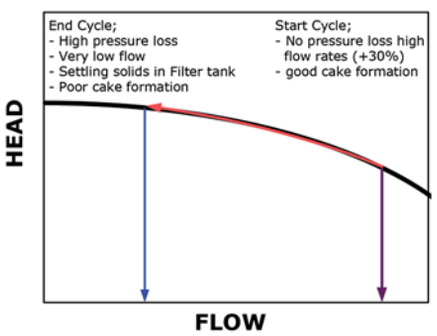

Figure 3—Filter cake formation and flow rate

the flow decreases with the increase in the system head required (Figure 3). This will continue until the flow of the pump is reduced to a certain predetermined rate that corresponds to an increase in the resistance head through the filter. At this stage cleaning is required. In this set-up the pumps are not used in the design condition so the system is not working very efficiently. These differences in flow rate influence the filter cake consistency. Initially there is a high flow rate (up to 30% of the design flow) and a very firm filter cake is formed, but at the end of the cycle, when the filter cake builds up resistance, the flow drops rapidly and the cake becomes 'fluffy', unstable, and holds a high content of liquid sulphur.

A consistent filter cake can be achieved by maintaining a constant flow over the entire filtration cycle. Selection of an appropriate design and size of filter will save on initial investment, and reduce operating costs due to:

- Less losses of sulphur in the filter cake
- Easier cake removal
- Longer filtration cycles
- Less ash passing the filter
- Longer life of the catalyst bed in the convertor.

Furthermore, extra energy savings are possible since the liquid sulphur pump is running at its optimal setting throughout the filtration process.

Conclusion

A well-designed filter system can save CAPEX cost. The filtration efficiency will be improved, leading to longer catalyst life in the converter bed. This reduces the overall OPEX cost.

Reference

Donovan, J.R. and Barnett, B.J.. 1959. Filtration of molten sulfur. Industrial and Engineering Chemistry, vol. 51, no. 2. pp. 165–168 ◆

http://dx.doi.org/10.17159/2411-9717/2017/v117n11a4

Two years of operation at Kansanshi's sulphuric acid plant

by B. Mumba*, D. Lourie†, and P. Ng'ambi*

Synopsis

Kansanshi Mining plc's copper smelter in Solwezi, Zambia started production in March 2015 and has now been operating for over two years. The sulphuric acid plant has performed well during this period with an average availability of about 93%. However, issues arose in the plant which were not evident during the design phase and became evident only after operation for an extended period, predominatly around the converter. Other areas where operating issues were encountered were wet electrostatic precipitator performance, blower power consumption, converter bed temperature profile, and converter internal duct reinforcement. This paper provides details on the issues and the solutions implemented.

Keywords
sulphuric acid plant, converter bed temperature, wet electrostatic precipitator, acid mist capture, preheater.

Introduction

In March 2015 Kansanshi Mining plc commenced operation of a greenfield copper smelter near Solwezi, Zambia. The smelter is designed to treat 1.2 Mt of copper concentrate per year. Concentrate is smelted in an Isasmelt furnace, and the matte is subsequently converted to blister copper in Peirce-Smith converters (PSCs). The off-gases from the Isasmelt furnace and the PSCs are directed to wet gas cleaning systems and then to a contact sulphuric acid plant (SAP).

Acid plant operation and performance

Overall, the SAP has performed well, allowing rapid ramp-up of the smelter to its design capacity of 1.2 Mt/a. The sophisticated control philosophy for the acid plant-smelter interface has allowed for relatively trouble-free operation with the smelter. The acid plant can easily handle transitions in gas flow and SO_2 concentrations resulting from the operation of PSCs. The goal for the future is to maintain the high availability of the acid plant through improvements in maintenance. There is also a desire to maximize acid plant throughput to maximize production of both copper and acid. While the operation and performance of the acid plant has been nearly trouble-free, some of the more interesting issues that we overcame are presented later in the paper.

Plant availability

Availability of the plant has exceeded 93.1% on average, with over 99% availability in the best month (see Figure 1). KMP's definition of availability is the time that the acid plant is ready and available to receive gas from either the Isasmelt furnace or from the PSCs. Downtime due to site power outages is not included in acid plant availability.

Acid production

The maximum daily production achieved to date is 4077 t.

Figure 2 shows the steady ramp-up of smelter throughput and the corresponding increase in acid production. For the months of March through to February 2017, acid production exceeded nominal design capacity for the plant. From September 2015 to January 2016 concentrate treatement, and therefore acid production, was limited due to lack of concentrate. Production was low in February 2016 due to the planned shutdown to repair the SAP converter, and in August 2016 due to a shutdown to repair damaged bricking in the Isasmelt furnace.

* *First Quantum Minerals Ltd, Zambia.*
† *DKL Engineering Inc., Canada.*

 This paper was first presented at the 6th Sulphuric Acid 2017 Conference', *9–12 May 2017, Southern Sun Cape Sun, Cape Town.*

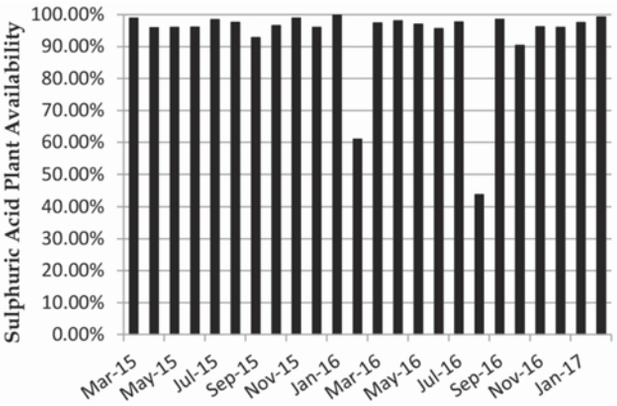

Figure 1—Acid plant monthly availability

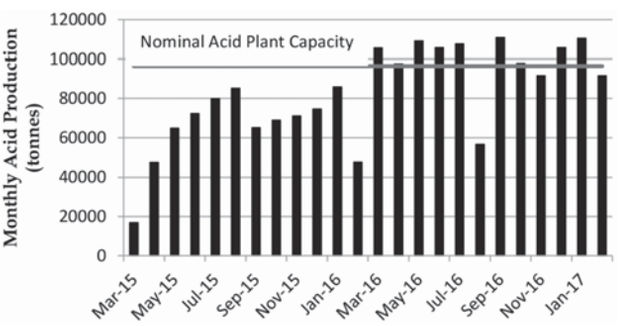

Figure 2—Monthly sulphuric acid production

Electrical power consumption

Specific power consumption for the acid plant when the production rate is above 3500 t/d is less than 100 KWh/t of acid produced, with some days in the low 90s (see Figure 3). SAP electrical power consumption figures include all process drives in the gas cleaning, contact, strong acid, cooling water, and effluent handling areas.

Converter

The converter is 17.5 m diameter with a 7.2 m diameter central core that houses two internal gas-to-gas heat exchangers. The central core is also used to direct gases into the converter via ducts in the core.

Converter bed temperature profile

The converter was designed with multiple temperature measurements in the catalyst beds. Beds 1 and 4 are equipped with two inlet, two mid-bed, and two outlet temperature measurements located 180° apart. Beds 2 and 3 are equipped with two inlet and two outlet temperature measurements only. A mid-bed thermowell is provided but a thermocouple is not installed.

Accurate temperature measurements are important for the proper operation of the converter to maximize conversion and to prevent damage to the catalyst and converter, particularly in bed 1. In a large converter, multiple temperature measurements also provide a better idea of the temperature profile across the catalyst bed.

Since the startup of the plant the bed 1 outlet temperature was always lower than the mid-bed temperature reading by up to 50–60°C. Also, there was a significant difference between the two outlet temperatures by up to 20°C (see Figure 4). Initially the cause was believed to be the placement of the thermowells in the gas space rather than in the catalyst bed itself.

This theory was proved by bending one bed 1 outlet thermocouple so that the end was closer to the bottom of the bed (see Figure 5). The result was a 20°C higher temperature reading, but the outlet temperature was still less than the mid-bed temperature reading. The conclusion is that thermocouples in the gas space do not provide a true temperature reading.

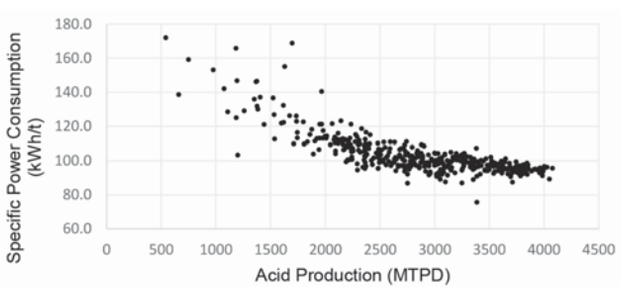

Figure 3—Acid plant specific power consumption

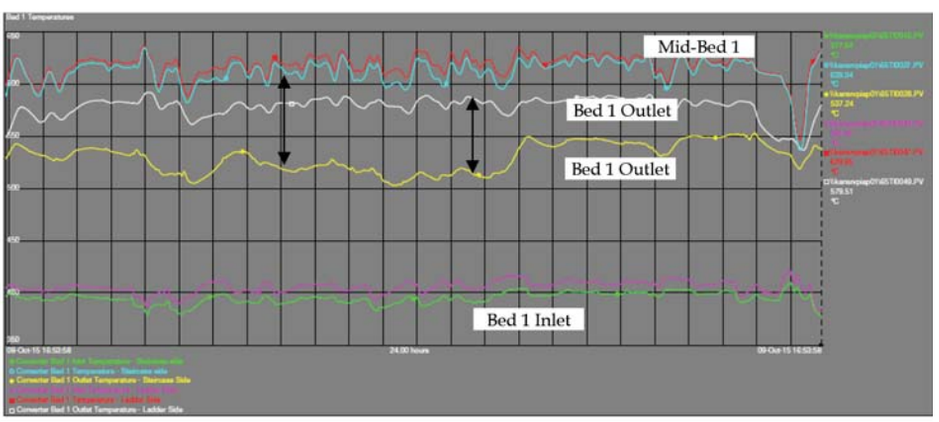

Figure 4—Bed 1 temperatures

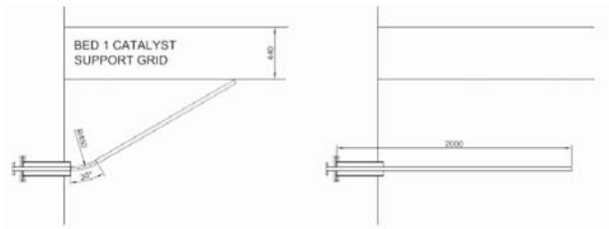

Figure 5—Thermocouple bending

Based on the temperature observations, the thermocouples were relocated during the February shutdown to provide more reliable readings. Furthermore, additional thermocouples were installed in the bed 1 inlet and outlet to obtain a better idea of the temperature profile across the bed. The additional temperature readings in bed 1 have helped to diagnose previous operating problems with one side of the catalyst bed going cold. A smelter outage in August 2016 provided an opportunity to enter the converter for an inspection. It was discovered that the catalyst in bed 1 was blown around, with a deep trench formed around the outside wall (see Figure 6).

When the gas exits the windows in the central core it travels across the top of the bed and impacts on the sloping roof, which directs the gas to the outside wall. The gas is deflected down into the catalyst bed with a high enough velocity so that the catalyst and hold-down rings are blown to the centre of the bed, forming the trough around the perimeter.

The top layer of catalyst and ceramic rings were screened to separate them and a small amount of makeup catalyst was added. The catalyst bed was levelled and ceramic balls instead of ceramic rings were used as a hold-down layer around the circumference of the bed.

When the plant was restarted there was a surprising benefit of levelling the bed and eliminating the trough. All temperature readings (six in total) at the bed inlet started to indicate within 5°C of each other, compared to a 10–15°C difference before the shutdown. The same improvement occurred with the bed outlet temperatures. The temperature readings now indicate a more even temperature and gas distribution across the bed, indicating that the the perimeter trough was the main factor in poor temperature distribution.

The August shutdown also revealed that the converter is subject to high-temperature scaling, like so many other stainless steel converters in the industry. During the shutdown the scale was cleaned from the bed outlets, heat exchangers, and gas ducts.

Bed 4 bypass

Soon after startup, problems were encountered in controlling the bed 4 inlet temperature. The design inlet temperature was 410°C but during operation the minimum temperature that could be achieved was about 430–440°C. The bypass damper around the internal hot reheat exchanger was always 100% open, indicating that possibly the bypass was either too small or too restrictive in terms of pressure drop.

To complicate the understanding of the issue, the SO_2 emissions from the stack were relatively low, even though the bed inlet temperature was too high and often higher than the bed outlet temperature.

Inside the internal hot reheat exchanger the bypass distributor consisted of 20 pipes with distributor caps to distribute the gas evenly and ensure good mixing of the hot gas and the colder bypass gas. It was determined that the distribution caps were too restrictive and did not allow sufficient cold gas to be bypassed with the available pressure drop. The solution was to increase the size of the openings in the distribution caps (see Figure 7).

The other issue in the discrepancy between the bed temperatures and SO_2 emission was not related to the bypass issue; it was the placement of the bed inlet thermocouples. Normally the bed inlet thermocouples are placed at the top of the catalyst bed between the hold-down layer of quartz/ceramic and the catalyst. In this case the thermocouples were placed in the gas space just below the division plate with bed 2 (see Figure 8). It is believed that the bed 4 inlet thermocouples were measuring higher temperatures due to the radiation from the hotter division plate (bed 2 outlet temperature approx. 526°C). The influence of the bed 2 outlet temperature on the bed 4 inlet temperature is evident when the plant is shut down. The bed 4 inlet temperature rises and then follows the bed 2 outlet temperature as it cools, which indicates that the true bed 4 inlet temperature is lower than the measured temperature.

Internal duct reinforcement

During an investigation into raising the design pressure for the converter it was discovered that the internal duct returning gas from the inter-absorber tower to bed 4 was designed for the wrong differential pressure, and as a result there was a risk that the internal duct would deform. The solution was to install three reinforcing rings inside the duct to prevent it from deforming due to high differential pressure. The repair required a shutdown and cooldown of the acid

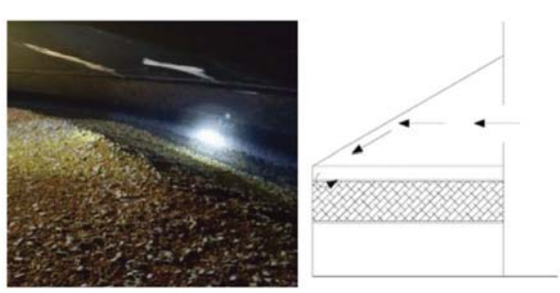

Figure 6—Bed 1 catalyst and gas flow to the bed

Figure 7—Bed 4 byass caps before and after modification

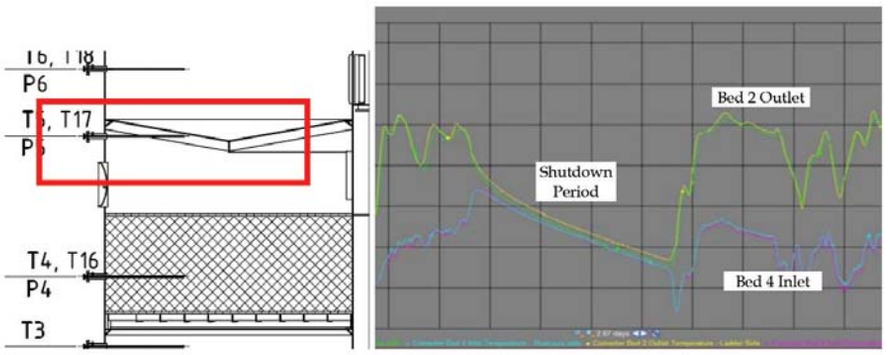

Figure 8—Location of bed 4 inlet thermocouples (graph), and bed 2 outlet and bed 4 inlet temperature trends during shutdown

plant and converter. The repair was done during a 10-day shutdown of the smelter in February 2016 and is detailed in the following section.

Plant shutdown for converter repairs

Planning for an acid plant shutdown began as soon as the risk of the duct deformation was known. The opportunity was taken to make corrections to the bed 4 bypass caps and converter thermocouples. Issues that were considered during shutdown planning were:

- Minimize length of the shutdown
- Confined space working conditions
- Temperature of the interior of the converter
- Seasonal conditions (Zambia's wet season)
- Multiple entry and exit points for safety
- Unknown condition of the interior duct (had the duct collapsed?)

To our knowledge, this type of repair has never been done before under similar circumstances.

A ventilation and cooling scheme was prepared (see Figure 9). The plan was to hot-purge the converter to remove SO_2 and SO_3 from the catalyst and then cold-purge to cool the entire vessel. The lowest temperature that the converter could be cooled to was the blower outlet temperature (approx. 75°C). This temperature was too high for vessel entry so another means of cooling the converter core was required.

During a normal plant shutdown the converter manways would be opened and allowed to cool with ambient air. This procedure would have taken a long time, particularly for the central core of the converter where there would be little or no ventilation. The shutdown was scheduled for the wet season so there was a risk of introducing large amounts of moist air into the converter and exposing the catalyst to moisture.

To provide ventilation and cooling a 75 kW axial ventilation fan was installed to blow ambient air directly into the core to cool and ventilate the work area. The downstream ducts were isolated to prevent ambient air being blown through the catalyst beds (particularly bed 4). Inflatable duct balloons were used to provide isolation in the ducts in two locations (see Figure 10).

The duct balloons ensured that the cooling air was directed through the converter core and not through the catalyst bed. A temporary power line was routed to the fan from one of the absorber acid pumps power supplies so that the motor control centre (MCC) and variable frequency drive (VFD) of the pump could be utilized to power and control the fan. Having a VFD on the fan proved invaluable. During the initial cooldown the fan was run at full speed. However, once work commenced and the steel temperature had reduced, the fan was operated at a reduced speed to avoid excessive noise and air velocity in the working area.

Two entry points into the work area were provided. The first was at the top of the central duct at the inlet elbow. This would be the first entry point, allowing access to the bottom hot reheat exchanger tubesheet plate where a hole would be

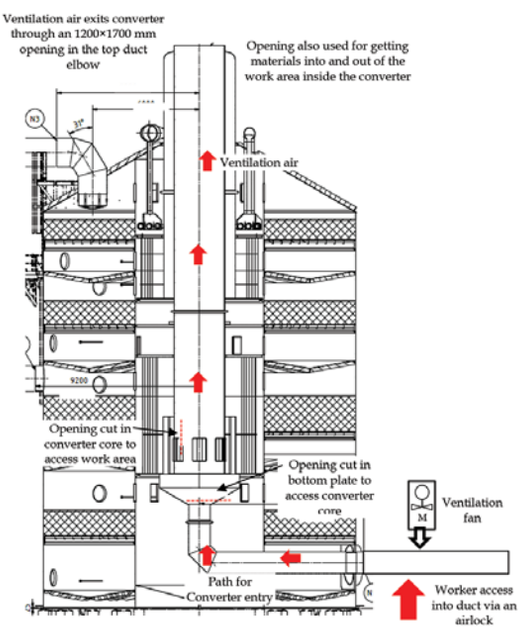

Figure 9—Converter ventilation and access plan

Figure 10—Duct balloons used for isolation

cut to provide the second entry point. Access was by a manbasket suspended from a crane. The top entry point was where materials and equipment would be lowered into the converter. A permanent platform was fabricated and installed to allow easy future access to the top of the converter. Once the opening in the bottom tubesheet plate was cut, the second entry point through the bypass duct was opened. This was the main access route for personnel working on the planned repairs.

Post-shutdown operation

After the modifications to the converter internals it was expected that control of bed 4 inlet temperature would improve. Although the bed 4 inlet temperature control improved, an unexpected consequence of the modification was the loss of bed 3 temperature control under certain operating conditions.

The design has a common bypass duct that splits to send cold gas to bed 3 and bed 4. At times, both bed 3 and bed 4 temperature control dampers open to 100%, indicating that the common duct is unable to provide sufficient cold bypass to control the inlet temperature of bed 3 and bed 4. The problem is currently under investigation to find a suitable solution.

Wet electrostatic precipitators

The wet electrostatic precipitators (WESPs) consist of four trains of primary and secondary units. The design flow through each train is 79 721 Nm^3/h.

WESP performance/acid mist

The WESPs are equipped with sightglasses to monitor their performance. A sightglass is also provided in the main outlet duct to monitor the optical clarity of the gas going to the drying tower. During initial operation of the plant, observations through the duct sightglass showed poor acid mist collection when operating at low voltages and high gas flows. Voltages were increased to improve WESP performance, but issues were then experienced with the band heaters (see below).

A CCTV camera was installed at the sightglass so the quality of the gas could be monitored in the control room, allowing easier correlation of WESP performance and subsequently quality of the gas. When the problems with the band heaters were resolved, the maximum WESP operating voltage setting was raised to 60 kV. At this operating voltage an optically clear gas would be expected to be produced, but at high gas flow rates acid mist could still be observed through the duct sightglass.

A qualitative grading system for gas quality was developed to assist in evaluating WESP performance. The scale ranged from Zero Visibility, Very Poor, Poor, Good, Very Good, to Optically Clear (see Figure 11). The gas quality was correlated with the gas flow through the WESP. In general, higher gas flows and lower operating voltages resulted in poorer WESP performance.

It was noted very early during the initial plant operation that the temperature of the gas entering WESP train no. 1 was higher than for the other three trains. The reason for this is that the air leaving the SO_2 stripper is delivered into the WESP inlet header near the entrance to train 1. The higher operating temperature results in a slightly worse performance, which is apparent when the secondary voltage and current are compared with the readings for the other trains.

A trial was conducted that involved closing the air to the SO_2 stripper and observing the performance of the WESPs in the sightglass. The temperature of the gas in train 1 decreased and its performance improved, as indicated by the secondary voltage and current. The mist that was visible in the sightglass cleared, but was still visible at high throughput.

The WESP electrodes were realigned during the August 2016 shutdown, which created an opportunity for further adjustment of WESP operating parameters. To resolve the mist breakthrough issue the vendor, Outotec Sweden, sent a team to the site to review the parameters of both the primary and secondary WESPs. Adjustments were made to the WESP primary current limit (*Ip*), secondary current limit (*Us*), and the timing for increasing primary current by 1 A after

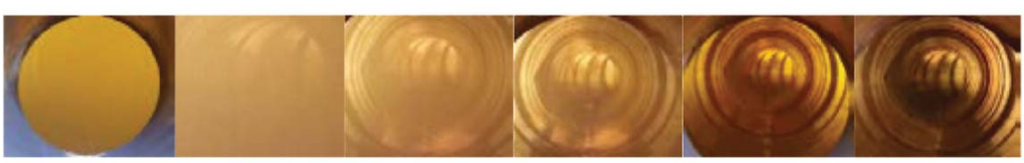

Figure 11—WESP performance grading system

Table I

WESP parameters

Parameters		*Ip*	*Us*	Slow ramp
Primary filters (WESP 1-4)	Before After	90 A 120 A	70 kV 75 kV	800 ms 200 ms
Secondary filters (WESP 5-8)	Before After	100 A 120 A	60 kV 75 kV	800 ms 150 ms

flashover (slow ramp). The adjusted settings are shown in Table I.

After the adjustments the flashovers per unit increased from 6 per minute to 16 per minute. The flashover rate is an important parameter for increasing the overall filter efficiency. These adjustments improved the WESP performance at high flow rates from 'very poor' to 'good' (see Figure 12). Mist quantification was conducted on the smelter scrubbers (PS converters and Isasmelt furnace) and the WESP outlets to ascertain how much mist was being captured (see results in Table II). The design mist exiting WESPs is 25 mg/Nm^3.

Increasing the voltage and primary current settings on the WESPs increased the risk of burning the collecting tubes at low flow rates. In mid-February 2017 a significant deterioration in performance was noticed on three of the secondary WESPs, which proved to be due to burned collecting tubes. After the incident a separate parameter set for low flow and startup situations was set for the WESPs, with significantly reduced limits on the primary current and a lower maximum secondary voltage limit. The low flow parameter set is automatically activated by the DCS when the gas cleaning plant dry flow drops below 150 000 Nm^3/h or if the WESPs are turned off. Normal operating parameters are automatically restored when the GCP dry flow is higher than 180 000 Nm^3/h.

Band heaters

The WESPs are designed with totally enclosed insulator compartments which are kept hot with electric band heaters to prevent condensation on the ceramic insulators. The band heater temperature is measured and controlled by varying the power to the heaters. Initial operation of the WESPs was at relatively low voltage (approx. 35 kV).

As the WESP voltage was increased to achieve better collection efficiencies the WESP would trip due to a fault in the band heater temperature measurement circuit. The instrument input cards that received the band heater temperature signal from the field were failing. With theassistance of the vendor, it was determined that this was likely due to the temperature signal cables being run too close to the WESP main grounding cables. When a flashover occurred in the unit an electromagnetic pulse ran down the grounding cable, which then induced a current in the temperature signal cable. The resulting power spike in the signal cable caused the input card to fail.

Installing a steel shield between the cables did not resolve the issue. The existing signal cables were then replaced with fully shielded cables that were rerouted away from the grounding cables, and additional shielding installed around the earth cables, which resolved the issue. This allowed the WESP to be set for higher operating voltage levels without the units tripping.

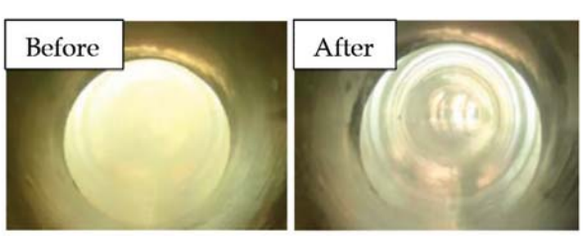

Figure 12—Comparison of visibility at WESP outlet before and after parameter adjustment

Table II

WESP performace test results

PS converters	Primary smelter	WESP outlet
3153 mg/m^3	380 mg/m^3	4 mg/m^3

WESP flushing

WESPs flushing is done to clean the collecting tubes of dust that has collected on the inside surface. Proper flushing of the WESPs was not possible due to a problem in the fabrication of the flushing piping and nozzles, which caused the spray nozzles to fall off. Also, the spray pattern of some of the nozzles was blocked by fogging water piping. The collecting tubes that were not adequately flushed experienced greater buildup of dust than those that were properly flushed.

The vendor supplied replacement spray nozzles and piping. Piping that blocked the sprays was relocated. Flushing of the WESPs is now much improved.

The WESP flushing pump was equipped with a constant speed electric motor. When a WESP is flushed, automatic valves open and close sending liquid to the flushing spray nozzles. The sudden opening and closing of these valves resulted in water hammer in the piping. The solution was to install a VFD. Flow is now increased and decreased at a slow rate, which avoids water hammer in the piping.

Preheater

Unplanned plant outages do occur due to equipment problems in the smelter and acid plant. Once all gas sources to the acid plant stop, the main blowers go on full recycle. If the outage is short, both blowers will be kept running. Even on full recycle there is still some gas that flows to the acid plant, which causes the converter beds to cool. If restart of the smelter is delayed, one blower is shut off, which reduces the rate of cooling of the converter. If the shutdown is further extended, all blowers are stopped and the converter isolated to conserve heat in the catalyst. The acid plant converter is able to restart without the use of the preheater after a 36-hour stoppage.

During normal operation, the preheater is isolated with help of blanks at both preheater inlets to the first and fourth passes. Blanking is done to avoid cold sulphur dioxide gas ingress from the cold heat exchanger to the first pass, causing the converter to cool. When the preheater needs to be used due to a process upset or after a long shutdown, the blanks have to be removed before starting the preheater.

To bring the preheater online the delta *P* across the tubes has to be more than 1.5 kPa to avoid causing damage to the tubes. To achieve this, the main sulphur dioxide blower has to be running before the preheater is turned on. This creates a problem when a preheater has to be tested during normal plant operation, as this would necessitate removing the

blanks and eventually cooling the bed during the test

In order to resolve this problem an independent external 75 kW motor axial fan and air outlet port were installed on first pass inlet duct. The modification allows the operations team to test the preheater as and when required without disturbing the process.

Blower power consumption

During the plant performance test, data was collected to determine whether the blowers were operating at the expected design setting. The plant flow and pressure drop were close to the expected design settings, but the blower power consumption was significantly higher than expected. Possible causes such as power measurement errors were quickly eliminated. In the end, the most likely cause identified was leakage through the blower recycle damper.

The analysis of the blower operation used the suction and discharge pressure and the flow to the contact section. Gas flow measurement is done downstream of the blowers and the recycle duct. The arrangement is such that the blowers can be operating in partial recycle and the flow meter would not register the additional flow in the recycle because of its location downstream of the recycle duct. The blower power consumption would be higher than what the differential pressure across the blower and the flow would otherwise indicate.

To verify this theory, flow measurements were taken in the recycle duct with the recycle damper fully closed. A flow was measured in the duct, which confirmed the theory and explained the higher electrical power consumption that was measured.

The solution was to install a tight shutoff damper upstream of the existing control damper. In initial tests, the moment the tight shutoff damper was closed the blower current decreased and the inlet guide vanes closed more for the same operating conditions. The power savings over the life of the plant are significant.

Acid plant debottlenecking study

Currently, the acid plant is designed to handle a maximum of 42 000 Nm³/h of SO_2. After smelter ramp-up it became obvious that whenever sulphur in the concentrate feed was high, giving a sulphur factor above 160 Nm³/h of SO_2 per ton concentrate smelted, the acid plant became a restriction for smelter production. During 2016, smelter production was restricted for a total of 98 days due to acid plant capacity. This restriction prompted us to request Outotec to perform a debottlenecking study for the acid plant in order to investigate possibilities for increasing the plant capacity. The results of the study are compiled in Table III. The modifications are expected to increase acid plant capacity by 3%, from 42 000 Nm³ of SO_2 per hour to 43 260 Nm³/h. The modifications will be implemented in the upcoming Isa furnace rebricking shutdown in August 2017.

Table III

Debottlenecking study results

Action	ΔP
Replace currently installed venturi flow meter with an ultrasonic one	-0.5 kPa
Increase free window area in converter at catalyst bed inlets by cutting new windows	-3.0 kPa
Guiding plates in windows for better gas flow distribution	0 kPa
Install 9 candles in IAT (currently 90 installed, but altogether 99 can be installed)	-0.2 kPa
Additional catalyst	+0.7 kPa
Relocation of a SX acid cooler from old acid plant to increase acid cooling capacity	0 kPa

Acknowledgement

We would like to thank Kansanshi Mining PLC for permission to present this paper.

References

Mumba, B., deVries, D., and Mohsler, S. 2015. Zambia's newest copper smelter and sulphuric acid plant. *Sulphur 2015, Proceedings of the 31st Annual Conference of Sulphur and Sulphuric Acid*, Toronto, Canada, 9–12 November. CRU Group.

Mumba, B. and Louie, D. 2016. Two years of operation for Kansanshi's sulphuric acid plant. *Proceedings of the Sulphur 2016 International Conference and Exhibition*, London, UK., 7–10 November. CRU Group. ◆

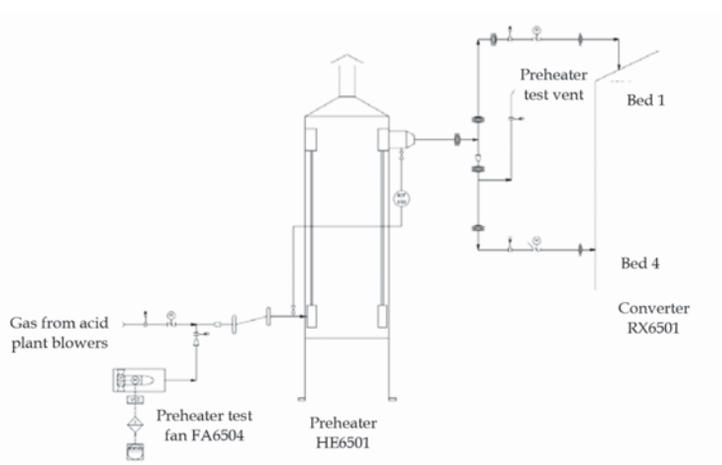

Figure 13—Preheater test equipment

The Society of Mining Professors (SOMP) in collaboration with the Mining Engineering Education South Africa (MEESA) and The Southern African Institute of Mining and Metallurgy (SAIMM) is proud to host

Society of Mining Professors 6th Regional Conference 2018

Overcoming challenges in the Mining Industry through sustainable mining practices

12–13 March 2018 — Conference
14 March 2018— Technical Visit

Birchwood Hotel and Conference Centre, Johannesburg, South Africa

BACKGROUND

The Mining Engineering Education South Africa (MEESA) will host the Society of Mining Professors (SOMP) 6th Regional Conference with the theme: *Overcoming challenges in the Mining Industry through sustainable mining practices*. The Society of Mining Professors is a vibrant Society representing the global academic community and committed to making a significant contribution to the future of the minerals disciplines. The main goal of the Society is to guarantee the scientific, technical, academic and professional knowledge required to ensure a sustainable supply of minerals for mankind. The Society facilitates information exchange, research and teaching partnerships and other collaborative activities among its members. MEESA is comprised of the School of Mining Engineering at the University of Witwatersrand, the Department of Mining Engineering at the University of Pretoria, the Department of Mining Engineering at the University of Johannesburg and the Department of Mining Engineering at the University of South Africa.

The 6th Regional Conference gives a platform to academics, researchers, government officials, Minerals Industry professionals and other stakeholders an opportunity to interact, exchange and analyse the challenges and opportunities within the Minerals Industry. For any country to develop technologically and economically there must be a strong link between its industry, government & academic institutions. This conference will put together the role-players of the Mineral Industry from within and outside South Africa.

RATIONALE FOR SOCIETY OF MINING PROFESSORS (SOMP) REGIONAL CONFERENCE

The main aim of this conference is to facilitate information exchange. It is known that the mining industry is currently faced with big challenges ranging from the technical skills shortage, deep ore bodies, declining ore grades, challenges linked to processing ores with complex mineralogy, water quality and supply to the ever escalating energy costs and sustainability amongst others (Musiyarira et al., 2014). To address some of these challenges there must be a strong link between its industry, government & academic institutions. This will only happen when all the role-players collaboratively work together. The set-up of this conference is such that it allows the interaction between the Minerals Industry players and the academics.

CONFERENCE APPROACH

The conference will feature peer reviewed technical presentations from academic, government and Industry professionals on a wide range of topics. While outlining the Conference programme, great emphasis is laid on participants' interaction in addition to the presentations. The conference will be structured as follows:

FEATURES

- Two-day technical programme with peer-reviewed papers
- Relevant discussion workshops
- Field trips and site tours
- Networking opportunities
- Keynote lecturers

FACILITATOR

The Conference is being organised by Society of Mining Professors (SOMP) in collaboration with the Mining Engineering Education South Africa (MEESA) and The Southern African Institute of Mining and Metallurgy (SAIMM). The Conference presenters are well-known and highly respected experts in their fields, and will cover a wide range of topics. Presentations will be followed by discussions.

TARGET AUDIENCE

The Conference will be of benefit to the Minerals Industry professionals, academics, non-government, government officers and other stakeholders.

EVENT MANAGEMENT SAIMM

For all enquiries please contact:
Chair: Associate Prof Rudrajit Mitra
Telephone: +27 (011) 717 7572 I Email: rudrajit.mitra@wits.ac.za

Head of SOMP Committee on Capacity Building: Dr Harmony Musiyarira

Head of Conferencing: Camielah Jardine
SAIMM, P O Box 61127, Marshalltown 2107
Tel: +27 (0) 11 834-1273/7 · E-mail: camielah@saimm.co.za
Website: http://www.saimm.co.za

Society of Mining Professors
Societät der Bergbaukunde

SAIMM
THE SOUTHERN AFRICAN INSTITUTE OF MINING AND METALLURGY

Conference Announcement

http://dx.doi.org/10.17159/2411-9717/2017/v117n11a5

Potassium silicate concretes in sulphuric acid environments at ambient and low temperature in South Africa

by J.D. Hancock

Synopsis

The paper examines the ongoing development of quartz aggregate potassium silicate concretes at the C&H Laboratories. The original concrete using a sodium fluosilicate setting agent was found to have site problems in South Africa under certain conditions, but not in the UK. The bonding system was modified for local applications, and examples of successful site applications are provided. During 2016 an alternative setting agent only available in South Africa was identified, and this has led to the work on a new acid-resistant concrete that utilizes solid potassium silicate rather than a liquid silicate.

Keywords
acid-resistant concrete, crushing strength, setting agent, sodium fluosilicate, potassium silicate.

Introduction

Over 20 years ago, C&H Laboratories, a refractory testing and development laboratory, was requested to develop an acid-resistant concrete for flooring and bund areas that was user-friendly and suitable for installation under typical South African site conditions.

The refractory industry in South Africa has a long history of involvement in acid-resistant materials. Acid-resistant bricks were made in South Africa for many years by Vereeniging Refractories until the closure of the plant in 2016. Figure 1 shows a cut section of a semi-vitrified red acid brick with a typical black core.

All alumina-silicate bricks have good resistance to acid attack and the choice of red, fawn, white acid, or even andalusite bricks was frequently based on price *versus* the available size tolerances of each grade.

Potassium silicate lining materials have been commercially available overseas for many years and are recognized for their excellent resistance to all acids except hydrofluoric acid (Corrosionengineering.com, 2006). Typically, such potassium silicate materials were based on a siliceous aggregate and sodium fluosilicate as a setting agent. The potassium silicate was supplied in large drums for addition on-site. The standard crushing strength of such concretes was 14 MPa after 1 day and 24–28 MPa after the final cure was reached after 7 days.

One special note pertains to many of these products. Once it has set and will be exposed to water before it is exposed to acid, the surface needs to be pre-treated with an acid mixture of 1 part commercial strength (33%) hydrochloric acid to 2 parts water. For applications in South Africa it would be an advantage to find a formulation that would be stable to water without the need for acid pre-treatment.

Although the use of fluosilicate and a condensed aluminium phosphate is prohibited as the setting agent in some European specifications, it is used locally. Only one sample of such a concrete was found for testing and hence the results may not be typical of such products. Crushing strength after 1 day was 6–14 MPa, and 11–25 MPa after 28 days.

Figure 1—Cut section of a red acid brick

* *C&H Group of Companies, South Africa.*
 ISSN 2225-6253. This paper was first presented at the 6th Sulphuric Acid 2017 Conference', *9–12 May 2017, Southern Sun Cape Sun, Cape Town.*

Table

Mass loss on acid-resistance testing

Test method	Red acid brick	Andalusite VR 60
Segar and Kramer ASTM C279-511	1.4 to 3.0 5 to 7 %	1.2% 0.09%

Initial experimental work

Conventional concretes

Crucibles and test cubes were cast using two concretes – both based on a quartz aggregate, with one using white Portland cement and the other a 50% alumina calcium aluminate cement. The latter had been developed a few years earlier for alkali-resistant flooring. Sulphuric acid concentrations of 20% and 50% were used for the tests. All tests had to be developed in-house as there are no definitive testing methods for acid-resistant castable.

The destruction of the white Portland concrete crucible by the 50% acid is shown in Figure 2. The damage to the crucible with the refractory cement was less severe and is shown in Figure 3.

The test cubes in the immersion tests showed a major reduction in strength, with the sample in 50% acid suffering complete destruction.

Potassium silicate concretes

A quartz aggregate concrete was formulated in the laboratory using potassium silicate liquid and sodium fluosilicate setting agent. Crushing strength after 24 hours was typically 25 MPa, increasing to 30 MPa after 1 day of air-drying. The product was stable in a static water immersion test after the air-drying.

This product was licensed for manufacture in South Africa and good results were obtained with a wide range of acids, including sulphuric. However, one consideration quickly became apparent as regards the finishing off of such linings when cast as floors rather than cast behind

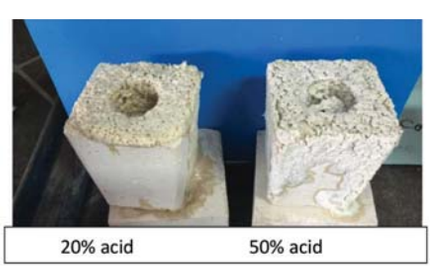

Figure 2—Acid testing of white Portland concrete

Table

Immersion testing of refractory concrete (30 days' exposure)

Medium	Change in crushing strength relative to sample in air
Water 20% acid 50% acid	-37% -37% Expansile destruction

shuttering. Potassium silicate concretes tend to form a skin on exposure to wind or direct sunlight, and finishing of an installation must be completed before this occurs. The walls of the structure shown in Figure 4 were cast behind shuttering, but the surface tears in the floor had to be patched with a mortar version of the castable.

As a result of its success in South Africa the product technology was licensed to the UK. Some clients requested independent testing of the resistance to acid attack, and the results of one such test are shown in Table III. The test samples were immersed in 50% sulphuric acid 18 hours after casting.

Over 150 t of the concrete was supplied for use in sulphur pits at ADGAS in the UAE, Exxon plants in Baytown and Singapore, and the Shell plant at Stanlow UK. Applications in plants at which contact with sulphuric acid can occur are listed in Table IV.

The problem in South Africa

While no problem was ever reported in any of the sulphuric acid applications in the UK, a very specific problem was encountered on one site in South Africa. An example of the effect is shown in Figure 5.

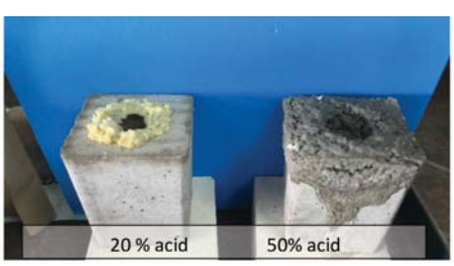

Figure 3—Acid testing of refractory concrete

Figure 4—Surface tearing of a potassium silicate concrete floor

Table

UK acid immersion test results in 50% sulphuric acid

Sample size	Age (d)	Cold crushing stength (MPa)
100×100×100 mm 100×100×100 mm	28 56	36.0 38.0

Soil Mechanics Civils (UK) tested to BS EN 12390-2000 Data supplied by R. Bowmer, Durosil Products UK

Table

Applications in the UK chemical industry

Lambson Chemicals	Bridgewater
Zenecca DTBA	Seal Sands
Rhodia	Chesterfield
Huntsman Tioxide	Grimsby
UCB Films	Wigan
United Utilitie	Rochdale
Albion Chemicals	Sandbach
Great Lakes Chemicals	Amiwch
Surface Specialities	Wigton
Incos Chlor	Runcorn
Yuasa Batteries	–
Tungstone Batteries	–

Figure 5—Surface scaling of acid-resistant concrete in wet/dry sulphuric acid conditions

According to some very old commercial literature (J. Crosfield & Sons, 1965) this surface scaling is associated with the expansile crystallization of sodium sulphate on a dry surface. In the UK there is a standard whereby the acid surface is kept constantly wet. However, no mention of this effect could be found in any documents published in the last 15 years. Consequently, some additional experimental work was undertaken.

Additional experimental work

The standard acid concrete was cast as 76×76×76 mm cubes and crucibles for testing with 20% and 50% sulphuric acid. A reference cube was used for a comparison of the 30-day strength in air. The cubes were air-dried for 3 days and then totally immersed in the liquids for 30 days. The crucibles were filled with liquid and topped up as required. The results of these tests (Table V) show some reduction in strength compared to the water-immersed and air-dried reference sample. This contrasts with the results of the UK laboratory tests, in which the cubes were not allowed to air-dry but were stripped from the moulds and placed directly into the acid.

The crucible tests, designed to simulate a wet to dry environment, showed surface scaling of the sample with 20% acid, but no scaling with 50% acid (Figure 6).

Table

Immersion testing of standard acid concrete (30 days' exposure)

Medium	Change in crushing strength relative to air value
Water	Nil
20% sulphuric acid	-15%
50% sulphuric acid	-5%

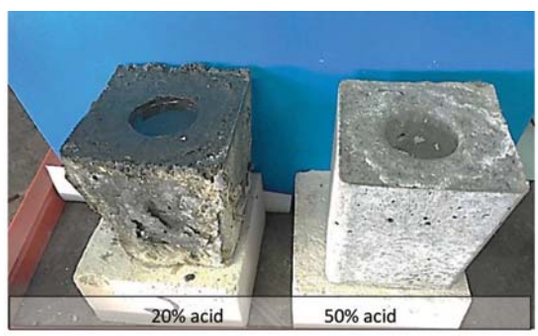

Figure 6—Surface scaling of acid concrete with 20% acid

Table VI

Immersion testing of modified concrete

S-Grade concrete exposed for 30 days	Change in crushing strength relative to air sample
Water	Nil
20% acid	-5%
50% acid	Nil

Formulation of S-Grade

Mixes were prepared in the laboratory with a reduced level of fluosilicate plus additives which might modify the chemistry and prevent the surface scaling.

One additive was found to be very successful and the results of crucible and cube tests are shown in Figure 7 and Table VI.

There have been many applications of the S-Grade silicate concrete in sulphuric acid conditions in South Africa. Some of these are shown in Table VII

Installation advantages

The following information was gathered from on-site observations during installations. This is to give an indication of the benefits of using a castable rather than any other acid-proofing methods.

(a) High slump concrete that can be mixed and installed with civil concrete equipment and methods
(b) Low permeability with no apparent cracking or shrinkage, therefore there is no need to install a membrane
(c) Casting in panels entails fewer joints, which results in no penetration at joints due to crystallization of chemicals in joints

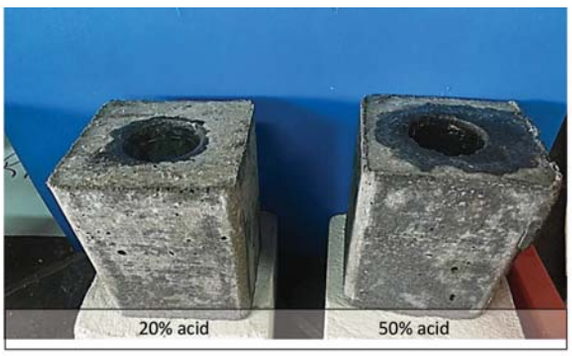

Figure 7—S-Grade concrete with no surface scaling

Table

Some larger applications of the modified concrete in sulphuric acid conditions

Date	Location	Application
2012	Secunda	Loading bay road
2012	Natal	Sugar mills
2012	Phalaborwa	Fertilzer plant
2013	Phalaborwa	Fertilizer plant
2014	Sasolburg	Sulphur pit
2014	Nelspruit	Loading bay road
2014	Nelspruit	Bund floor
2014	Nelspruit	Bund wall
2015	Gauteng	Bund area
2015	Phalaborwa	Loading bay road
2015	Nelspruit	Bund area
2015	Nelspruit	Acid pit
2015	Gauteng	Bund area
2015	Mpumalanga	Bund area & road
2015	Secunda	Bund area
2016	Gauteng	Bund area
2016	Secunda	Bund area
2016	Phalaborwa	Fertilizer plant
2016	Nelspruit	Channel
2016	North west	Bund area

Burger, P. Burg Refractories South Africa

(d) Set equipment on castable structure and overlays in 24 hours (at 21°C)
(e) Stable in the presence of water
(f) No need to wait 28 days for concrete to dry out to 10% moisture, as it can be laid on green concrete
(g) Can be laid over dried acid-attacked concrete after removal of loose materials and acid residue
(h) No cutting around plinth ensures better sealing
(i) Precast shapes for weir wall, guide blocks, gulleys, troughs *etc.* can be cast in days
(j) Excellent adhesion to civil concrete, earthworks, and acid-resistant brick
(k) Quick installation time compared with cutting, shaping, or more traditional methods.

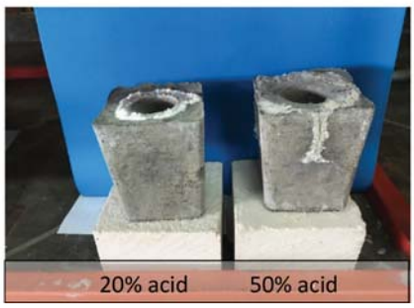

Figure 8—Crucible tests with powder potassium silicate

Table

Immersion testing of concrete (30 days' exposure)

Medium	Change in crushing strength relative to air sample
Water	Nil
20% acid	35%
50% acid	Destroyed by expansile cracking

New setting agent 2016

An ideal potassium silicate concrete for site work would involve just the addition of water to a dry bagged material containing a soluble potassium silicate powder and setting agent.

In 2016 a locally manufactured material was identified as a possible setting agent for use with dry powder potassium silicate. The results of initial strength and acid resistance tests looked very promising. The reaction mechanism was based on soluble boric acid in the setting agent reacting with the soluble potassium silicate in water. Unfortunately, tests with sulphuric acid showed both cracking and a significant strength reduction (Figure 8 and Table VIII).

Conclusions

The original formulation of the acid-resistant concrete continues to be used in the UK and no problems of surface scaling have been reported by the technology licensor. The manufacture of this product was discontinued in South Africa following the scaling problem on one site, and it was replaced by the S-Grade version in 2009. No problems with scaling have been reported from any site.

The ideal concrete for site use would be a totally dry mix utilizing a powdered potassium silicate and no requirement for an acid pre-wash. Laboratory work is continuing to find a setting agent that will function in sulphuric acid conditions.

References

Corrosionengineering.com. 2006. The amazing acid resistance of potassium silicate concrete http://www.corrosion-engineering.com/newsletterarticleshtml/TheAmazingAcidResistanceofPotassiumSilicateConcrete.html

J. Crosfield & Sons UK. 1965. Silicate brochure. Reviewed and reprinted May, 1965. ◆

http://dx.doi.org/10.17159/2411-9717/2017/v117n11a6

An example of the use of advanced fibre-reinforced plastics in sulphuric acid plants

by P.M. Fouché

Synopsis

Anglo American Platinum treats the off-gas from its primary and converter furnaces at Waterval Smelter Complex in two sulphuric acid plants. In this paper the processes and the background to the decision to use fibre-reinforced plastics (FRPs) as a major construction material are briefly discussed. The applicable design codes and design optimization that was required to reach and exceed the life expectancy of the plant are addressed. The discussion is then broadened to design concepts used in the plant, FRP maintenance quality requirements, and the inspection and testing programme. This programme was introduced to establish the condition and monitor the degradation of FRP equipment compared to original code requirements, the resin supplier's recommendations, and good FRP engineering practice. Some guidance is given on the availability and use of FRP testing laboratories and how the lessons learned can be incorporated into procurement technical specifications. This paper seeks to improve the understanding of FRP maintenance within the sulphuric acid community, thereby reducing costly failures and the associated downtime.

Keywords

sulphuric acid plant, fibre-reinforced plastic(FRP), design code, condition monitoring, maintenance.

Introduction

The acid plants at Anglo Converter Plant (ACP) treat two streams of off-gas. One stream is from the top submerged-lance furnace and contains 8–13% SO_2; this gas is treated in a dry double-contact double absorption (DCDA) plant.

The other stream is from two six-in-line electric furnaces that produce relatively low concentrations of SO_2 – 0.3 to 2%. This strength is too low for treatment in a DCDA plant as it will not remain autothermal and would require significant amounts of heat input to achieve the desired results. The process used for this stream is the Petersen-Fattinger process (the only one of its kind in the world), based on the lead chamber process (Davenport *et al.*, 2006). It is capable of producing only 75% H_2SO_4, which is then used to dilute the acid in the absorption towers of the DCDA plant. The process uses NOx as a catalyst. Thus not only is the H_2SO_4 in the process dilute, it is hot from the conversion and contains up to 5 ppm nitrosyl in the form of nitrosyl sulphuric acid. This represents a very corrosive environment that only specialized materials can withstand.

The plant has been in use since 2002. Over the period of operation of the plant it was realized that more detail was required on the maintenance of the fibre-reinforced plastics (FRPs) used in the plant if the design life was to be exceeded. A condition assessment and reliability programme was therefore launched, that would enable maintenance planning and thus longer operating periods between maintenance stops, lower maintenance costs, and extended plant life.

Materials and methods

Fibre-reinforced plastic as a major construction material

Due diligence required that various materials needed to be considered for the vessels, ducting, and associated piping in the weak acid sections (<96% H_2SO_4), where common steel grades would not be able to resist corrosion.

Three options were available: brick-lined mild steel, FRP, and highly alloyed stainless steel. The concern of brick flakes clogging the plate heat exchangers, as well as the additional weight and the difficulty and cost of repairs, quickly ruled out bricks as an option.

Table I illustrates the two remaining options scored on a scale of 0 to 5 with regard to various attributes.

The table illustrates clearly that FRP was the preferred material of construction

FRP was selected due to:

- A wider tolerance to process excursions
- Easier repairs

* *Anglo American Platinum, South Africa.*

 ISSN 2225-6253. This paper was first presented at the 6th Sulphuric Acid 2017 Conference', *9–12 May 2017, Southern Sun Cape Sun, Cape Town.*

Table I

Materials trade-off study

Risk	FRP	Special alloyed steel	Comments
Corrosion	****	***	Available data indicate that FRP can handle higher temperatures at the specified concentrations. No history for nitrosyl sulphuric acid on either material
Erosion	****	***	The passive layer formed on alloyed steels can be eroded by high-velocity acid. FRP erosion conditions can be minimized through careful design
Quality	***	****	Quality systems for both materials are well established, but FRP requires a significant manufacturing QC programme since nondestructive testing is limited
Fabrication	*****	***	FRP can be more easily fabricated then these steels due to the strict welding code requirements; welds are also susceptible to contamination
Maintenance	****	**	FRP materials are freely available and repairs are more easily carried out than for steel. No hot work is required and repairs can be done *in situ*. The alloys have long delivery times
History of use	****	*	Extensive use of FRP in Anglo Platinum's refineries, but very limited history with these alloys
Safety	****	***	Welding and grinding associated with metalwork can be a fire hazard. Risk of hydrogen explosion if steel is corroded. The styrene in resins is a fire risk
Process excursions	****	***	Steel's passive layer can be undercut and removed quickly during excursions
Availability	****	**	Resin of the type required in this application is not manufactured locally but is shipped in regularly and in large enough quantities not to be a concern. Steel availability was in question at the time and long lead times were expected
Failure indication	***	*	If acid penetrates the FRP structure, tell-tale signs will appear before catastrophic failure. Thus FRP is more forgiving than steel
Cost	***	**	Resins are sensitive to oil price, but much less expensive than the high-Si and -Ni steels.

- Better availability
- Better history of use, along with advances in vinyl ester resins
- The excessive cost and weldability issues associated with the metals in question.

Fibre-reinforced plastics – manufacturing background

FRPs or polymers are composites consisting of a resin matrix containing reinforcing fibres such as glass or carbon that have greater strength or stiffness then the resin. FRP is used as a material of construction in many industries, from concrete reinforcement to aerospace. The term 'advanced composites' is often used to describe FRPs with carbon or high-performance aramid fibres. Hand lay-up, filament winding and pultrusion are discussed due to their extended use in industrial component manufacture.

Resin

Resins are liquid polymers that when catalysed cure to a solid state. Resins selected for ACP acid plant are epoxy vinyl ester resins, either bisphenolic or novalac on the basis of the resin manufacturer's recommendations and local Refinery experience. Resins have a shelf life, once activated, of six months generally and once catalysed should cure within 30 minutes to provide adequate application time and prevent burning of the resin due to the exothermic reaction of curing. Styrene (Figure 1) is added to resins to increase wettability and reduce viscosity. (Palmese, La Scala, and Sands, 2013)

Reinforcements

ACP acid plant uses E-CR glass manufactured by Owens Corning. The chemical resistance offered by ECR glass, with the proven track record of Owens Corning, has proven to be a winning combination. In some cases when process conditions have dissolved the resin, the glass remained (Figure 2).

Hand Lay-up

Hand lay-up is one of the manufacturing methods used for FRP. Sections of chopped strand mat are cut, wetted with resin, and applied to moulds or other prepared surfaces. This method is used almost exclusively for site joints and patch

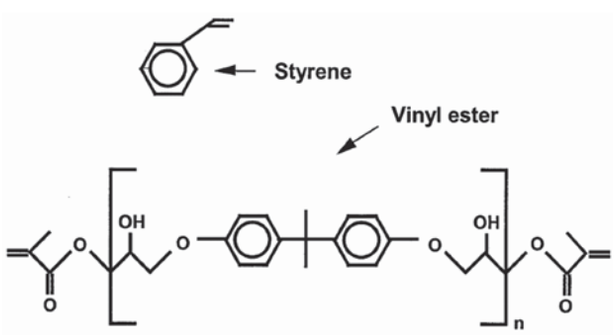

Figure 1—Styrene and vinyl ester structures

Figure 2—C glass tissue remaining after resin is dissolved

repairs. As the name suggests, hand lay-up is a manual task that is very labour-intensive. ACP acid plant vessels were manufactured by hand lay-up. Filament winding was not available at the time.

Filament Winding

Woven filaments, in the form of unidirectional roving or woven roving, are wound around a mould or mandrel while being wetted by resin in a continuous process to produce pipes, ductings, and vessels (Figure 3). This method has an improved glass-to-resin ratio compared to hand lay-up and thus stronger, thinner vessels can be manufactured. Additional capital expenditure is required from the manufacturer for the equipment (Mouton, 2007)

Pultrusion

Structural forms like I-beams, channels, rods, bars, and tubing are moulded through an open-ended moulding process whereby fibres are wetted with resin and pulled through a heated die, thus curing the component (Figure 4). Various resin-to-fibre ratios can be obtained. (Mouton, 2007). This process is used to manufacture packing support beams for process vessels and has a significant advantage over lined steel.

Composite Construction

Design codes specify three discrete sections to a wall. Firstly, the internal corrosion barrier; this is the section that will be exposed to the process and is generally 3 mm thick. If a component was correctly designed, manufactured, and operated this will be the only element that may require maintenance. The structure is the section of the wall that provides strength. If this is attacked by the process, structural integrity is in question. Lastly there is an external corrosion barrier. This section is very thin and includes an ultraviolet filter to protect the resin in the structure from damage.

Leaks and splashes can expose the outside surface to process conditions and this should be considered in the design of the external chemical barrier.

The FRP in chemical barriers can be substituted with fluoropolymers for process conditions that exceed current resin capabilities.

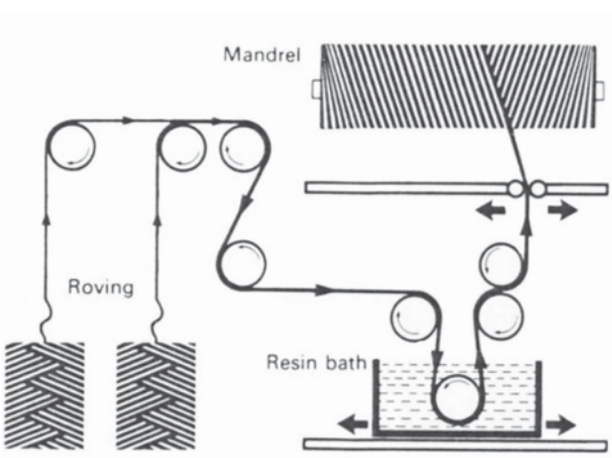

Figure 3—Filament winding (Mouton, 2007)

New vessel requirements

Nondestructive testing of FRPs is still very limited, thus there should be extensive controls in place during manufacturing to ensure the quality of the end product. A component's condition monitoring programme starts during manufacturing, and if some items are missed it can impair the effectiveness of the programme significantly.

FRP components require internal inspection to determine whether there is deterioration of the corrosion barrier. This opportunity is available only during plant stoppages, and in most cases only certain sections of the internals can be inspected. Records of these inspections should be kept and evaluated to understand degradation over time and thus ascertain the expected equipment life, as well as to locate hot spots requiring more attention than other areas or components. For this exercise, component manufacturing data is required, including the manufacturing code, resins used, fibre lay-up, thickness, process conditions, and previous repairs conducted.

Design Codes

FRP components are generally manufactured to BS4994:1987 for vessels, and BS7159 for piping. The vessel code is dated, and as such a new code, EN 13121, was implemented. However, the BS code is still preferred by manufacturers. Care should be taken when modifications to vessels are considered as Category 1 vessels will require approval by an Approved Inspection Authority (AIA). AIAs for nonmetallic materials are not very common and thus modification costs are substantially increased.

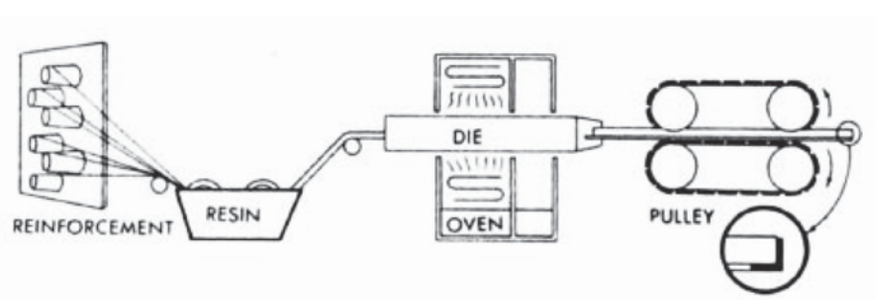

Figure 4—Representation of continuous pultrusion (Mouton, 2007)

Cut-outs

A key consideration in evaluating the fabrication of the component and for future evaluations of component condition is keeping and cataloguing cut-outs from the component when nozzles and manways are fitted. These are preferred to representative panels since they are more representative of the laminate. These can be sent for laboratory analysis, as explained later.

Sample Plates

Sample plates are good substitutes if cut-outs are unavailable. Sample or representative plates can be requested to be manufactured by the same laminator, with the same resin, glass, and lay-up, at the same time as the component, to be analysed at a later date. For accurate life expectancy estimation it is indispensable that either cut-outs or representative panels are stored in a safe place for future use.

Quality Dossier

Since the FRP fabricator is responsible for the entire fabrication process of the component, this document is of great import and should contain at least the following:

1. Scope
2. A quality assurance plan
3. An organogram for the project
4. Drawings (general arrangements showing joint location and site joints, manufacturing drawings showing lay-up and joint details) signed off by AIA if required
5. Quality control plan
6. Laminating schedules
7. Materials and blending certificates
8. Laminator qualifications
9. Gel time tests (daily), including gel time tester calibration certificate
10. Material safety data sheets for all chemicals
11. Daily temperature and humidity tests
12. Sample schedules
13. Applicable specifications (including site flange, fastener, and gasket specifications)
14. Acceptance criteria (defects and tests)
15. Defect reports
16. Additional requirements if fluoropolymer linings are involved:
    a. Material certificates (of the original pellet stock and from the sheet manufacturer)
    b. Welding procedure
    c. Welder qualification
    d. Spark test result (insist on a graphite lining behind welds to allow this)
17. Certificate of compliance to the pressure equipment regulations and SANS 347 if applicable
18. Inspection release from manufacturing site
19. Takeover certificate from transporting company
20. Takeover certificate from end user (upon delivery to site)
21. Final acceptance certificate (after installation, depending on scope)
22. Design calculations (remember lifting points)
23. If modifications are made to site components, GA drawings of the equipment involved to update site libraries.

Quality assurance plan for equipment in service

Obtaining information on an old plant is sometimes impossible. Vessels might have been manufactured by a company that no longer exists, and libraries on site are not always updated with all repairs conducted. In such a case, history must be interpreted from available data.

Plant inspections

A new starting point needs to be defined. The current plant condition needs to be assessed. This process begins with plant inspections. The general condition of the vessel can be assessed fairly accurately through manway inspections. If any areas of concern are noted, internal inspections may have to be carried out.

To ensure that plant inspections add as much value as possible a good template, should be used. This will ensure that no details are missed.

A very handy tool for inspections is a Barcol hardness tester (Figure 5). By using this tester in and around the manway, the extent of the process attack on the chemical barrier of the FRP vessel can be very easily determined. A Barcol hardness tester is used to determine the cure of a laminate. Values in the 40-60 range are acceptable for new components, and the test will also reveal softening of the laminate due to process attack. Test results above 30 are acceptable in principle, although the true value of these tests will be revealed only when consecutive test values can be trended to show a long-term graph. Statistical process control can then be used to identify significant deviations that would warrant action.

Plant inspection is also the best way to select samples, as areas of concern can be noted

Figure 5—Barcol test on a new duct

Sample selection

The next step in building a history for an item constructed of FRP is to select a representative sample for destructive testing. The sample should represent the area of most severe attack, hence the area most likely to fail first, and therefore enable an estimation of the expected remaining life.

That is difficult to do, as cut-outs of the structure of the vessel are required. Since the condition of the structure is not known at this stage, this is not recommended. A better strategy is to use the manway cover as a vessel sample. First, the age of the manway cover relative to the vessel should be confirmed. As this is not likely to be the area of worst attack it will not be the last sample to be tested, but will provide a good starting point.

Laboratory tests

A standard manway cover 600 mm in diameter yields enough samples to provide statistically relevant results for the required destructive tests. These tests are:

- Ignition loss
- Tensile strength
- Lap sheer
- Flexural strength
- Differential scanning calorimetry
- Dynamic mechanical analysis.

Further Barcol hardness tests are also conducted to enable comparison with plant tests. Correct sample labelling on site is essential to avoid confusion at the laboratory.

Ignition loss tests

These tests are carried out by weighing a sample, heating it in a furnace to remove all resin, and then reweighing the sample. The weight of the residual glass is then recorded as a percentage of the total initial weight. Design codes give guidance as to the expected glass weight percentages required, depending on the type of glass reinforcement used.

Tensile strength test

This test is undertaken on a reinforcement sample machined to the code dimensions (length and thickness), suitably conditioned, by applying a direct vertical load at a defined speed, at ambient temperature, and monitoring the extension and load value until the sample fails.

The tensile strength of the specimen is the load at which the load extension curve becomes nonlinear, whilst the ultimate tensile strength (UTS) is the load at which the specimen fails. For reinforcement laminates the UTS is expressed as ultimate tensile unit strength (UTUS), which is the strength (force) per unit width, per unit mass of reinforcement.

The code gives minimum recommended values to be used in the design.

Lap shear strength

Shear strength is the maximum load (stress) needed to produce a separation fracture by a shearing action between the layers of the reinforcements (glass), and is a good indication of interlayer bonding characteristics. The code gives minimum values for good bonding.

Flexural strength

Flexural strength of a laminate is a measure of its ability to withstand forces that cause bending.

Tests are normally carried out on both sides of the test sample to include the corrosion barrier. Design code strain limiting factors of 0.2% are applied.

Barcol hardness tests

Hardness is a common mechanical property that is measured for FRP materials. Hardness is the resistance of a material to penetration of its surface. The greater the resistance to penetration, the harder the material. Such penetration of material is simply due to movement of the molecules in the FRP polymer, which is resisted by intermolecular forces called crosslinks. The resistance is closely related to the strength of the material

Differential scanning calorimetry (DSC)

Differential scanning calorimetry measures the effects associated with phase transitions and chemical reactions that relates to the degree (Mouton, 2007) of cure of a laminate (Figure 6). These effects are noted as a transitional temperature (T_g) when such phase transitions occur (Bruce *et al.*, 2002). The closer the actual T_g value to the recommended value, the better the corrosion resistance of the resin. The values are nominally close to the heat distortion temperature value given by the resin suppliers for pure cast resin.

Recommended values for the maximum service temperature based on the T_g value are given for the specific chemical environment. Post-cure of a resin helps to ensure that the optimum T_g is obtained.

Dynamic mechanical analysis (DMA)

DMA is a more modern technique that is not published in the public domain by resin suppliers but is being increasingly used in conjunction with DSC testing. It is a technique used to study and characterize materials, in particular the viscoelastic behaviour of polymers. Simply put, it is a measurement of the 'stiffness' of a resin. The lower the relative value of stiffness, the more the likelihood that the resin polymer will have a lower corrosion resistance and hence an increased propensity for a reduced life-cycle. The DMA value is obtained by applying a sinusoidal stress either on a three-point basis or on a double-cantilever load basis, and the strain in the material is measured. In the three-point test the specimen is supported on its ends and a sinusoidal load is applied in the centre. In a double-cantilever test the specimen is fixed at one end and a load is applied at the end of the specimen. (Technical Risk Management Services, 2016).

Once these tests are completed the following information is available for the sample:

- Actual laminate makeup compared to prescribed makeup
- Remaining structural strength compared to original strength
- Chemical attack depth.

This information enables the remaining service life of the vessel to be estimated.

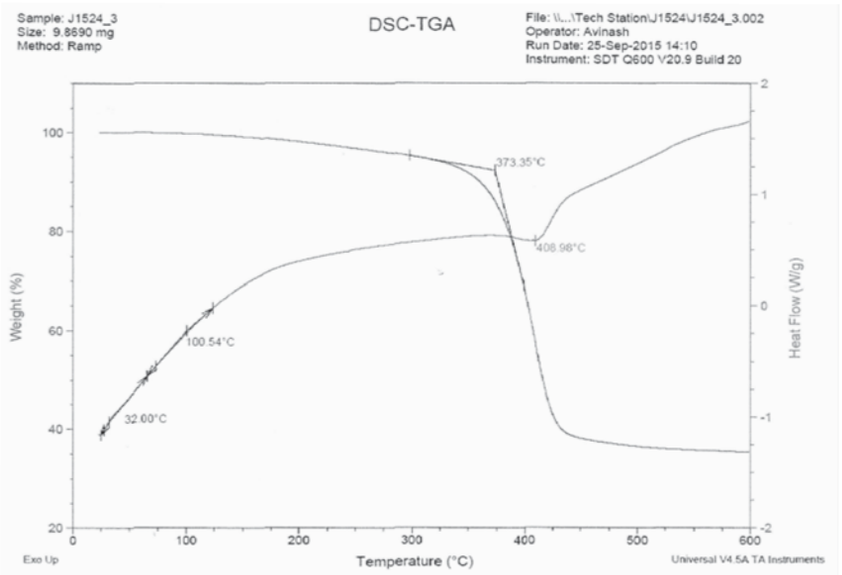

Figure 6—Example of a typical DSC graph

Support activities for continued maintenance excellence

Quality assurance and quality control

If site maintenance work is to be trusted to result in safe operation, systems have to be in place to ensure the work is done to specification.

Before any maintenance work is conducted on process equipment, site maintenance procedures are required. These form part of quality assurance, and should include;

- Daily temperature and humidity recording
- Daily gel time tests (Figure 7).

These results are used to ensure that catalyst addition is correct, to enable full cure and prevent resin burn on site work and thus reduce unnecessary downtime.

Records of the above should be kept for monthly inspection. A gel time testing procedure should be available, including the use of a calibrated stirrer.

Resin drums should clearly indicate the resin type, promotion date, and expiry date. This will ensure that the correct resin is used for the application and that it will reach full cure.

Generic laminating schedules should be available for different joints. Joint kits should be made up for different size joints containing the correct glass lay-ups. Nozzles, stubs, flanges, pipes, and bends of the required sizes should be available in stock. This ensures quick response times when failures affect plant operation while ensuring good quality of work. Laminators should laminate a test plate to be analysed for compliance to the principle code.

Site maintenance monitoring

Plants are ever-changing; opportunities for sampling must not be missed. Flange failures due to incorrect torqueing practices require stub replacements; the removed stub should be inspected to determine if analysis is required. Pump modifications require piping re-alignment; the piping should be inspected to determine if sampling should take place.

A large GA of the plant should be available with indications of repairs undertaken. This should link to repair files on record. Over time, hot-spots can be identified and failure analysis instituted.

Supplier qualification

FRPs can be as technical or simple as you make it. Just as there are many people capable of welding two pieces of angle iron together, there are many capable of laminating one piece of fibre on top of another. These people are referred to as the 'bucket-and-brush brigade' – they are not the people you

Figure 7—Gel time test

want repairing high-pressure or hazardous chemical piping. Yet they will have a cost advantage compared to a company capable of producing the quality assurance noted earlier in this document.

To ensure that underqualified companies are not contracted for site work, the FRP or nonmetallic service scope should be clearly defined by the responsible engineer. The scope should include a supplier qualification requirement. Companies should be scrutinized against a list of requirements and scored in terms of competence. Companies scoring lower may be used for low-risk work but should not be used for the design and fabrication of a new process vessel, for example.

A simple matrix is used for such a rating. A company is ranked on a 3×3 matrix regarding technical capability and management effectiveness, as shown in Table II.

A company capable of doing engineering design and manufacturing of large vessels would score in the first or second column, depending on the exact resources available

If such a company has ISO9001 certification and is capable of producing all the documentation listed above, it can score in the first or second rows, depending on a detailed document review. Such a company can potentially be trusted with large project work and site maintenance of process equipment.

This evaluation should, however, be undertaken by a subject matter expert against a set requirements document to avoid allegations of impropriety.

Discussion and recommendations

The system used at Anglo Converting Process acid plant requires supervision. It has enabled the identification and prevention of potential failures that would have resulted in extended downtime. It also provides a solid base for the condition monitoring principles that were implemented.

From the above process, some general recommendations can be made for acid plants:

- Ensure inspections are done using a template, with subject matter experts present if the inspector is not an expert
- Use good illumination, high-powered torches are recommended.
- Buy a Barcol hardness tester and check the calibration before inspection (test discs are provided)
- Ensure that gel time tests are done daily and recorded
- Specify post-cure as part of component manufacturing. This will ensure full curing of purchased components. It will also accentuate defects, and thus it is not favoured by manufacturers, but it ensures that only the best components are delivered to the site. Bruce *et al.* (2002) state that the degree of cure in vinyl esters depends on the cure temperature. A post-cure cycle at 80°C will increase the cure percentage and thus improve the resistance of the component to chemical attack.

Resin manufacturers recommend a useful life of 10 years for FRP components. ACP acid plant has been in operation for 15 years, and with the use of the quality assurance plan detailed in this article a further ten years is expected. This significantly influences the return on capital calculations made in feasibility studies. Through continued innovation some new techniques are available that can assist the plant engineer. Pultrusion is one such technology. ACP acid plant has been using pultruded packing support beams successfully. Resin technology is continually evolving, so testing opportunities should always be considered. Components can be pigmented for colour coding or aesthetic purposes, but this is not good practice as it makes visual inspection ineffective. If colour coding is required, thin strips can be pigmented or at the very least a strip of the component should be left unpigmented. termed the 'Bradbury strip' after the consultant that recommended it. Pigmenting should not be wholly discarded, however; a duel chemical barrier with a pigmented layer in-between allows for easy assessment of the remaining thickness of the barrier. Another innovation in condition monitoring is the inclusion of graphite powder in a resin layer between the chemical barrier and structure. Monitoring the electrical resistance between the process and this layer enables immediate detection of chemical barrier failure. If the selected laminate has adequate history in the design conditions there is a possibility of cost saving by installing dual laminates. Since chemical attack should be limited to the chemical barrier (CB) the structural laminate can be made with a less resistant resin, as long as the external CB is also made from the same resin as the internal CB in case of process leaks and splashes.

Table II

Quality rating system

	Technical resources and capabilities		
Management effectiveness	A1 B1 C1	A2 B2 C2	A3 B3 C3

Acknowledgements

Anglo American Platinum Ltd. for permission to publish. I also gratefully acknowledge contributions of Sam Venter, Phil Bradbury, Fibre-Wound and Prof Mark Walker

References

Bruce, K.F., Travis, A.B., Molly, A.S., and John, W. G.J. 2002. Thermochemical response of vinyl-ester resin ARL-TR-2653. US Army Research. Laboratory, http://www.arl.army.mil/arlreports/2002/ARL-TR-2653.pdf

Davenport, W., King, M., Rogers, B., and Weissenberge, A 2006. Sulphuric acid manufacture. *Proceedings of Southern African Pyrometallurgy 2006*, Cradle of Humankind, South Africa, 5–8 March. p. 116. http://www.saimm.co.za/Conferences/Pyro2006/001_Davenport.pdf

Mouton, J. 2007. Increasing the use of fibre-reinforced composites in the Sasol group of companies: a case study. DTech thesis, Durban University of Technology, South Africa. http:// http://ir.dut.ac.za:8080/jspui/handle/10321/144

Palmese, G., La Scala, J.J., and Sands, J.M. 2013. Multimodal vinyl ester resins. European Patent EP20050804814.

Technical Risk Management Services. 2016. Plant engineering condition assessment NOX absorber #1 535 - CM - 350 J1521/001. ◆

SAIMM: Diamonds — Source to Use 2018 Conference

'Thriving in Changing Times'

11 June 2018 — Workshop: SAMREC/SAMVAL Reporting – Diamond Projects
12–13 June 2018 — Conference • 14 June 2018 — Technical Visits
Birchwood Conference Centre (Jet Park, Johannesburg)

BACKGROUND

Being the seventh conference in the series, the ***Diamonds – Source to Use*** conferences target the full spectrum of the diamond pipeline from exploration through to sales and marketing. The last conference in this series (***Diamonds – Still Sparkling***) was held in Botswana in 2016 and it is now returning to Johannesburg, where it was last held in 2013

Keynote Speakers

The State of the Diamond Market
E. Blom, *Blom Diamonds (Pty) Ltd*

Financing Diamond Projects
J. Campbell, *Botswana Diamonds PLC*

OBJECTIVE

The objective of the conference is to provide a forum for the dissemination of information relating to the latest tools and techniques applicable to all stages of the diamond industry; from exploration, through mine design, processing, to cutting, marketing and sales.

WHO SHOULD ATTEND

- Geologists
- Mineral (Diamond) Resource Managers
- Mining Engineers
- Process Engineers
- Consultants
- Suppliers
- Sales/marketing
- Diamantaires
- Mine Managers
- Mining Companies
- Students.

TOPICS

- Geology and exploration
- Mine expansion projects
- Mining, metallurgy and processing technology
- Rough diamond sales and marketing
- Cutting, polishing and retail
- Financial services and industry analysis
- Industry governance, beneficiation and legislation
- Mine-specific case-studies
- Value optimization.

Sponsors:

Imexsar DMS Ferrosilicon

SAIMM
THE SOUTHERN AFRICAN INSTITUTE OF MINING AND METALLURGY

For further information contact:
Camielah Jardine • Head of Conferencing · SAIMM
P O Box 61127 • Marshalltown 2107
Tel: (011) 834-1273/7
Fax: (011) 833-8156 or (011) 838-5923
E-mail: camielah@saimm.co.za • Website: http://www.saimm.co.za

Conference Announcement

http://dx.doi.org/10.17159/2411-9717/2017/v117n11a7

Sulphuric acid plant optimization and troubleshooting

by J. Hanekom

Synopsis

In an ideal world in which sulphuric acid plant operators could have anything they wish for, many would request an acid plant that never experiences corrosion, never has gas leaks, and never needs catalyst screening. And yet that is not the reality. All sulphuric acid plant operators experience acid mist carryover from sulphuric acid towers at some stage. If this is not detected and corrected quickly, extensive damage can be caused to downstream equipment. Not all mist carryover issues are related to poorly performing mist eliminators. This paper presents a review of the entire tower as a unit and discusses how process conditions, packing, acid distribution, mechanical factors, or mist eliminators affect the performance of the tower, as well as early detection and troubleshooting tools and methods.

Keywords
acid mist carryover, process conditions, packing, acid distribution, mechanical factors, mist eliminators.

Introduction

Unfortunately, there is no 'silver bullet' to optimize overall performance of a sulphuric acid plant. Plant equipment and operation must be viewed holistically to effectively integrate improvements to sustain efficient operation and profitability. This paper illustrates how tower and plant performance can be improved by an integrated approach that addresses both tower gas/acid distribution and mist elimination.

Tower design – acid distribution and packing

Proper dry tower design, maintenance, and operation impact overall plant performance and economics. Running the dry tower outside design conditions can lead to mist carryover into the blower and excessive acid carryover in the plant, resulting in corrosion, crusting of catalyst beds, and excessive acid in areas where it should not be present.

When designing a tower, it is therefore important to consider the following aspects of tower design:

- Acid distribution
  - Uniform and accurate acid distribution
  - Limiting mist generation
  - Wetting the walls
- Gas distribution
  - Gas velocity
  - Optimum inlet gas nozzle and packing support design
- Liquid/gas contact
  - Packing performance
  - Gas and acid conditions
- The greater the open area in the tower, the less the pressure drop

An improvement of the drying tower (DT) acid distribution will reduce sub-micrometre acid mist formation. Figure 1 shows the effect of water vapour slipping past the DT as measured by the exit dry tower water dew point. This water vapour eventually combines with SO_3 in the process gas, resulting in sulphuric acid vapour entering the inter-pass absorption tower (IPAT). Normal dew point temperature is less than -40°C; however, well-performing dry towers have much lower dew points. This can be a low as -50 to -60°C. The higher the dry tower dew point, the higher the inlet acid vapour content entering the IPAT and the higher the potential for acid mist formation once the gas enters the IPAT and cools below the sulphuric acid dew point.

The amount of sub-micrometre acid mist formed in the IPAT *versus* the amount of acid vapour condensing on wetted packing surfaces depends on the amount of acid vapour entering the IPAT, the concentration of nucleating agents in the gas (*e.g.* very fine dust particles from air or from ash resulting from sulphur burning) and fine particles from upstream metallurgical process, along with how the IPAT is designed and operated.

* *Sulphur EMEA, MECS, South Africa.*
 ISSN 2225-6253. This paper was first presented at the 6th Sulphuric Acid 2017 Conference', *9–12 May 2017, Southern Sun Cape Sun, Cape Town.*

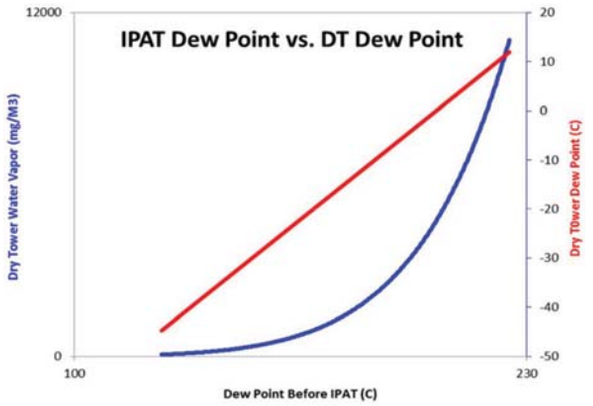

Figure 1—Effect of water vapour slipping past the dry tower

Improved mist elimination in the DT also helps reduce the acid vapour level at the inlet to the IPAT, since any acid mist reaching the downstream sulphur burner will decompose to H_2O and SO_3 and ultimately result in more acid vapour at the inlet to the IPAT.

On metallurgical acid plants the DT are often blamed for poorly performing upstream wet electrostatic precipitators (WESPs) often found in these plants. Sub-micrometre mist from WESP will pass through the drying tower and accumulate in the blower. The WESP sight glasses should always be optically clear.

Tower design

When designing an acid tower, it is imperative to keep the following in mind:

1. Good absorption of SO_3 (absorbing towers) or H_2O (drying tower)
   = Uniform distribution
2. Low mist generation (saturation or overloading of mist eliminators)
   = No droplet carryover
3. Safe and reliable operation / maintenance
   = Easy access, no sulphate build-up, no plugging
4. Acid quality => low Fe content
   = Steel with low corrosion rates (Figure 2a).

Uniform acid distribution is achieved by even irrigation of the packing both in the centre and near the walls, and of an equal flow per pour point (Figure 2b).

Droplet carryover can be avoided if the acid is discharged slowly, just under the packing without decreasing the tower open cross-section.

Flat packing support grids, such as the ZeCor® packing support grids, ensure equal packing thickness and equal gas distribution, and require no maintenance. The open area is more than 80% and the packing (random Intalox saddles) is installed directly on top of the grid. No grid blocks or cross-partition rings are required. ZeCor® packing support grids are easy to install and are supplied in easy-to-handle sections.

Tower dew points as an early indicator of potential issues

Dew point is defined as the temperature at which water in a gas condenses. The dew point for sulphuric acid plants is in

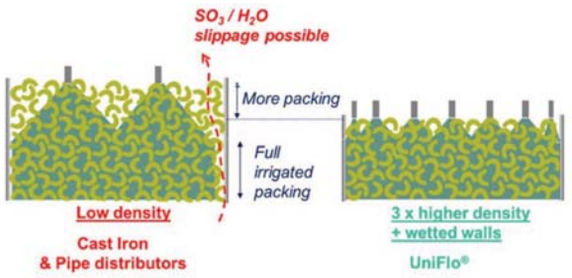

Figure 2a—Difference between low and high-density irrigation acid distributor

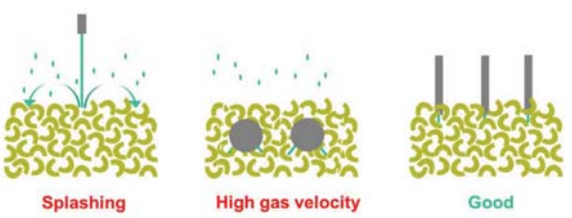

Figure 2b—Acid droplets above the ceramic packing

fact the point at which the first droplet of sulphuric acid condenses. However, the quantity is so small that it is invisible to the naked eye. An effective way for sulphuric acid plant operators to obtain accurate readings of the dew point is to use a vacuum pump to take measurements at the outlet of the dry tower if it is a suction tower. Dew-point measurement is an early detection method for any potential issues.

The H_2O volume is 30 times that of H_2SO_4, making the water dew point visible first. For example:

Vapour pressure over 96% H_2SO_4 at 65°C (typical DT operating point) mmHg

- H_2O 0.02
- H_2SO_4 0.0007
- SO_3 0.000002

The dew point matters because it affects drying tower efficiency, a crucial factor in plant optimization and one that has an impact on the life of a plant. As mentioned above, any moisture in the process gas will increase the dew point temperature before the IPAT. This will also increase the risk of acid condensation in economizers and in the converter during long hot shutdowns, increasing corrosion and damage to catalyst structure.

The impact of mist eliminators on tower performance

Tower performance is also affected by the choice of mist eliminator. Many different mist eliminator options are available in the market. They all intend to capture submicrometre liquid and soluble mists. However, they don't all function in the same way. Three mechanisms are used to capture mist –impaction, interception, and diffusion. MECS products use all three of these mechanisms – the impaction mechanism with the help of mesh pads, the interception mechanism with a combination of mesh pads and glass fibre, or the diffusion mechanism with the help of fibre beds to collect mist effectively.

Fibre bed collection intercepts particles ranging in size from <1 μm to larger particles >3 μm, trapping them in the fibre bed as shown in Figure 3.

The focus of this paper will be on diffusion bed mist eliminators, which are predominantly used in IPAT and final absorption towers (FAT) in modern acid plants. Some plant still uses impaction/interception-type mist eliminators in the FAT

Diffusion bed mist eliminators are produced by wrapping glass fibre (in rope form) around an inner cage of metal wire or by compressing bulk glass fibre between two metal cages. The commonly used diffusion bed mist eliminators are the ones where glass fibre rope is wrapped around an inner cage – ES-type mist eliminators.

Two methods are used for placing fibre roving onto a mist eliminator – angle wrap and parallel wrap. The positioning of the fibre has a significant impact on the efficiency of the mist eliminator, as demonstrated with the help of thermographic imaging (Figures 4 and 5). Angle-wrapped mist eliminators tend to allow less heat to escape than parallel-wrapped fibre beds.

Velometry testing of angle- and parallel-wrapped fibre bed mist eliminators also shows a difference in performance (Table I, Figures 6 and 7).

Whatever the type of mist eliminator chosen, it is normally easy to install, but not to remove. Maintenance must be carried out on site. It is therefore vital, at installation, that enough space is planned for maintenance and parts replacement.

Although mist eliminators are relatively simple devices, it is important that they are installed properly. Many factors will affect the efficiency of a mist eliminator:

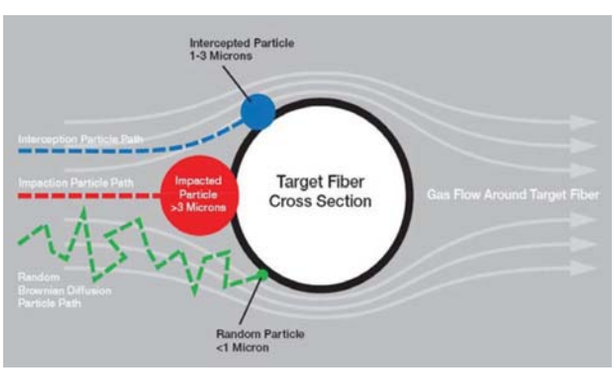

Figure 3—Fibre bed collection

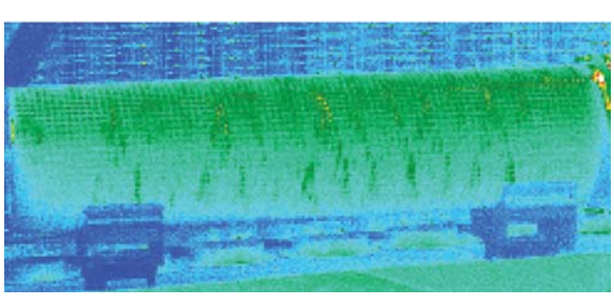

Figure 4—MECS ES angle-wrapped mist eliminator

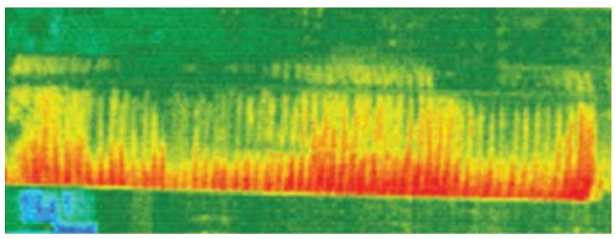

Figure 5—A parallel-wrapped mist eliminator

Table I

Results of velometry tests (ft/min)

Item	Test Vb	Max. Vb	Min. Vb
Standard packed (angle-wrapped) ES	30	102	1
Hand-packed (parallel-wrapped) ES	30	685	4

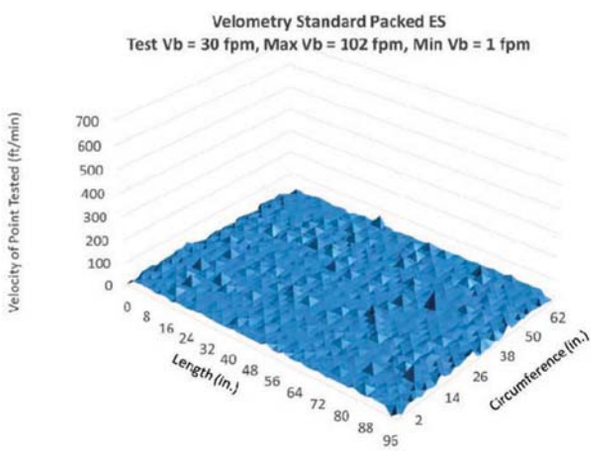

Figure 6—Velometry graph of an angle-wrapped mist eliminator

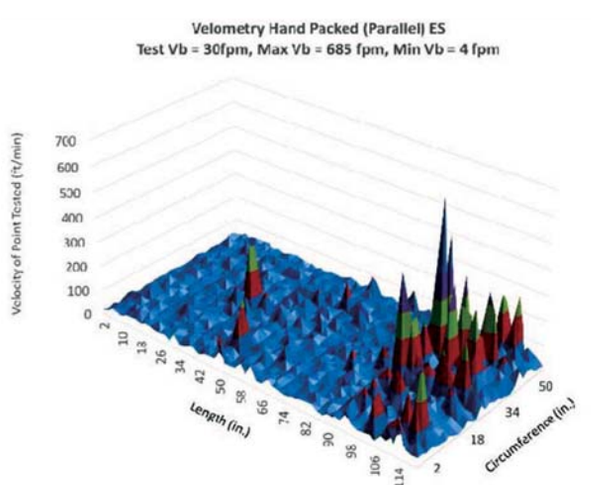

Figure 7—Velometry graph of a parallel wrapped mist eliminator

- ➤ Orientation of the mist eliminator – hanging or standing
- ➤ Type of gaskets used

Figure 8—Dry tower stick test, before (left) and after (right)

- Is it installed on a pedestal or directly on the tube sheet?
- Are the correct flange bolts used and are they torqued properly?
- Are seal pots or seal pipe used?
- Are seal pots filled up with acid before start-up?

Troubleshooting: a systematic approach

Preventing high acid mist carryover requires an understanding of its possible root causes. This involves a good knowledge of the plant design, an insight into the plant maintenance history (*e.g.* have there been tower distribution problems in the past?), a familiarity with the functioning of mist eliminators, plans for dealing with expected mist, and awareness of what constitutes a problem symptom.

Problem symptoms

These may include an abnormal drop in pressure, re-entrainment, 'drip acid', stack opacity e.g. EPA method 9, and measurements that show high exit loading. Downstream systems such as high stack opacity, high EPA 8 emissions, or a charred stick often have the same root cause (SO_3/H_2SO_4 vapour) or can be due to very specific causes:

What to avoid

Although it is possible to run a plant with partially blinded candles, *i.e.* a blocked mist eliminator, there is a substantial risk of damaging the cages. In the case of sulphur sublimation, the best approach is to shut down the plant and wash or replace the mist eliminator elements. Hanging elements should never be operated with a dP more than 680 mmWC (27 inWC).

Fouled packing results in sulphate accumulation in mist eliminators and an increase in operating pressure drop.

Sulphuric acid plant operators can deploy a range of testing and troubleshooting methods aimed at addressing a variety of root causes for problems. They can vary from plotting element pressure drop divided by the actual gas flow *versus* time, to acid vapour and acid mist stick tests, drip acid volumes and concentration, dry tower stick tests, the installation of viewports and, of course, physical inspections, though these require shutdowns and will lead to a loss of production unless the inspections are scheduled to coincide with planned turnarounds.

Several ways to identify the reason for acid mist carryover from acid towers are listed below. The most common fault-finding method is a stick test on the outlet of the tower (Figure 8). The condition of the stick after 30 seconds, 1 minute or 3 minutes gives a sound qualitative assessment of acid mist carryover.

Summary of testing/troubleshooting methods

- *Pressure drop and flow rate history*—plant records and while operating
- *Stick test*—while operating
- *Drip acid measurements*—while operating
- *Physical inspection*—during plant shutdown
- *View ports*—requires planning and shutdown to install
- *Smoke test*—primarily for checking leaks at gaskets, liquid seals, and tube sheet
- *Tyndall beam*—while operating – requires some finesse/practice
- *Water dew-point*—while operating
- *Acid dew-point*—while operating – not commonly used (expensive equipment)
- *MECS method 104*—requires planning and hot shutdown to install sampling nozzles and/or full-bore 4-inch gate or ball valves—last resort if other troubleshooting methods do not identify root causes.

Conclusion

Improving the performance of an acid plant is not a simple matter. Equipment cannot be placed in a haphazard, piecemeal fashion. Rather, the entire acid plant must be viewed holistically and improvements need to be made in a way that consider the interplay of all the various unit operations. Acid mist emissions cannot be reduced by simply optimizing tower operation, nor by simply enhancing mist capture. Indeed, the operational performance, and ultimately, the profitability, of many sulphuric acid plants will be improved only by incorporating and maintaining efficient tower acid distribution and superior mist elimination. This holistic approach is likely to reduce maintenance costs, avoid loss of production, and reduce stack acid mist emissions. ◆

http://dx.doi.org/10.17159/2411-9717/2017/v117n11a8

Computational model of large-capacity molten sulphur combustion spray efficacy and process efficiency

by K. Brown*, K. Bade*, and R. Schick*

Synopsis

The use of precision spray injectors with advanced technology nozzles in the combustion of molten sulphur represents an active and growing field. The efficient combustion of large volumes of molten sulphur is a clear requirement in the phosphate industry. Spraying Systems Company, along with our industry partners, has conducted significant research in the laboratory as well as in full-scale industrial settings to arrive at optimized process solutions for this application.

Additionally, computational models have been developed to allow for the assessment and optimization of the sulphur combustion efficacy. Over the past decade there have been rapid advancements in computer and software technologies for simulation of complex applications. These strides have allowed for more complex simulations at reasonable cost, such as the design of spray injectors with stress analysis coupled with fluid dynamics and heat transfer.

This paper presents the results of a detailed spray injection modelling study demonstrating the scale-up of the spray solution as well as the 100% spray combustion requirement at these elevated sulphur flow capacities. Through the use of the models developed here, the sulphur combustion was improved beyond that which was possible using experimental results.

Keywords

molten sulphur combustion, atomization, injector modelling, computational fluid dynamics, CFD.

Introduction

Sulphur trioxide (SO_3) is commonly used in the manufacture of sulphuric acid, oleum, chlorosulphonic acid, and other compounds. One method of obtaining SO_3 gas for these processes is through the combustion of molten sulphur. The sulphur is liquefied and fed into the combustion chamber of a furnace through one or more injectors. These precision spray injectors are a critical component in the process. The injectors convert large quantities of molten sulphur into an atomized spray of sulphur particles. Control of the particle size is a critical factor in ensuring rapid vapourization and complete combustion within the combustion chamber. Unburned sulphur can deposit outside of the combustion zone, which results in process inefficiency and increased maintenance.

This work outlines the design considerations for a successful sulphur combustion injection system. The process details injector selection and empirical characterization of the injector. Additionally the injection system design is evaluated via computational fluid dynamics (CFD) to ensure the intended performance characteristics in the combustion chamber. These simulations address velocity profiles, temperature profiles, droplet tracking (devolitization), and other relevant characteristics of the application.

These injectors have a significant role to maintain over long time periods, in a harsh environment. The environment is characterized by extremely high temperatures and turbulent flow conditions. The injectors are fairly long and must remain in operation, maintenance-free, for up to 25 years. In order to optimize design and verify proper material selection, FSI is required to ensure performance and reliability for the design life of the injectors. This work outlines the design considerations for a successful sulphur combustion injection system. The process details injector design verification, based on the selection and preliminary design from previous work. These simulations address velocity profiles, temperature profiles, flow-induced vibration, and other relevant characteristics of the application.

Theoretical considerations

Atomization

Atomization is used in many spray applications to produce droplets with a high surface area to volume. Often this high ratio results in much more efficient use of the spray droplets in evaporative and/or combustion processes. In general, atomizers that cause the greatest physical interaction between the liquid and vapour are most effective.

* *Spray Analysis and Research Services, Spraying System Company, Johannesburg, South Africa.*
 ISSN 2225-6253. This paper was first presented at the 6th Sulphuric Acid 2017 Conference', *9–12 May 2017, Southern Sun Cape Sun, Cape Town.*

Jet breakup

A liquid jet exhausted into air may be in a laminar or turbulent state. A laminar jet, which contains fluid particles that are travelling in parallel at the exit plane, may be created by utilizing a rounded inlet, having no mid-flow disturbances, and using a high-viscosity liquid. Turbulence in jets, which aids in jet breakup, may be encouraged through high flow velocities, large tube sizes, general surface roughness, rapid cross-sectional changes, and perturbations due to flow obstructions or vibrations. The Reynolds number (Re), which relates pressure and viscous forces, may be used to determine the likelihood of a flow to be laminar (low Re number) or turbulent (high Re number). The critical Reynolds number identifies where laminar flow will undergo the transition to turbulent flow. For pipe flow, the critical Reynolds number (Re_{crit}) is approximately 2300. When a flow transitions from laminar to turbulent flow, the mechanisms governing jet breakup change and cause a decrease in jet breakup length.

Liquid sheet breakup

Fraser and Eisenklam (1953) defined and described three liquid sheet breakup regimes: rim, perforated sheet, and wave. Liquid surface tension and viscosity are the primary properties that determine which mode(s) of disintegration occur. Liquid sheet breakup through 'rim' disintegration often occurs with high-viscosity, high-surface-tension type liquids. In rim disintegration the liquid mass becomes thicker at the free edges, which ultimately form liquid threads that break up into large drops, whereas the internal area disintegrates and forms smaller drops.

In a 'perforated sheet' type breakup, many holes are developed in the liquid sheet. The edges of these holes become thicker as the holes grow and more fluid mass is combined at each hole edge. The holes continued to grow until they encounter other rims and coalesce. Drops of many different sizees are created. 'Wave' disintegration occurs when wave motions within the liquid sheet cause fluctuations with distinct wavelengths. These waves break up into whole or half wavelength sections and surface tension reforms the sections into strands. These strands then disintegrate into drops. Wave disintegration creates drops that vary the most in size.

Drop breakup

Atomization is the process by which a liquid jet is disintegrated by aerodynamic forces. These aerodynamic forces, which cause the liquid to form into small drops and often to further break down into droplets, are created by the velocity of the liquid jet relative to its surroundings. The breakdown of drops in a spray can be summarized with an internal/external force assessment. The external aerodynamic pressure is balanced by the surface tension in order for the internal drop pressure to remain at a constant level, which it must do in order to sustain its drop size. In the event that the external forces are too large to be balanced though an increase in effective surface tension, the surface tension will be drastically increased through a decrease in the diameter of the drop (drop splitting). The process of drop splitting takes place until the surface tension pressure is large enough to counteract the aerodynamic drag pressure at all points on the drop's surface. The drop size at this equilibrium level is known as the critical drop size. The mechanisms that cause the breakup of drops can be further identified by considering some of the more complex aspects of 'real-world' conditions.

In turbulent flow fields the relative velocity between a drop and the surrounding gas will be very high, either locally or on a global scale. The turbulent field will impart a dynamic force on the drop, which will determine the largest drop size that can exist in equilibrium due to the energy in the most disruptive turbulence scales (E). With dynamic turbulent forces present, the Weber number, which for low-viscosity liquids relates the deforming external pressure forces to the reforming surface tension forces of a liquid drop in air, can be evaluated for low-viscosity liquids and used to estimate the maximum drop size based on these scales.

In high-viscosity (low Reynolds number) flow fields, where dynamic forces no longer control breakup, the surface tension forces and viscous forces work to deform and reform liquid drops. It is generally very difficult to atomize liquids that have a high liquid-to-air viscosity ratio. In these high-viscosity flows, variations in the air viscosity make little difference to the atomization process. Also, high-viscosity liquid-phase spray material delays the breakup of drops and impedes atomization, which is why more aggressive methods, such as air-blast atomization, are often used.

In practice

Hydraulic nozzles

Hydraulic nozzles are pressure-driven nozzles that spray a single fluid. Many different types of hydraulic nozzle designs exist, which aim to produce a variety of spray patterns from a continuous stream to a dispersed spray. These nozzles rely solely upon high liquid-to-gas relative velocities at exhaustion to achieve atomization. Liquids with low viscosity and high velocities atomize more readily; therefore hydraulic nozzles may suffice.

Two-fluid (pneumatic) nozzles

The mixing of two fluids (usually one liquid phase and one gaseous phase) by a nozzle may be accomplished either internally or externally to the nozzle body. In an internally mixing nozzle, the liquid flow and gas flow interact upstream of the final discharge orifice. In this case, the mixture exits as a single mixed flow, which widens with a reduced liquid flow velocity due to the pressurized gas. An internally mixing nozzle is optimum for high-viscosity fluids in a low flow rate application, since the breakup of this type of flow is more difficult. However, the flow rate of each fluid is then coupled, and to reach a desired operating condition, both flow rates must be tuned.

In an externally mixing nozzle the two fluid flows do not interact until after exiting the final nozzle orifice. These nozzle types may be designed to generate various spray characteristics depending on the atomizing air pressure. However, due to the uncoupling of the two fluid streams, these nozzles are much less efficient in their use of the atomizer fluid. Also, externally mixing nozzles do not offer the possibility of the liquid flow to 'back up' into the gas flow orifice; this may be a benefit in certain processes.

Fluid considerations

The spray angle of a nozzle represents the expected coverage

of a spray exiting from the nozzle. The theoretical spray angle (the angle in the near-exit region) will diminish at larger downstream distances. Higher viscosity liquids will tend to form less divergent sprays, whereas lower viscosity liquid sprays disperse more easily into a wide spray. The surface tension of the spraying liquid has a direct effect on the spray angle. Liquids with lower surface tensions form wider sprays.

The liquid properties such as (dynamic) viscosity, density, and surface tension directly affect and determine the spray type and quality that is created at a given operating condition. Liquid viscosity is representative of the propensity of a fluid to take the shape of its surroundings. A high-viscosity fluid (syrup-like) will resist conforming to its surroundings and will move very slowly. The liquid viscosity directly affects the pattern at which a liquid will spray. High-viscosity liquids require a higher pressure to spray due to their resistance to flow and will naturally form narrower sprays. Liquid density is directly proportional to the capacity of a spray. Density represents the mass-to-volume ratio for a liquid and therefore spraying a high-density liquid at a given velocity will result in a higher capacity spray. Liquid surface tension is a property representative of the internal force that holds a liquid together. This internal tension affects the liquid spray's minimum operating pressure, spray angle, and drop size. A higher surface tension will require a higher operating pressure, reduce the spray angle, and produce larger drop sizes.

The properties of molten sulphur are highly temperature-dependent, and thus the temperature of the liquid feed through the injector is required to be tightly controlled. This is achieved by means of steam-jacketed lining. Steam must be continually circulated to maintain the desired physical properties of the molten sulphur and corresponding spray performance. Table I lists representative liquid properties and their general effects. Figures 1a and 1b detail the temperature-dependent properties of sulphur density and viscosity.

Injector property considerations

Nozzle construction materials may vary from lightweight plastics to case-hardened metals. The material that is most suited to an application depends directly on the spray substance, spray environment (corrosive, heated, *etc.*), and desired spray characteristics.

Typical furnace temperatures are in the range of 900–1500°C. In order to function properly the injector must withstand the external temperatures, internal temperatures, and exposure to process fluids and internal forces. There are many readily available heat-resistant injector materials such as type 310, 304, 316, or 309 stainless steel or similar materials; the combination of material and design must be evaluated and optimized for each application.

Injector design

Spraying Systems' patented design of an 'Enhanced efficiency nozzle for use in molten sulfur combustion' provides a

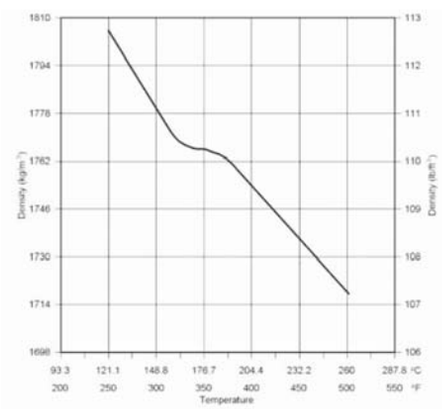

Figure 1a—Variation in sulphur density with temperature (Sulphuric-Acid.com, 2005)

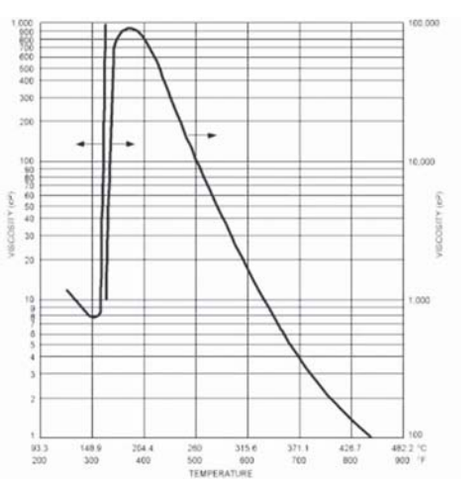

Figure 1b—Variation in sulphur viscosity with temperature (Sulphuric-Acid.com, 2005)

Table I

Atomization and fluid properties (after Schick, n.d.)

Fluid property	Increase in operating pressure	Increase in specific gravity	Increase in viscosity	Increase in liquid temperature	Increase in surface tension
Pattern quality	Improves	Negligible	Worsens	Improves	Negligible
Capacity	Increases	Decreases	Nozzle dependent	Fluid- and nozzle dependent	No effect
Spray angle	Increase/decrease	Negligible	Decreases	Increases	Decreases
Drop size	Decreases	Negligible	Increases	Decreases	Increases
Velocity	Increases	Decreases	Decreases	Increases	Negligible
Impact	Increases	Negligible	Decreases	Increases	Negligible
Wear	Increases	Negligible	Decreases	Fluid- and nozzle- dependent	No effect

refined solution to the sulphur feed injection process. There are options for hydraulic and two-fluid (pneumatic) injection of molten sulphur. The use of an unobstructed feed path for cleaning provides for easy maintenance with a uniform distribution of small to medium drop size throughout a range of flow rates. Where large turndown ratios are required, a transversely intersecting steam (or gas) flow greatly improves the ability to maintain efficacy and efficiency of the combustion process by tightly controlling the atomization of the molten feed. In addition to these features, the unit allows for thermal expansion and withstands the temperature loading in the burner without bending. Steam-jacketed designs allow for tight control of the molten sulphur temperature and related rheological fluid properties. Injectors can be manufactured to specified lengths in various materials, in compliance with ASME B31 3-2010 standards. Figure 2 provides a representation each type of design configuration.

The Spraying Systems sulphur-burning nozzles offer many advantages, some of which are:

- Uniform spray distribution to fit exact coverage with maximum atomization for a given amount of flow
- Controlled spray velocity
- Each injector nozzle is custom-designed to exact specifications to maximize performance
- Ability to provide good atomization at relatively low ΔP (30–40 psi liquid; 50–60 psi steam)
- Large non-clogging passages
- Rugged, durable construction
- Ongoing research for improved product
- Designs are patent-protected
- 25 years of continuous service.

Experimental testing

Test set-up and data acquisition

For drop sizing, the nozzle was mounted on a fixed platform 72 inches (1.82 m) from the floor. A fixed assembly held the nozzle in place and data was acquired at 36 inches (0.91 m) downstream of the nozzle exit. Drop size and velocity data was collected at various operating conditions.

A two-dimensional Artium Technologies PDI-200MD (Schick, n.d.; Sulphuric-Acid.com, 2005; ANSYS, 2010; Fluent Inc, 2007) system was used to acquire drop size and velocity measurements. The solid-state laser systems (green 532 nm and red 660 nm) used in the PDI-200MD are Class 3B lasers and provide 50–60 mW of power per beam. The lasers were operated at an adequate power setting to overcome interference due to spray density.

Figure 2—Patented sulphur-burning injector 53686-1 with 1/2BA-309SS70 hydraulic nozzle (top) and FM10A two-fluid nozzle (bottom)

The transmitter and receiver were mounted on a rail assembly with rotary plates; a 40° forward scatter collection angle was used. For this particular test, the choice of lenses was 1000 mm for the transmitter and 1000 mm for the receiver unit. This resulted in an ideal size range of about 4.0–1638 μm diameter drops. The optical set-up was used to ensure acquisition of the full range of drop sizes while maintaining good measurement resolution. The particular range used for these tests was determined by a preliminary test run where the $D_{V0.5}$ and the overall droplet distribution were examined. For each test point, a total of 10 000 samples were acquired. The experimental set-up can be seen in Figures 3a and 3b.

The $D_{V0.1}$, $D_{V0.5}$, D_{32}, and $D_{V0.9}$ diameters were used to evaluate the drop size data. This drop size terminology is as follows.

- $D_{V0.1}$ is a value where 10% of the total volume (or mass) of liquid sprayed is made up of drops with diameters smaller or equal to this value
- D_{32}: Sauter mean diameter (also known as SMD) is a means of expressing the fineness of a spray in terms of the surface area produced by the spray. SMD is the diameter of a drop having the same volume-to-surface area ratio as the total volume of all the drops to the total surface area of all the drops
- $D_{V0.5}$: volume median diameter (also known as VMD or MVD) is a means of expressing drop size in terms of the volume of liquid sprayed. The VMD is a value where 50% of the total volume (or mass) of liquid sprayed is made up of drops with diameters equal to or smaller than the median value. This diameter is used to compare the change in average drop size between test conditions
- $D_{V0.9}$ is a value where 90% of the total volume (or mass) of liquid sprayed is made up of drops with diameters smaller or equal to this value.

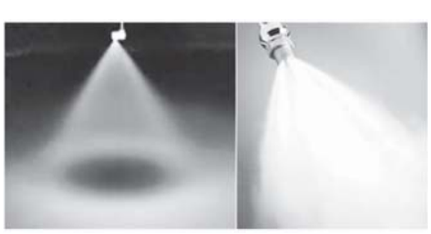

Figure 3a—BA WhirlJet (left) and FM10A (right)

Figure 3b—PDI testing set-up

By analysing drop size based on these standardized drop statistics it is possible to objectively characterize the quality and effectiveness of this atomizing nozzle for the prescribed application.

Test fluids and equipment

All testing was conducted using water. Liquid flow to the system was supplied using a high-volume pump at full capacity. The liquid flow rate to the atomizer was monitored with a MicroMotion D6 flow meter and controlled with a large bleed-off valve. The MicroMotion flow meter is a Coriolis mass flow meter that measures the density of the fluid to determine the volume flow. The meter is accurate to ±0.4% of reading. Liquid pressures were monitored upstream of the nozzle with 0–1.73 MPa class 3A pressure gauges. Photographs of the set-up and operation of the test nozzle are shown in Figures 3a and 3b.

Test conditions

Data was acquired for multiple flow conditions. These tests involved the interaction of various liquid pressure levels and flow rates for five flow capacities (see Figures 5 and 6 in the Results section) in order to characterize the nozzle's spray at various testing conditions and determine optimal operating conditions for this application.

Numerical simulations

CFD methods

Computational fluid dynamics (CFD) is a numerical method used to solve fluid flow problems. Today's CFD uses extremely large numbers of calculations to simulate the behaviour of fluids in complex environments and geometries. Within the computational region, CFD solves the Navier-Stokes equations to obtain velocity, pressure, temperature, and other parameters that may be required. CFD recently became a popular design and optimization tool with the help of commercially available software and advanced computer technology. The CFD simulation problem called for the assessment of liquid sulphur combustion inside the combustion chamber. The sulphur is atomized via spray nozzles in order for efficient burn-off.

The commercially available CFD package ANSYS FLUENT (version 12.1) was used for the simulation of sulphur combustion with air as an oxidizer. Air and combustion gases inside the horizontal combustion chamber were set as primary phase flow (Eulerian approach). The primary phase used coupled models (momentum, turbulence, energy, species mixing, and combustion), which required boundary conditions (BCs). Table II shows the BCs for the primary phase. This problem consisted of inlet BC and outlet BC, set as 'mass flow rate inlet' and 'constant pressure outlet' respectively. At the inlet a mixture of gas with oxygen and nitrogen (air) was employed. These had to be separate since oxygen is needed in the combustion process.

The sulphur injection was set as secondary phase (Lagrangian approach) where the inlet BCs are based on spray injection parameters as determined empirically. The Lagrangian particles were set as 'combusting'. Table III shows the injection BCs of the injection nozzle. The Lagrangian particles were tracked using a discrete phase model (DPM). During computation, heat and mass transfer were coupled between primary and secondary phases.

The sulphur injection was set as secondary phase (Lagrangian approach) where its inlet BCs are based on spray injection parameters as determined empirically. The Lagrangian particles were set as 'combusting'. Table III shows the injection BCs of the injection nozzle. The Lagrangian particles were tracked using a DPM. During computation, heat and mass transfer were coupled between primary and secondary phases.

To generate the computation domain (mesh) for the combustion chamber shown in Figure 4, Gambit (version 2. 3.16) was utilized. The mesh consisted of 3 986 432 million mixed cells. Due to its size and modelling complexity, the simulation required significant computer power and processing time.

Table II

Primary phase BCs

Boundary condition	Units -	Inlet Mass flow	Outlet Constant pressure
Vol. flow rate	Nm^3/h	308 000	–
Mass flow rate	kg/s	113.9	–
Pressure	barg	0.569*	0**
Temperature	°C	122	1160***
Area	m^2	6.5	8.0
Av. velocity	m/s	19.67	126.8

*Set as operating pressure
**Set with respect to operating pressure
***Target temperature

Table III

Injection BCs

	Units	Hydraulic (BA)	Pneumatic (FM)
Total mass flow rate	kg/s	14.647	12.2
Pressure	barg	11	
Temperature	°C	132	1323
Number of injectors	–	5	5
Mass flow rate/inj.	kg/s	2.929	2.44
Injection velocity	m/s	35	35
D minimum ($DV_{0.01}$)	mμ	37	11
D mean ($DV_{0.50}$)	mμ	505	66
D maximum ($DV_{0.99}$)	mμ	1087	144
Spread parameter (RRD)	–	3.0	2.4

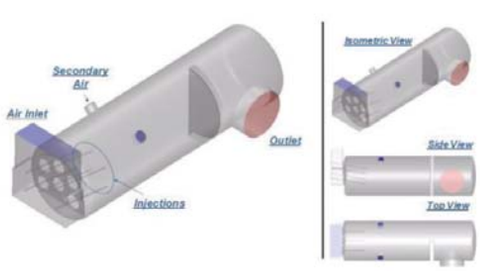

Figure 4—Sulphur combustion chamber

The primary phase, which consisted of the gas mixture, was mainly dependent on temperature as large temperature variations were expected. The gas was treated as an incompressible ideal gas (no pressure variation, whereas operating pressure is used in the Ideal Gas Law), with physical properties such as density, heat capacity, viscosity, thermal conductivity *etc.* set to be dependent on temperature. The operating pressure was set based on air inlet pressure (see Table II). The walls had a common (standard) set-up, with no slip, adiabatic (insulated), and reflect for the combusting particles.

For the combustion study, a species mixing model was used to accommodate combustion with oxygen from air. The evaporation and combustion of the liquid sulphur, using dispersed-phase modelling capability, was employed to compute coupled gas flow and liquid spray physics as mentioned previously. The mixture fraction/PDF equilibrium chemistry model was used to predict the combustion of the vapourized fuel. This approach allows the simulation of combustion by solving a transport equation for a single conserved scalar, the mixture fraction. Property data for the species is accessed through a chemical database and interaction is modelled using a β-PDF.

The basis of the non-premixed modelling approach is that under a certain set of simplifying assumptions, the instantaneous thermochemical state of the fluid is related to a conserved scalar quantity known as the mixture fraction, f. The mixture fraction can be written in terms of the atomic mass fraction (ANSYS, 2010):

$$f = \frac{Z_i - Z_{i,ox}}{Z_{i,fuel} - Z_{i,ox}} \quad [1]$$

where Z_i is the elemental mass fraction for element i. The subscripts 'ox' and 'fuel' refer to the values at the oxidizer and fuel stream inlet respectively.

The β-PDF shape is given by Equations [2]–[4].

$$p(f) = \frac{f^{\alpha-1}(1-f)^{\beta-1}}{\int f^{\alpha-1}(1-f)^{\beta-1}\,df} \quad [2]$$

where

$$\alpha = \bar{f}\left[\frac{\bar{f}(1-\bar{f})}{\overline{f^2}} - 1\right] \quad [3]$$

and

$$\beta = (1-\bar{f})\left[\frac{\bar{f}(1-\bar{f})}{\overline{f^2}} - 1\right] \quad [4]$$

Radiation was modeled with the P-1 radiation model. This is a simplified radiation model that is based on the more general P-N model, which is based on the expansion of the radiation intensity I into an orthogonal series of spherical harmonics (ANSYS, 2010). For combustion applications where the optical thickness is large, the P-1 model works reasonably well. In addition, the P-1 model can easily be applied to complicated geometries with curvilinear coordinates (ANSYS, 2010).

Results

Experimental results

The results of the PDI measurements provide a representative characterization of the atomizer effectiveness at the 36-inch downstream investigation location. The results are provided in Table III. The Sauter mean diameter (D_{32}) as well as other representative diameter statistics based on the volume flow are presented. These results allow the qualitative evaluation of the dependence of drop size on the liquid flow rate and pressure.

CFD results

The CFD results provide great insight into the mixing mechanisms and spray interactions in complex environments such as combustion. The boundary conditions, as described above, mimic the intended real-world operation of this sulphur feed injection nozzle and provided quality inputs for numerical analyses. These CFD calculations, based on the k-epsilon turbulence model, were allowed to run through hundreds of iterations until a steady-state solution was realized. This solution was deemed acceptable when the calculation residuals (changes in the results from one iteration to the next) were negligibly low and good convergence was achieved. Figure 6 illustrates the path lines of the gas flow traced through the combustion chamber. This provides a preliminary assessment of the injection locations, which due to the relative momentum of the gas stream, influence the droplet trajectories and particle tracks. An increased velocity profile is apparent at the six entry points of air into the chamber. This will affect the droplets, pulling drops towards the base of the combustion chamber. If this effect is large, there is potential for wall impingement, resulting in wall damage and reduced efficiency of the process.

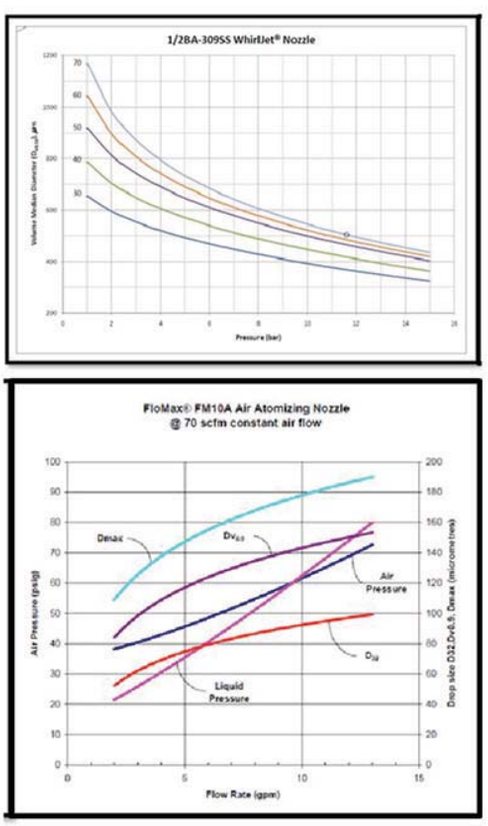

Figure 5—Spray characterization results

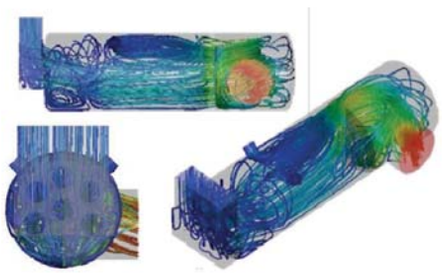

Figure 6—Gas path lines through combustion chamber

Additionally, the effects of the secondary air on the general flow can be assessed. The secondary air has a significant effect on the top three injected sprays. This secondary air is poorly distributed through the combustion chamber.

The velocity profile demonstrates the high velocity magnitude of both fluids as they enter the mixing and combustion region. As would be expected, there are very low velocity regions in the combustion chamber near the walls and the mixed flow has a fairly uniform mid-level velocity profile as it moves through the primary combustion area (see Figure 6).

The combustion was considered through with a non-premixed modelling approach. The property data for the species was accessed through a chemical database and the interaction was modelled using a β-PDF. The results of the combustion based on species contents are shown in Figure 7.

The primary focus of this study was to verify that the sulphur injection droplets were fully devolatilized prior to the exit of the combustion chamber. Failure to achieve this could lead to downstream damage and increased cost of operations. From Figure 7, it is evident that sulphur combustion is complete prior to the baffle wall. From the injection planes (the right-hand side of Figure 7), it is evident that the oxygen from the secondary air results in faster combustion rates at the top of the combustion chamber compared to the lower regions. This trend is mirrored by the oxygen profiles within the combustion chamber.

The combustion of the sulphur injections can also be examined through visualizing the spray emitted from the injectors. An initial DPM concentration (DPMC) value was used to define the spray plume boundary (SPB) and visualize the spray region, as shown in Figure 8. The isosurface of DPMC was based on matching peaks of CFD DPMC value and experimental volume flux at measured with the PDI. To obtain the cut-off DPMC, the cut-off volume flux point at about 0.002 $cm^3/cm^2/s$ was matched with 0.001 kg/m^3.

With the hydraulic atomizer, there is some potential for droplet impingement with the base of the spray chamber (this region is highlighted in red). From the top view (shown on the left-hand side of Figure 8), there is no evidence of wall impingement along the sides of the combustion chamber; however, sulphur spray occupies the full diameter of the combustion chamber. This would indicate that the spray angle of the injector is optimal for the application. This is fully mitigated in the case of the two-fluid atomizer (shown on the right). The FloMax two-fluid atomizer is able to better control the drop size of the molten injection. This allows for faster combustion and mitigates the risk of contact with the walls of the combustion chamber.

The resulting temperature profiles for the combustion chamber were examined. The temperature profiles are displayed in Figure 9. Temperatures were not uniform from top to bottom. This is due primarily to the fact that the secondary air adds cooler air and also acts as an additional source of oxygen to improve the combustion. The rate of combustion is slightly higher towards the top of the combustion chamber.

Temperatures at the outlet were found to be around 1400°C. This is slightly above the measured values of 1100–1200°C. This error could be improved with a more complex combustion model and more complex radiation model. However, the simulation does prove to be a reasonable assessment of the sulphur combustion application.

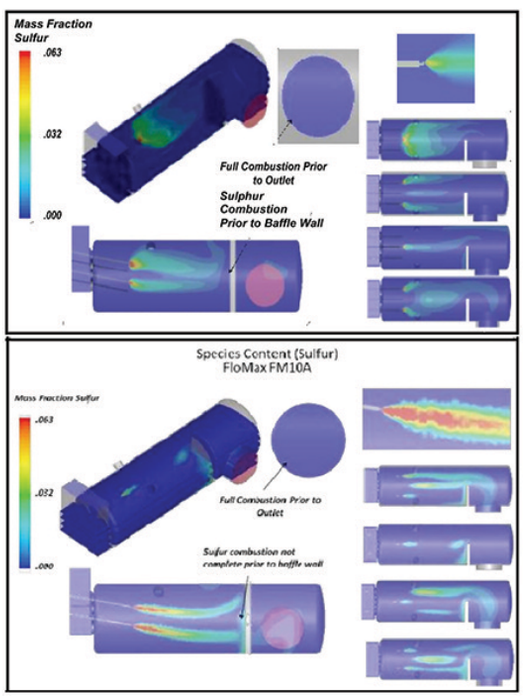

Figure 7—Mass fraction of sulphur

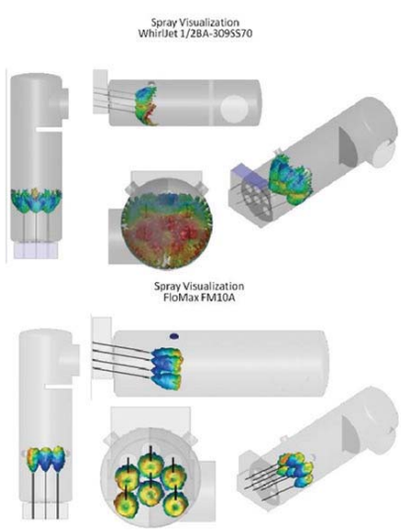

Figure 8—Spray visualization in the combustion chamber

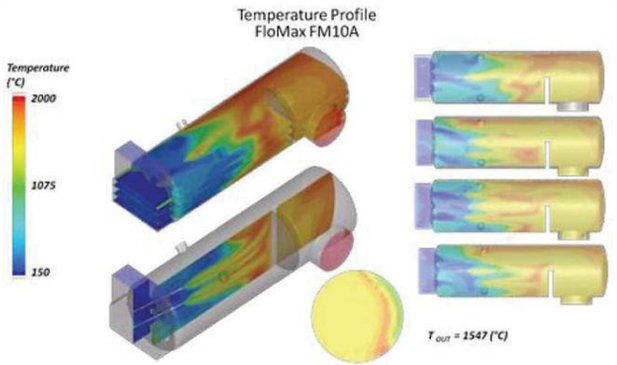

Figure 9—Temperature profiles in the combustion chamber

Structural considerations

CFD and FEA analysis was performed to determine temperature, pressure, and velocity flow around the injectors. The results of this work are shown in Figures 10–13. Temperatures were determined to peak at 570°C, which is within the expected range for this application. The main body of the injector has a well-controlled temperature range, due to the recirculating steam design. The highest temperature occurs at the outer edge of the injector tip.

The thermal load on the lance has multiple sources. Heat transfer from the combustion process and gas stream acts on the outer surface of the injector. The recirculating steam supplies further heat from the internal chamber of the steam-jacketed injector. The final contribution to the thermal load is from the molten sulphur feed. The maximum temperature of the injector of 570°C is well below the melting point for stainless steel.

Velocity results are shown in Figures 11–12. Multiple scales are used to investigate the steam flow initially, and in the injector tip. The velocity in the steam line far exceeds the flow of the molten sulphur through the nozzle. Owing to the high viscosity of the molten sulphur, the velocity at the exit orifice is 25 m/s. This is as expected for the injector style and operating conditions.

The pressure distribution through the injector is shown in Figure 13. Again, due to the high viscosity of the molten sulphur, there is a significant pressure drop across the injector.

The cantilevered injector was modelled using a fixed surface at the flange location. The pressures were accounted for: from the combustion chamber, steam jacket, and internal sulphur flow. The maximum stress concentration is located at the base of the lance, near the flange. The stress results are contained in Figure 14. The maximum stress, of 271 kilopounds per square inch (ksi)[1] exceeds the yield strength of stainless steel of 33 ksi. It is evident that supports will be required for this application.

Modal analysis was performed to determine the dynamic natural response of our model when subjected to free vibration. Overall mass and stiffness were used to determine the various periods at which the injector will naturally resonate, which could potentially lead to failure. The natural frequency was compared to the vortex shedding frequency determined during failure analysis.

Six modes were used to analyse vibration in the injector, although the first is the most probable vibration mode. The six vibration modes are: (1) side-to-side vibration, (2) up and down vibration, (3) side-by-side vibration along a fixed point at the centre of the lance, (4) up and down vibration along a fixed point at the centre of the lance, (5) side-by-side vibration along two fixed points in the lance, and (6) up and down vibration along two fixed points in the lance. The results of the modal analysis are contained in Table IV.

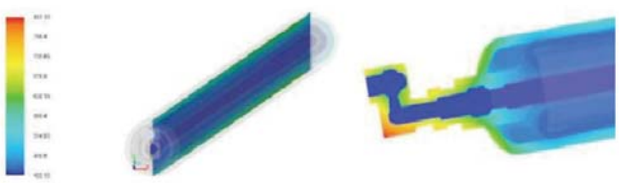

Figure 10—Temperature profiles in the injector

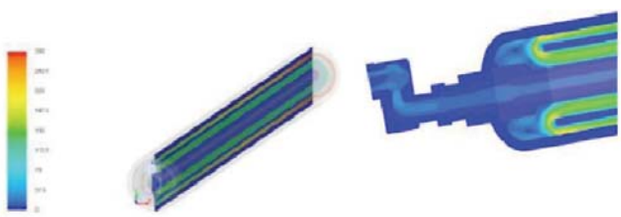

Figure 11—Velocity profiles in the injector (steam focus)

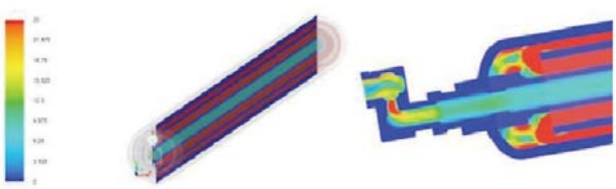

Figure 12—Velocity profiles in the injector (nozzle tip)

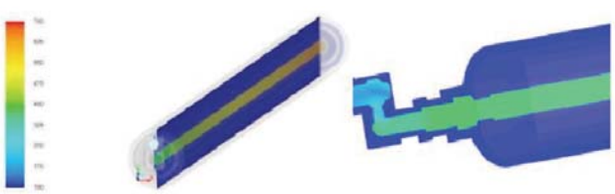

Figure 13—Pressure profiles in the injector (nozzle tip)

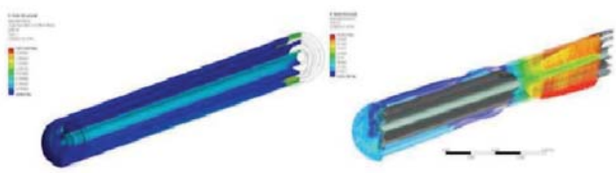

Figure 14—Stress analysis of the injector

[1]0.1450 ksi = 1 MPa

Table IV

Modal analysis

Mode	Frequency (Hz)	Maximum stress (ksi)
1	2.167	37.3
2	2.168	37.4
3	2.516	44.6
4	2.923	51.8
5	14.212	231
6	14.212	231

Discussion and conclusions

Engineering optimization of injectors

The optimal nozzle design for sulphur feed injection for this combustion application incorporates the Spraying Systems patented nozzle, optimized based on the results of tests presented in this report. The Spraying Systems nozzle can provide the necessary spray characteristics with minimal wall impingement and full combustion of injected sulphur. Drop sizes ranging from less than 37 μm to greater than 1087 μm were created at the selected operating conditions.

The results of the CFD analyses provide insight into the internal mixing mechanics of the sulphur combustion process and allow for better optimization. High-accuracy, steady-state simulations of the nozzle gave a better understanding of the governing mixing forces, and their relative effects on the internal mixing and combustion is evident. It is clear from these models (see Figures 6–9) that the injected molten sulphur will thoroughly combust, without interactions leading to increased operational costs or equipment damage.

The hydraulic and two-fluid atomizers were compared to provide a general design aid. Multiple performance variations were identified through the empirical and simulation investigations. The in-depth analysis of these results, and those from previous tests, provides an experimental, computational, and analytical basis for the optimization of sulphur combustion injectors. With improved knowledge of the internal mechanics and the external spray pattern, the performance of the nozzle at these operating conditions can be optimized very effectively.

A sulphur-burning injector was analysed to determine its suitability for use in in a combustion chamber at normal operating conditions. An optimized injector design was incorporated into a lance. Due to the length requirement of the injector, structural analysis was required to determine suitability for long-term, maintenance-free service. A full analysis was performed for the injector; including fluid flow analysis, structural analysis, and one-way fluid structure analysis (Figures 10–14).

Acknowledgement

The authors thank Mr. Wojciech Kalata of Spraying Systems Co. for his assistance with this project.

References

ANSYS. 2010. Fluent Theory Guide, Release 13.0. November 2010.

Bachalo, W.D. 1994. Experimental methods in multiphase flows. *International Journal of Multiphase Flow*, vol. 20 (suppl.). pp. 261–295.

Bachalo, W.D. 1980. A method for measuring the size and velocity of spheres by dual beam light scatter interferometry. *Applied Optics*, vol. 19, no. 3. pp. 363–370

Bachalo, W.D. and Mauser, M.J. 1985. Spray drop size and velocity measurements using the phase/doppler particle analyzer. *Proceedings of the 3rd International Conference on Liquid Atomisation and Spray Systems*, Imperial College, London, 8–10 July 1985, vol. 2. pp. VC/2/1–12.

Bachalo, W.D. and Mauser, M.J. 1984. Phase/doppler spray analyzer for simultaneous measurement of drop size and velocity distribution. *Optical Engineering*, vol. 23, no. 4. pp. 583–590.

Blevins, R.D. 1990. Flow Induced Vibration. Krieger Publishing, Malabar, FL.

Fluent Inc. 2007. FLUENT 6.3 User's Guide.

Lefebvre, A.W. Atomization and Sprays. Hemisphere Publishing. pp. 1-78.

Naudascher, E. and Rockwell, D. 1994. Flow Induced Vibrations: An Engineering Guide. Dover Publications

Schick, R.J. Not dated. A guide to drop size for engineers. Spraying Systems Co., *Bulletin* 459. Wheaton, IL.

Sulphuric-Acid.com 2005. Properties of sulphur. http://www.sulphuric-acid.com/TechManual/Properties/ properties_sulphur.htm ◆

BM
BASE METALS
2018

Copper Cobalt Africa

In Association with

The 9TH Southern African Base Metals Conference

9–12 July 2018

Avani Victoria Falls Resort, Livingstone, Zambia

SAIMM is proud to host the Second Copper Cobalt Africa Conference in the heart of Africa

To be held in Livingstone, Zambia, this anticipated and prestigious event provides a unique forum for discussion, sharing of experience and knowledge, and networking for all those interested in the processing of copper and cobalt in an African context, in one of the world's most spectacular settings - the Victoria Falls.

The African Copper Belt is again experiencing a resurgence of activity following the commodity downturn of recent years. A significant proportion of capital spending, project development, operational expansions, and metal value production in the Southern African mining industry take place in this region. The geology and mineralogy of the ores are significantly different to those in other major copper-producing regions of the world, often having very high grades as well as the presence of cobalt. Both mining and metallurgy present some unique challenges, not only in the technical arena, but also with respect to logistics and supply chain, human capital, community engagement, and legislative issues. This conference provides a platform for discussion of a range of topics, spanning the value chain from exploration, projects, through mining and processing, to recycling and secondary value addition.

For international participants, this conference offers an ideal opportunity to gain in-depth knowledge of and exposure to the African copper and cobalt industries, and to better understand the various facets of mining and processing in this part of the world.

Jointly hosted by the Mining and Metallurgy Technical Programme Committees of the Southern African Institute of Mining and Metallurgy (SAIMM), this conference aims to:

- Promote dialogue between the mining and metallurgical disciplines on common challenges facing the industry
- Enhance understanding of new and existing technologies that can lead to safe and optimal resource utilization
- Encourage participation and build capacity amongst young and emerging professionals from the Copper Belt region.

The organizing committee looks forward to your participation.

Conference Topics

- Mineralogy
- Exploration and new projects
- Open-cast mining
- Underground mining
- Rock engineering
- Mine planning
- Mineral resource management
- Minerals processing
- Pyrometallurgy
- Hydrometallurgy
- Current operational practices and improvements
- Project development and execution
- Novel technologies for this industry
- Socio-economic challenges
- Recycling
- Waste treatment and minimization
- Environmental issues
- Geometallurgical modelling

To add your name to the mailing list and to receive further information, please e-mail your contact details to: Gugu Charlie Conference Co-ordinator
Saimm, P O Box 61127, Marshalltown 2107, Tel: +27 (0) 11 834-1273/7
E-mail: gugu@saimm.co.za, Website: http://www.saimm.co.za

SAIMM
THE SOUTHERN AFRICAN INSTITUTE OF MINING AND METALLURGY

http://dx.doi.org/10.17159/2411-9717/2017/v117n11a9

SEM image processing as an alternative method to determine chromite pre-reduction

by G.T.M. Mohale, J.P. Beukes, E.L.J. Kleynhans, P.G. van Zyl, J.R. Bunt, L.R. Tiedt, A.D. Venter, and A. Jordaan

Synopsis

The specific energy consumption (SEC) of the pelletized chromite pre-reduction process is the lowest of all FeCr production processes commercially applied. This process also eliminates the use of chromite ore fines that could result in furnace blow-outs or so-called bed turnovers, yields a high chromium (Cr) recovery, and can produce a low-sulphur (S) and -silicon (Si) FeCr. However, this process requires extensive operational control due to the variation in pre-reduction levels and carbon contents of the pre-reduced, pelletized furnace feed material. The wet chemical analytical method currently applied for the determination of chromite pre-reduction is time-consuming. In this paper, the development of an alternative method consisting of scanning electron microscopy (SEM) micrograph image processing is presented. A strong linear correlation (R^2 = 0.919) between chromite pre-reduction (%), as determined by wet chemical analysis, and the new method was obtained. Further development could result in the industrial application of the method, which could contribute significantly to the metallurgical stability and enhanced process control of the pelletized chromite pre-reduction process.

Keywords

chromite pre-reduction, solid-state reduction of chromite, scanning electron microscopy (SEM), image processing, metallurgical carbon balance.

Introduction

Chromite ore has remained the only commercially viable source of new chromium (Cr) units since its discovery (Riekkola-Vanhanen, 1999). South Africa holds the majority of the world's exploitable chromite reserves (Cramer, Basson, and Nelson, 2004). More than 90% of all chromite is smelted using pyrometallurgical carbothermic reduction to form various grades of ferrochrome (FeCr) – a crude alloy principally containing Cr and iron (Fe) (ICDA, 2013). Over 80% of FeCr is used for the production of different stainless steel grades (ICDA, 2013; Murthy, Tripathy, and Kumar, 2011; Abubakre, Muriana, and Nwokike, 2007). Stainless steel products play an important role in modern-day society due to their resistance to corrosion (Riekkola-Vanhanen, 1999).

The FeCr industry utilizes various pre-processing and smelting methods, with the following being the most well-defined (Beukes, Dawson, and van Zyl, 2010; Naiker, 2007; Daavittila, Honkaniemi, and Jokinen, 2004; Riekkola-Vanhanen, 1999).

- Conventional semi-closed or open submerged arc furnace (SAF) operations that mainly utilize coarse chromite, flux, and carbonaceous reductant feed materials. This process requires the lowest capital input, since minimal pre-processing of the feed materials is necessary. However, it is the least environmentally friendly and the least efficient in terms of Cr recovery and specific energy consumption (SEC), *i.e.* MWh/ton FeCr produced
- Closed SAF operations that mainly utilize oxidative sintered chromite pellets, as well as coarse flux and reductant as feed materials (*e.g.* Outotec process). A significant proportion of green- and brownfield FeCr developments over the last two decades utilize this technology
- Closed SAF operation combined with pelletized pre-reduced chromite, as well as coarse fluxes and reductants as feed material (*e.g.* the Premus process applied by Glencore-Xstrata Alloys)
- Closed SAF with plasma or direct current (DC) arc operation that can be fed fine material exclusively, which eliminates pre-processing of raw materials. However, this process option has the highest SEC.

In this paper, the focus is on the pelletized chromite pre-reduction process (also referred to as solid-state reduction of chromite), which is applied at two FeCr smelters in South Africa that currently account for a combined production capacity of about 1.13 Mt of FeCr annually (Jones, 2014; Beukes, van Zyl, and Ras, 2012). FeCr smelters applying this

* *Chemical Resource Beneficiation North-West University, Potchefstroom Campus, South Africa.*

 ISSN 2225-6253. Paper received Jan. 2017; revised paper received Mar. 2017.

process are also being developed in China, but information regarding production capacities of these facilities is not yet available in the public domain. In the pelletized chromite pre-reduction process, fine chromite ore, a clay binder, and a carbon reductant are dry-milled, agglomerated (pelletized), and pre-reduced (solid-state reduction) in a rotary kiln at temperatures up to 1 400°C (Niayesh and Fletcher, 1986). The pre-reduced pellets are then charged hot, immediately after exiting the kiln, into a closed SAF (Beukes, Dawson, and van Zyl, 2010; Naiker, 2007). If chromite pellets made from typical South African chromite ore are pre-reduced to approximately 45%, the SEC of the pelletized chromite pre-reduction process is approximately 2.4 MWh/t FeCr, which is the lowest of all FeCr production processes commercially applied (Kleynhans *et al.*, 2017a; Beukes, Dawson, and van Zyl, 2010; Takano *et al.*, 2007; Naiker, 2007; Niayesh and Fletcher, 1986). The SEC is of particular importance, since electricity consumption is the single largest contributor to the overall FeCr production costs (Kleynhans *et al.*, 2017b; Biermann, Cromarty, and Dawson, 2012; Daavittila, Honkaniemi, and Jokinen, 2004). Other advantages associated with the application of the pelletized chromite pre-reduction process are that it: (i) eliminates the use of chromite fines that could sinter on the surface of the furnace bed materials, which could trap evolving gases and can result in blow-outs or so-called bed turnovers, (ii) yields a high Cr recovery of approximately 90%, (iii) can produce low-sulphur (S) FeCr due to the use of a highly basic slag, and (iv) can produce a relatively low-silicon (Si) FeCr, since the bed conductivity is not only dependent on lumpy carbon reductant content, due to the conductivity of the basic slag that makes it possible to operate at lower excess carbon ratios (McCullough *et al.*, 2010; Beukes, Dawson, and van Zyl, 2010; Naiker, 2007; Botha, 2003).

Apart from the high capital costs associated with the pelletized chromite pre-reduction process option, its main disadvantage is the extensive operational control that is required due to the variation in pre-reduction levels and carbon contents of the furnace feed material (Naiker, 2007). In practice, this implies that the metallurgical carbon balance has to be changed regularly to prevent the process from becoming carbon-deficient (traditionally referred to as 'under-coke') or too rich in carbon ('over-coke'). A carbon deficiency results in incomplete chromite reduction, with increased Cr losses to the slag, as well as significant increases in the molten slag viscosity that lead to difficulty in tapping the furnace. An over-carbon situation leads to increased conductivity of the bed material, resulting in lower power input if the electrodes cannot be raised high enough, as well as poor electrode penetration, which is also associated with tapping difficulties if the electrodes are raised too high, or if the power input is excessively limited.

The wet chemical analytical technique currently applied to determine the level of chromite pre-reduction (Kleynhans *et al.*, 2017a, 2016, 2012; Neizel *et al.*, 2013) is time-consuming, making it difficult and expensive to deal with large numbers of samples. Therefore, smelters applying the pelletized chromite pre-reduction process in South Africa currently collect a composite pellet sample from the discharge of a rotary kiln during an eight-hour working shift, which is then sent to the on-site laboratory for the appropriate analyses. The results typically become available only during the latter half of the eight-hour working shift after the samples were submitted. This implies that the carbon metallurgical balance are updated based on the analysis of pre-reduced pellets that were fed eight to sixteen hours earlier into the closed SAF, which contributes significantly to the instability of the smelting process.

In an attempt to develop a technique that would determine the level of chromite pre-reduction faster, a new analytical method using a combination of scanning electron microscopy (SEM), image processing, and computational techniques was investigated. Image processing is increasingly being applied in minerals processing and engineering (*e.g.* Jingzhong, Kewen, and Fan, 2013).

Materials and methods

Materials

The raw materials utilized in the industrial application of the pelletized chromite pre-reduction process consist of fine chromite ore, a carbonaceous reducing agent, and a clay binder (Kleynhans *et al.*, 2017a, 2017b, 2016, 2012; Neizel *et al.*, 2013; Beukes, Dawson, and van Zyl, 2010; Naiker, 2007). Samples of metallurgical-grade chromite (<1 mm), anthracite breeze (<1 mm), and fine FeCr (<1 mm) were received from a large South African FeCr producer applying the pelletized chromite pre-reduction process. Industrially produced pre-reduced pellets that had already been milled in preparation for the determination of the pre-reduction level using wet chemical analysis were obtained from the same FeCr producer. The chemical compositions of the chromite, anthracite, and FeCr samples are presented in Table I.

Wet chemical determination of pre-reduction

As previously mentioned, the degree (%) of chromite pre-reduction is currently determined using a wet chemical method. This method, applied by laboratories associated with FeCr smelters utilizing the pelletized chromite pre-reduction process, was described by Kleynhans *et al.* (2017a, 2016, 2012) and Neizel *et al.* (2013). In this method, the degree of chromite pre-reduction is calculated using the following equation:

$$\text{chromite pre} - \text{reduction } \% = \frac{\frac{\%\ \text{Sol Cr}}{34.67} + \frac{\%\ \text{Sol Fe}}{55.85}}{0.0121} \quad [1]$$

The soluble Cr (% Sol Cr) and Fe (% Sol Fe) in Equation [1] are extracted by reflux leaching of a pre-determined mass of the pre-reduced material with a hot sulphuric/phosphoric acid solution. The % Sol Cr in this aliquot is then established by means of the oxidation of the soluble Cr with potassium permanganate ($KMnO_4$) and subsequent volumetric titration with ferrous ammonium sulphate ($(NH_4)_2SO_4$) using diphenylamine sulphonate as an indicator. The % Sol Fe in the untreated aliquot is determined similarly, the only difference being that potassium dichromate ($K_2Cr_2O_7$) is used as the titrant. In this analytical method, the % Sol Cr and % Sol Fe represent these metals in the metallized state, *i.e.* the zero oxidation state. However, the level of Cr and Fe metallization is not directly related to the total pre-reduction, since pre-reduction is more commonly related to the removal of oxygen (Barnes, Finn, and Algie, 1983). Therefore, a

Table I

Chemical characterization of the metallurgical-grade chromite (<1 mm), anthracite breeze (<1 mm), and fine FeCr (<1 mm) received for a large FeCr producer. These materials were used to prepare laboratory-prepared pellet mixtures, described in the text

FeCr							
	%Cr	%Si	%Fe	%P	%Slag	%C	%S
Wt. %	50.32	3.07	36.65	0.01	2.08	7.20	0.05

Chromite				Anthracite			
ICP wt. %		EDS wt. %		ICP wt. %		EDS wt. %	
Cr_2O_3	45.37	Cr	27.21	SiO_2	10.09	Si	2.53
FeO	25.39	Fe	15.33	$Al2O_3$	3.13	Al	0.89
Al_2O_3	15.21	Al	6.39	FeO	1.62	Fe	1.19
MgO	9.83	Mg	6.37	CaO	0.8	Ca	0.18
SiO_2	1.72	Si	3.70	MgO	0.35	-	-
CaO	0.22	Ca	0.48	P	0.011	-	-
P	<0.01	Ti	0.37	S	0.59	S	0.68
-	-O	40.16	-	-	C	76.9	
			-	-	O	17.63	
				Proximate analysis			
				FC		75.08	
				Inherent Moisture		0.26	
				Ash		17.79	
				Volatiles		6.87	

constant of 34.67 was calculated by dividing the molar mass of Cr by 1.5, and a constant of 55.85 for Fe was determined by dividing the molar mass of Fe by 1. These constant factors were derived from the stoichiometrically balanced chemical reaction equations, wherein 1.5 mole of CO (containing 1 mole of oxygen removed from the oxide) forms in the metallization reaction for 1 mole of Cr, and 1 mole of CO forms in the metallization reaction for 1 mole Fe (Barnes, Finn, and Algie, 1983). Lastly, the constant 0.0121 is a chromite reduction value for typical South African metallurgical-grade chromite ore, which is calculated from (total Cr/34.67 + total Fe/55.85)/100. Although this value is indicated as a constant in Equation [1], it was actually calculated for each analysis to compensate for different chromite compositions.

Material preparation prior to SEM analysis

In this study, both laboratory-prepared pellet mixtures, as well as industrially produced pre-reduced chromite ore pellets, were utilized to validate the new analytical technique. The laboratory-prepared mixture compositions were prepared in such a manner that the mixtures mimicked different pre-reduction levels, which ranged from 15, 30, and 45, to 60% pre-reduction. Three sets of these mixtures were prepared, with each set containing varying carbon contents, *i.e.* 1, 3, and 5 wt.% fixed carbon (FC). The laboratory-prepared mixtures, which consisted of FeCr, chromite ore, and anthracite were dry-milled to the particle size specifications for industrial pre-reduction feed material, *i.e.* 90% of the particles smaller than 75 µm (D_{90} = 75 µm) (Neizel *et al.*, 2013; Kleynhans *et al.*, 2012). A Siebtechnik laboratory disc mill equipped with a tungsten carbide grinding chamber was used to avoid possible iron contamination. 50 g mixtures of raw materials were milled for 2 minutes to obtain the desired size specification. The particle size distribution was verified by laser diffraction particle size analysis utilizing a Malvern Mastersizer 2000. For this purpose, a much-diluted suspension of milled mixture was ultrasonicated for 60 seconds prior to the particle size measurement, in order to disperse the individual particles without the use of a chemical dispersant.

The laboratory-prepared pellet mixtures, as well as the industrially produced pre-reduced pellets that had already been milled in preparation for the determination of the level of pre-reduction, were mounted in resin and polished for cross-sectional SEM micrograph imagery. 1 g of the respective pellet mixtures was placed in 25 mm diameter mounting cups. The epoxy resin solution ratio was 100 g of resin to which 12 g of a slow-curing agent was added (50:6 mass ratio). The epoxy resin solution was stirred thoroughly in a plastic beaker for 3 minutes, then placed in a Speedivac vacuum degassing chamber model VDC 12, which ensures the elimination of air bubbles. A few drops of epoxy resin were added to each of the 1 g mixtures and mixed slowly to avoid stirring air into the mixture, but thoroughly to ensure homogenous mixtures. The mounting cups were then replaced in the vacuum chamber to remove any air bubbles. Additional epoxy resin was then added on top of these mixtures (over a label) to completely fill the 25 mm mounting cup. The mixtures in the mounting cups were then allowed to set overnight.

The epoxy resin-mounted samples were polished using an SS20 Spectrum System Grinder polisher, operated at an average speed of 300 r/min for grinding and 150 r/min for polishing. A 250 mm platinum 2 green cameo magnetic disc (comparable to 220-280 grit), a 250 mm platinum 4 red cameo magnetic disc (comparable to 600 grit), as well as 9, 3, and 1 µm diamond paste polishing cloths were used. The two

rough grits were operated by using continuous water flow as cleaner and lubricant, whereas diamond paste suspension poly lubricant was applied on the diamond paste cloths to obtain a smooth polished surface. Analytical grade ethanol was used to wipe the surfaces clean after polishing.

SEM image acquisition

Prior to SEM analysis, polished samples were rendered conductive by carbon coating in a Dentom vacuum DV-502A. An FEI QUANTA 250 FEG scanning electron microscope with an integrated OXFORD X-max EDS system, applying a backscattered electron compositional signal that operates with a 15 kV electron beam, at a working distance of 10 mm, 300 ns scan speed, and a magnification of 800×, was used to acquire SEM micrographs of the polished samples for further computational processing. Ten images were captured for every sample from random areas so that they were representative of the entire sample.

Image processing and analysis

All SEM micrographs were imported into and processed in MATLAB (MathWorks, 2017).

Results and discussion

Hypothesis

Elements with higher atomic numbers are indicated by lighter greyscale in SEM micrographs, while elements with lower atomic numbers are indicated by darker greyscale. For the composite chromite pellets considered in this paper, chromite ore particles that were not pre-reduced are therefore typically indicated as grey particles since they contain both heavy (Cr and Fe) and light elements (Si, Al). In contrast, metallized particles/droplets that form as a result of pre-reduction are typically indicated as white particles, consisting mostly of Fe and Cr. Kleynhans *et al.* (2012) presented SEM micrographs of an industrially pre-reduced chromite ore pellet indicating this principle. The EDS feature of the SEM-EDS used in this study was also used to confirm that particles appearing almost white in the polished samples contained mostly Fe and Cr. Considering the aforementioned, the basic hypothesis applied in the development of this new analytical technique was that the pixel count of white pixels (representing metallized particles), divided by the combined pixel count of white and grey (representing chromite particles) pixels can be directly related to the level of chromite pre-reduction determined by the current wet chemical method. This hypothesis can be mathematically expressed as:

$$\text{chromite pre} - \text{reduction } \% \cong \text{white pixel } \% = \frac{\text{white pixel count}}{\text{white pixel count} + \text{grey pixel count}} \quad [2]$$

Basic algorithm

The abovementioned basic approach was refined into a general algorithm consisting of several steps.

- The ten SEM micrograph images of a specific polished sample were cropped to the same size to remove the footer information (working distance, magnification) from each image.
- The ten cropped micrographs were stitched together into one image in order to ensure that image processing was not performed on a single micrograph, which might not be statistically representative of the overall sample.
- The pixel count of white pixels in the stitched image was determined, which represented metallized particles according to the hypothesis. A typical example of the application of this methodology is presented in Figure 1. Figure 1a indicates an original greyscale SEM micrograph, while Figure 1b is a zoomed-in section for illustration purposes. The actual pixels in greyscale can be seen on this zoomed-in image. This greyscale map was then converted into a matrix in MATLAB

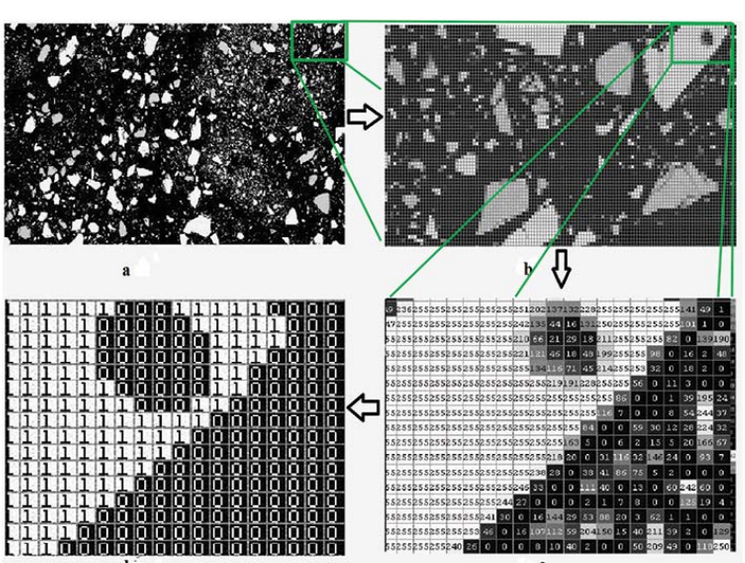

Figure 1—An example of a SEM micrograph processing scheme. (a) Original micrograph, (b) a zoomed-in area showing actual pixels, (c) showing greyscale intensity numbers of the corresponding pixels, (d) the converted binary black and white image

containing the actual greyscale intensity number array that ranges from 0 to 255, with 0 being black and 255 indicating white, as shown in Figure 1c. This greyscale intensity number matrix was then converted into a binary matrix of black and white, which is indicated by 0 and 1, respectively in Figure 1d. This was achieved by applying a fixed threshold value of 0.98. In Figure 2, an example of an image consisting of ten stitched SEM micrographs is presented, together with a histogram indicating the number of pixels as a function of the greyscale numbers 0 to 255, as well as the correlating threshold values from 0 to 1. In practice, the fixed threshold value of 0.98 implies that the number of white pixels was regarded as the pixels occurring at greyscale values larger than the correlating threshold number of 0.98.

- SEM micrograph image acquisition is subject to minor artefacts, *e.g.* noise from the SEM detector. Therefore, noise filtering was applied on the white pixel areas to avoid random white pixels from contributing to the white pixel count. Any individual white pixel that was not next to another white pixel was discarded in this step.
- The number of greyscale pixels, representing the pre-reduced and non-pre-reduced chromite ore particles, was then determined. Two threshold values were determined for this purpose, with the number of greyscale pixels between these threshold values regarded as being representative. However, fixed threshold values could not be utilized, since the degree of metallization achieved influenced the range of greyscale levels observed for pre-reduced chromite particles. The criteria for the selection of the two threshold values can be explained by also considering the example presented in Figure 2. The epoxy resin in which the sample material was mounted and the carbon reductant (anthracite) formed part of the black pixel areas that are typically represented by greyscale colours correlating to a threshold value of < 0.2. Therefore, these pixels were not considered in this greyscale pixel count calculation. The range of appropriate greyscale was determined by varying the threshold value between 0.2 and 0.98 in steps of 0.02. This was performed in an iterative loop in MATLAB, which enabled the testing of all possible greyscale threshold ranges between 0.2 and 0.98. This approach is further explained in the method validation section.
- The last step in the method was to determine the white pixel percentage, as indicated in Equation [2].

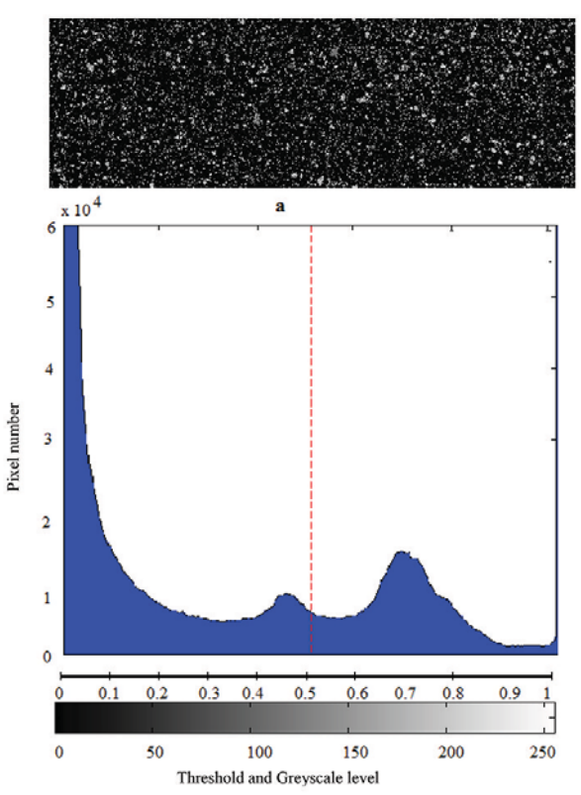

Figure 2—An example of (a) ten SEM micrograph images stitched together and (b) a histogram of pixel numbers as a function of greyscale level and the corresponding threshold values

Validation of the analytical technique with laboratory prepared pellets mixtures

In Figure 3, the correlation between the white pixel percentage (Equation [2]), determined with the algorithm described earlier and the chromite pre-reduction levels (%) of the laboratory-prepared pellet mixtures, are presented. It is evident from these results that there was a strong linear relationship (R2 = 0.998) between the white pixel percentage and the level of pre-reduction determined by the conventional wet chemical method.

From Figure 3 it is clear that the method can be applied successfully to determine the level of chromite pre-reduction, at least for laboratory-prepared samples. However, these laboratory-prepared samples do not exactly represent the real-world samples. Firstly, the metallized particles represented by FeCr particles in these laboratory-prepared samples were totally liberated from the chromite particles, as is illustrated in Figure 4. Additionally, the greyscale intensity of the chromite particles was relatively constant, since these

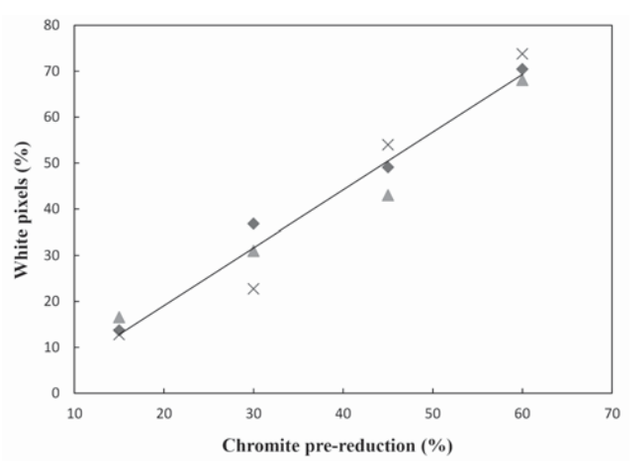

Figure 3—Correlation between white pixel percentage and chromite pre-reduction (%) for laboratory-prepared pellet mixtures. The diamonds, triangles, and crosses represent 1, 3, and 5 % carbon content, respectively

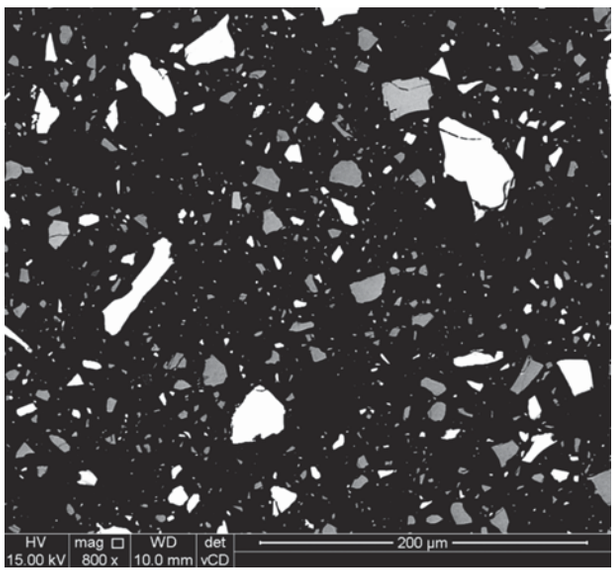

Figure 4—Polished sectional SEM micrograph of a typical laboratory-prepared pellet mixture

samples were not actually pre-reduced at elevated temperatures. This implies that the greyscale threshold ranges (step 'v' in the algorithm), which should be representative of the chromite particles, could have been chosen by checking the greyscale intensity numbers of a couple of chromite particles manually. Therefore, testing of the method on the laboratory-prepared samples was only the first step in the validation of the method.

Validation of the analytical technique with industrially pre-reduced pellets

In Figure 5, a typical SEM micrograph of a mounted polished industrial pre-reduced pellet mixture is presented. In contrast to the laboratory-prepared mixture (Figure 4), most metallized particles (white areas) are associated with chromite grains, since the metallized particles actually form from the chromite during pre-reduction at elevated temperatures. In addition, the greyscale intensity of the chromite particles varies substantially. When Cr and Fe migrate from the chromite spinel to the metallized phase, the remaining chromite particle(s) will consist of a higher percentage of elements with lower atomic numbers and will consequently appear darker than the non-pre-reduced chromite particle(s). Therefore, the importance of selecting an appropriate greyscale range, between two matching threshold values, as indicated in Figure 2 and step 'v' of the algorithm, becomes apparent. These two threshold values cannot be selected manually, since the range of appropriate greyscale intensity that matches pre-reduced and non-pre-reduced chromite particles cannot be predicted.

Actual chromite pre-reduction levels up to 80% have been achieved commercially on an industrial scale. However, according to thermodynamic calculations Cr oxides reduce at higher temperatures than Fe oxides (Kleynhans *et al.*, 2017a; Niemelä, Krogerus, and Oikarinen, 2004; Dawson and Edwards, 1986). Therefore, chromite pre-reduction above 60% is relatively uncommon in an industrial setting, since this would require elevated temperatures and exposure periods that become less feasible on a commercial scale. The industrial pre-reduced pellet mixtures received from the FeCr producer had pre-reduction levels varying between 38 and 50%. Figure 6 indicates the relationship between Cr and Fe metallization during chromite pre-reduction as a function of exposure time at 1 200°C (adapted from Dawson and Edwards, 1986). In this figure, the metallization and pre-reduction of the industrial pre-reduced pellet mixtures received are also indicated. It is evident that the increase in pre-reduction with time is not linear. However, for the purpose of the development of the alternative analytical technique, it was assumed that the level of pre-reduction over the pre-reduction percentage range of the industrial pre-reduced pellets received can be approximated by a straight-line correlation, as indicated by the dashed black linear line in Figure 6.

If the abovementioned assumption is valid, the white pixel percentage (according to Equation [2]) would be correlated to the chromite pre-reduction levels determined by the wet chemical technique (Equation [1]). This implies that the two threshold values determined in an iterative manner in step 'v' of the algorithm represent the optimal range of greyscale of the pre-reduced and non-pre-reduced chromite particles must stay constant to determine the white pixel percentage for the entire range of pre-reduction levels of the industrial pre-reduced pellet mixtures. From the results presented in Figure 7, it is evident that this is indeed the case. The chemically determined level of chromite pre-reduction (Equation [1]) of the industrial pellet mixtures correlated very well with the white pixel percentage calculated according to Equation 2 ($R^2 = 0.919$) for industrial pellet mixtures originating from two different rotary kilns.

Possible industrial application of the method

The objective of this study was to investigate the possible development of a SEM image processing method that would

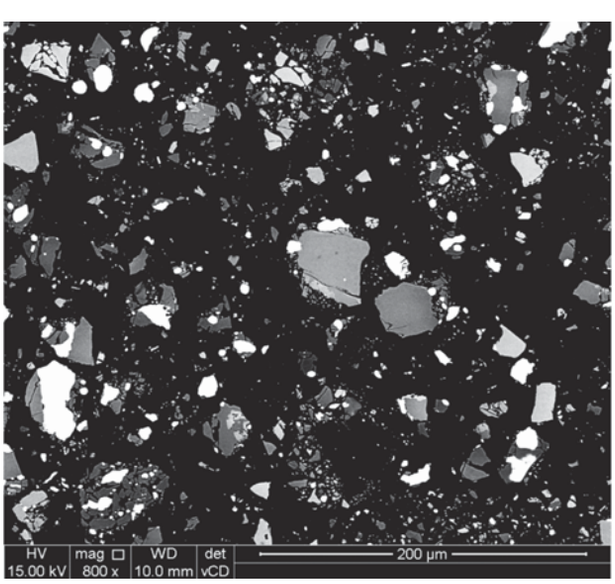

Figure 5—Polished sectional SEM micrograph of a typical industrial pre-reduced pellet mixture

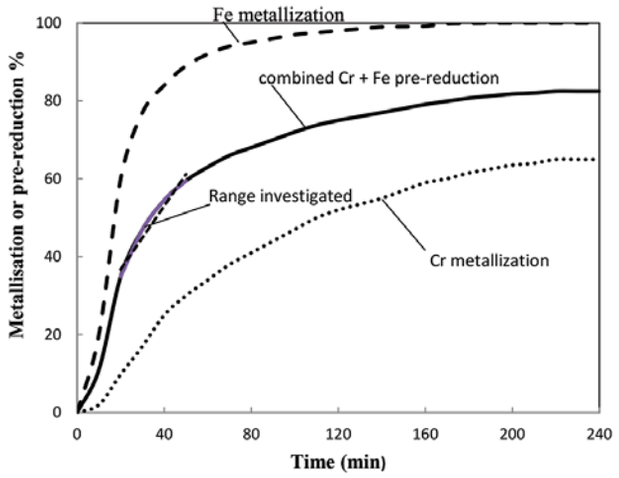

Figure 6—The pre-reduction of chromite in terms of the of metallization rates of iron, chromium, and their combination (adapted from Dawson and Edwards, 1986). The pre-reduction range evaluated in this study is illustrated by the dotted straight line that is superimposed on the pre-reduction line

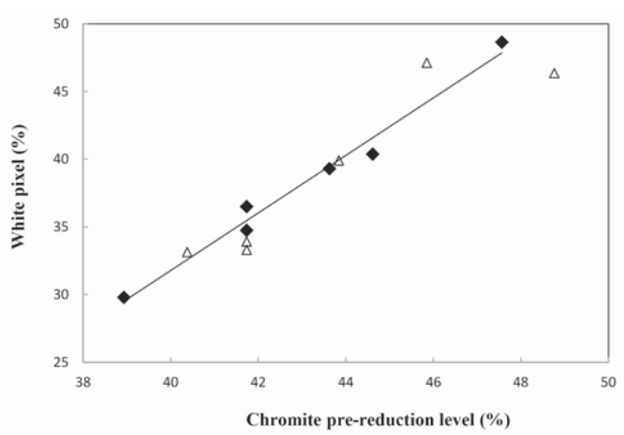

Figure 7—Correlation between white pixels percentage and chromite pre-reduction levels (%) of industrial pre-reduced pellets originating from two different kilns

enable the faster determination of chromite pre-reduction than the currently applied wet chemical method. From the results, it seems feasible that the developed method can be applied to determine chromite pre-reduction. However, two issues need to be addressed. Firstly, it needs to be established how the method can be applied to deliver quicker results, and secondly, the method needs to be validated over a wider range of pre-reduction levels than were considered in this study (38 to 50% pre-reduction).

Although not investigated as part of this study, it is suggested that actual pre-reduced pellets can be split into two halves, one of which can be polished relatively quickly. Industrial pre-reduced chromite pellets are strong enough to be polished in this manner (Kleynhans *et al.*, 2012). These polished cross-sectional pellets can then be mounted in fit-for-purpose aluminium mounting stubs, with metal grub screws to hold the pellets in place. This would eliminate the need to carbon-coat the pellets, since such cross-sectional polished pellets would be conductive. SEM micrographs can then be obtained for these polished pellets without the necessity for setting the sample material in a resin matrix prior to polishing. In this study, only milled pre-reduced pellets were received, and this aspect of method development was therefore not considered in the current scope of work.

As indicated in Figure 6, the industrial pre-reduced material mixtures considered in this study were within a limited range of pre-reduction levels, *i.e.* 38 to 50 %. The results indicated that this range of pre-reduction could be linearly related to the white pixel percentage (Figure 7). However, according to the nonlinear increase in chromite pre-reduction presented in Figure 6, it might not be possible to accurately relate the white pixel percentage to the level of pre-reduction with only a single set of optimally determined greyscale threshold values (step 'v' in the algorithm). Therefore, it is proposed that reference standards are prepared to represent various ranges of pre-reduction. These standard samples could be prepared by splitting pellets into two halves, one of which could be analysed using the wet chemical method to determine pre-reduction, while the other half could be polished and mounted as described in the previous paragraph. An analysis of a pellet with an unknown level of pre-reduction should then be conducted simultaneously (and at the same SEM settings) with a set of standard pellets with known levels of pre-reduction. This

would imply that a two-value threshold greyscale range (as indicated in step 'v' of the algorithm), which is applicable to the pre-reduction range covered by that specific set of standard pellets, would be determined. If the level of pre-reduction that was derived from the white pixel percentage of the unknown sample fell outside the range covered by the standards, then the unknown sample should be re-analysed with another set of standard samples that do represent the appropriate range.

Conclusions

As far as the authors could ascertain, the method described in this paper is the first SEM image processing method developed for the determination of chromite pre-reduction and described in the peer-reviewed public domain. In this method, the white pixel percentage (Equation [2]) is determined. A strong linear correlation ($R^2 = 0.919$) between chromite pre-reduction (%) determined by wet chemical analysis and white pixel percentage was observed for industrially pre-reduced pellets from two different kilns. This demonstrated that the method can be applied in industry to determine chromite pre-reduction accurately. Adaptations of the investigated method, which include polishing of pre-reduced pellets without setting in epoxy resin and the preparation of standards to be analysed with an unknown sample, are proposed to make the method industrially viable. Such a method could significantly reduce the effective turnaround time for determination of chromite pre-reduction, which would result in improved metallurgical control of the pelletized chromite pre-reduction process.

References

Abubakre, O.K., Muriana, R.A., and Nwokike, P.N. 2007. Characterization and beneficiation of Anka chromite ore using magnetic separation process. *Journal of Minerals and Materials Characterization and Engineering*, vol. 6, no. 2. pp. 143–150.

Barnes, A.R., Finn, C.W.P., and Algie, S.H. 1983. The prereduction and smelting of chromite concentrate of low chromium-to-iron ratio. *Journal of the South African Institute of Mining and Metallurgy*, vol. 83, March. pp. 49–54.

Beukes, J.P., Dawson, N.F., and van Zyl, P.G. 2010. Theoretical and practical aspects of Cr(VI) in the South African ferrochrome industry. *Journal of the Southern African Institute of Mining and Metallurgy*, vol. 110, no. 12. pp. 743–750.

Beukes, J.P., van Zyl, P.G., and Ras, M. 2012. Treatment of Cr(VI)-containing wastes in the South African ferrochrome industry - a review of currently applied methods. *Journal of the Southern African Institute of Mining and Metallurgy*, vol. 112, no. 5. pp. 347–352.

Biermann, W., Cromarty, R.D., and Dawson, N.F. 2012. Economic modelling of a ferrochrome furnace. *Journal of the Southern African Institute of Mining and Metallurgy*, vol. 112, no. 4. pp. 301–308.

Botha, W. 2003. Ferrochrome production through the SRC process at Xstrata, Lydenburg Works. *Journal of the South African Institute of Mining and Metallurgy*, vol. 103, no. 6. pp. 373–389.

Cramer, L.A., Basson, J., and Nelson, L.R. 2004. The impact of platinum production from UG2 ore on ferrochrome production in South Africa. *Journal of the South African Institute of Mining and Metallurgy*, vol. 104, no. 9. pp. 517–527.

Daavittila, J., Honkaniemi, M., and Jokinen, P. 2004. The transformation of ferrochromium smelting technologies during the last decades. *Journal of the South African Institute of Mining and Metallurgy*, vol. 104, no. 9. pp. 541–549.

Dawson, N.F. and Edwards, R.I. 1986. Factors affecting the reduction rate of chromite. *Proceedings of the 4th International Ferro-alloys Congress*, Rio de Janeiro, Brazil, 31 August – 3 September. Finardi, J., Nascimento, J,O, and Homem de Melo, F.D. (eds). Associacao Brasileira dos Produtores de Ferro-Ligas-Abrafe, Sao Paulo. pp. 105–113.

ICDA. 2013. Statistical Bulletin 2013. International Chromium Development Association, Paris, France.

Jingzhong, H., Kewen, X., and Fan, Y. 2013. An approach to distinguish and detection in nodular cast iron metallographic analysis. *Advances in Information Sciences and Service Sciences*, vol. 5, no. 3. pp. 10–16. DOI:10.4156/AISS.vol5.issue3.2

Jones, R. 2014. http://www.pyrometallurgy.co.za/PyroSA/. Accessed 1 June 2014.

Kleynhans, E.L.J., Beukes, J.P., van Zyl, P.G., Kestens, P.H.I., and Langa, J.M. 2012. Unique challenges of clay binders in a pelletised chromite pre-reduction process. *Minerals Engineering*, vol. 34. pp. 55–62. DOI:10.1016/j.mineng.2012.03.021

Kleynhans, E.L.J., Neizel, B.W., Beukes, J.P. and van Zyl, P.G. 2016. Utilisation of pre-oxidised ore in the pelletised chromite pre-reduction process. *Minerals Engineering*, vol. 92. pp. 114–124. DOI:10.1016/j.mineng.2016.03.005

Kleynhans, E.L.J., Beukes, J.P., van Zyl, P.G., Bunt, R.J., Nkosi, N.S.B., and Venter, M. 2017a. The effect of carbonaceous reductant selection on chromite pre-reduction. *Metallurgical and Materials Transactions B*, vol. 48. pp. 827-840. DOI:10.1007/s11663-016-0878-4

Kleynhans, E.L.J., Beukes, J.P., van Zyl, P.G., and Fick, J.I.J. 2017b. Techno-economic feasibility of a pre-oxidation process to enhance prereduction of chromite. *Journal of the Southern African Institute of Mining and Metallurgy*, vol. 117, no. 5. pp. 457–468.

MathWorks. 2014. http://www.mathworks.com, 2017. [Accessed 10 January 2017].

McCullough, S., Hockaday, S., Johnson, C., and Barcza, N.A. 2010. Pre-reduction and smelting characteristics of Kazakhstan ore samples. *Proceedings of the 12th International Ferroalloys Congress (INFACON XII)*, Helsinki, Finland. Vartiainen, A. (ed.). Outotec Oyj. pp. 249-262.

Murthy, Y.R., Tripathy, S.K., and Kumar, C.R. 2011. Chrome ore beneficiation challenges & opportunities – A review. *Minerals Engineering*, vol. 24, no. 5. pp. 375-380. DOI:10.1016/j.mineng.2010.12.001

Naiker, O. 2007. The development and advantages of Xstrata's Premus Process. *Proceedings of the 11th International Ferroalloys Congress (INFACON XI)*, New Delhi, India. Das, R.K. and Sundaresan, T.S. (eds.). Indian Ferro Alloys Producers Association. pp. 112–119.

Neizel, B.W., Beukes, J.P., van Zyl, P.G., and Dawson, N.F. 2013. Why is $CaCO_3$ not used as an additive in the pelletised chromite pre-reduction process? *Minerals Engineering*, vol. 45. pp. 115–120. DOI:10.1016/j.mineng.2013.02.015

Niayesh, M.J. and Fletcher, G.W. 1986. An assessment of smelting reduction processes in the production of Fe-Cr-C alloys. *Proceedings of the 4th International Ferroalloys Congress (INFACON IV)*, Rio de Janeiro, Brazil, 31 August – 3 September. Finardi, J., Nascimento, J,O, and Homem de Melo, F.D. (eds.). Associacao Brasileira dos Produtores de Ferro-Ligas-Abrafe, Sao Paulo. pp. 115–123.

Niemelä, P., Krogerus, H., and Oikarinen, P. 2004. Formation, characterisation and utilisation of CO-gas formed in ferrochrome smelting. *Proceedings of the 10th International Ferroalloys Congress (INFACON X)*, Cape Town, South Africa. South African Institute of Mining and Metallurgy, Johannesburg. pp. 68–77.

Riekkola-Vanhanen, M. 1999. Finnish expert report on best available techniques in ferrochromium production. *Finnish Environmental Institute*, Helsinki. pp. 1–50.

Takano, C., Zambrano, A.P., Nogueira, A.E.A., Mourao, M.B., and Iguchi, Y. 2007. Chromites reduction reaction mechanisms in carbon-chromites composite agglomerates at 1773 K. *ISIJ International*, vol. 47, no. 11. pp. 1585–1589. ◆

http://dx.doi.org/10.17159/2411-9717/2017/v117n11a10

Target fragmentation for efficient loading and crushing – the Aitik case

by A. Beyglou, D. Johansson, and H. Schunnesson

Synopsis

Blast-induced fragmentation has a significant influence on the operational efficiency of open pit mines, especially on loading and crushing, the two immediate tasks after blasting. This study presents an empirical method to determine the target fragmentation for efficient loading and crushing at the Aitik mine in Sweden. In the study, the loading efficiency of rope shovels was correlated to the energy consumption and throughput of a gyratory crusher. Two photographic techniques were utilized to assess the feed fragmentation, considering the lithological origin of the ore as an indicator of hardness. The results indicate ore hardness is most influential in mid-range fragmentation, with a marginal effect in coarser fragmentations. The influence of fragmentation is more pronounced in the coarse region, with a sudden reduction in efficiency for P_{80} values coarser than 800 mm. The results suggest tailoring the fragmentation to a P_{80} of 600–800 mm could lead to higher operational efficiency at Aitik.

Keywords

open pit, fragmentation, loading, crushing, energy, efficiency.

Introduction

Energy efficiency in operations is vital to achieving sustainability in the mining and metals sector. On the one hand, adverse environmental aspects of inefficient energy consumption and their consequent costs to mining companies are driving the industry towards leaner and more responsible operations. On the other hand, high prices of energy, volatile markets, and falling commodity prices put pressure on mines to cut costs and optimize their operations as a whole. Consequently, increasing efficiency has become a priority in many base and precious metals mines.

A great deal of the total energy consumption in most mine sites can be traced to comminution, the process of reducing the size of rock particles to extract their valuable components. Despite differences in their quantitative figures, most studies agree that milling, *i.e.* crushing, grinding, and separation, is the largest consumer of energy (Napier-Munn, 2015; Ballantyne and Powell, 2014). Although the energy, and eventually costs, for each unit operation are site specific, the figures suggest a more or less equal share in costs for mining and milling processes. Curry, Ismay, and Jameson (2014) evaluated the total costs of 41 open pit operations and found that around 40% of the total costs correspond to operational mining activities, while milling typically accounts for 49%. Therefore, any improvement in the efficiency of either the mining or the milling operation contributes to the overall economy of the operation. There is, however, a fundamental difference between the two; process optimization in the mine revolves around blast-induced fragmentation as the final deliverable of the mine to the crusher, while the crusher product is the initial input for the mill. Such a distinction defines the crusher as the link between the mine and the mill. It also signifies the necessity to assess the downstream effects in a stepwise manner along the comminution process, *i.e.* direct influence of run-of-mine (RoM) fragmentation on loading and crushing, before the next comminution stage.

This study examines the influence of fragmentation on loading and crushing in mines. The goal is to define an optimum range of fragmentation to yield maximized productivity in these two processes. Such information can be implemented in future models to evaluate the overall influence of fragmentation on the entire mining process, thus helping to improve operations. A gyratory crusher was observed for 20 days and digital images of the crusher feeder were used to assess the fragmentation of each truck cycle, both quantitatively and qualitatively. The fragmentation was then correlated to ore type and efficiency to evaluate its margins of influence on loading and crushing.

Background

From a mine-to-mill point of view, blasting is a crucial step in the comminution chain. The

* *Luleå University of Technology, Luleå.*

 ISSN 2225-6253. Paper received Jun. 2016; revised paper received Feb. 2017.

procedures before blasting determine the level of fragmentation and uniformity of the particle size distribution. This, in turn, dictates the efficiency of subsequent tasks in the operation, including loading and crushing. The effects of fragmentation are first seen in loading; no matter what type of machinery is used, fragmentation plays a leading role in loading efficiency. A well-swollen muckpile with a fragmentation tailored to the type and size of the machinery will yield fewer passes and smoother, more efficient loading compared to an inconsistent and disproportionately fragmented muckpile (Williamson, McKenzie, and O'Louglin, 1983; Hawkes, Spathis, and Sengstock, 1995; Onederra *et al.*, 2004; Singh and Narendrula, 2006).

The efficiency and productivity of loading equipment have been studied extensively, especially for electric rope shovels. However, because several qualitative and quantitative descriptors are also associated with loading, it is difficult to determine the individual influence of any one of these on efficiency. For example, loading is influenced by fragmentation, make and design of loading equipment, operator proficiency, loading trajectory, swell, and muckpile shape and looseness (Bellairs, 1987; Hendricks, 1990; Singh and Narendrula, 2006).

Early studies on electric shovels attempted to correlate digging performance of shovels to muckpile fragmentation by using time studies combined with logs of voltage and current in the hoist and crowd motors of rope shovels (Williamson, McKenzie, and O'Louglin, 1983; Hendricks, 1990; Patnayak *et al.*, 2008). Dipper fill factor, dipper payload, dig rate, and frequency of dig cycles have also been used as performance indicators for rope shovels (Onederra *et al.*, 2004; Halatchev and Knights, 2007).

According to Hendricks (1990) and Onederra *et al.* (2004), dig cycle times are not specifically related to digging effort or fragmentation. But digging trajectory, which depends on operator skills, has a great influence on shovel performance. Using geostatistics and data from monitoring systems, Halatchev and Knights (2007) showed basic key performance indicators (KPIs) such as shovel payload can be used to evaluate digging performance and muckpile properties. Based on 20 production blasts in two open pits, Sanchidrián, Segarra, and López (2011) developed a model for loader productivity which took into consideration the rock strength and density, as well as explosive energy and dipper capacity. Hansen (2001) reported measurements of dipper payload for improving shovel performance as well. Patnayak *et al.* (2008) confirmed the large variability in performance indicators and stressed that these studies should be conducted over a larger number of load cycles to yield meaningful results. All these studies emphasize the complexities involved in assessing loading performance. Owing to operator dependence and variability in muckpile conditions, researchers have not as yet been able to establish a definite correlation of muckpile properties with loading efficiency, but it is possible to evaluate loading performance by statistically assessing basic KPIs over a large number of load cycles.

The next step in the production chain is primary crushing. This is the second mechanical breakage step after blasting; it prepares the RoM ore for further processing in the mill. Crushing typically consumes much less energy than grinding, but it still accounts for a large portion of energy costs in a typical mine operation, and its product has an enormous influence on downstream processes (Murr *et al.*, 2015).

Gyratory crushers play an important role in large scale mines as primary crushing units. As crushing is the link between the mine and the mill, it has two-fold potential for process improvement. Crushing efficiency is determined not only by the design and operational factors of the crusher itself, but also by characteristics of the RoM feed. Therefore, any effort to improve the energy efficiency of crushers must consider both factors, not to mention the requirements for the crusher's product (Evertsson, 2000; Herbst, Lo, and Flintoff, 2003).

The power drawn by gyratory crushers depends on many factors, including size distribution, hardness and shape of the feed, as well as liner profile, feeding rate, closed side setting (CSS), eccentric speed and stroke of the mantle. This complex and dynamic system has been simulated in several models (McKee and Napier-Munn, 1990; Evertsson, 2000; Pothina *et al.*, 2007). Studies show that fragmentation and ore hardness are the most prominent feed characteristics affecting crushing energy consumption (Eloranta, 1995). After much research, scientists at the Julius Kruttschnitt Mineral Research Centre (JKMRC) developed a simulation package to optimize mineral processing circuits (McKee and Napier-Munn, 1990). Included in this package is a model for predicting crusher power draw and product size distribution. However, these models have been developed as tools for the optimization of the entire mineral processing circuit and do not comply with stand-alone crushers (Pothina *et al.*, 2007). Moreover, they are based on comminution theories, such as Bond's work index (Bond and Whitney, 1959), and they depend on a large database of site-specific and machine- specific data gathered over years of research. The complexity and extensive data requirements of these models make them difficult to use in typical industrial conditions.

Pothina *et al.* (2007) developed an analytical model for energy consumption of gyratory crushers by using CSS and feed size variations. However, the feed fragmentation in this model is based on the Kuz-Ram model (Cunningham, 1983) and is assumed to be a function of burden and spacing, regardless of all other factors affecting blast fragmentation. In reality, it is well known that blast-induced fragmentation in mines varies because of several uncontrollable factors. Variations in lithology, structural geology, explosive performance and precision of drilling and blasting are some of the factors leading to inconsistencies in RoM fragmentation. Therefore, such assumptions about the relationship between burden/spacing and crushing energy are of little practicality in day to day production blasts.

For a specific site, an empirical approach yields more hands-on conclusions. It provides a simple but statistically reliable understanding of the influence of the feed size of a certain ore on the energy consumption of a certain crusher. In practice, the mine has the ability to produce different ore fragmentations by manipulating the blasting set-up. It is, therefore, possible for the mine to tailor the feed material in such way that loading and crushing are performed at peak efficiency. Despite the aforementioned uncertainties in blast fragmentation, having a target fragmentation in mind for a

specific ore helps the mine modify the blast set-up to yield a fragmentation as close as possible to the target. This has a great influence on operational efficiency in the long term.

Aitik mine

At 3 km long, 1.1 km wide, and 450 m deep, Aitik is one of the largest open pit copper mines in the world. It is situated about 60 km above the Arctic Circle in northern Sweden and has been owned and operated by Boliden Mineral AB since 1968. The Aitik deposit comprises metamorphosed plutonic, volcanic, and sedimentary rocks. The ore zone consists of biotite gneiss, biotite schist, and muscovite schist with dykes of pegmatite cutting through.

Despite its low grade ore (0.22% copper on average), Aitik is considered one of the most efficient open pit mines in operation. In 2015, its annual production of ore reached more than 36 Mt, yielding about 67 kt of copper, 61 t of silver, and 2 t of gold. Its efficiency stems from its in-pit crushing and conveying system, as well as advanced technological infrastructure and monitoring systems. These permit the mine to audit and improve the operation continuously. In fact, the well-coordinated fleet management system and comprehensive data collection during all stages of operation provided a solid platform for this study. Data from different sources could be extracted and utilized to correlate fragmentation to both loading and crushing.

Data collection and methods

The goal of this study was to investigate the effects of fragmentation on the efficiency of loading and crushing. It also considered rock hardness, as crushing efficiency is sensitive to the hardness of the ore. Because different factors are important at different stages of a mine's production, it is crucial to define a unit mass of ore and follow it up the production chain. The most suitable unit for such a purpose in a fully operational mine is the haul truck, as it can be tracked from the muckpile to the crusher by means of fleet data. A schematic illustration of the ore-tracking method and factors extracted at each stage is presented in Figure 1.

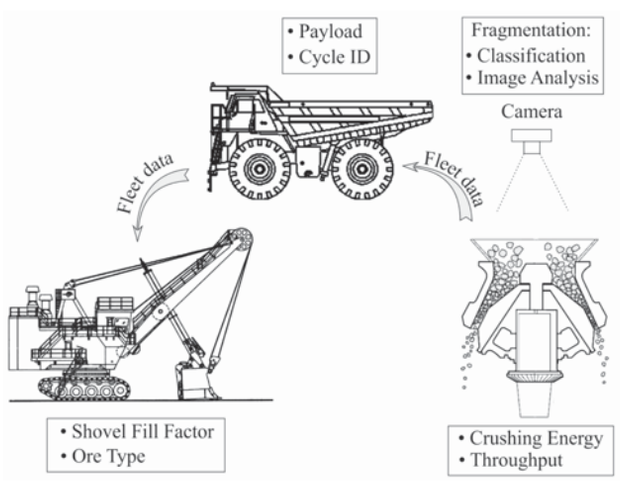

Figure 1—Scheme of data follow-up and ore tracking during loading, hauling, and crushing

As seen in Figure 1, the data corresponding to each truckload was acquired by back-tracking it from the targeted crusher to the muckpile. Each ore unit (*i.e.* one truckload) was photographed after the truck dumped it in the crusher inlet. The photographs were used to assess the fragmentation using image analysis and ordinal classification. The energy consumption in the crusher was recorded for the entire cycle and was normalized to the tonnage of crushed ore. By incorporating fleet data, each truck could be traced to its corresponding rope shovel, thus allowing loading efficiency and the coordinates of the ore unit to be extracted as well. The loading coordinates were later cross-referenced with geological data to define the lithological origin of the ore. Unfortunately, complex geology, uncertain mechanical properties, and low spatial resolution of lithological information in the mine did not permit a strict distinction of ore types for the studied cycles. Hence, the mine was roughly divided into two main areas: north and south. During the study, the mined ore in the north area had a large content of muscovite schist, while the south ore contained a high amount of biotite gniess. A summary of the mechanical tests on specimens of these ores is presented in Table I.

All truckloads were traced back to their original coordinates in the mine and were distinguished to be from either the north or south area. This over-simplified distinction between the two is due to uncertainties in the lithological content of truckloads as well as large variations in hardness between different specimens. As the mechanical properties of these ores do not fit within the scope of this study, the results were simply separated by origin. Therefore, the following comparisons of the two ores do not take into consideration the numerical difference in hardness of the material, but simply indicate the origin of the ore as either north or south, considering that south ore is generally harder than north ore. Additionally, since the nominal density of both ore types is identical, density differences were not considered in the analysis of loading or crushing and are not given in what follows.

Given the large quantity of the data in this scheme, each of the aforementioned stages included careful filtering and selection procedures to keep external factors at bay. The 20-day study period provided fully compatible data for 225 truckloads, equivalent to approximately 50 kt of ore.

Fragmentation

Assessing blast-induced fragmentation has been one of the most challenging tasks for both researchers and the industry. Until now, the only reliable method to quantify the

Table I

Comparison of hardness of the two main ore types in Aitik

Main ore	North [MPa]	South [MPa]
	Muscovite schist	Biotite gneiss
Schmidt hammer (Sjöberg, 1999)	46.0	81.1
Point load test (Valery *et al.*, 2002)	28.6	112.1
Point load test (Bergman, 2005)	67.1	121.0
UCS (Hantler, 2015)	73.5	127.8

sizedistribution of a muckpile has been physical sieving, yet it yields reliable results only if the process is carried out carefully using adequately large samples and in a controlled environment. Because of its time-consuming and costly nature, this method is generally disregarded by industry and the research community; few studies present full-scale sieving results, and they all agree on its practical difficulties (Ouchterlony, Bergman, and Nyberg, 2010; Wimmer *et al.*, 2015).

Since the 1980s, photographic techniques have been used as non-contact measurement tools to estimate the size distribution of muckpiles. Image-based fragmentation assessment started with the visual comparison of muckpiles to scaled photographs; it later advanced to 2D image analysis techniques, and more recently broadened to include more complicated 3D analysis using laser scanning or photogrammetric methods (Thurley, Wimmer, and Nordqvist, 2015). One of the simplest methods of using photographs to assess fragmentation is to compare the target muckpile to reference images of standardized muckpiles. An early example of this method is the 'Compaphoto' technique, introduced by Aswegen and Cunningham (1983). The technique is based on visual comparison of the target muckpile to scaled photographs of standardized muckpiles and uses the Rosin Rammler function to estimate the particle size distribution. In a recent study, Wimmer *et al.* (2015) used a similar but customized approach in the so-called quick rating system (QRS). This method was developed to classify the fragmentation of LHD bucketloads into four classes of median fragment size (P_{50}) and three subclasses of uniformity index (n) varying from 0.6 to 2.2. These researchers also compared the results from a rating system, 2D and 3D image analysis, and physical sieving of LHD bucketloads. They reported that the quick rating system showed consistent results between users, except for fine-medium material of an inhomogeneous character. The method was also found reliable – if used carefully – and accurate in comparison with 2D image analysis.

2D image analysis techniques have been studied extensively, with various disadvantages pointed out by several researchers (Hunter *et al.*, 1990; Chavez *et al.*, 1996; Maerz and Zhou, 1998; Lathham *et al.*, 2003; Thurley and Ng, 2005; Sanchidrián *et al.*, 2009; Spathis, 2009). Because of the method's shortcomings, the repeatability of 2D image-based measurements is generally poor. Segregation of differently sized particles in a muckpile, the lay and aspect ratio of fragments, overlapping fragments, insufficient and biased sampling, imaging inconsistency (lighting, scaling, and perspective), inaccurate automatic delineation, and time-consuming and user-dependent manual delineation are some of the drawbacks of this technique. If done carefully, however, 2D image analysis can provide insights into the trends of variations in fragmentation; these trends may not describe the entire size distribution accurately, but they are still more practical than physical sieving and have been proven useful over years of experience in the industry.

The errors and shortcomings of both classification and image analysis techniques are well known. However, with consistent measurement procedures and statistically reliable sampling, researchers can identify the trends of variation with either method. Maerz and Zhou (1998) state:

'Processes such as blasting [and crushing] can be characterized by looking at the relative differences between two measurements, and consequently the absolute error is not important.'

On the one hand, the advantage of the classification method lies in its fast and straightforward procedure which allows a large number of samples. However, it only shows subjective trends in the mean RoM fragmentation with little information on the details of size distribution. 2D image analysis, on the other hand, is limited to a much smaller number of samples because of the time-consuming delineation procedure. Yet it yields a detailed quantitative assessment of particle size distribution. Given their respective strengths and weaknesses, this study used both 2D image analysis and ordinal classification of fragmentation and compared the results.

The gyratory crusher at Aitik includes two bays where the trucks dump the ore directly into the crusher inlet. Each bay is equipped with several closed-circuit cameras with real-time feed and a stationary camera aimed at the crusher inlet. In this study, the bay cameras were used to double-check the time-tag of dumps, while the camera aimed at the inlet was used to assess the feed fragmentation for each crushing cycle. This latter camera provided a continuous video feed at two frames per second, and fragmentation was based upon single frames of each cycle sampled every five seconds, as each cycle typically took 4–6 minutes to finish. Consequently, each crushing cycle was assigned a series of images with a five-second interval. A sample image of the crusher inlet with its dimensions is presented in Figure 2.

The study assessed the feed fragmentation of crushing cycles in two stages. In the first stage, all image sequences were classified into five ordinal categories, with class 1 the finest and class 5 the coarsest fragmentation. In the second stage, eight cycles from each class were selected and then analysed using Split-Desktop image analysis software (Kemeny *et al.*, 2002).

One of the authors performed the five-class rating of the cycles based on a visual comparison of all images of the cycle with a series of predefined sample images for each class. Figure 2 shows samples of each class. The choice of guide samples for classes was based on image analysis of three sample images per class. The median fragment size (P_{50}) and 80% passing size (P_{80}) values of images were extracted before classification and used to define more or less equal size-spans for each class in such way as to cover the entire range of observed fragmentation. The numerical values were not used to classify cycles, as the rating was solely qualitative, *i.e.* comparing the image sequence of each cycle to guide samples and rating them from 1 to 5. The range of pre-defined values for the P_{50} and P_{80} of each class is presented in Table II.

The image sequences from selected cycles were inspected carefully for any external factor affecting the crushing cycle and feed size at the crusher inlet, *e.g.* interruptions in the cycle due to boulders. The circular steel protector of the mantle was visible in almost all images, hence its diameter was measured and used as a scale to estimate fragment size. Since the camera was stationary and perpendicular to the crusher inlet, all images included identical viewpoints, thus minimizing errors introduced by perspective. The crusher

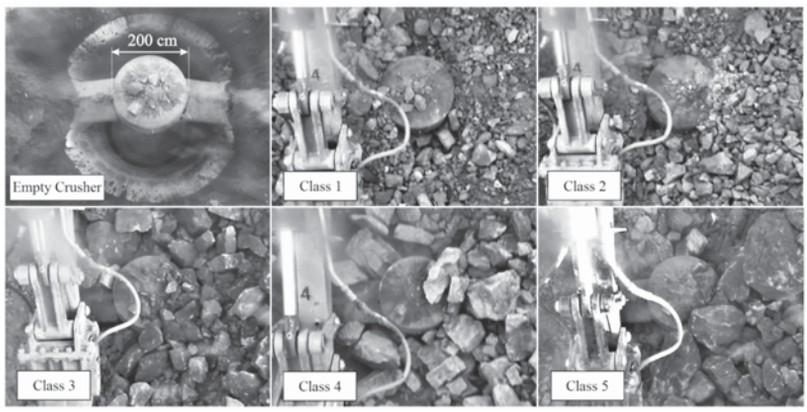

Figure 2—Guide samples for ordinal classification of fragmentation at the crusher inlet

Table II

Pre-defined approximation of P_{50} and P_{80} sizes for fragmentation classes

Class	P_{50} ± stdev. [mm]	P_{80} ± stdev. [mm]
1	209 ± 39	464 ± 51
2	336 ± 54	615 ± 73
3	510 ± 59	785 ± 74
4	653 ± 77	994 ± 105
5	820 ± 91	1174 ± 156

inlet was lit by artificial light to reduce lighting variations. Finally, all images were enhanced by increasing their contrast and sharpened using the Unsharp Mask tool in Adobe Photoshop™ for better particle delineation (Wimmer *et al.*, 2015).

All images were delineated manually by only one user to minimize the user-dependency of the results. Due to uncertainties in theoretical estimation of fines, no fines factor was used in the analysis, and only visible particles were included in size distribution curves (Spathis, 2009). Finally, the 50% and 80% passing sizes for each cycle were extracted and correlated to the loading and crushing efficiency of cycles. However, it should be mentioned again that despite all efforts to minimize errors, the image analysis technique is not in any way comparable to full-scale sieving. The P_{50} and P_{80} values are not expected to represent the true size distribution of the feed. Thus, the results can only be considered quantitative figures suitable to compare the size distributions of different feeds and identify trends.

Crushing efficiency

The gyratory crusher studied here is an Allis-Chalmers Superior 60-109. The diameter at the lower part of the mantle is 2770 mm, and the closed side setting (CSS) of 160–180 mm determines the crusher product. Depending on the characteristics of the ore, the coarsest particles after crushing vary from 350 to 400 mm in size (Bergman, 2005). During the study, the CSS and the eccentric speed of the crusher were kept constant, so the only variable was the torque applied on the motor for effective breakage, measured in terms of power draw (kW). The power draw at the crusher motor was sampled every nine seconds. The raw data was then broken down into crushing cycles by cross-referencing the power draw curve to the fleet logs, and each cycle was given a unique ID.

Only the single-dump cycles were selected for further analysis. The single-dump cycles, as opposed to multi dump (choked) cycles, correspond to the crushing cycles in which the material from a single truck is dumped into the feeder; no other material is dumped until the cycle is finished. Figure 3 shows samples of single-dump and multi-dump cycles of the crusher. The reason for this selection is that gyratory crushers perform slightly differently under choked conditions (Eloranta, 1995). A choked crusher will go through a continuous material flow with heavier particle interaction and a varying force of gravity. This, in turn, could introduce bias into the energy consumption measurements. In addition, at the study mine, the blending of material in multi-dump cycles made it impossible to trace the ore to a specific coordinate in the mine, possibly compromising the material follow-up as well as energy and tonnage estimation.

All crushing cycles included in the study were from single dumps. Each cycle started as soon as the material entered the idle crusher and ended when all the material had passed through and the status returned to idle. In this way, the start and end of all cycles could be distinguished precisely, and the influence of the rise and fall in torque of the motor was evident for all cycles. Furthermore, the duration of each cycle could be accurately extracted for further analysis of momentary throughput.

The energy consumption in the crusher was calculated for each cycle by integrating the area under the power-time curve (Figure 3). The consumed energy was normalized to the tonnage of the crushed material from the fleet logs, and energy consumption per unit mass was extracted and presented in kWh/t for each crushing cycle. As the tonnage and duration were known for each cycle, the instantaneous throughput of the crusher could also be calculated.

Loading efficiency

The load and haul fleet at Aitik mine comprises a variety of electric and hydraulic shovels combined with differently sized haul trucks. Loading efficiency is comparable only between

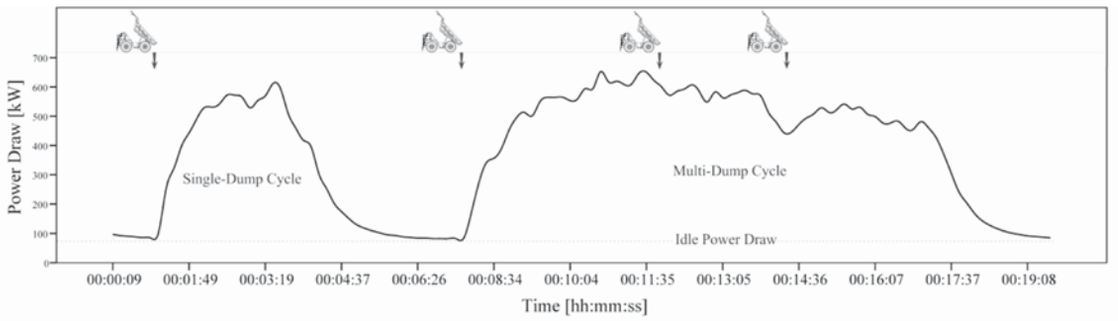

Figure 3—Power-time curve for single- and multi-dump crushing cycles with their corresponding dump log

Table III

Summary of the results from classification of feed fragmentation

		Ore type	Truck count	Crushing energy [kWh/kt]		Crusher throughput [t/min]		Shovel fill factor [%]	
				Mean	Stdev.	Mean	Stdev.	Mean	Stdev.
Fragmentation Class	1	North	29	70.46	19.59	80.01	18.3	87.88	10.34
		South	10	82.91	13.71	75.70	11.21	78.67	9.96
	2	North	35	92.36	21.49	79.12	20.55	90.89	7.46
		South	24	137.04	34.66	68.05	16.16	93.32	8.44
	3	North	36	117.95	28.80	74.46	20.34	84.30	9.87
		South	33	149.21	28.77	64.99	17.34	80.58	14.13
	4	North	15	176.38	31.71	57.52	10.16	74.12	11.95
		South	20	192.30	36.16	52.89	14.92	65.32	10.08
	5	North	11	190.03	19.18	57.39	9.27	63.49	13.11
		South	12	207.57	45.08	49.39	10.58	60.62	10.35

similar types and makes of machinery, as the mechanisms and capacities of different rope shovels vary widely. Consequently, all truck cycles included in the study were filtered to include only identical shovels loading identical trucks, namely P&H4100C shovels with an 81.7 t dipper capacity loading CAT793 trucks with a capacity of 227 t. When the truck payloads were comparable, the crushing cycles could be evaluated and the loading efficiency determined for identical shovel-truck combinations.

The studied trucks were normally loaded to full capacity by three to five shovel passes, depending on the fragmentation and diggability of the muckpile. The payload and number of shovel passes to fill a corresponding truck were used to estimate the mean payload of the dipper in each cycle. The mean payload of each dipper pass was compared to the nominal capacity of the dipper, and the mean fill factor was calculated and presented as a percentage of full dipper capacity.

Although loading is an operator-dependent task, this was not considered in the analysis because of the number of cycles and operators. However, in a previous study of Aitik, the authors compared the performance of different operators and concluded the influence of muckpile diggability on loading is greater than that of operator skills (Beyglou *et al.*, 2015). Therefore, the present study assumed the operator effect to be negligible, especially as similar operators operated all shovels in circulation during the study.

Results and analysis

A summary of the classification results is presented in Table III. Mean values for crushing energy, crusher throughput, and fill factor of shovel dipper are separated by ore type (north/south) and presented for each fragmentation class.

Table III shows that the crushing energy consumption gradually increases as fragmentation shifts from fine to coarse. Meanwhile, throughput shows a consistent decrease with increasing fragment size. The fill factor shows the highest loading efficiency for class 2 fragmentation (*i.e.*, finer fragmentation); it gradually decreases as fragmentation reaches the very coarse end (class 5). To determine the statistical distribution of values in each class, Figures 4–7 compare means and quartiles across fragmentation classes.

As seen in Figure 4, the mean energy consumption shows a consistent stepwise increase from class 1 (very fine) to 5 (very coarse). For all fragmentation classes, the south ore (harder ore) consumes more energy than the north ore (softer ore). The difference is largest for classes 2 and 3, implying that ore hardness is less influential for crushing very fine or very coarse fragmentations. In addition, the increase in energy consumption from class 4 to 5 is smaller than that between other classes in both ores, especially from class 3 to 4, which shows the largest difference. This indicates that fragmentation is less influential when the particles are larger than a certain size. This can be seen in the distribution plot as well. However, the distribution of the values exhibits rather large variation spans in all classes. Overall, the variations increase as fragmentation becomes coarser. The largest spans, for classes 4 and 5, show a more or less similar statistical range of variation. It is also apparent that the lower and upper quartiles lie relatively far

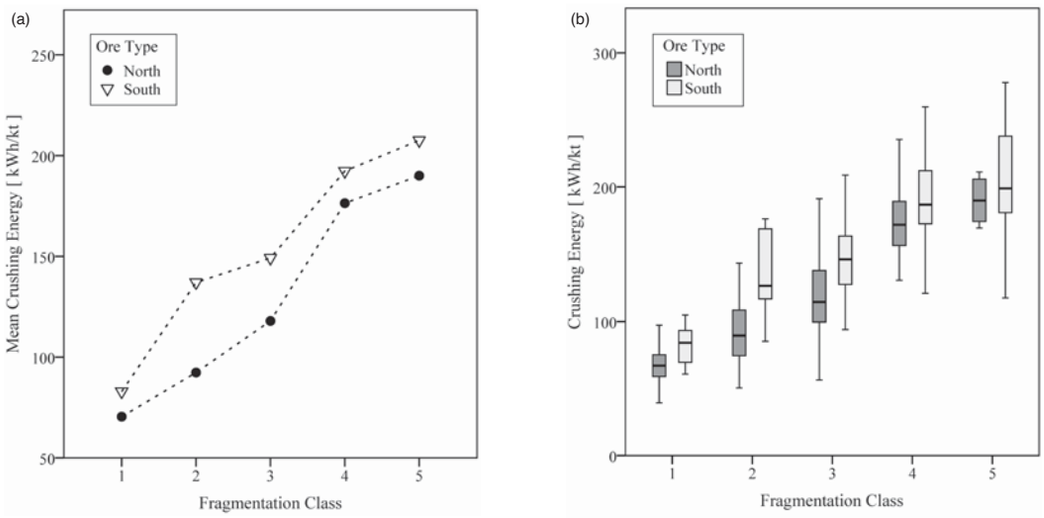

Figure 4—(a) Mean crushing energy, (b) statistical distribution of crushing energy within each fragmentation class

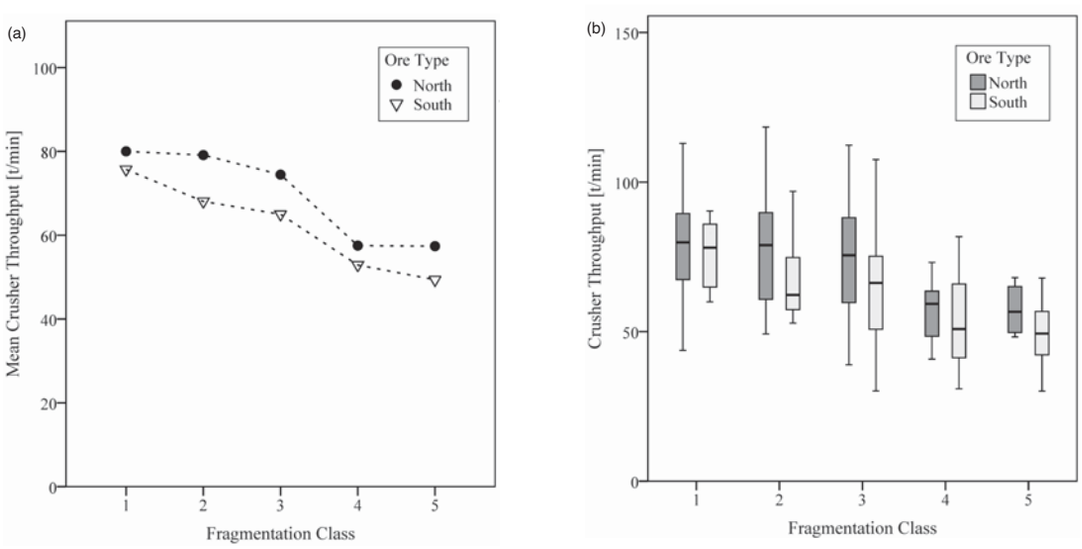

Figure 5—(a) Mean crusher throughput, (b) statistical distribution of throughput for fragmentation classes

away from the minimum and maximum values, suggesting that the statistical spread includes a wide scatter.

The analysis of mean crusher throughput (Figure 5) shows that the largest decrease in throughput occurs between class 3 and class 4. There is a slight decrease from classes 1 to 3, a significant drop from classes 3 to 4, and a marginal difference between classes 4 and 5. In all classes, the south ore shows a 5-10% reduction in throughput compared to the north ore. As in energy consumption, the differences between north and south ores are more pronounced in classes 2 and 3 and marginal in classes 1, 4, and 5. The distribution of throughput demonstrates large variations in classes 1 through 3, with more or less similar ranges in all quartiles, and classes 4 and 5 showing comparatively smaller, but identical throughputs overall.

The fill factor of the shovel dipper (Figure 6) shows a dissimilar trend. Firstly, the influence of ore type is not as pronounced for loading as for crushing. North and south ores show closely comparable means and medians. Secondly, the fill factor in class 1 is lower than in class 2, indicating medium-fine fragmentation has higher diggability than very fine fragmentation. The fill factor gradually decreases from classes 2 through 5. The quartiles in the distribution plot also show a decrease, with a marginal difference between the two ores.

The results of the classification of feed fragmentation give an overview of the trends in loading and crushing efficiency over a relatively large sample population (n=225). In contrast, the image analysis results, presented in Figure 7, provide a detailed view of about 40 single crushing cycles. Since P_{80} and P_{50} of the size distributions were strongly correlated (Figure 7a), the image analysis results are presented only in terms of P_{80}. More or less similar trends were observed for P_{50}, but are not presented here.

The plot of crushing energy against P_{80} of the feed (Figure 7b) demonstrates a correlation similar to that found

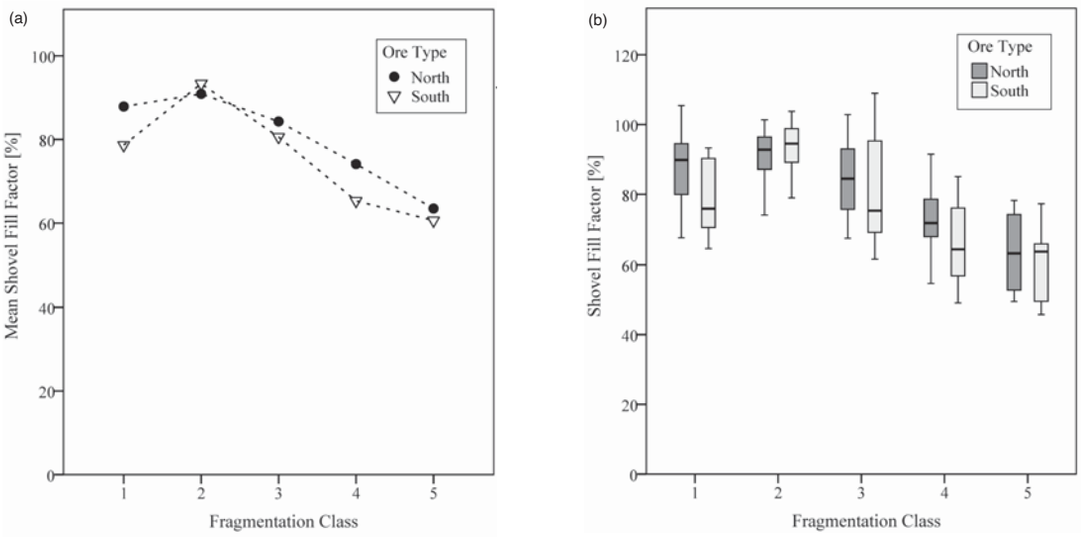

Figure 6—(a) Mean fill factor of shovels, (b) statistical distribution of fill factor within fragmentation classes

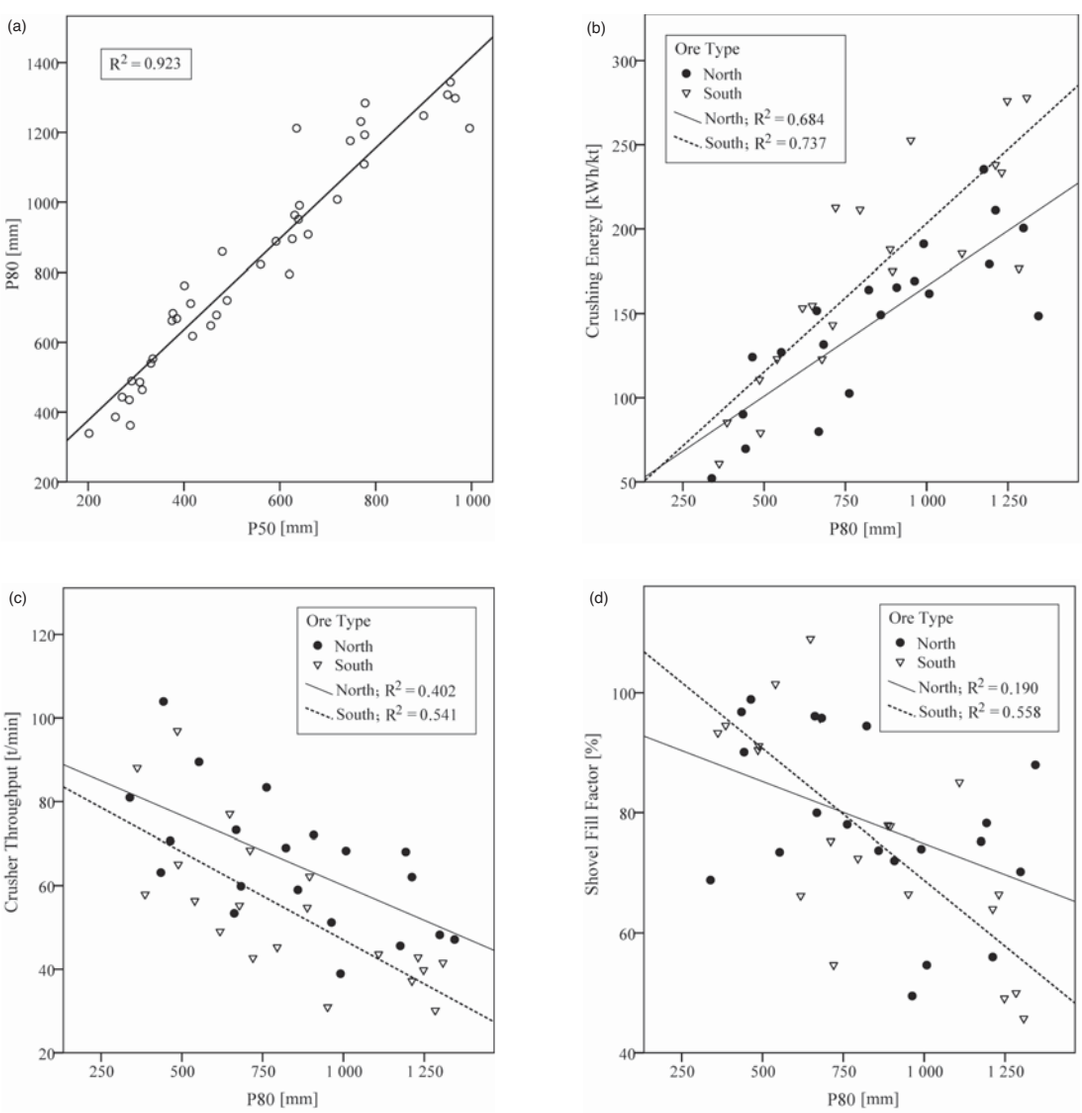

Figure 7—Image analysis results. (a) Correlation between P_{50} and P_{80} of all analysed images, (b) crushing energy plotted against P_{80}, (c) crusher throughput versus P_{80}, (d) shovel fill factor plotted against P_{80} of the feed

in the classification results. The energy consumption increases as fragmentation reaches the coarse end of the spectrum. The regression lines show that south ore generally consumes more energy during crushing, though the difference is marginal in the fine end of the fragmentation range and increases with P_{80}. The difference between the ores is more pronounced in the mid-range (P_{80}=600–800 mm) and includes large scatter at the coarse end. This agrees well with the results obtained from classification; however, the variations at the coarse region of the plot could imply that factors other than ore type and fragmentation have influenced the energy consumption.

The throughput of the crusher (Figure 7c) also shows a decreasing trend as fragmentation becomes coarser, but the low correlation coefficients imply that in single crushing cycles, the throughput is not only affected by fragmentation, but also by external factors such as feeding rate (material flow) and shape of fragments. The regression lines show that, on average, south ore yields less throughput than north ore, but the values do not show a strong correlation to either size or ore type in this number of samples (n=40). The fill factor of the electric shovels (Figure 7d) shows an even weaker correlation with P_{80}. The trend of the overall envelope suggests diggability decreases with increasing P_{80}. But the correlation coefficients are rather small, and no distinct difference is observed between the two ores, as all points lie within a similar, wide statistical range. This could arguably be due to inaccuracies in fragmentation measurements, or other factors related to the machinery; either way, the large scatter does not allow a definite conclusion about the loading efficiency.

Summary and conclusion

This study analysed the feed fragmentation of 225 single-dump crushing cycles statistically in an ordinal manner. It considered the fragmentation for 40 of the cycles using an image analysis tool and correlated the results to the crushing energy consumption per unit mass, throughput of the crusher and fill factor of the shovel dipper. The crushing cycles were traced to their loading origin and subjectively separated by estimated ore hardness. During the study period, the CSS of the crusher was kept constant, as was the rotational speed of the mantle. The loading efficiency was compared for identical electric rope shovels. The classification and image analysis were conducted in a systematic manner with images from a single stationary camera aimed at the crusher inlet. The findings are summarized as follows.

- The results indicate a consistent difference between the soft and hard ores in their crushing efficiency. Both the classification and the image analysis show that, regardless of size distribution of the feed, the harder ore (south) involves higher energy consumption and lower throughput than the softer ore (north)
- The influence of ore hardness is most pronounced in mid-range fragmentation (classes 2 and 3), implying hardness matters less for very fine or very coarse fragmentations
- The largest change in both energy consumption and throughput of the crusher occurs between class 3 and class 4 fragmentations. This indicates that the efficiency decreases slightly as the fragmentation becomes coarser (from class 1 to 3), but as the fragmentation exceeds a certain size (between class 3 and 4), the efficiency drops considerably. Interestingly, for the very coarse fragmentations (class 5), the efficiency does not decrease significantly
- The loading efficiency shows no correlation to the hardness of the ore. The highest efficiency is observed in mid-fine range fragmentation (class 2). It decreases thereafter with increasing feed size
- The general trends in crushing and loading efficiency are consistent in both the classification and the image analysis results. However, a comparison of the results shows both methods include large scatters. The classification method provides a much larger sample population and is, therefore, statistically more representative than the image analysis of limited samples. Although both methods are image-based and include similar drawbacks, the trends in classification results are more reliable for subjective evaluations. This is more evident for the throughput and fill factors; they show very large scatters in both methods, but the broad sampling in classification leads to more representative results over a larger population
- Several shortcomings of image-based methods to assess fragmentation were observed in this field study. These observations were not easily measurable in a non-contact manner, but affected the results in one way or another. Segregation of material, lay and shape of fragments, overlapping fragments, and inhomogeneity within each sample (truck) were some of the factors causing inaccuracies, not only in fragmentation assessment but also in loading and crushing. Despite their limitations, these methods are the only available tools to measure fragmentation.

Finally, the findings of this study suggest that higher loading and crushing efficiencies can be achieved in Aitik mine. This could be accomplished by tailoring the blast-induced fragmentation to class 2 or 3, approximately equivalent to a P_{80} of 600–800 mm. Such target fragmentation could be achieved by using field trials to find the most economical blast set-up satisfying those requirements. Furthermore, the results suggest that the crushing efficiencies are different for north and south ores, something to consider in blast design and cost estimations. The target fragmentation for loading and crushing can be correlated to the operational parameters of the crusher and the efficiency of the mill to find the most suitable combination for efficient milling. Subsequent cost estimations for each unit operation can determine a combination of blast set-up, crusher setting, and milling parameters to eventually yield the highest overall chain value of this particular operation in the long term.

Acknowledgments

Boliden Mineral AB, especially the staff and management of the Aitik mine are gratefully acknowledged for the support and valuable input they provided during this study. This work was supported by Vinnova, The Swedish Energy Agency, Formas, LKAB, and Boliden Mineral AB through the SIP-STRIM programme.

References

Aswegen, H.V. and Cunningham, C.V.B. 1986. The estimation of fragmentation in blast muckpiles by means of standard photographs. *Journal of the South African Institute of Mining and Metallurgy*, vol. 86, no. 12. pp. 469–474.

Ballantyne, G.R. and Powell, M.S. 2014. Benchmarking comminution energy consumption for the processing of copper and gold ores. *Minerals Engineering*, vol. 65. pp. 109–114.

Bellairs, P. 1987. The application of geological and downhole geophysical data to blast pattern design, *Proceedings of the 2nd International Symposium on Rock Fragmentation by Blasting*, Keystone, Colorado. pp. 398–411.

Bergman, P. 2005. Optimisation of fragmentation and comminution at Boliden Mineral, Aitik Operation. Licentiate thesis, Luleå University of Technology, Sweden.

Beyglou, A., Schunnesson, H., Johansson, D., and Johansson, N. 2015. Adjusting initiation direction to domains of rock mass discontinuities in Aitik open pit mine. *Proceedings of the 11th International Symposium on Rock Fragmentation by Blasting*, Sydney, Australia. Australasian Institute of Mining and Metallurgy, Melbourne. pp. 385–391.

Bond, F.C. and Whitney, B.B. 1959. The work index in blasting. *Proceedings of the 3rd US Symposium on Rock Mechanics (USRMS)*. American Rock Mechanics Association. pp.78–90.

Chavez, R., Cheimanoff, N., and Schleifer, J. 1996. Sampling problems during grain size distribution measurements. *Proceedings of the 5th International Symposium on Rock Fragmentation by Blasting*, vol. 5, pp. 245–252.

Cunningham, C.V.B. 1983. The Kuz-Ram model for prediction of fragmentation from blasting. *Proceedings of the 1st International Symposium on Rock Fragmentation by Blasting*, Luleå, Sweden. vol. 2, pp. 439–453.

Curry, J.A., Ismay, M.J., and Jameson, G.J. 2014. Mine operating costs and the potential impacts of energy and grinding, *Minerals Engineering*, vol. 56. pp. 70–80.

Eloranta, J. 1995. Influence of crushing process variables on the product quality of crushed rock. PhD thesis, Tampere University of Technology, Finland.

Evertsson, C.M. 2000. Cone crusher performance. PhD thesis, Chalmers University of Technology, Göteborg, Sweden.

Halatchev, R.A. and Knights, P.F. 2007. Spatial variability of shovel dig performance. *International Journal of Mining, Reclamation and Environment*, vol. 21, no. 4. pp. 244–261.

Hansen, J. 2001. Electric rope shovel monitoring. *CIM Bulletin*, vol. 94, no. 1052. pp. 80–82.

Hantler, A. 2015. Crushing index – Aitik. Technical Report, no. 8HX286586.10, Pöyry Sweden AB.

Hawkes, P.J., Spathis, A.T., and Sengstock G.W. 1995. Monitoring equipment productivity improvements in coal mines. *Proceedings of EXPLO 95 Conference*, Brisbane. Australasian Institute of Mining and Metallurgy, Melbourne. pp. 127–132.

Hendricks, C. 1990. Performance monitoring of electric mining shovels. PhD thesis, McGill University, Montreal, Canada.

Herbst, J.A., Lo, Y.C., and Flintoff, B. 2003. Size reduction and liberation. *Principles of Mineral Processing*. Fuerstenau, M.C and Han, K.N. (eds). SME, Littleton, Colorado. pp. 61–118.

Hunter, G.C., McDermott, C., Miles, N.J., Singh, A., and Scoble, M.J. 1990. A review of image analysis techniques for measuring blast fragmentation. *Mining Science and Technology*, vol. 11. pp. 19–36.

Kemeny, J., Mofya, E., Kaunda, R., and Lever, P. 2002. Improvements in blast fragmentation models using digital image processing. *Fragblas*t, vol. 6, no. 3–4. pp. 311–320.

Latham, J.P., Kemeny, J., Maerz, N., Noy, M., Schleifer, J., and Tose S. 2003. A blind comparison between results of four image analysis systems using a photo-library of piles of sieved fragments. *Fragblast*, vol. 7, no. 2. pp. 105–132.

Maerz, N.H. and Zhou, W. 1998. Optical digital fragmentation measuring systems–inherent sources of error. *Fragblast*, vol. 2, no. 4. pp. 415–431.

McKee, D.J. and Napier-Munn, T.J. 1990. The status of comminution simulation in Australia. *Minerals Engineering*, vol. 3, no. 1. pp. 7–21.

Murr, D.L., Workman, L., Eloranta, J., and Katsabanis, T. 2015. Blasting influence on comminution. *Proceedings of the Sixth International Conference on Semi-autogenous and High Pressure Grinding Technology*, Vancouver, Canada. http://www.ceecthefuture.org/publications/5911/ [accessed 8 June 2016].

Napier-Munn, T. 2015. Is progress in energy-efficient comminution doomed? *Minerals Engineering*, vol. 73. pp. 1–6.

Onederra, I.A., Brunton, I.D., Battista, J., and Grace, J. 2004. 'Shot to shovel'-understanding the impact of muck pile conditions and operator proficiency on instantaneous shovel productivity. *Proceedings of EXPLO 2004 Conference*, vol. 3. Australasian Institute of Mining and Metallurgy, Melbourne. pp. 205–213.

Ouchterlony, F., Bergman, P., and Nyberg, U. 2010. Fragmentation in production rounds and mill throughput in the Aitik mine, a summary of development projects 2002–2009. *Report no.* 2010:3. Swebrec, Luleå University of Technology, Sweden (in Swedish).

Patnayak, S., Tannant, D.D., Parsons, I., Del Valle, V., and Wong, J. 2008. Operator and dipper tooth influence on electric shovel performance during oil sands mining. *International Journal of Mining, Reclamation and Environment*, vol. 22, no. 2. pp. 120–145.

Pothina, R., Kecojevic, V., Klima, M.S., and Komljenovic, D. 2007. Gyratory crusher model and impact parameters related to energy consumption. *Minerals and Metallurgical Processing*, vol. 23, no. 3. pp. 170–180.

Sanchidrián, J.A., Segarra, P., Ouchterlony, F., and López, L.M. 2009. On the accuracy of fragment size measurement by image analysis in combination with some distribution functions. *Rock Mechanics and Rock Engineering*, vol. 42, no. 1. pp. 95–116.

Sanchidrián, J.A., Segarra, P., and López, L.M. 2011. On loader productivity, rock strength and explosive energy in metal mining. *Proceedings of the Sixth EFEE World Conference on Explosives and Blasting*, Lisbon, Portugal. pp. 461–468.

Singh, S.P. and Narendrula, R. 2006. Factors affecting the productivity of loaders in surface mines. *International Journal of Mining, Reclamation and Environment*, vol. 20, no. 1. pp. 20–32.

Sjöberg, J. 1999. Analysis of large scale rock slopes. PhD thesis, Luleå University of Technology, Sweden.

Spathis, A.T. 2009. Formulae and techniques for assessing features of blast-induced fragmentation distributions. *Proceedings of the 9th International Symposium on Rock Fragmentation by Blasting*, Granada, Spain. pp. 209–219.

Thurley, M.J. and Ng, K.C. 2005. Identifying, visualizing, and comparing regions in irregularly spaced 3D surface data. *Computer Vision and Image Understanding*, vol. 98, no. 2. pp. 239–270.

Thurley, M.J., Wimmer, M., and Nordqvist, A. 2015. Blast fragmentation measurement based on three dimensional imaging in sublevel caving drawpoints and underground excavator buckets at LKAB Kiruna. *Proceedings of the 11th International Symposium on Rock Fragmentation by Blasting*, Sydney, Australia. Australasian Institute of Mining and Metallurgy, Melbourne. pp. 763–773.

Valery, W., Thornton, D., Jankovic, A., and Kristiansen, J. 2002. Mine to mill scoping study at Aitik Mine Boliden. *Technical Report no*. TM_REP 2002/006, Boliden Mineral AB, Sweden.

Williamson, S., McKenzie, C., and O'Louglin, H. 1983. Electric shovel performance as a measure of blasting efficiency. *Proceedings of the 1st International Symppsium on Rock Fragmentation by Blasting*, Luleå, Sweden. pp. 625–635.

Wimmer, M., Nordqvist, A., Righetti, E., Petropoulos, N., and Thurley, M.J. 2015. Analysis of rock fragmentation and its effect on gravity flow at the Kiruna sublevel caving mine. *Proceedings of the 11th International Symposium on Rock Fragmentation by Blasting*, Sydney, Australia. Australasian Institute of Mining and Metallurgy, Melbourne. pp. 775–791. ◆

http://dx.doi.org/10.17159/2411-9717/2017/v117n11a11

Mechanism and control of roof fall and support failure incidents occuring near longwall recovery roadways

by W. Zhu*, J. Xu*‡, and G. Xu†

Synopsis

Pre-driven longwall recovery roadways are commonly adopted for rapid extraction in the high-production mines of Shendong coalfield in China. A special roadway, the adapting roadway, is utilized to adapt the longwall roof and floor to match the recovery roadway. However, severe accidents such as roof falls and support failures frequently occurred where this recovery roadways layout was applied to relatively deep coal seams. This posed a serious threat to safe production, and effective recovery and relocation of the longwalls. By analysing different cases and mining conditions, theoretical investigation and numerical simulation were conducted based on the mechanisms of such incidents, and a systematic control approach was proposed. The controls involve a method to determine the applicability of the adapting roadway, the evaluation of incident potential, the means to reduce the likelihood of incidents, and an optimized method to determine the location of mesh installation. The findings were applied to multiple longwall faces in the Shendong coalfield and resulted in substantial benefits. The study findings and the proposed control approach can also be applied to other mines with similar problems.

Keywords

Shendong coalfield, pre-driven longwall recovery roadway, roof fall, support failure, adapting roadway, flexible mesh.

Introduction

As one of the eight largest coalfields in the world, the Shendong coalfield in China is typically characterized by shallow cover depth, simple geological conditions, and high coal quality. Shenhua Shendong Coal Group, the largest coal enterprise located in the coalfield, has established massive, fully mechanized longwall faces with a 10 Mt annual output. The technology of pre-driven longwall recovery roadways allows for the safe and rapid movement of equipment in longwall faces. This shortens the time required for longwall moves and substantially increases production (Barer and Listak, 1989; Liu and Chen, 1999).

Figure 1 shows the entry layout for longwall moves. Two entries that are perpendicular to the mining roadways are pre-driven near the stop line. The one close to the longwall face is called the main longwall recovery roadway, while the other is the secondary longwall recovery roadway. The two entries are connected with several crosscuts. In practice, the floor level at the working face usually does not match the level of the main longwall recovery roadway when the longwall face approaches the main longwall recovery roadway. The level of the longwall floor is either higher or lower than that of the longwall recovery roadway, which causes difficulties in extracting the longwall equipment. This is a common occurrence when the mining height exceeds the height of the longwall recovery roadway. This is because when the longwall face approaches the recovery roadway, the mining height needs to be reduced for the smooth extraction of equipment. The traditional way of matching the roof and floor of the longwall and recovery roadway is to measure the level of the longwall floor at every specific distance from the longwall recovery roadway (for example, 20 m, 18 m, 16 m, *etc.*). Then, by adjusting the mining height, the level of the longwall roof can also be well controlled. This is an effective, but time-consuming method. The use of the adapting roadway allows the miner to control the coal cutter so as to adjust the level of the longwall floor. This is a more efficient method and operation. To avoid roof falls and to ensure the safety of underground personnel, flexible mesh is usually installed at 15 to 20 m from the stop line.

As shallow coal resources are becoming depleted, the company has started to mine the deeper coal seams. Several longwall faces experienced rib spalling, gangue leak, and even roof fall accidents near the main longwall recovery roadways. In some severe instances, hydraulic cylinders were damaged and the longwall shearer became stuck due to roof fall. This posed serious threats to safe production

* *Key Laboratory of Deep Coal Resource Mining, Ministry of Education of China; School of Mines, China University of Mining and Technology, China.*

† *Department of Mining Engineering and Metallurgical Engineering, Curtin University, Western Australia, Australia.*

‡ *Corresponding Author.*

 ISSN 2225-6253. Paper received Oct. 2016; revised paper received Mar. 2017.

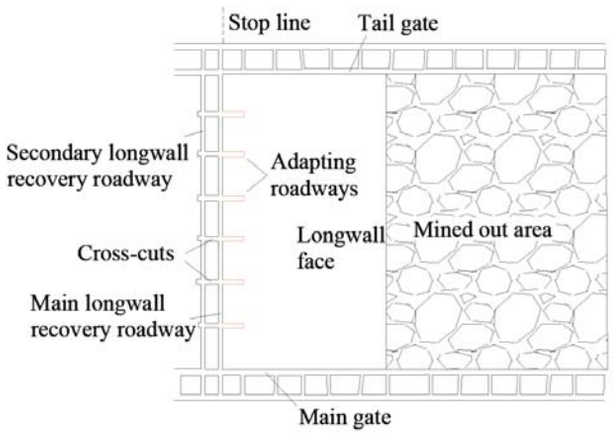

Figure 1—Layout of recovery roadways in Shendong coalfield

and successful removal of the equipment. Therefore, studying the mechanism of hydraulic support failure and roof fall in such conditions, and identifying feasible remedies, became urgent.

The technology of pre-driven longwall recovery roadways has been generally adopted due to its massive advantages (Barer and Listak, 1989; Liu and Chen, 1999), and the systematic assessment for it has been well-developed (Barczak, 2006; Wichlacz, Britten, and Beamish, 2009). With regard to roof management, numerous researchers have conducted in-depth, systematic studies on the design parameters for weak roof conditions (Tadolini, Zhang, and Peng, 2002; Zhang *et al.*, 2006; Lu, 2014; Kang *et al.*, 2015) and the relationship between the supporting system, strata movement, and ground subsidence (Tadolini and Barczak, 2006, 2008; Barczak, Chen, and Bower, 2003; Barczak, Tadolini, and Zhang 2006). The studies on mining-induced stress transfer, roof control technology, and the design of a support system have had a significant instructive effect on the application of pre-driven longwall recovery roadways in the field. The immediate roofs of the longwall recovery roadways in Shendong coalfield are commonly supported by intensive, high-powered hydraulic supports, resulting in fewer roof falls or leaks. However, because of the application of the adapting roadways, severe incidents such as hydraulic support failure and roof fall are more likely to occur when longwall faces approach the main longwall recovery roadways. Many past researchers focused on the study of roof fall at the longwall faces under conditions such as composite single key stratum with thick drift sand (Huang, 2002; Hou, 2000; Shi and Hou, 1996), the uphill section of valley terrains (Xu *et al.*, 2009, 2012; Zhu, 2011), and the mining of the upper pillars (Ju and Xu, 2013; Ju, Xu, and Zhu, 2015; Chen, 2014). However, few studies have focused on the support failures and roof fall incidents that occurred near the longwall recovery roadways.

Based on the above analysis and several incidents in the Shendong coalfield, we present the reasons for and mechanisms of support failure and roof fall incidents that occurred near the longwall recovery roadways, and propose comprehensive prevention countermeasures by using field observation, theoretical analysis, and FLAC^{3D} simulation. The outcome of this study has been successfully applied in Shendong coalfield for the prevention of incidents.

Incident case studies

Incident 1 – longwall 12401 and longwall 12402, Bulianta coal mine

Longwall 12401 and longwall 12402 of Bulianta coal mine were deployed at No.4 panel,1-2 coal seam. The coal seam is subhorizontal with a dip angle ranging from 1° to 3°. The mining height is approximately 4.3 m. The depth of cover near the longwall recovery roadway is between 253 and 260 m. The layout of the panel and entries is illustrated in Figure 2. The distances between the two longwall recovery roadways in longwall 12401 and longwall 12402 were 30 m and 35 m, respectively. The adapting roadways were 15 m long and 5 m wide. There were only two adapting roadways near the main gate in longwall 12401. Other parameters are shown in Figure 2.

When longwall 12401 face retreated 13 m from the main longwall recovery roadway, roof fall started above the no. 90-20 hydraulic supports (near the adapting roadway). Figure 2

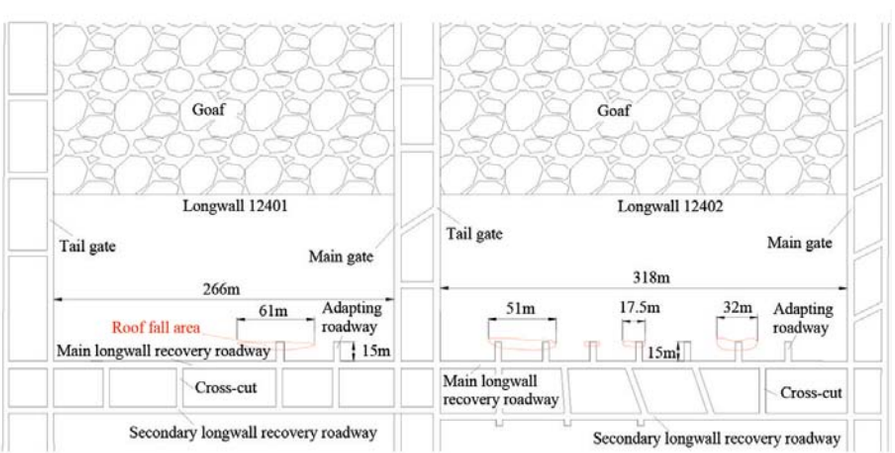

Figure 2—Roof fall areas and roadway layout of longwalls 12401 and 12402

shows the roof fall areas. The height of roof fall was between 1.0 m and 1.5 m. Such issues were very serious until the longwall face retreated to 7 m away from the main longwall recovery roadway. By injecting Marithan, a special coal strengthening grout, into the longwall face, the coal mass was stabilized and the face eventually completed extraction.

Similarly, in longwall 12402 face, roof fall occurred in multiple parts of the roof near the adapting roadways when the face retreated to 12.5 m from the main longwall recovery roadway. The roof fall areas were 1.5 m to 2.2 m high and 1.0 m to 1.7 m wide (refer to Figure 2). Injection of Marithan did not control the roof fall, and extraction of the longwall could not be completed until mining personnel upgraded the support by adding bolts and anchor cables.

Incident 2 – longwall 52304, Daliuta coal mine

Longwall 52304 was the first panel with 7.0 m-high support in 5^{-2} coal seam of Daliuta coal mine in Shendong coalfield. The coal seam has a dip angle ranging from 1° to 3°. The longwall 52304 panel was 4547.6 m long and 301 m wide, with a cover depth of 275 m near the main longwall recovery roadway. The adapting roadways were 20 m long and 4 m wide. The width of the main longwall recovery roadway was 6.8 m, and it was separated from the secondary longwall recovery roadway by 20 m pillars (refer to Figure 3a).

On 6 March 2013, mining at the longwall face stopped 20 m from the main longwall recovery roadway to wait for ground pressure to be established. The pressure did not appear, so the mining personnel decided to resume operation on the morning of 7 March. Periodic roof pressure manifested when the longwall face was retreated to 17.5 m away from the main longwall recovery roadway, when the flexible mesh was installed. On the afternoon of 8 March, there was a serious compressive closure of hydraulic cylinders in the no. 39 to no. 108 supports; and the available compression distance was less than 1 m for supports no. 86 to no. 88, causing inadequate space for the longwall shear and serious gangue leakage. From 9 to 22 March, due to the severe roof fall in the longwall face, the major work consisted mainly of the disposal of the massive stone blocks and the injection of Marithan grout into the coal mass. During that time, production was further delayed by many hours due to the breakdown of conveyor and transfer machines, thus only about 10 m (to 7 m from the main longwall recovery roadway) could be extracted. After the night shift on 23 March, the centre section of the longwall face remained 6 m from the main longwall recovery roadway, and workers continued hanging and fixing flexible mesh. The longwall face approached the end of the panel and finished production on 25 March.

Incident statistics and analysis

From the above cases studies, it can be seen that the roof fall incidents occurred mainly near the adapting roadways; and the support failures occurred due to the roof falls. The cause of the incidents can therefore be preliminarily attributed to the adapting roadways. A summary of the 51 longwall panels in the Shendong coalfield is listed in Table I for comparison. It can be seen that the widths and lengths of the adapting roadways in Shendong coalfield are generally 3 to 5 m and 10 to 20 m, respectively. With similar supporting systems, roof fall and support failure occurred only when the longwall panel depth was large. Therefore, the use of adapting roadways at greater than a certain depth may be the major possible cause. This hypothesis is further investigated by theoretical analysis and numerical modelling in the following sections.

Mechanism analysis

Theoretical analysis

The stress over the adapting roadway will transfer to the adjacent coal mass and cause abutment stress. The area outside the peak position of the abutment pressure is called the plastic zone. The coal mass near the wall has a lower

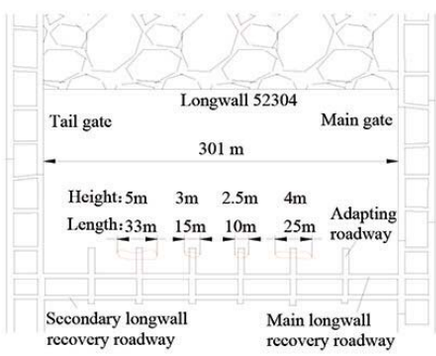

(a) Roof fall areas of longwall 52304

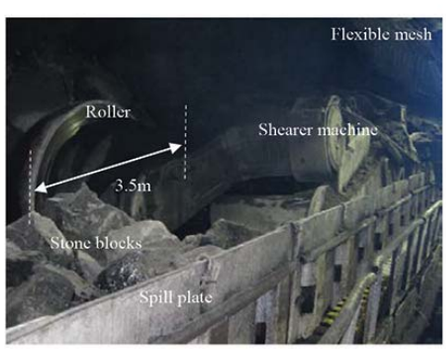

(b) The shearer was stuck

(c) Comparison of mining height before and after roof pressure

Figure 3—Scene of incident in longwall 52304

Table I

Adapting roadway parameters and roof fall situation in Shendong coalfield

Name of longwall faces	Mining height/m	Width /m	Length /m	Cover depth/m	Roof fall or not
22608~22615and22302~22309 of Daliuta mine	4.2	3.0~5.0	12~17.5	48~94	
22207-2and22302 of Bulianta mine	6.8	3.6,4.5	20,19.2	55,147	
12up201~12up208and22301~22306 of Huojitu mine	4.5	3.0~5.0	12~17.5	61~102	
12201~12203 of Shangwan mine	7.0	3.3	10~12	72~87	No
12103~12105and12201~12206 of Shigetai mine	3.5	3.3~5.2	10~18	77~98	
31406,31110-1 of Wulanmulun mine	4.4	No adapting roadway	190		
42104,42103-1 of Buertai mine	6.7	No adapting roadway	259,278		
12401,12402 of Bulianta mine	4.2~4.4	5.0	15	253,260	Yes
52304 of Daliuta mine	7.0	5.0	20	275	

stress than the *in situ* stress, and this area is called the fractured zone (Qian, Shi, and Xu, 2010) (refer to Figure 4). If x_0 denotes the width of the plastic zone and the stress distribution in the plastic zone is assumed as linear, the width of the fractured area can be expressed as:

$$x = \frac{x_0}{K} = \frac{m}{2K\xi f} \ln \frac{K\gamma H + C\cot\varphi}{\xi(p + C\cot\varphi)} \quad [1]$$

where K is the stress concentration factor, γH is overlying strata loading, p is the support resistance in the roadway, m is the thickness of the coal seam, C and φ are the cohesion and internal friction angle of the coal, respectively, f is the friction coefficient of the coal seam to roof or floor, ξ is the triaxial stress coefficient, and $\xi = (1-\sin\varphi)/(1+\sin\varphi)$.

Using specific parameters from the Shendong coalfield, the calculated width of the plastic zone is generally more than 9 m. This figure can be up to 20 m when the cover depth and mining height are relatively large (for instance, their values are 250 m and 7 m, respectively), with a 5 m wide fractured zone.

Similarly, the longwall face abutment stress will transfer to the coal mass near the adapting roadway when the longwall face approaches it. This additional stress is more likely to cause the coal mass in the fractured zone (induced by the adapting roadway) to completely lose its bearing capacity. Severe rib spalling will occur at the intersection of the adapting roadway and longwall face due to insufficient support. This can enlarge the hanging area of the roof and result in roof fall. The immediate roof generates the resistance in the hydraulic support to control the movement of the overlying strata. When roof fall reaches a certain extent, the immediate roof cannot impart sufficient resistance to the overlying key block (the broken hard stratum), which may cause the key block to rotate and slide down. The instability of the overlying strata can cause a sudden roof drop and induce a more serious roof fall (refer to Figure 5).

According to Equation [1], there is a positive correlation between the cover depth and the width of the fractured zone, hence the probability and severity of the incident will increase when the cover depth increases. To further analyse the mechanism of the roof fall and support failure in a longwall face caused by the adapting roadway, a further study of the influence of the adaptingroadway on the vertical stress in the coal mass and the deformation of the roadway was conducted, and is described in the next section.

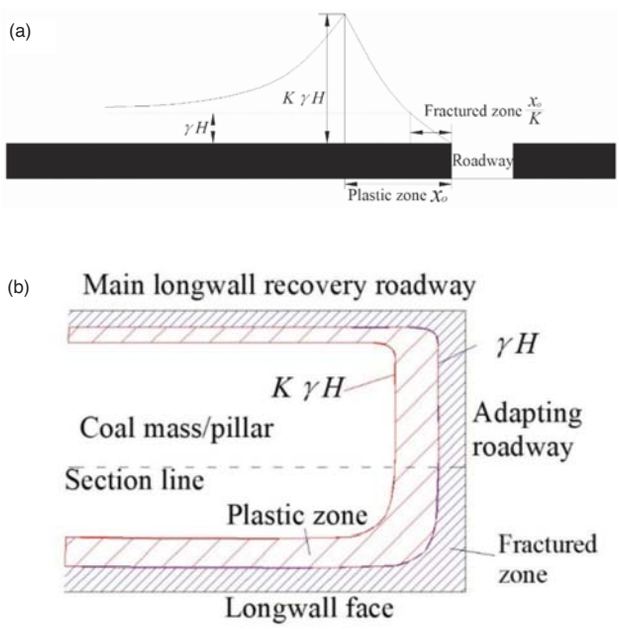

Figure 4—(a) Distribution of vertical stress in coal mass and (b) classification of deformation zone

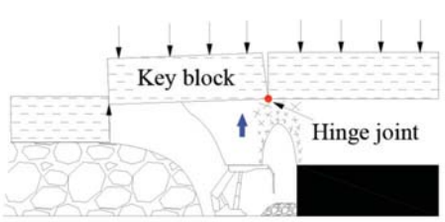

(a) Rib spalling results in roof fall

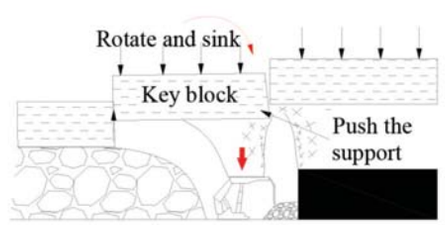

(b) Roof fall triggers support failure

Figure 5—Development of roof fall and support failure

Numerical simulation

The finite difference numerical code FLAC3D was used to simulate the influence of the adapting roadway stress distribution. The features of the rock strata were determined according to the actual rock strata in longwall 12401 of Bulianta coal mine and longwall 52304 of Daliuta coal mine, with some reasonable simplifications. The rock mechanics parameters in the model were determined by standard mechanical tests on borehole core samples from several production longwall panels in the Shendong coalfield (refer to Table II).

Four groups of models were established, each with a length, width, and height of 300 m, 200 m, and 120 m, respectively (refer to Figure 6a). The thicknesses of the coal seam and floor were 5 m and 20 m, respectively, and the cover depth of the coal seam was 100 m. The support parameters of the adapting roadway were in agreement with the parameters in the field. Table III shows the parameters and layouts of the adapting roadways in the four groups. A uniformly distributed vertical stress with a gradient of 0.025 MPa/m was applied to the top interface of the model to represent the overlying strata. The group one models were

Table II

Rock mechanics parameters for numerical simulation

Lithology	Bulk modulus (Gpa)	Shear modulus (Gpa)	Internal friction angle (°)	Cohesion (MPa)	Tensile strength (MPa)	Poisson's ratio	Volumetric weight (kg·m^{-3})
Medium sandstone	3.6	3.98	35	7.2	1.43	0.19	2600
Fine sandstone	2.32	2.17	27	5.3	0.92	0.25	2550
Siltstone	1.80	1.56	27	4.3	0.89	0.29	2300
Mudstone	1.47	1.42	22	2.5	1.01	0.24	2250
Coal	1.60	1.24	20	2.2	0.45	0.31	1350

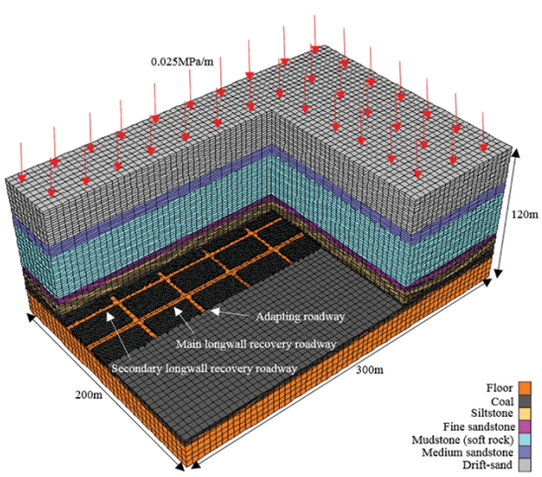

(a) Layout of the numerical model

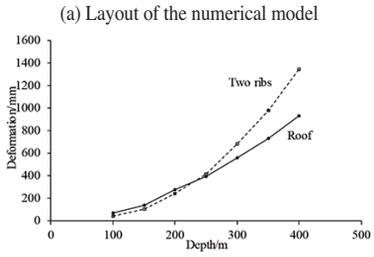

(b) Influence of cover depth on deformation of adapting roadway

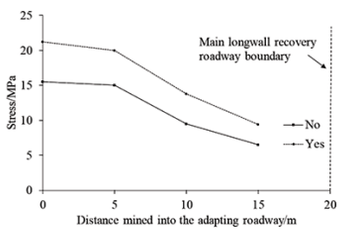

(c) Influence of adapting roadway on vertical stress in coal mass

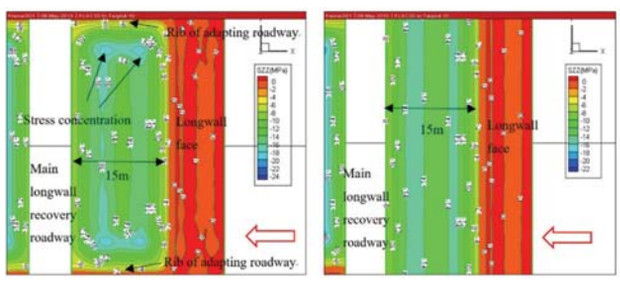

(d) Distribution of vertical stress in coal mass when longwall face was 15 m away from main longwall recovery roadway

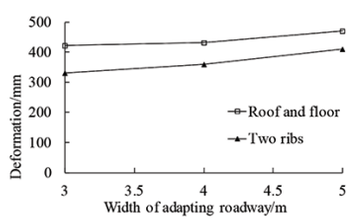

(e) Deformation of adapting roadway in different widths

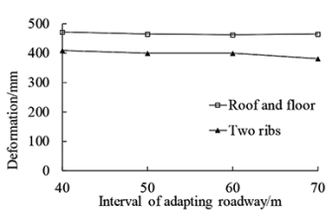

(f) Deformation of adapting roadway in different intervals

Figure 6—Results of the numerical simulation

Table III

Parameters and layout of the adapting roadways in four groups

Group	Cover depth/m	Width /m	Interval /m
1	100, 150, 200, 250, 300, 350, 400	5	40
2	250	5	40
		No adapting roadway	
3	250	3, 4, 5	40
4	250	5	40, 50, 60, 70

used to simulate the influence of cover depth on the deformation of the adapting roadway. Groups two to four were used to determine the impact of the use or non-use of adapting roadways, the width and interval of the adapting roadway on the vertical stress in the coal mass, and the deformation of the roadway. The dip was not considered because the coal seams in the Shendong coalfield are relatively flat. The bottom boundaryof the model was restricted in vertical movement, and the lateral boundary was restricted in horizontal movement. All the remaining areas, including the coal, roof, and floor, were assumed to have elastic-perfectly plastic behaviour as defined by the Mohr-Coulomb strength criterion.

Because the study focused mainly on the impact of the adapting roadway on the vertical stress in the coal mass and the deformation of the roadway when the longwall face approached the main longwall recovery roadway, the coal seam that was 40 m away from the adapting roadway was excavated immediately in the simulation to allow the overlying strata to deform to a steady-state condition. After that, the coal seam was excavated by a 5 m step in the simulation. Figure 6 shows the results.

The deformations of the roof and two ribs of the roadway increased rapidly with the cover depth (refer to Figure 6b), from 66.9 mm to 929 mm and 40 mm to 1340 mm, respectively, when cover depth increased from 100 m to 400 m. Figure 6c and Figure 6d show that the adapting roadway has a significant impact on the stress in the coal mass above the longwall face, resulting in the stress concentrating in the intersection of the adapting roadway and longwall face. The stress concentration factor is up to 3.4. Thus, large-scale fracturing of the coal mass will occur when the cover depth increases to a certain degree, which can trigger roof fall. Figure 6e and Figure 6f show that the width and the interval of the adapting roadway have little impact on deformation. From the results of the simulation, the conclusion can be drawn that the cover depth is a key factor that increases the vertical stress and the deformation of the adapting roadway.

Key factors and countermeasures

The coal mass in front of the longwall face is divided into several pillars by the adapting roadways, which will increase the degree of stress concentration and impair the bearing capacity of the coal mass. The adapting roadways can also increase the hanging area of the roof, which is very likely to trigger rib spalling and roof fall with increasing cover depth. This poses extreme difficulties for effective roof control. The mining rate is delayed by the installation of flexible mesh, which further increases the challenges of roof control. Based on the analysis in the previous sections, the maximum applicable cover depth of the adapting roadway was determined, and a method was developed to determine the optimum position of flexible mesh installation. Lastly, a flow chart is provided to evaluate the incident potential and to apply different countermeasures.

Maximum cover depth of adapting roadway

The longwall recovery roadways in the Shendong coalfield contain the main and secondary longwall recovery roadways, and the adapting roadways. The main factor triggering support failure and roof fall is the application of the adapting roadway beyond a certain cover depth. The results of numerical simulation indicated that the width and the interval of the adapting roadway have a minimal influence on its deformation. Thus, these parameters cannot be further optimized. However, the deformation of adapting roadways is sensitive to the cover depth, which indicates that there is a maximum depth for the application of adapting roadways.

Maximal cover depth based on the stability of the coal mass

When the longwall face is mined to the adapting roadway, the coal mass in front of the longwall face is divided into several independent coal pillars. The length of the adapting roadway is generally less than 20 m, and the interval between two roadways is usually more than 30 m. The bearing capacity of coal pillars decreases with the progress of the longwall face. Based on the Obert-Duvall/Wang formula, the strength of the coal pillar can be expressed by:

$$R = R_c(0.778 + 0.222\frac{B}{h}) \quad [2]$$

where R, B, and h are the strength, width, and the height of the coal pillar, respectively; and R_c is the cube compressive strength of the coal.

According to the typical arrangement of adapting roadways in Shendong coalfield, the value of h is 5 m, the length is 20 m, so the initial value of B is 20 m. From tests on massive coal samples from multiple regions in the Shendong coalfield, the value of R_c is determined to be 13.5 MPa. The maximum coal pillar strength can be calculated by using various distances mined into the adapting roadway. This is plotted in Figure 7 together with the maximum stress calculated from the numerical simulation. The figure shows that the stress in the coal pillar is greatest when the longwall

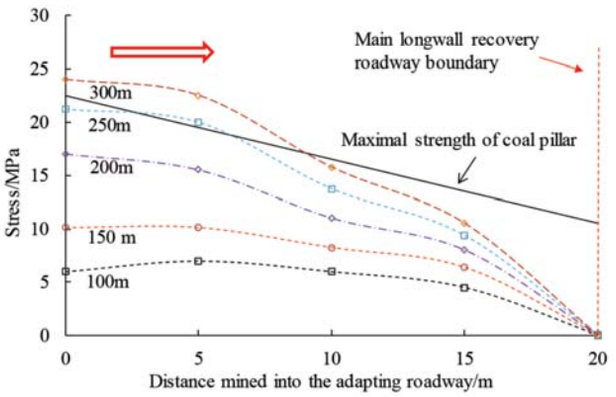

Figure 7—Comparison between stress and strength of coal pillar for different cover depths

face enters the adapting roadways. The advance abutment pressure transfers to the main longwall recovery roadway, or even further, as mining progresses (Kang *et al.*, 2015; Batchler, 2016), hence the stress in the coal pillar shows a downward trend. Therefore, support failure and roof fall are more likely to occur when longwall faces have just entered the adapting roadways. This was demonstrated by the three case studies presented above, in which the incidents occurred when the longwall faces had just entered the adapting roadway by 2 m to 3 m.

Figure 7 also reveals that when the cover depth reaches 250 m, the stress in the coal pillar exceeds its maximum strength when the longwall face has entered the adapting roadway by 3 m to 7 m. When the cover depth is less than 200 m, the coal pillar remains in a safe condition. Therefore, the applicable maximum depth of the adapting roadways is determined to be between 200 m and 250 m.

Maximal cover depth based on roadway deformation

During the last stage of mining, the longwall face is connected to the main longwall recovery roadway by adapting roadways. The deformation of the adapting roadways is closely related to the stability of coal walls and the roof control. Therefore, for the safe excavation of the longwall face it is critically important to control the deformation of the adapting roadway within a certain range. Table IV shows the level of difficulty in controlling the deformation of roadways (Chen and Lu, 1994). According to these criteria, roadway maintenance is relatively easy when the deformation is between 200 mm and 500 mm. Based on site experience in this coalfield, the roadway is generally considered to be relatively easy to control under shallow cover when the deformation of the roadway is less than 350 mm. This is used as the threshold deformation.

Figure 8 shows the deformation change with cover depth for roof and floor, and ribs. It can be seen that the cover depths corresponding to 350 mm deformation of the roof, and ribs are 212 m and 229 m, respectively. Therefore, from the perspective of the difficulty of roadway maintenance, the adapting roadway is inapplicable when the cover depth of the longwall face exceeds 212 m.

Therefore, considering both criteria for coal pillar stability and the manageability of roadway deformation, the applicative maximum depth of the adapting roadways is determined to be 212 m. The existing adapting roadways at greater depths should be considered for backfill (Figure 9a), or a new main longwall recovery roadway should be excavated at the end of the adapting roadways (Figure 9b). For new panels that are deeper than 212 m, the method of drilling holes from the longwall recovery roadway in the direction of the longwall face and filling the holes with lime for marking purposes can be used together with elevation survey methods.

Optimum position of mesh installation

The flexible mesh is usually installed at a distance of 15 to 20 m from the main longwall recovery roadway. In the initial period of mesh installation, a large area of the roof is exposed and it is critical to maintain good roof conditions. In practice, workers usually choose an empirical time and location to start installing mesh, which may encounter periodic roof pressure, and trigger support failure and roof fall. For instance, in the case of longwall 52304 in the Daliuta coal

Table IV

Rank of maintenance of underground roadways

Level	Easy	Medium	Hard	Hardest
Deformation of roadway/mm	< 200	200~500	500~1000	> 1000

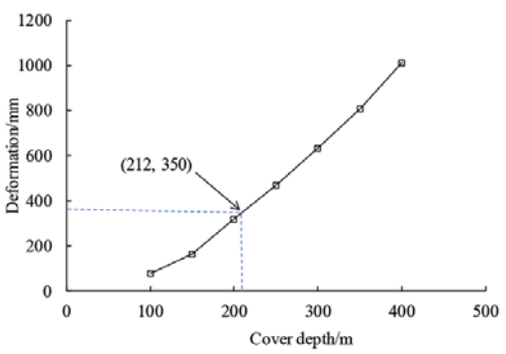

(a) Deformation of roof and floor with different cover depths

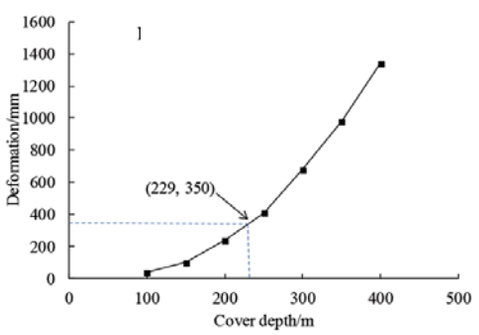

(b) Deformation of two ribs with different cover depths

Figure 8—Threshold of easy control of adapting roadway deformation

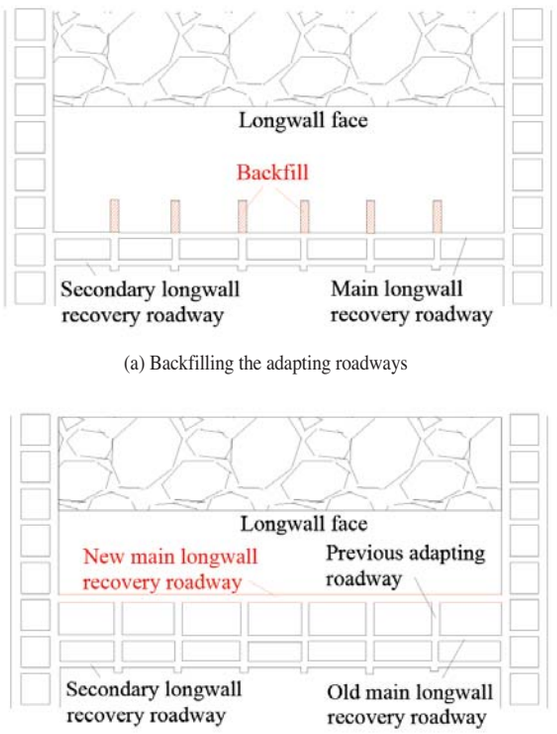

Figure 9—Optimization of extraction roadways

mine, mesh installation coincided with the last periodic roof pressure, which aggravated the accident.

Figure 10 illustrates the parameters that are related to mesh installation. By studying multiple mesh installation cases in the Shendong coalfield, the position of the mesh installation can be expressed as:

$$\begin{cases} X = X_{\min} \sim X_o & L_z < X_{\min} \\ X = L_z + n \times d & X_{\min} \le L_z < X_{\min} + L_c \\ X = L_z - L_c & X_{\min} + L_c \le L_z \end{cases} \quad [3]$$

where X is the position of the mesh installation, $X_{\min}$ is the minimum mesh installation length, X_o is the maximum mesh installation length (the length of flexible mesh), L_z is the position of the last periodic roof pressure from the main longwall recovery roadway, L_c is the persistence length of periodic roof pressure, n is an influence coefficient with a value between 2 and 4, and d is the cutting depth of the shearer, which usually equals 0.8 m in the Shendong coalfield.

The mesh installation needs to consider all the parameters related to ground pressure and the installation method. The periodic roof pressure can be predicted by the observation and analysis of previous periodic roof pressure frequency. If the position of the predicted periodic roof pressure is less than $X_{\min}$, the position of mesh installation can be selected at the miners' discretion between the minimum and maximum mesh installation lengths. However, if the position of the predicted periodic roof pressure is greater than $X_{\min}$ but less than the sum of the maximum mesh installation length and the persistence length of periodic roof pressure, the position of the mesh installation should start 2 to 4 cuts before the predicted periodic roof pressure as mesh installation a relatively time-consuming process. When the position of the predicted periodic roof pressure is greater than the sum of the maximum mesh installation length and the persistence length of periodic roof pressure, the mesh should be installed after the periodic roof pressure. If the length of flexible mesh is insufficient according to this design, metal mesh should be used for continued protection.

Incident potential and prevention

Incident potential in such conditions can be evaluated based on the study above. The countermeasures are proposed to eliminate risk, and to ensure the safe and smooth excavation of the longwall face. Figure 11 shows a detailed flow chart for evaluation and prevention. The evaluation starts with assessing whether the adapting roadways have been excavated. If they have been excavated, the cover depth should be confirmed to be less than 212 m. Otherwise, the adapting roadways need to be backfilled, or a new main longwall recovery roadway needs to be excavated at the end of the adapting roadways. For flexible mesh installation, the periodic roof pressure should be predicted based on previous periodic roof pressure frequency, and the optimum mesh installation position should be confirmed to ensure safe excavation of the longwall face.

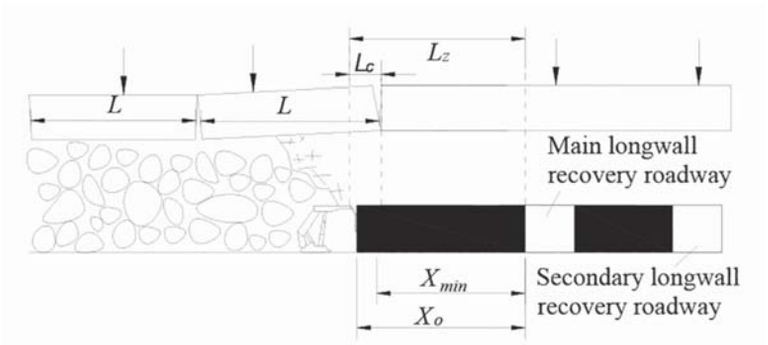

Figure 10—Diagram of relevant parameters for installing mesh

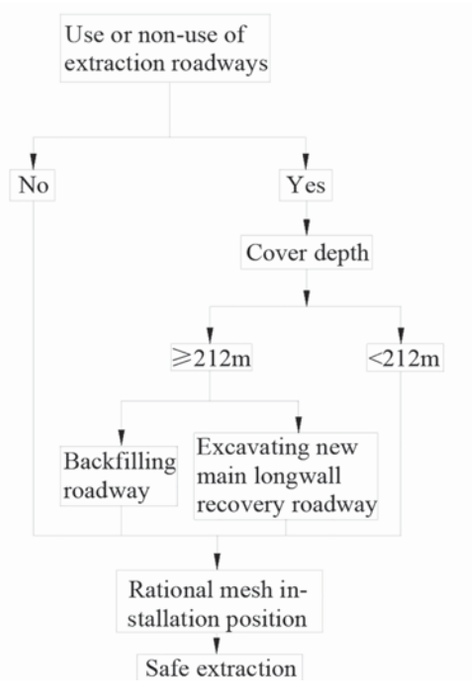

Figure 11—Flow chart of incident potential and prevention

Field trials

Longwall 12405 and longwall 12406 of Bulianta coal mine

The geological conditions of longwall 12405 and longwall 12406 of Bulianta coal mine were similar to longwall1 2401, and the adapting roadway of longwall 12405 had been excavated in advance. Considering that the cover depth of the two longwall faces reached 225 m, a new main longwall recovery roadway was excavated at the end of the adapting roadway in longwall 12405 (using the method shown in Figure 9b). Due to the cover depth exceeding the maximum applicable depth determined in the previous section, the adapting roadways were not excavated in longwall 12406, and the width of pillars between the main and secondary longwall recovery roadway was increased. No incidents occurred in both panels, and the production was smooth and rapid.

Longwall 52303 of Daliuta coal mine

Longwall 52303 was the successive longwall face to longwall 52304, and the geological conditions of the two longwall faces were the same. Considering that the cover depth of longwall 52303 reached 287 m, a new main longwall recovery roadway was excavated at the end of the pre-driven adapting roadways. The mesh installation was also optimized using the method discussed previously. According to the frequency of the six previous periodic roof pressures, the average step was 17 m and the persistence length was 4.6 m. The nearest periodic roof pressure manifested 33.8 m from the main longwall recovery roadway, thus the predicted next periodic roof pressure distance was 16.8 m. The minimum mesh installation length was 12 m. According to Equation [3], the mesh installation position should be 19.2 m. Therefore, the researchers suggested the mesh should be installed at 19.2 m instead of the empirical position of 16 m used previously. The mining practice indicated that the mining pressure during mesh installation was normal and the periodic roof pressure occurred at 15.5 m when the mesh installation was completed. By using this procedure, roof fall was prevented.

Since then, all of the adapting roadways are decommissioned when the cover depth of longwall faces exceeds 212 m in the Shendong coalfield. The mesh installation positions in all longwall faces are also determined by Equation [3]. With the use of such countermeasures, no incidents of roof fall and support failure occurred when longwall faces approached the recovery roadways, which demonstrates that the proposed countermeasures are appropriate and effective.

Conclusions

The Shendong coalfield commonly adopts pre-driven longwall recovery roadways, which greatly improves the rate of extraction. The special roadways, adapting roadways, are also usually pre-driven to ensure the rapid and precise match of the longwall and recovery roadway floor. With the increase in mining depth, several support failure and roof fall incidents occurred near the longwall recovery roadway area, which posed a threat to the safety of underground personnel and the mining operation. By analysing case studies of different incidents and the mining layouts, theoretical investigations and numerical simulation were conducted. It was found that the adapting roadways were the main cause of the roof fall incidents. The adapting roadway increases the roof exposure area and divide the coal mass in front of the longwall face into several separate coal pillars. This dramatically increases deformation of the coal mass and roof

control difficulties. When the cover depth reaches a certain value, failure of the coal mass can occur over a large area, triggering serious accidents such as roof falls and support failure.

By considering coal pillar stability and the manageability of the deformation of the roadways, the maximum applicable depth of the adapting roadways is determined to be 212 m. A method is also proposed to determine the optimum flexible mesh installation position. This systematic approach is presented in a flow chart, which can also be applied to other mines under different conditions.

In particular, for the Shendong coalfield, studies have shown that the adapting roadways should not be used at a cover depth of more than 212 m; and if these roadways are already pre-driven, they should be backfilled or a new main longwall recovery roadway should be excavated at the end of the adapting roadways. The optimum position of mesh installation should be chosen according to determination of mine pressure, and the result can be different from the one determined empirically. The findings have been applied successfully to several longwall faces, with safe and smooth production and longwall moves, which demonstrated their effectiveness.

Acknowledgements

The authors would like to express their gratitude to the State Key Research Development Program of China (2016YFC0501100) and the Fundamental Research Funds for the Central Universities (2015XKMS098) for their financial support. The authors are also grateful to Shenhua Shendong Coal Group Co., Ltd. for its financial support that assisted the China University of Mining and Technology's research project and the field test, in particular Chen Sushe for his help during the field observation and Dayang Xuan for his advice.

References

Barczak, T.M. 2005. A retrospective assessment of longwall roof support with a focus on challenging accepted roof support concepts and design premises. *Proceedings of the 25th International Conference on Ground Control in Mining*, Morgantown, West Virginia, 2–4 August 2005. West Virginia University. pp. 232–243.

Barczak, T.M., Chen, J., and Bower, J. 2003. Pumpable roof supports: developing design criteria by measurement of the ground reaction curve. *Proceedings of the 22th International Conference on Ground Control in Mining*, Morgantown, West Virginia, 5–7 August 2003. West Virginia University. pp. 283–293.

Barczak, T.M., Tadolini, S.C., and Zhang, P. 2005. Evaluation of support and ground response as longwall face advances into and widens pre-driven recovery room. *Proceedings of the 25th International Conference on Ground Control in Mining*, Morgantown, West Virginia, 2–4 August 2005. West Virginia University. pp. 1–3.

Batchler, T. 2016. Analysis of the design and performance characteristics of pumpable roof supports. *International Journal of Mining Science and Technology*. doi:10.1016/j.ijmst.2016.10.003

Bauer, E.R. and Listak, J.M. 1989. Productivity and equipment removal enhancement using pre-driven longwall recovery rooms. *Proceedings of the 1989 Multinational Conference on Mine Planning and Design*, Lexington, Kentucky, 23-26May 1989. pp. 119–124.

Chen, S.S. 2014. Dynamic mine strata pressure control technology of full-mechanized coal mining face passing through concentrated coal pillars in above seam. *Coal Science and Technology*, vol. 42, no. 6. pp. 140–143.

Chen, Y.G. and Lu, S.L. 1994. Strata Control Coal Mine Roadways in China. China University of Mining and Technology Press, Xuzhou. pp. 51–52.

Hou, Z.J. 2000. Analysis of combinatorial key strata stability in shallow coal seam with thick loose bed. *Journal of China Coal Society*, vol. 25, no. 2. pp. 127–131.

Huang, Q.X. 2002. Ground pressure behavior and definition of shallow seams. *Chinese Journal of Rock Mechanics and Engineering*, vol. 21, no. 8. pp. 1174–1177.

Ju, J.F. and Xu, J.L. 2013. Prevention measures for support crushing while mining out the upper coal pillar in close distance shallow seams. *Journal of Mining and Safety Engineering*, vol. 30, no. 3. pp. 323–330.

Ju, J.F., Xu, J.L., and Zhu, W.B. 2015. Longwall chock sudden closure incident below coal pillar of adjacent upper mined coal seam under shallow cover in the Shendong coalfield. *International Journal of Rock Mechanics and Mining Sciences*, vol. 77. pp. 192–201.

Kang, H., Lv, H., Zhang, X., Gao, F., Wu, Z., and Wang, Z. 2015. Evaluation of the ground response of a pre-driven longwall recovery room supported by concrete cribs. *Rock Mechanics and Rock Engineering*, vol. 49, no. 3. pp. 1–16.

Liu, X.Q. and Chen, S.S. 1999. Application of technology of pre-driven recovery rooms in fully mechanized coal mining faces. *China Coal*, vol. 25, no. 10. pp. 36–37.

Lu, H.W. 2014. The mechanism of stability of pre-driven rooms and the practical techniques. *Journal of China Coal Society*, vol. 39, no. SI. pp. 50–56.

Qian, M.G., Shi, P.W., and Xu, J.L. 2010. Ground Pressure and Strata Control. China University of Mining and Technology Press, Xuzhou, pp. 221-222.

Shi, P.W. and Hou, Z.J. 1996. Law of roof breaking movement of shallow seams in Shenfu CMA. *Journal of Xi'an Mining Institute*, vol. 16, no. 3. pp. 204–207.

Tadolini, S.C. and Barczak, T.M. 2006. Design parameters of roof support systems for pre-driven longwall recovery rooms. *Transactions of the Society for Mining Metallurgy and Exploration*, vol. 318. pp. 87.

Tadolini, S.C. and Barczak, T.M. 2001.Rock mass behavior and support response in a longwall panel pre-driven recovery room. *Proceedings of the 6th International Symposium on Ground Support in Mining and Civil Engineering Construction*, Cape Town, South Africa, 30 March–3 April 2008. Southern African Institute of Mining and Metallurgy, Johannesburg. pp. 167–182.

Tadolini, S.C., Zhang, Y., and Peng, S. 2002. Pre-driven experimental longwall recovery room under weak roof conditions–design, implementation, and evaluation. *Proceedings of the 21st International Conference on Ground Control in Mining*, Morgantown, West Virginia, 6–8 August 2002. West Virginia University. pp. 1–10.

Wichlacz, D., Britten, T., and Beamish, B. 2009. Development of a pre-driven recovery evaluation program for longwall operations. *Coal 2009: Proceedings of the Coal Operators' Conference*, Wollongong, New South Wales, 12-13 February 2009. Aziz, N. (ed.). University of Wollongong and the Australasian Institute of Mining and Metallurgy. pp. 23–36.

Xu, J.L., Zhu, W.B., Wang, X.Z., and Yi, M.S. 2009. Classification of key strata structure of overlying strata in shallow coal seam. *Journal of China Coal Society*, vol. 34, no. 7. pp. 865–870.

Xu, J.L., Zhu, W.B., Wang, X.Z., and Zhang, Z.J. 2012. Influencing mechanism of gully terrain on ground pressure behaviors in shallow seam longwall mining. *Journal of China Coal Society*, vol. 37, no. 2. pp. 79–85.

Zhang, P., Mishra, M., Trackemas, J., Zeglen, E., Huff, C., Peng, S.S., and Chen, J. 2006. Pre-driven longwall recovery room under weak roof conditions–design, evaluation, and monitoring. *Proceedings of the 25th International Conference on Ground Control in Mining*, Morgantown, West Virginia, 2–4 August 2005. West Virginia University. pp. 221–228.

Zhu, W.B. 2011. Study on the instability mechanism of key strata structure in repeating mining of shallow close distance seams. *Journal of China Coal Society*, vol. 36, no. 6. pp. 1065–1066. ◆

http://dx.doi.org/10.17159/2411-9717/2017/v117n11a12

Ore transport system selection for the Sintoukola potash project in the Republic of Congo

by P. Kluge*, D. Limpitlaw†, and W. Swanepoel*

Synopsis

Material transport is one of the major components of a bulk mining system, and the selection of the most appropriate material transport system can have a significant bearing on the success of a mining project, particularly in Africa. This paper presents a three-criterion methodology for assessing a mine transport system. The three criteria are focused on operability, economic analysis (using the net present cost (NPC) methodology), and safety, health, and environment.

The methodology is demonstrated in a case study assessment of truck hauling *vs* overland conveyor belt for the Sintoukola potash project in the Republic of Congo. The results show that for the given project configuration, an overland conveyor belt is preferred on the basis of all three criteria.

Keywords

bulk materials handling, ore transport system selection, overland conveyor belt, hauling, net present cost, Congo Brazzaville.

Introduction

The repeated performance of a number of fundamental processes lies at the heart of the mining process. These processes constitute the mining cycle (Singh and Saperstein, 1992). These fundamental processes are commonly referred to as 'unit operations' and comprise: fragmentation, loading, and haulage/transportation. There are also a number of auxiliary unit operations (such as site preparation and provision for services) but these are not discussed here. This paper deals with the selection of an ore transportation system for a planned potash mine in the Republic of Congo (Congo Brazzaville, RC).

The Sintoukola potash project

The Sintoukola potash project is a greenfield potash project located approximately 90 km north of the city of Pointe Noire in the RC. The project is located on the coastal plain between the Mayombé Mountains in the east and the Atlantic Ocean in the west. The potash deposit occurs within the Lower Cretaceous Loeme Evaporite Formation and is approximately 300 m below the surface. This evaporite sequence in the Congolese coastal basin comprises horizontal, undulating layers of salt. The targeted ore mineral is sylvinite (KCl), although carnallitite ($KMgCl_3 \cdot 6H_2O$) is also present. The sylvinite is interbedded with halite (NaCl) and other salts.

The project consists of a planned underground board-and-pillar mine, a 35 km transport corridor to the coast, and a process plant and ship loading facility for export of potash to foreign markets. Underground access will be via a twin vertical shaft system. The mine and haulage/processing facilities are to be located in two of the administrative regions or *sous-préfectures* (Madingo Kayes and Loango) in the Kouilou Department.

The project currently consists of a measured and indicated resource of 573 Mt of sylvinite, providing a sufficient reserve for a 23-year life of mine using a conventional underground mining method to produce 2 Mt/a of muriate of potash (MoP).

In order to achieve this production, 6.9 Mt/a (960 t/h) of run-of-mine (RoM) ore will be mined using a room-and-pillar method, utilizing continuous miners. The RoM ore will then be transported to a dedicated processing plant located 35 km from the mine at the coast. Due to the hydrophilic nature of the salts, the ore needs to be kept dry at all times. At the processing facility, the potash salt (KCl) will be separated from the waste salt (NaCl), dried, stored, and then loaded onto barges for transhipment to ocean-going vessels using a custom-built jetty facility. The waste salt will be pre-diluted and then discharged into the ocean.

A comprehensive trade-off study of all transport solutions was conducted in the early stages of the prefeasibility study (PFS). This paper describes the methodology followed to select the materials transport system for

* *Kore Potash Limited.*

† *Centre for Sustainability in Mining and Industry, University of the Witwatersrand, South Africa.*

 ISSN 2225-6253. Paper received Nov. 2015; revised paper received Jun. 2016.

Ore transport system selection for the Sintoukola potash project in the Republic of Congo

Figure 1—Location map

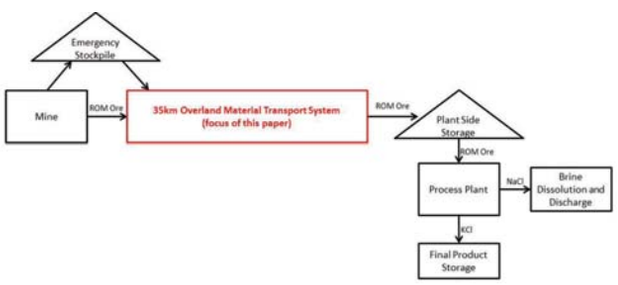

Figure 2—A simple diagram showing the material storage and transport segments

moving the ROM ore from the mine site to the process plant. The selection of the materials transport system was undertaken subsequent to the PFS and in preparation for the feasibility study (FS), based on new fieldwork data that had become available.

Bulk ore transport

For bulk commodity mines, ore transport is particularly critical as it commonly constitutes a significant component of overall capital and operating costs. Generally, the materials handling component makes up 30-75% of a mine's operating cost (Karande and Chakraborty, 2013). In Central Africa, as in many developing regions, mineral projects have to invest substantially in establishing transport infrastructure. Existing infrastructure is frequently over-utilized, has poor levels of availability, and/or is not fit for purpose. Consequently, selecting the ore transport system for the Sintokoula potash project is crucial to the project's viability.

The PFS for the project was completed in 2012 and recommended a fleet of road-train haul trucks using a dedicated haul road. The haul road system was selected after a comprehensive trade-off study conducted in mid-2011, which considered conveyors, rail, road, and a pipeline for material transport in combination with different plant locations and layouts. Rail and conveyors were initially discarded on account of their high upfront capital costs, while the pipeline was eliminated for operability reasons.

After the completion of an on-site geotechnical investigation programme, it became apparent that the costs of haul road construction were significantly underestimated during the original trade-off study. In addition, an independent review of the PFS indicated that the costs for overland conveyors may have been overestimated. According to Saxby and Elkink (2010), the operating costs of conveyor belts for distances between 25 and 40 km should be approximately 20% of those of truck transport. These authors reported that single-flight conveyor lengths increased from around 5 km to 20 km between 1985 and 2005. Consequently, fewer flights, with reduced re-handling of ore, are required to cover large distances. This trend has significantly improved the competitiveness of conveying systems.

In addition, with the completion of the Environmental and Social Impact Assessment (ESIA), a better understanding of the social and health and safety context of the area highlighted the risks inherent in an around-the-clock road hauling operation. It was therefore decided to revisit the material transport system selection in 2013, by comparing an overland conveyor option to the PFS road hauling option.

Transport system selection

There are numerous factors to consider when selecting a transport system. Karande and Chakraborty (2013, p. 2) list criteria such as 'better utilization of manpower, providing product flexibility, increasing productivity, decreasing lead time, reduction in handling cost, increased efficiency of material flow, and enhancement of production process' as just some of the criteria to consider. They emphasize that the decision-making process should use a multi-criteria analysis approach.

Many complex analytical methods, such as the analytical hierarchical process, exist for this type of multi-criteria decision-making, and the applications in the mining industry have been described by Kluge and Malan (2011), among others. Owusu-Mensah and Musingwini (2011) elaborate on how this method was used to select an ore transport system for a lower tonnage at a Ghanaian gold mine. The emphasis in this paper, however, is on explaining a simply weighted multi-criteria process that can be more easily and simply applied in a project setting, without the use of complex matrix algebra or other tools and systems.

Pratt (2008) suggests that the assessment of materials transport systems focuses on the following fundamental questions:

- How reliable are they? What is the degree of technical risk in a business context?

- What levels of flexibility do they offer?
- How capital-effective are they? What returns are indicated by the balance of capital and operating cost estimates?

In modern mining practice, environmental, and social impacts of projects must also be considered alongside the traditional technical and economic considerations when optimizing projects – bulk ore transport systems have the potential for high environmental and social impacts.

For the Sintoukola project, the selection of the transport system was based on:

- Minimizing capital and operating costs over the working life of the system
- Optimizing operability of the system
- Minimizing environmental consequences of operation of the system
- Maximizing environmental benefits of the system alignment
- Minimizing safety risks of system operation.

Consequently, the project team decided to follow a three-pronged approach in assessing the transport system:

- Operability: the criteria listed by Karande and Chakraborty (2013) and the questions regarding reliability and flexibility proposed by Pratt (2008) were grouped into one category focused on the impact of the material transport system on the overall project system. This includes power, water, employees, stockpile sizing, availability, and maintenance
- Net present cost (NPC): as economic profitability and return on investment underlie all mining projects, it is important to consider the impact that the choice of transport system will have on project value. This includes an analysis of operating, capital, and sustaining capital costs, resulting in comparison on NPC terms
- Safety, health, and environment assessment: the focus here is to both identify 'show-stoppers', that immediately exclude a system from further consideration, and to weigh and compare those impacts that can be mitigated.

For the sake of simplicity, all three criteria used in the assessment were considered to be of equal importance. Each will now be discussed in turn. The focus of the trade-off study discussed below is to compare an overland conveyor belt with the PFS base case of using a fleet of 25 road-train trucks to transport RoM ore on a dedicated haul road.

Operability assessment

Two workshops were held with conveyor belt consultants, the project infrastructure engineers, and the owner's team, which included the authors of this paper. The objective was to determine the impact of switching from hauling to a conveyor on the overall project configuration, identify critical flaws, and assess the potential for reducing project complexity and improving the project operability and reliability. The following points were identified:

- Fuel and power supply
- Backup power requirements
- Availability and maintenance
- Labour requirements
- Reduction in surface facilities
- Sizing stockpiles for system downtime
- Scalability.

Fuel and power

Fuel supply logistics are considerably more complex for truck-based hauling. Fuel needs to be transported via tanker from Pointe Noire and special fuel storage and truck re-fuelling infrastructure needs to be provided. Although the cost benefit of reducing this infrastructure has not been accounted for in the NPC analysis, it results in an improvement in project operability.

The overland conveyor is expected to require between 3.5 MW and 5 MW of installed power capacity. This increases the base case power demand for the project by between 6% and 9%. The increase is considered small enough to not materially affect the design of the electrical reticulation system. Drives and booster drives can be readily powered from the planned transmission line connecting the mine site and process plant. The oil price is expected to be more volatile than the gas price (gas is used to generate electricity in the RC), which also makes the conveyor option preferred.

The planned emergency power supply is insufficient to sustain operations in the case of a grid interruption. It is sized to ensure that personnel can be evacuated safely and that equipment can be responsibly shut down. If the preference is to shut down the overland conveyor only when it is empty, additional backup power will need to be considered. These possible additional costs have not been considered in the NPC analysis. This might lead to an increase in project complexity, if restarting with a loaded conveyor belt is not feasible.

Availability, downtime, and maintenance

Haul trucks are collectively expected to be available almost continually. The only major downtime can result from problems at the loading or offloading facility or a major interruption on the haul road. The two conveyors in series are expected to have a lower availability. Each conveyor has an availability of 94%, resulting in a system availability of 88%. The resulting lower capacity can be offset by increasing the design capacity of the belts and allowing for larger stockpiles. Furthermore, planned belt downtime should be scheduled to coincide with plant maintenance. Nevertheless, the increased stockpile requirements at the mine and plant lead to increased project complexity.

A large truck workshop is required to maintain the hauling fleet. The conveyor belt can be maintained by a smaller team with a smaller workshop. The exclusive presence of sand to a depth of 40 m provides poor geotechnical conditions for the construction of platforms, storage yards, and workshops. Reducing or eliminating the footprint of this infrastructure is therefore of great benefit to the operation. These costs savings have not been included in the NPC analysis, but this leads to a reduction in project complexity.

A tear on the belt will require 2–3 days' downtime to splice. Provision for downtime of up to a week has been made in the cost assumptions. At the mine site, when the storage is full, a temporary stockpile is available for

emergencies, so mining operations will not be interrupted. To ensure that no production interruptions occur at the plant site, a significantly larger dome or a warehouse, similar to that used for product storage, will need to be constructed. For this analysis it was assumed that two domes with total storage capacity of 120 kt will be constructed. A reassessment of the planned stockpile sizing is recommended, to ensure that it is adequate. The requirement for larger stockpiles and the possibility of major production interruptions when using a conveying system increase the complexity of the project

Scalability

There is a possibility for an expansion of mine production in the future. A haul road is easily scalable, as additional trucks linearly increase transport capacity. However, both loading and offloading facilities will be operating at maximum capacity and thus need to be replicated to increase production.

Conveyor belts are designed for a fixed capacity and upscaling requires additional capital outlay for a second belt. However, the incremental cost for specifying a larger capacity belt at the design phase is relatively small. The capacity required for the current Sintoukola production is 1080 t/h while the cost estimates made for the project by two suppliers were based on 1600 t/h and 2400 t/h systems. It is suggested that a belt with larger capacity be installed from the outset. Production can then be increased when required without the outlay of additional capital. This implies that if a sufficiently large belt is installed initially, the conveyor belt actually increases the future operability in the case of a production expansion. The large operating cost advantages of a conveyor belt would then also be further enhanced.

Labour

The truck hauling option requires almost 100 staff, while the conveyor will require fewer than 40. This reduces the strain on the employee facilities, as well as general overheads. These costs savings have not been included in the NPC analysis, but this leads to a reduction in project complexity, as fewer people need to be accommodated in the project camp.

The operability review could identify no major flaw with an overland conveyor. In fact, many project areas have reduced project complexity and improved operability with the use of a conveyor belt. The major factor that requires addressing is the correct sizing of the mine and process plant stockpiles, but allowance for larger stockpiles has been made in the NPC assessment.

Economic analysis

The cost comparison consists of capital, sustaining capital, and operating costs. Using these parameters a NPC comparison can be made. All costs discussed in this section are in US dollars.

Capital costs for hauling

The haul road capital costs form the basis for the cost comparison. The various components of the capital costs are listed in Table I.

- Fencing, earthworks and forest clearing, crossing culverts, and remoteness factor are explicitly costed for the conveyor options, but were included in direct capex for truck hauling
- The haulage option did not require additional service and access roads and did not require electrical installations
- The capital cost of the haul road is estimated to be $116 million, with the trucks and trailers comprising an additional $16 million.
- Loading and offloading includes the loading and offloading infrastructure as well as the associated product storage at the mine and process site. For the truck hauling option, the cost of these facilities is approximately $62 million, which can be divided as follows:
  - Storage at mine site: $12 million
  - Loading at mine site: $25 million
  - Offloading at process plant site: $14 million
  - Storage at process plant site: $11 million.
- A contingency of 15% was used for the haul road and road trains
- Engineering, procurement, construction, and management (EPCM): 12.5% was used for the haul road as applied in the PFS
- 1.2% was used for insurance as per the PFS.

Capital cost for overland conveyor

The overland conveyor will be approximately 35 km long, will be fully covered, and for the purpose of this evaluation consists of two flights. Three estimates of conveyor costs, considered to be at a Class 5/4[1] level of accuracy, were supplied by three different suppliers and were used in this comparison. The capital costs are compared in Table I. The following assumptions were used for the individual line items.

Supplier 1 based the direct capex figures on a previous project database derived from a belt system consisting of three 11.7 km flights, with a capacity of 1600 t/h and a belt speed of 3.5 m/s. This system was estimated to cost $92 million. Although the belt at Sintoukola will likely be configured in two flights, it was felt that this cost for a three-flight belt was comparable for this distance.

Supplier 2 based direct capex on a project in South Africa at the time of this study. A belt with a capacity of 2400 t/h and belt speed of 6.5 m/s was costed at approximately $1769 per metre or $83 million. Supplier 3 provided the estimate prepared for the original trade-off study in 2011 at $201 million. Fencing costs are based on the assumption that both sides are fenced for 35 km at $10 per metre.

The haul road costs include a cost of $900 000 per kilometre for site clearance and earthworks. It was assumed that the costs for the conveyor will be 15% of these as a conveyor can accommodate significantly steeper angles and therefore requires less cut and fill. This was confirmed in an independent assessment by an engineering company, who estimated the earthworks requirements and costs if a conveyor was superimposed on the haul road corridor. Their estimated cost of approximately $2 million for earthworks is in the same order of magnitude as the 15% factor applied.

[1] AACE International Recommended Practice No. 18R-97

The cost of the service road was estimated as $3.5 million by the project infrastructure consultants. This equates to $100 000 per kilometre. With the conveyor option, there will be no haul road to provide vehicle access to the process plant and mine site, and an additional 14 km of access road must be constructed at a cost of $2 million per kilometre.

The haul road costs include $70 000 per kilometre for crossing culverts. It was assumed that the costs for the conveyor will be 50% of these, as conveyor crossings are comparatively simple.

Each of the two belts will have a booster drive, which means a total of four drives is required. As one drive will be located at the process plant site, three take-offs from the overhead line with associated infrastructure are required. These were estimated to cost $5 million in total.

The 'remoteness allowance' attempts to capture the additional cost of construction in the RC rather than South Africa. This is mostly as a result of higher transport, concrete, and supervision costs.

Loading and offloading costs include the loading and offloading infrastructure as well as the associated product storage at the mine and plant site. As the loading and offloading arrangements for the conveyor are expected to be much simpler than for the road trains, these costs can be reduced. Storage at the plant site will need to be increased significantly due to lower system availability for a conveyor compared to a haul truck fleet. For the conveyor option, the loading/offloading cost is $50 million, which can be divided as follows:

- Storage at mine site: $12 million
- Loading at mine site: $5 million
- Offloading at process plant site: $3 million
- Storage at process plant site: $30 million.

Given the higher level of uncertainty in the conveyor costs, a contingency of 20% was used. An EPCM cost of 10% was recommended for the conveyor belt by the suppliers. 1.2% was used for insurance as per the PFS.

It can be seen from Table I that the capital cost estimates provided by suppliers 1 and 2 are similar and only marginally higher than those for the hauling option. The original conveyor capex estimate used in the first trade-off study is approximately $90 million higher.

The following capital savings on the PFS cost estimate resulting from the installation of an overland conveyor were not considered here:

- Smaller workshop footprint and requirements
- Savings on the employee facilities due to a smaller workforce
- Reduced fuel farm requirements and refuelling facilities
- Reduced earthworks at mine and process plant site, no turning loops, and smaller loading and offloading infrastructure.

Sustaining capital

The sustaining capital is shown in Table II. Sustaining capital for the truck hauling option consists mainly of maintaining the drainage systems and the relaying of tarmac on the haul road as well as infrequent truck fleet replacements. A factor of 2% on initial capital, as recommended by Saxby and Elkink (2010) was used to determine annualized sustaining capex on the conveyors.

The sustaining capital costs are considerably higher for the conveyors, which can be expected given the increased amount of mechanical and electrical equipment.

Operating costs

Annual operating costs of the truck hauling option at steady state are $27.6 million, which is made up of the following:

- $0.07 per ton loading facility

Table I

Comparison of capital costs ($ thousand)

Option	Hauling	Conveyor Supplier 1	Conveyor Supplier 2	Conveyor Supplier 3
Direct capex	115 664	92 000	82 539	201 600
Fencing	Included	700	700	Included
Earthworks and forest clearing	Included	4 725	4 725	Included
Service road	Not required	3 500	3 500	Included
Access road	Not required	27 440	27 440	Included
Crossing culverts	Included	1 225	1 225	Included
Electrical	Not required	5 000	5 000	Included
Remoteness allowance	Included	5 000	5 000	Included
Loading and offloading	63 135	50 000	50 000	40 000
Contingency	26 820	37 918	36 026	48 320
EPCM	25 702	22 751	21 616	28 992
Insurance	2 467	2 730	2 594	3 479
Total initial capex	**233 789**	**252 989**	**240 365**	**322 391**

Table II

Comparison of sustaining capital costs ($ thousand per annum)

Option	Hauling	Conveyor Supplier 1	Conveyor Supplier 2	Conveyor Supplier 3
Sustaining capex (LoM) Sustaining capex ($ thousand per annum)	36 400 1 820	5 060	4 807	6 448

- $2.85 per ton haul truck operations and maintenance
- $1.12 per ton haul road maintenance.

Supplier 3 estimated the operating costs of the conveyor system at just under $4 million per annum. Supplier 1 estimated the operating cost for three conveyors in series at $0.67 per ton, resulting in an opex of $4.5 million per annum. Calculating the operating costs from first principles results[2] in a cost of $4.2 million per annum. This was used for the supplier 2 option. From Table III it is apparent that the operating cost estimates by the various suppliers, as well as those derived from first principles, lie in a narrow range. These costs are also in agreement with the assertion by Saxby and Elkink (2010) that conveyor operating costs for these distances should be approximately 20% of those for trucking.

NPC comparison

Using the cost inputs discussed above, a NPC analysis based on a discount rate of 10% was used to assess the total costs of the material transport systems. The base year was 2013. The results are shown in Table IV and in the plot of cumulative NPC values in Figure 3.

An improvement of between $125 million and $140 million in NPV is possible by changing from hauling to conveying. Even using the supplier 3 estimate that was deemed 'conservative' results in a better NPV than hauling.

Environmental, health, safety, and social analysis

A desktop assessment comparing the potential impacts and risks associated with the road-train trucking option and overland conveyors was undertaken to complement the technical and economic assessments. Four categories were used: environment, health and safety, social impacts, and closure. Sub-categories were weighted according to importance. A weight of 1 was assigned to sub-categories of low importance and a weight of 3 to critical sub-categories. The performance of the two modes of transport was then compared in each sub-category with poor performance attracting a score of 1 and excellent performance a score of 3. These scores were multiplied by the weighting to obtain the weighted scores, which were summed to determine the overall relative performance in each category. These results are presented below.

Environmental performance

Belt conveyors operate relatively quietly and dust is an issue only at loading and discharge points, where it can be contained and dealt with (Unmacht and Alspaugh, 2009). Measured sound levels for conventional belt conveyors transporting 10 000 t/h at 5 m/s in the coal industry range[3] between 113 dB(A) and 119 dB(A) per 100 m of length. 'Low-noise' conveyors operate at levels down to 101 dB(A) per 100 m (Brown, 2004). For Rio Tinto's Simandou project, sound pressure levels of 119 dB(A) were reported for Komatsu haul trucks and 117 dB(A) for Cat 777 trucks. The sound pressure levels expected for the road trains would be lower than these figures.

[2] 4 MW power, 30 local employees, 3 expats, 5 vehicles, 3% of mechanicals for spares

[3] This is an order of magnitude greater than the mass flow rate for Sintoukola.

Table III

Comparison of operating costs ($ thousand per annum)

Option	Hauling	Conveyor Supplier 1	Conveyor Supplier 2	Conveyor Supplier 3
Opex ($ thousand per annum)	27 674	4 590	4 200	3 840

Table IV

Comparison of NPC ($ thousand)

Option	Hauling	Conveyor Supplier 1	Conveyor Supplier 2	Conveyor Supplier 3
NPC	410 394	287 428	271 956	352 146

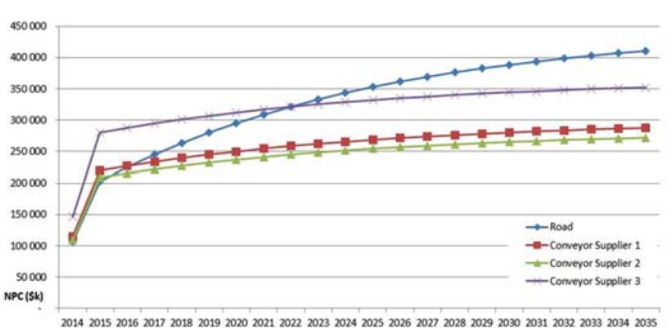

Figure 3—NPC analysis of the various options ($ thousand)

Carbon dioxide (CO_2) emissions from a belt transport system are reduced by factors in the range 1.2–1.4 kg/t.km relative to truck haulage (Raaz and Mentges, 2011). For a distance of 35 km and an annual production of 6.9 Mt, this equates to a potential reduction in CO_2 emissions of 289 800 to 338 140 t annually. The relative environmental performance of the two systems is summarized in Table V.

Health and safety performance

Belts can be monitored and operated remotely from a central control room, removing operators from possible risk areas (Unmacht and Alspaugh, 2009). There will be reduced risk of night-time accidents as other users will not be able to utilize the conveyor route to the degree possible with a haul road. Pedestrians are at risk with the haul truck option to a greater degree than with the overland conveyors. The potential risks of unauthorized access are consequently lower.

Conveyor belts require a significant amount of heat to commence combusting, but once ignited, the fire cannot easily be controlled (le Roux, 2004). Belts are likely to be capable of self-sustained combustion (Table VI).

Social performance

A disadvantage from a social perspective is that conveyor systems are less labour-intensive than trucks and require only one person per km for operation[4]. This equates to approximately 40 people for a belt *versus* more than 100 for the truck option. This disadvantage is offset by the lower potential social impacts (Table VII).

Closure

Overland conveyors can accommodate steeper gradients than road trains and thus the need for cut and fill is reduced. Current conveyor technology can tolerate inclines of up to 35°, while haul trucks are limited to gradients of not much more than 5° (Metzger, 2007; Unmacht, and Alspaugh, 2009). While a more realistic maximum incline for an overland conveyor is probably around 12°, this still represents a significant reduction in cut and fill volumes required and thus a reduced rehabilitation footprint on closure. Conveyors are also able to curve in the horizontal plane and can avoid hills (Table VIII).

The contention that trucks have higher CO_2 and dust emissions, suffer from more erratic labour costs (due to larger labour complements), have higher maintenance requirements (while conveyors have longer lifespans), and have high noise levels (Superior Industries, 2009) is supported by this study. In the comparative assessment, conveyors scored a total of 110 *versus* 62 for trucks. This represents a significant advantage over trucks from an environmental, social, and health/safety perspective.

[4] Industry rule of thumb

Table V

Environmental criteria performance comparison (note higher risks obtain a lower score)

Environmental aspects	Weighting	Belts Score	Trucks Score	Belts Weighted score	Trucks Weighted score
Noise	2	2	1	4	2
Dust/particulates	3	3	3	9	9
Exhaust gases	1	3	1	3	1
Carbon footprint	1	3	1	3	1
Light pollution/visual intrusion*	2	3	1	6	2
Animal strike	2	3	1	6	2
Spills (hydrocarbon/product)	3	2	1	6	3
Land surface impact (cut and fill)	3	3	1	9	3
Hydrocarbon logistics	1	3	1	3	1
Sub-total				49	24

*Assuming that the belt is not illuminated

Table VI

Health and safety criteria performance comparison (note higher risks obtain a lower score)

Health and safety aspects	Weighting	Belts Score	Trucks Score	Belts Weighted score	Trucks Weighted score
Risk of accident and injury	3	2	1	6	3
Risk of unauthorised access	3	3	1	9	3
Night operation	2	3	1	6	2
Driver fatigue	2	3	1	6	2
Fire	3	1	2	3	6
Sub-total				30	16

Table VII

Social criteria performance comparison (note higher risks obtain a lower score)

Social aspects	Weighting	Belts Score	Trucks Score	Belts Weighted score	Trucks Weighted score
Control of access to the national park	3	3	2	9	6
Social disruption (village migration)	3	3	1	9	3
Employment	3	1	3	3	9
Ease of underpass construction	2	2	1	4	2
Sub-total				25	20

Table VIII

Closure criterion performance comparison (note higher risks obtain a lower score)

Closure aspects	Weighting	Belts Score	Trucks Score	Belts Weighted score	Trucks Weighted score
Removal of infrastructure	2	3	1	6	2
Sub-total				6	2

Summary and conclusion

This paper presented a three-criterion methodology for assessing a mine transport system. The methodology was then demonstrated on a case study assessment of truck hauling *vs* overland conveyor belt for the Sintoukola potash project in the Republic of Congo. Table IX summarizes the performance of the two considered transport methods for the three considered criteria.

With similar capital costs, but significantly lower operating costs, the NPC analysis showed that an overland conveyor belt should be clearly preferred over a fleet of haul trucks for this application. The improvement in project value is expected to be between $125 million and $140 million.

During two workshops, no major critical flaws could be identified with the overland conveyor. Some project component complexity is increased, while in other areas operational improvements can be realized as a result of an overland conveyor.

An assessment based on environmental, health and safety, social, and closure factors was undertaken with specific focus on comparing trucks and conveyor belt. The conveyor belt was preferred in all four aspects.

It was concluded by the project team that an overland conveyor should be preferred to the haul road, and this key change to the project configuration will be taken into the feasibility study.

Table IX

Summary of all three criteria

Criterion	Conveyor	Hauling
Operability		
Fuel and power	Preferred	
Availability, maintenance		Preferred
Scalability	Preferred	
Labour	Preferred	
Economic analysis	$270m–$285m	$410m
Net present cost	Preferred	
SHE Analysis		
Environmental	Preferred	
Health and safety	Preferred	
Social	Preferred	
Closure	Preferred	

References

Brown, S.C. 2004. Conveyor noise specification and control. *Proceedings of Acoustics 2004*, Gold Coast, Australia, 3-5 November. Mee, D.J., Hooker, R.J., and Hillock, I.D.M. (eds.). Australian Acoustical Society. pp. 269–276.

Karande, P. and Chakraborty, S. 2013. Material handling equipment selection using weighted utility additive theory. *Journal of Industrial Engineering*, vol. 2013, Article ID 268708.

Kluge, P. and Malan, D.F. 2011. The application of the analytical hierarchical process in complex mining engineering design problems. *Journal of the Southern African Institute of Mining and Metallurgy*, vol. 111, no. 12. pp. 847–855.

Le Roux, H. 2004. Conveyors come under scrutiny after Northam Platinum mine fire. *Mining Weekly*, 29 October.

Metzger, D. 2007. Long distance conveying – long term savings. *Technical Bulletin*, Superior Industries LLC, Morris, MN. 7 pp.

Owusu-Mensah, F. and Musingwini, C. 2011. Evaluation of ore transport options from Kwesi Mensah Shaft to the mill at the Obuasi mine. *International Journal of Mining, Reclamation and Environment*, vol. 25, no. 2. pp. 109–125.

Pratt, A.G.L. 2008. Mine haulage – options and the process of choice, *Proceedings of the Tenth Underground Operators' Conference*, Launceston, Tasmania. Australasian Institute of Mining and Metallurgy, Melbourne. pp 179–188.

Raaz, V. and Mentges, U. 2011 Comparison of energy efficiency and CO2 emissions for trucks haulage vs in-pit crushing and conveying of materials. *Proceedings of the SME Annual Meeting.* Society for Mining, Metallurgy and Exploration, Inc., Littleton, CO. 6 pp.

Saxby, P. and Elkink, J. 2010. Material transportation in mining – trends in equipment development and s*election. Australian Bulk Handling Review*, March/April 2010.

Singh, M.M. and Saperstein, L.W. 1992. Production operations. *SME Mining Engineering Handbook*, 2nd edn. Vol.1. Hartman, H.L. (ed.). Society for Mining, Metallurgy and Exploration, Inc., Littleton, CO, USA. pp 677–802.

Superior Industries. 2009. Overland conveyor systems. Superior Industries LLC, Morris, MN. 4 pp.

Unmacht, D. and Alspaugh, M. 2009. Harnessing gravity – the new rock conveying system planned for National Cement's Lebec plant. https://www.worldcement.com/magazine/world-cement/may-2009/ 4 pp. ◆

http://dx.doi.org/10.17159/2411-9717/2017/v117n11a13

Investigation of Western Australia's rehabilitation fund as a fiscal policy solution for South African abandoned mines

by D. Klopper* and J-A. Wessels*

Synopsis

South Africa's mining legacy has resulted in a large number of abandoned mines which pose ongoing environmental threats. The regulatory framework makes no provision for cases of abandoned mines, nor does the legislation delegate due responsibility or have an approved strategic plan for their rehabilitation. A mixed methods approach was taken to investigate the challenges related to South African abandoned mine sites and to compare South Africa's legal provisions for abandoned mine site management with those of Western Australia, specifically the Mining Rehabilitation Fund (MRF) Act. Surveys and semi-structured interviews were conducted to ascertain industry attitudes towards the viability of Western Australia's fiscal policy solution for South Africa. Industry stakeholders are reluctant to accept responsibility for previous mine-owners' actions and the lax legislative controls under which mines operated in the past. It was found that the current implementation and enforcement of legislation in South Africa is lacking in some regards, but if all responsible parties work towards a common goal of funding the rehabilitation of abandoned mines the Western Australian fund may be a feasible fiscal policy solution for South Africa.

Keywords

abandoned mines, rehabilitation, fiscal policy solution, South Africa, Western Australia.

Introduction and background

Abandonment of mine sites in South Africa (RSA) and Western Australia (WA) is both an ongoing occurrence and a legacy issue. This is due to a lack of legislative controls and impact assessment in the past, and a lack of financial provisioning and planning for closure at present. Abandoned mine sites (orphaned mine sites or legacy sites) are classified by the United Nations Environmental Programme (UNEP, 2000, p.6) as:

'*... mines that are no longer operational, are not actively managed, are not rehabilitated, causing significant environmental or social problems, and for which no-one is currently accountable for the rehabilitation or remediation of the site.*'

Abandoned mines have the potential to cause significant environmental impacts (Swart, 2003; Menéndez, 2005). Closure plans may underestimate the significance of impacts and closure costs and therefore the required financial provisions (Swart, 2003, p. 489; Menéndez, 2005; Auditor-General of South Africa (AGSA), 2009; UNEP FI, 2012, p. 23).

According to Swart (2003), a site is abandoned when the owners are liquidated or when the owners are traceable but do not necessarily have the capability or financial means to carry out sufficient post-closure rehabilitation. The sites are not classified as *derelict and ownerless mines* (D&O), which bear legal ramifications as responsible persons are untraceable. The AGSA (2009, p. 1) of South Africa notes that the regulatory framework 'does not provide for cases of abandoned mines' nor does the legislation delegate due-responsibility or 'have an approved strategic or business plan' for their rehabilitation.

The Council for Geoscience (CGS) officially listed a total of 5 906 abandoned sites in RSA as of May 2008 (AGSA, 2009, p. 6) of which the 'majority had closed down prior to 2002 when the Minerals and Petroleum Resources Development Act 28 of 2002 (MPRDA) (South Africa, 2002) came into effect.' According to the Auditor General (2009, p. 5) during the 2007/08 and 2008/09 financial years the DMR estimated the cost of the rehabilitation of these sites to be R30 billion. Of the 5906 abandoned mine sites in RSA, the CGS classified 1730 as high-risk sites which would cost an estimated R28.5 billion to rehabilitate. This amount excludes the cost of long-term acid mine drainage (AMD) treatment for affected sites and further operating costs such as for the stabilization of tailings, revegetation, or pumping of water to prevent shafts from flooding and decanting (AGSA, 2009, p.,5). The RSA Treasury does not have access to sufficient funds, justifying the need for a fiscal policy solution.

* *School of Geo- and Spatial Science, Unit for Environmental Sciences and Management, North-West University, Potchefstroom, South Africa.*

 ISSN 2225-6253. Paper received Jul. 2016; revised paper received Jan. 2017.

According to Peck *et al.* (2005, p. vii) the negative impacts of mining practices could be adequately mitigated with the guidance of a stringent legislative framework and the implementation of 'sustainable policy-, capacity- and institutional- developments.' Western Australia, which faces similar challenges with funding for rehabilitation of abandoned mine sites, has passed the Mining Rehabilitation Fund Act 33 of 2012 (MRF) (Western Australia, 2012) to alleviate the financial burden on government. This study explores the opportunity of the MRF to provide a fiscal policy solution for the rehabilitation of South African abandoned mines and to instigate real and measurable action.

Methodology

The research methods included an in-depth qualitative literature review on existing bodies of knowledge (Grant and Booth, 2009), a comparative analysis between the legal provisions for abandoned mine sites management in RSA and WA, and semi-structured interviews with 25 stakeholders in the mining sector. Although the interviews were conducted before the National Environmental Management-Regulations (NEM-R) (South Africa, 2015) were introduced, the regulations do not impact the way legislation is implemented in South Africa.

The qualitative literature and interview data was coded and tabled based on 'interconnected categories of knowledge' (Creswell, 2013). Three quantitative questions in the survey measured the respondents' 'degrees of agreeability and the intensity of their feelings by means of Likert-type questions' (Bryman, 2012, p. 712) toward the various aspects of the viability of the MRF as a fiscal policy solution for South African abandoned mines. The comparative analysis aimed to enhance the understanding of the workings of the two legislative frameworks.

The Western Australian MRF as a fiscal policy solution

The South African legislative framework does not mention abandoned mines specifically but it is inferred from sections 28 and 24R(1) of the National Environmental Management Act 107 of 1998 (NEMA) (South Africa, 1998) and section 34(a) of the MPRDA (South Africa, 2008) that the mining right holder remains liable for their abandoned mines (which are a source of pollution) and the sustainable closure thereof until a closure certificate is issued by the Minister of Mineral Resources. Botham (2012, p. iv) is quoted as saying 'in South Africa no mine closure certificates have ever been issued under either the Minerals Act of 1991 or the MPRDA of 2002', possibly due to the difficulty in ensuring the long-term sustainability of rehabilitation and the prevention of environmental liabilities or risks in the future. The Department of Environmental Affairs (DEA) and the Department of Mineral Resources (DMR) do not claim responsibility for the sites and technically consider all holders of mining rights responsible for their abandoned sites.

Western Australia's abandoned mines total 11 411 (Geological Survey of Western Australia, 2016), for which the rehabilitation costs are estimated to be between A$4 billion and A$6 billion (Leybourne, 2014). As indicated by Morrison-Saunders and Pope (2013, p. 212), the sites pose a 'social, environmental and financial challenge for the government', and a financial burden on taxpayers. In hopes of addressing the issue, the MRF was implemented to encourage concurrent rehabilitation practices, prevent further abandonment of sites adding to the already burdensome legacy, and to generate funds for the rehabilitation of the legacy mines.

The MRF is a 'government-administered, pooled fund' (Western Australia, S5 of Act 33 of 2012), and according to section 8(1)-(2) of the MRF Act (Western Australia, 2012) the interest generated by the fund will be used to rehabilitate those sites which form part of the legacy of abandoned mines. According to section 9A of the MRF Act (Western Australia, 2012) 'tenement holders are not excused from carrying out mine closure and rehabilitation as stipulated in the approved mining plans and programmes'. The MRF will only provide funds for the rehabilitation of abandoned mining areas 'after every effort has been made to trace responsible parties and recover funds' (Western Australia, 2013a, p. 2), and only in the event of the mine undergoing premature closure and being unable to complete closure as planned due to lack of financing will the capital held in the fund be accessed to assist in the rehabilitation of these abandoned sites. A Mining Rehabilitation Advisory Panel is established under the MRF Act (Western Australia, 2012) section 33, whose members function as advisors on matters relating to administration and implementation of the Act. The first rehabilitation efforts of the MRF were realized in 2015-16 when five sites were selected for rehabilitation to be managed by the Abandoned Mines Program (Western Australia, 2016a) and carried out according to the Abandoned Mines Policy (Western Australia, 2016b).

The MRF requires that all holders of mining authorizations in WA make an annually recalculated, non-refundable contribution to the MRF of approximately 1% of the total estimated mine closure liability for each site (Western Australia, 2013a). This is based on, and proportionate to, the 'disturbance data and outstanding rehabilitation on the site' as required by section 12 of the MRF Act (Western Australia, 2012) and by the DMP (Western Australia, 2013a, p. 4). If mining impacts are concurrently managed and rehabilitated, the annual levy will decrease. The promulgation of the MRF Act was well received in the Western Australian mining industry and 95% of tenement holders had submitted disturbance reports for 2013-14 and 98.8% for 2015-16 (Western Australia, 2016c).

The WA MRF functions as a replacement for the performance bond system which quarantined funds (Western Australia, 2010, p. 4), and since the introduction of the MRF, more than Aus$ billion in security bonds was returned to the mining sector to help free up funds for concurrent rehabilitation activities (Western Australia, 2016c, p. 1). In extreme cases, retirement bonds were not retired if the DMP CEO determined that a site poses a high risk of rehabilitation liability which would not be adequately covered by the payment of the annual levy. Regarding the financial incentives for WA mines, in a Norton Rose Fulbright (2013) article dated August 2013, it was noted that previously the main incentive for meeting rehabilitation obligations was the required performance bond. The annual levy as required by the MRF Act, which only requires 1% of total closure costs,

may not be sufficient in encouraging exhaustive rehabilitation, considering a mine would have to operate for 100 years before the full rehabilitation costs would be reached, hence it may be a small price to pay with little incentive for environmental cleanup. Entirely doing away with the security bonds leaves room for underfunding if the end-of-life liabilities are underestimated and if concurrent rehabilitation activities are not wholly provided for. This again places the burden of responsibility on the government and taxpayers. Critics say that the implementation of the MRF came at a bad time when commodity prices were in a downward trend. Seventy-three mining projects suspended operations and four collapsed entirely shortly after having been returned their security bonds, resulting in underfunding of rehabilitation activities (Barrett, 2016; Masige, 2016).

Clark and Clark (2005, p. 68) mention the comparable role of governments around the world to 'enact and implement appropriate policy and legislation', thereby protecting themselves from major financial burdens and persisting environmental concerns. The new South African NEM-Regulations (South Africa, 2015) pertaining to the financial provision for prospecting, exploration, mining, or production operations encourage concurrent rehabilitation and make it a priority, changing the rehabilitation protocol as of 20 November 2015. Appendix 3 has introduced more stringent requirements for annual rehabilitation plans to be risk-monitored, measurable, compiled with the help of specialists, and auditable. It requires the reporting of shortcomings experienced during the year, ensuring continual growth through lessons learned. The RSA DEA requires financial provisioning for remediation and rehabilitation actives and decommissioning and closure, as stated in section 6 of the NEM-R (South Africa, 2015), in the form of bank guarantees, trust funds, and cash deposits, as per section 8(1) of NEM-R (South Africa, 2015).

Adopting a policy such as this in South Africa could address many of the financial challenges associated with abandoned mines. The success of the policy will be determined by how it is adapted to fit the unique requirements of South Africa and whether or not it can be implemented and enforced effectively.

Results and analysis

Categories of responses, identified from literature and interview data, identify the challenges related to abandonment of mine sites in South Africa, which are presented in Figure 1.

It may be deduced from literature and interviews that stakeholders in the industry believe that the relevant government departments, such as the DMR and DEA do not do everything in their legislative power to ensure that current mining practices do not add to the burden of abandoned mines. The responses indicate that enforcement of existing legislation may be lacking, past and present polluters are not held accountable, and little guidance is offered to mining companies with regard to what is expected of them according to best-practice standards. The guideline document of the DMR, which all mining companies in South Africa rely on to calculate the financial provisions necessary for closure, has not been updated since 2005 and there has been no other form of assistance afforded to mines in terms of guideline documents for the preparation of environmental management plans (EMPs) or programmes (EMPrs) or mine closure plans until the release of the NEM-Regulations (South Africa, 2015). This has resulted in underestimations of closure costs, thereby increasing the likelihood of mining sites being

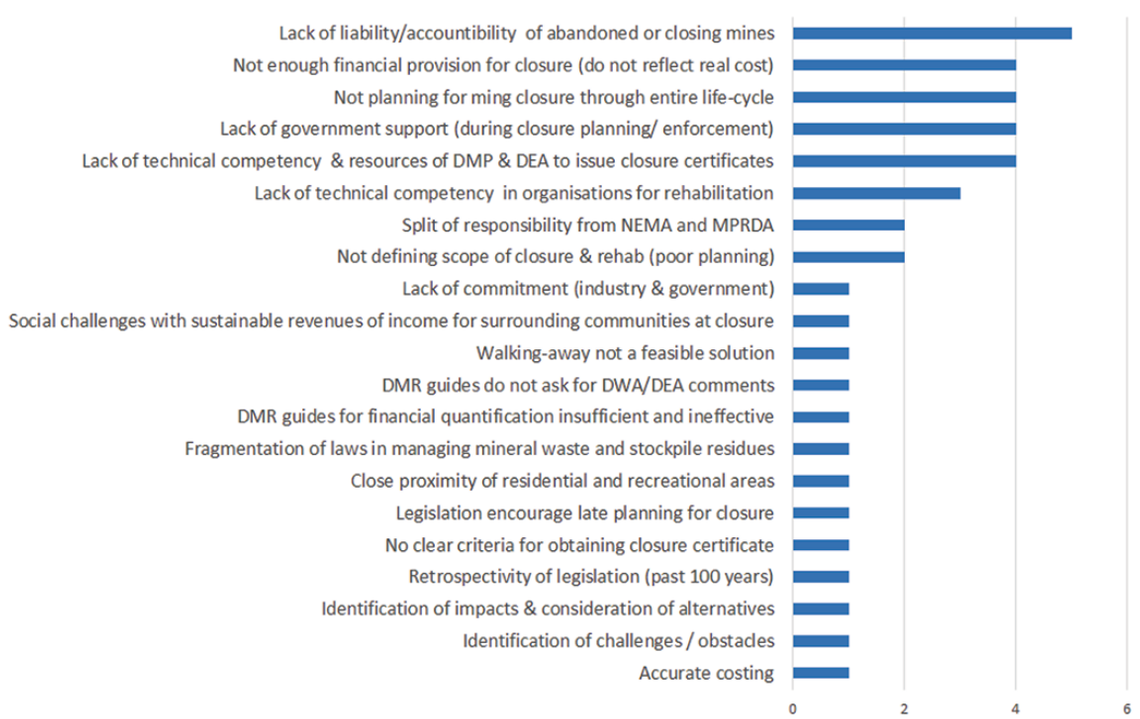

Figure 1—Frequency graph of survey responses on possible challenges related to mine site abandonment

abandoned due to a lack of funding for rehabilitation, monitoring, and maintenance post-closure. There are no lessons learned across the industry as every company approaches mine closure planning individually, resulting in the same scenarios of inefficient practices and continued abandonment of sites.

The survey questions, as part of the interviews with stakeholders, shed light on the perceived viability of a fiscal policy solution such as the MRF to deal with the issues of abandoned sites and continued abandonment of sites. The first survey question asked whether the respondents thought the MRF would be beneficial for South Africa. The responses are concentrated in the 'partly agree' category, closely followed by 'agree' and 'strongly agree', indicating a great inclination to the agreeability of the benefits which such a policy could afford to South Africa. The second question measured the agreeability of the respondents to the viability of a solution such as the MRF for South Africa's abandoned mines. Once again the respondents' answers indicate that they agree as to the viability of the proposed fiscal policy solution. However, some respondents felt they 'strongly disagreed', indicative that although the policy may be highly beneficial, the viability thereof in the South African context is more uncertain. The last survey question asked agreeability to the statement that the South African government is capable of adopting and supporting (*i.e.* implementing) such a fund. The responses varied, with the majority of stakeholders 'strongly disagreeing' and the rest 'strongly' to 'partly agreeing'. The faith in the South African government's ability to implement legislation is uncertain and this will need to be addressed before any further legislation is drafted so that industry stakeholders may be assured that the implementation thereof will be fair and consistent.

The NEM-Regulations (South Africa, 2015) have attempted to address some of the identified problems. This entails more stringent monitoring requirements for the calculations of financial provisions, as seen in S14. Appendix 3 of the NEM-Regulations provides for the minimum content of an annual rehabilitation plan, providing better guidance concerning what is expected of mining operators. According to S2(a) of Appendix 3, mines are required to 'review concurrent rehabilitation and remediation activities already implemented', and S2(d) 'identify and address shortcomings experienced in the preceding 12 months of rehabilitation', thereby ensuring that the most- and least-effective practices are identified. The threat of emergent liabilities has afforded an excuse for the DMR to not grant mine closure certificates. This is a major factor behind the abandonment of mines as mining companies do not make provision for indefinite monitoring and maintenance of their sites. Appendix 4 of the NEM-R (South Africa, 2015), which provides for the minimum content of a final rehabilitation, decommissioning, and mine closure plan, requires detailed and accurate financial planning, impact mitigation, and post-mining land use plans. These guidelines may just be what is necessary for mining companies to attain closure as they now have more details regarding the ministry's expectations of them.

Table I is a comprehensive summary of the comparative analysis of the two frameworks on the legal provisions specifically dealing with abandoned mine site management in the two countries.

The Environmental Protection Act (EPA) 76 of 1986 shows the intention to not only prevent further pollution, but also delegates responsibility to prevent, as far as possible, any environmental damage and mitigate the damage which cannot be prevented, as seen in section 16 which provides for the 'functions of authority' with respect to the 'prevention, control and abatement of pollution and environmental harm'. For cases of sudden and unexpected closure, as guided by sections 24 and 88 of the Mines Safety and Inspection Act 62 of 1994 (Western Australia, 1994), the closure process will be sped up, a decommissioning plan will need to be drafted, and the Mine Closure Plan needs to be reviewed within 3 months of abandonment (Western Australia, 2013). Up until the time of a closure certificate being issued, the mining operations remain the responsibility of the holder or other responsible appointed party, as directed by section 114B of the Mining Act 107 of 1978.

Sections 28 and 24R(1) of NEMA (South Africa, 1998) and section 43(1) of the MPRDA (South Africa, 2002) support the polluter-pays principle and provide for retrospective action in terms of liability for the pollution and degradation of the environment. The DMR has developed the National Strategy for the Management of D&O Mines (DMR, 2009) but a strategic plan is yet to be developed to deal with the rehabilitation of abandoned mines. As per section 46 of the MPRDA (South Africa, 2002) 'Parliament should set aside funds to employ a third party for the rehabilitation of a prematurely abandoned site where it is urgently needed to prevent environmental degradation'. These funds, according to section 46(1) are to be 'retrieved from the right holder'. Currently abandoned mines are not being factored into the parliamentary budget, as indicated by the Mineral Resources Minister (Wait, 2012).

Section 15 of the Mining Act Regulations (Western Australia, 1981) provide for 'expenditure conditions' and require that mining operators provide for a performance bond, according to section 126, which serves as a form of financial security for closure rehabilitation, and section 60(1) of the Mining Act states 'the applicant for an exploration license shall lodge … a security for compliance with the conditions to which the exploration license … will … be subject'. The MRF Act (Western Australia, 2012) has now replaced the bonds system as the mandated financial security and makes use of a government-administered 'pooled fund' (Western Australia, 2013a, p. 2), into which annual levies are paid. As the mines still operate under the Mining Act (Western Australia, 1978) they remain responsible for financing the rehabilitation of site according to the approved mine closure plan as per Western Australias Guidelines for Preparing Mine Closure Plans (DMP and EPA, 2011, p. 26). The purpose of the MRF Act (Western Australia, 2012), according to section 6 thereof, is 'to provide a source of funding for the rehabilitation of abandoned mine sites and other land affected by mining operations carried out in, on or under those sites'.

Section 8 of the NEM-Regulations (South Africa, 2015) provide for the use of a financial guarantee and trust fund system to ensure financial provision for mine closure. There is, however, no policy in place to rehabilitate abandoned mine sites and South Africa could benefit from the implementation of a fiscal policy solution such as that of Western Australia.

Table I

Summary of the comparative analysis between South Africa and Western Australia's applicable legislation

		SOUTH AFRICA		WESTERN AUSTRALIA	
Comparative categories		**Source**	**Relevant extract(s) & comments**	**Source**	**Relevant extract(s) & comments**
Constitutional & legislative provision	Constitution on the environment	Constitution of RSA	**S24(a),(b)(i-iii)**	Constitution of WA & Commonwealth Constitution	Neither Constitution specifically mentions the environment.
	Provides for national legislation to protect environment		**S146(2)(vi)**, defines & establishes sustainability principles & the DMR's constitutional mandate.		The Commonwealth of Australia makes legislative provision in the forms of other Acts which deal specifically with the environment.
	Relevant environmental & mining legislation		NEMA, NEM-R, MPRDA & MPRD-R		EPAct, EPBCA, MRF Act & MA
Mine Closure-, Annual Rehab- & Environmental Management Plans (EMP)	Are Mine Closure Plans/EMPs required?	MPRDA & NEM-R	EMP is required which aids in guiding mines in effective closure. Final Mine Closure Plans not required until mine closure is imminent, but kept up to date with annual rehab plan.	The Guidelines for the Preparation of Mine Closure Plans & MA	Mine Closure Plan to be submitted as part of the Mining Proposal (**S70O** of the MA amendments).
	When to be made available?	NEMA, NEM-R & MPRDA	EMP required before the mining permit is issued.		Internationally accepted best practice: plan for closure before commencement of any activities.
	How often should they be updated?	MPRD-R & NEM-R	**S55**; as stipulated in the EMP otherwise annually.		Reviewed throughout life of mine & submitted to DMP every three years for approval.
	Are there government developed guidelines for their formulation?	MPRD-R	**S51& S52** provide a basic idea of the contents of an EMP.	The Guidelines for the Preparation of Mine Closure Plans (DMR & EPAuth, 2011)	Suggest the structure and content of the Mine Closure Plan and provide all the necessary legal and best practice information regarding Mine Closure Plans.
		NEMA & MPRDA & MPRD-R	Provide for mine closure principles (MRPD-R, **S56**) & provide generic descriptions for *contents of closure plan* (MPRD-R, **S62**).		
		Info. Series 12 (DEAT, 2004)	Supportive text (clearly stipulated that this is not a guideline document) to support with the formulation of EMPs.		
		NEM-R	Appendices 3 & 4.		
Management of abandoned mines & emerging liabilities	Responsible parties post-closure	NEMA & MPRDA	NEMA **S24R(1)**, **S28** & MPRDA **S43(1)** supports "polluter pays principle" & holds polluters responsible for degradation caused before promulgation of NEMA & indirect pollution as a result of polluting activities. Polluters remain responsible even when ceased to exist.	EPAct	**S16:** Appointed authorities responsible for encouraging protection of the environment.
				MRF Act	. **S9A:** person responsible for site & rehab thereof at time of it being declared abandoned, is liable to pay a cost into MRF as debt due to state. Once established that liable person is unable to provide for rehab, MRF comes into effect & rehabilitates.
		NEMA & MPRDA	MPRDA **S 46(1):** if holder ceased to exist or is liquidated & rehab is required, Minister must "*take necessary measures to prevent further pollution or degradation*", after which Minister may recover costs of remediation from responsible party (previous holder of mining right)	MA	**S114B:** *continuation of liability after expiry, surrender or forfeiture of mining tenement* & don't excuse previous holders from closure liabilities
	Legislative provisions for abandoned mines		There is no legal document in place which specifically deals with abandoned mines. The legislation does not delegate due-responsibility or have an approved strategic or business plan for the rehab of sites.	MSI Act & MRF Act	MSI Act **S42(1)(a):** notify DMP before abandonment & cessation of activities. **S88:** *plans for abandonment or suspension.* Mine Closure Plan: updated within 3 months to include decommissioning- & care & maintenance plans. MRF Act **S8**: funding rehab of abandoned mines.
Financial provision & guarantees for rehab post-closure	Financial provisions for mine closure	MPRDA, MPRD-R & NEM-R (entire document)	**S23(1), S10(k) & S53** (MPRD-R) Financial provision must be provided before EMP may be approved or environmental authorisation awarded. Financial guarantees are required.	MRF Act	Mines are responsible for providing finances for rehab in any form they deem fit. The mandatory financial provision is made by paying annual levies into the MRF (**S11**).
	Calculations of financial provisions	Quantum guideline (DME, 2005) & NEM-R	Administrated by the DMR – quantum guideline is principle guideline document for calculating closure costing. Last updated in 2005. NEM-R **S11(2)** requires annual updating of financial provisions.	MRF Act & Regulations	MRF Regulations provide comprehensive guide for calculations of the annual levy payable. The financial provisions for rehab of sites may be provided in any form & may be calculated based on previous guidelines (DMR & EPAuth) which are no longer obligatory.

Terms and abbreviations used in Table I

Commonwealth Constitution	Commonwealth of Australia Constitution Act of 1900
Constitution of RSA	Constitution of the Republic of South Africa Act 108 of 1996
Constitution of WA	Western Australia's Constitution Act 23 of 1889
EPAct	Environmental Protection Act 87 of 1986
EPBCA	Environmental Protection, Biodiversity Conservation Act 91 of 1999
Quantum guideline	Guideline document for the evaluation of the quantum of closure-related financial provision provided by a mine
MA	The Mining Act 107 of 1978
MPRDA	Minerals and Petroleum Resources Development Act 28 of 2002
MPRD-R	MPRD Regulations of 2004
MRF Act	Mining Rehabilitation Fund Act 33 of 2012
MSI Act	Mines Safety and Inspection Act 62 of 1994
NEMA	National Environmental Management Act 107 of 1998
NEM-R	National Environmental Management Regulations of 2015, GG 39425

Discussion

The continued abandonment of mine sites in South Africa points to some crucial shortcomings in the implementation of, and enforcement of, existing legislation. The lack of competency, both in the mining sector and government, with regard to the compilation of Mine Closure Plans and EMPs, continues to supplement the abandonment of sites as the quality of documents varies greatly and government simply does not have adequately trained personnel or policy guidelines to assess the quality of documents produced or to enforce existing laws. This perpetuates the cycle of inefficient closure planning and tolerates the bare minimum with regard to efforts made to comply with legislative requirements. Before November 2015 mining companies had to rely on the out-of-date *Guideline document for the evaluation of the quantum of closure related financial provision* (South Africa, 2005), which resulted in serious shortfalls regarding financial provision for closure.

Government's legislative mandate is to provide guidance for the formulation of procedures and assess these procedures to ensure compliance. It is hoped that the new NEM-Regulations (South Africa, 2015), which provide more stringent guidance on what is expected regarding financial provision for mine closure, will address this problem of underestimations and prevent further abandonment of mines. This will, however, only make an impact if the legislation is properly implemented. An investigation into the implementation and impacts of the new regulations may present a further research opportunity.

The comparison of the legislative frameworks of South Africa and Western Australia highlighted some key areas of shortcomings which potentially lead to the abandonment and ongoing degradation of sites. Based on the literature review it is evident that South Africa, unlike Western Australia, has no specific policy in place to deal with the legacy of abandoned mines and does not have the financial means to undertake

such a mammoth task. Secondly, the existing legislation that aims to prevent further abandonment of sites is not properly implemented. The assessment of the interview and literature data revealed that government does not draft up-to-date and stringent guidelines for mines and that mines then do not carry out proper assessment and monitoring procedures. Best-practice industry guidelines could help alleviate some of the strain on the industry and the NEM-Regulations (South Africa, 2015) have started to address this. Mine closure plans do not provide for life-long monitoring of mines where operations have ceased and oftentimes don't provide finances for the ongoing monitoring and maintenance of the site. By permitting mining activities, the government also enters into an agreement that it will take over responsibility for the site once rehabilitation is completed according to the mine closure plan and a closure certificate is issued. Based on the responses, it is evident that the South African government does not easily accept responsiblilty for the implications related to mining.

Once mining operations have ceased, the site still needs to be monitored and maintained and proactive measures need to be taken to maintain the natural ecosystems in good health for the benefit of the entire country. The survey responses indicate that there is a displacement of liabilities and lack of accountability, which leads to the question of who is to take responsibility for these sites as they continue to degrade the environment and infringe on South Africans' constitutional rights.

From comparative analysis of the legislative frameworks and the literature review, it is evident that policies, regulations, guidelines, and legislative documents need to be aligned with one another in order to support unified goals and provide a clear indication of what is expected of mining plans and development projects. When a legal framework is not properly implemented and up-to-date, all-encompassing legislation cannot be drafted, irresponsible mining practices ensue, and rehabilitation is not done properly, giving rise to a state of constant environmental deterioration.

Interview responses indicated that stakeholders in the mining industry regard it as unjust to hold current mining operators responsible for the wrongdoings of past miners and the ineffective legislation which permitted the neglect of the environment. The crux, however, lies in the mining activity itself, which if not approached correctly, is wholly unsustainable. In essence, if mining operators draw their profits from the environment, they should be willing to pay a percentage of their income to assist in dealing with the persistent negative impacts of the mining industry's activities as a whole. As can be seen from the Western Australian example, it is possible to obtain the support of the industry, as long as the enforcing party, in this case the government or a third party, does its part in ensuring that it provides proper guidance and fair enforcement and implementation of the legislation, free of corrupt activities. A vehicle such as the Western Australian fund may thus be a feasible fiscal policy solution for South African abandoned mines, when and if all parties involved give their support to the cause.

References

Auditor-General of South Africa (AGSA) 2009. Report of the Auditor-General to Parliament on a performance audit of the rehabilitation of abandoned mines at the Department of Minerals and Energy, South Africa. Pretoria. http://cer.org.za/wp-content/uploads/2011/10/AG_Report_on_abandoned_mines-Oct-2009.pdf [accessed 12 April 2014].

Australian Commonwealth. 1900. Commonwealth of Australia Constitution Act 1900. Parliament of the United Kingdom, Westminster.

Barrett, J. 2016. Australian miners leave clean-up bill after taking the cash, *Reuters*, 1 August 2016. http://www.reuters.com/article/us-australia-mining-environment-idUSKCN10D094 [accessed 18 January 2017].

Botham, N.D. 2012. A critical analysis of mine closure process as followed by the De Beers Oaks Diamond Mine, Limpopo, South Africa. MA thesis, University of Johannesburg.

Bryman, A. 2012. Social Research Methods. 4th edn. Oxford University Press, New York.

Clark, A.L. and Clark, J.C. 2005. An international overview of legal frameworks for mine closure. Environmental Law Alliance Worldwide. http://www.elaw.org/node/3715 [accessed 9 June 2014].

Creswell, J.W. 2013. Qualitative Inquiry and Research Design: Choosing Among Five Approaches. 5th edn. Sage, Thousand Oaks, CA.

Department of Mines and Petroleum and Environmental Protection Authority (DMP and EPA). 2011. Guidelines for preparing mine closure plans June 2011. Government of Western Australia, Perth. http://edit.epa.wa.gov.au/EPADocLib/Guidelines-for-preparing-mineclosure-plans-210611.pdf [accessed 25 August 2014].

Department of Mineral Resources (DMR). 2009. The national strategy for the management of derelict and ownerless mines in South Africa. Government Printer, Pretoria.

Geological Survey of Western Australia (GSWA). 2016. Mines and mineral deposits (MINEDEX). http://www.dmp.wa.gov.au/Mines-and-mineral-deposits-1502.aspx [accessed 17 January 2017].

Grant, M.J. and Booth, A. 2009. A typology of literature reviews: an analysis of 14 review types and associated methodologies. *Health information and Libraries Journal*, vol. 26, no.2. pp.91–108.

Leybourne, M.L. 2014. Ensuring rehabilitation into the future - The Western Australian Mining Rehabilitation Fund. *Proceedings of the Life-of-Mine Conference 2014*, Brisbane, Queensland, 16 July 2014. Australasian Institute of Mining and Metallurgy, Melbourne. pp. 441–448.

Masige, S. 2016. Failed mine rehabilitation fees could have taxpayers footing the bill. *Australian Mining*, 3 August 2016. https://www.australianmining.com.au/news/failed-mine-rehabilitation-fees-taxpayers-footing-bill/ [accessed 18 January 2017].

Menéndez, J.M.A. 2005. Harmonising policy and technology: environmental regulation of mine waters in the United Kingdom and European Union. PhD thesis, University of Newcastle.

Morrison-Saunders, A. and Pope, J. 2013. Mine closure planning and social responsibility in Western Australia: Recent policy innovations. *SR Mining 2013, Proceedings of the 2nd International Conference on Social Responsibility in Mining*, Santiago, Chile, 5-8 November 2013. Centre for Social Responsibility in Mining, Sustainable Minerals Institute, University of Queensland. Chapter 3.

Norton Rose Fulbright. 2013. Mine site closure in WA and the new Rehabilitation Fund. http://www.nortonrosefulbright.com/knowledge/publications/102325/mine-site-closure-in-wa-and-the-new-rehabilitation-fund [accessed 24 Nov. 2016].

Peck, P., Balkau, F., Bogdanovic, J., Sevaldsen, P., Skaalvik, J. F., Simonett, O., Thorsen, T.A., Kadyrzhanova, I., and Svedberg, P. 2005. Mining for Closure; policies and guidelines for sustainable mining practice and closure of mines. Environment and Security (EnvSec) Initiative Project, UNEP, UNDP, OSCE, and NATO. https://www.commdev.org/mining-closure-policies-and-guidelines-sustainable-mining-practice-and-closure-mines [accessed 21 May 2014].

South Africa. 1996. Constitution of the Republic of South Africa Act 108 of 1996, Government Gazette, vol. 378, no. 17678. 8 May 1996.

South Africa. 1998. Department of Environmental Affairs (DEA). National Environmental Management Act 107 of 1998, *Government Gazette*, vol. 19519, no.1540. 27 November 1998.

South Africa. 2002. Department of Mineral Resources (DMR). Mineral and Petroleum Resources Development Act 28 of 2002. *Government Gazette*, vol. 23922, no. 1273. 10 October 2002, as amended. Mineral and Petroleum Resources Amendment Act 49 of 2008, *Government Gazette*, vol. 526, no. 32151, 21 Apr. 2009, as amended.

South Africa. 2004. Department of Mineral Resources (DMR). Mineral and Petroleum Resources Development Regulations (MPRD-R), No. 527 of 2004. *Government Gazette*, 10 October 2002.

South Africa. Department of Minerals and Energy (DME). 2005. Guideline document for the evaluation of the quantum of closure-related financial provision provided by a mine. Government Printer, Pretoria.

South Africa. Department of Environmental Affairs (DEA). 2015. National Environmental Management Regulations: Regulations pertaining to the financial provision for prospecting, exploration, mining or production operations, *Government Gazette*, vol. 39425, no. 1147, 20 November 2015.

Swart, E. 2003. The South African legislative framework for mine closure. *Journal of the South African Institute of Mining and Metallurgy*, vol. 103, no. 8. pp.469–492.

United Nations Environmental Programme (UNEP). 2000. Mining and sustainable development II: Challenges and perspectives. United Nations Environment Programme Division of Technology, Industry and Economics, Paris, France.

United Nations Environmental Programme – Finance Initiative (UNEP-FI). 2012. *Chief Liquidity Series*, Issue 3: Extractives Sector. Geneva, Switzerland: UNEP-FI. http://www.unepfi.org/work_streams/water/liquidity [accessed 19 June 2014].

Wait, M. 2012. DMR rehabilitates derelict and ownerless mines, not abandoned sites. *Mining Weekly*, 17 September http://www.miningweekly.com/article/dmr-rehabilitates-derelict-and-ownerless-mines-not-abandoned-sites-2012-09-17 [accessed 14 May 2014].

Western Australia. 1889. Constitution Act 23 of 1889. State Law Publisher, Perth.

Western Australia. 1978. Mining Act 107 of 1978. State Law Publisher, Perth.

Western Australia. 1981. Mining Regulations of 1981. State Law Publisher, Perth.

Western Australia.1986. Environmental Protection Act 87 of 1986. State Law Publisher, Perth.

Western Australia. 1994. Mines Safety and Inspection Act 62 of 1994. State Law Publisher, Perth.

Western Australia. 1999. Environment Protection and Biodiversity Conservation Act 91 of 1999. State Law Publisher, Perth.

Western Australia. Department of Mines and Petroleum (DMP). 2010. Policy Options for Mining Securities in Western Australia: Preliminary Discussion Paper. Government of Western Australia; DMP, and, EPA, Perth. http://www.dmp.wa.gov.au/documents/100957_Policy_Options.pdf [accessed 10 May 2014].

Western Australia. 2012. Mining Rehabilitation Fund (MRF) Act 33 of 2012.

Western Australia. Department of Mines and Petroleum (DMP). 2013a. Mining Rehabilitation Fund Guidance. Perth. http://www.dmp.wa.gov.au/Documents/Environment/ENV-MEB-382.pdf [accessed 18 January 2017].

Western Australia. 2013b. Mining Rehabilitation Fund Regulations (MRF-R) of 2013. Government Gazette, vol. 2423, no. 95. 21 June 2013.

Western Australia. Department of Mines and Petroleum (DMP). 2016a. Abandoned mine program. Government of Western Australia, DMP. http://www.dmp.wa.gov.au/Environment/Abandoned-mines-projects-18193.aspx [accessed 17 January 2017].

Western Australia. Department of Mines and Petroleum (DMP). 2016b. Abandoned mines policy. Perth: Government of Western Australia, DMP. http://www.dmp.wa.gov.au/Documents/Environment/ENV-MEB-201.pdf [accessed 17 January 2017].

Western Australia. Department of Mines and Petroleum (DMP). 2016c. Mining rehabilitation fund: yearly report 2016. Government of Western Australia, DMP, Perth. ◆

Conference Announcement

ASM Conference 2018

'Fostering a regional approach to ASM transformation in sub-Saharan Africa'

10–11 SEPTEMBER 2018

Nasrec, Johannesburg (Electra Mining)

BACKGROUND

The number of people involved in artisanal and small-scale mining (ASM) activities have been increasing globally. In Africa, specifically, the figures are estimated to be 9 million. This is an increase from an estimated 3 and 3.5 million in 1999. Presently, the ASM sector accounts for the largest mining workforce in Africa. Since ASM became part of the development agenda in the 1970s, many developing countries have acknowledged the sector's importance in its role in local socio-economic development and have initiated a series of interventions aimed at formalizing the sector. In parallel, significant amount of research has been conducted to understand the sector and to address the negative externalities associated with the sector which for many decades have hindered the development of the sector in line with the respective national development agendas and on the African continent, the Yaoundé Vision on ASM and the African Mining Vision (AMV). To date, ASM remains a contentious issue characterized by misconceptions brought by the lack of clarity on the definition of ASM and issues surrounding its legitimacy as a source of livelihood.

While some countries have success stories to share in terms of the formalization of the ASM sector, South Africa has lagged behind developments in the rest of Africa with possible devastating consequences to its economy and people. Over the past few years, South Africa has seen an escalation of illegal ASM activities predominantly in the gold sector. This upsurge is driven by the limited economic opportunities in the country amid high unemployment rate and rising poverty levels. The loss of employment in the formal mining sector has also contributed to the scourge of illegal mining. Well over 300 lives have been lost in illegal mining activities between 2012 and 2016 and these are linked to rock falls, explosive accidents, gas poisoning, security and police battles and turf wars.

As a signatory to the AMV, it has become crucial for South Africa to diversify and create a mining sector that harnesses the potential of ASM to advance integrated and sustainable local socio-economic development. Accordingly, it is also important for mining practitioners to use their knowledge of mining to ensure that ASM operators work safely, effectively and efficiently to ensure the future viability of the South African mining industry, while leveraging opportunities for local socio-economic development.

This conference aims to provide a platform which brings together stakeholders working in the ASM sector to share experiences and learn from each other. Specifically, the conference seeks to expose South Africa to the successes and failures of ASM formalization efforts as seen in other developing countries particularly in the SADC region. In this context, this conference endeavour to explore policy and legislative changes that would optimize the current ASM legislative framework in South Africa in line with the aspirations of the AMV to deliver on the objectives of the National Development Plan. The conference aims to consider the implications of the future mining industry in South Africa where ASM is rejected on the one hand, and where ASM is encouraged and properly regulated on the other and used as a tool of poverty alleviation. With South Africa being amongst the largest mineral producing countries in the world, this conference will also explore the relationship between the large-scale mining (LSM) sector and ASM sector in the country with a view of bridging the gap between the two sectors for shared socio-economic benefits.

This conference seeks to go beyond the sharing of knowledge and encompasses the transfer of skills and experiences as well. The objectives of the conference are to:

- Understand the spectrum of ASM activities in Africa *e.g.* legal *vs* illegal *vs* extra-legal
- Explore the importance of ASM in the context of sustainable livelihood framework
- Understand gender perspectives on ASM
- Explore the legitimacy of ASM in the context of criminalization and/or decriminalization
- Explore policy and legislative changes to optimize ASM legislative framework
- Draw lessons from past and current formalization efforts as seen in developing countries
- Understand the relationship between LSM and ASM sectors
- Explore potential synergies between the LSM and ASM sectors
- Consider best practices in terms of health, safety and environmental concerns of ASM
- Understand attendant issues as they relate to the ASM mining value chain
- Consider innovative machinery and techniques to ensure that ASM can be done effectively and safely

- Develop lessons from other developing countries in so far as the formalization of ASM
- Consider the African Mining Vision and its domestication at country-levels.

WHO SHOULD ATTEND

- Government Officials and Regulators
- Academics, Trainers and Educators
- ASM operators
- ASM associations
- Mine Affected Communities
- Civil Society Organizations
- Community liaison officials at the mines
- ASM consultants
- Closure practitioners
- Community engagement practitioners
- Health and Safety Practitioners
- Development practitioners
- Futurists and forward thinkers

For further information contact:
Head of Conferencing: Camielah Jardine • SAIMM
Tel: +27 11 834-1273/7 Fax: +27 11 833-8156 or +27 11 838-5923
E-mail: camielah@saimm.co.za • Website: http://www.saimm.co.za

SAIMM
THE SOUTHERN AFRICAN INSTITUTE OF MINING AND METALLURGY

http://dx.doi.org/10.17159/2411-9717/2017/v117n11a14

Development of a predictive model of fragmentation using drilling and blasting data in open pit mining

by J.D. Silva*, J.G. Amaya†, and F. Basso‡

Synopsis

This article presents predictive statistical models for fragmentation in open pit mines using drill-and-blast data. The main contribution of this work is the proposing of statistical models to determine the correlations between operational data and fragmentation. The practical use of these models allows the drill-and-blast parameters, *i.e.* burden, spacing, explosive, among others, to be optimized in order to obtain a more efficient size distribution.

Keywords
open pit blasting, linear models, blast fragmentation.

Introduction

The drill-and blast-process (D&B), the main objective of which is to remove the ore from its *in situ* position, aims at generating a degree of fragmentation that permits loading and transporting the ore to the processing plant, and which minimizes energy consumption in comminution. Moreover, in those processes where the ore is treated by heap leaching operations, D&B also seeks to generate the conditions to maximize copper extraction on the leach pads through a better-controlled size distribution profile.

In the literature, several models are described that are aimed at predicting the fragmentation obtained by the D&B process. However, the greatest difficulty in applying them successfully in normal operations is the complex calibration required, considering different D&B practices in different types of rock. Therefore, the quality of calibration must be improved to obtain an applicable predictive model for D&B operations.

The main variables and parameters that define D&B practice are burden (B), spacing (S), quality and quantity of the explosive charged into the blast-holes (Q), stemming (T), and firing pattern. This article aims to establish an empirical model that uses D&B data to predict P_{80}, P_{50}, and P_{20}, defined as the 80%, 50%, and 20% passing sizes, respectively. From these variables it is possible to infer the size distribution of the feed to downstream processes.

Fragmentation by blasting

Basis of modelling

In general, mathematical models that allow any physical phenomenon to be reproduced in a simplified manner fall into one of three categories. First, there are models based on 'site-specific' correlations and trends that have local application, and therefore are difficult to extrapolate to other settings. The most sophisticated models are those that rely on the fundamental principles of physics, such as fracture mechanics and/or the theory of detonation, as for blasting. Between these two approaches are the so-called mechanistic empirical models, which are cost-effective since they predict appropriately in most situations of interest, without requiring a degree of unmanageable complexity in their practical implementation (supercomputers and excessive processing time, typical of research – essentially academic).

Figure 1 shows schematically the difference among these three approaches to fragmentation by blasting. For the reasons given above, it is not surprising that most of the knowledge regarding fragmentation has evolved in line with empirical-mechanistic models, especially the approach proposed by Cunningham (1983, 1987, 2005), which has been the subject of countless case studies, both in quarries and mining, and there are many references in the literature on its applicability. Evidence collected globally and the contribution of several researchers

* *UAI Mining Center, Faculty of Engineering and Sciences, Universidad Adolfo Ibañez Santiago, Chile.*

† *Center for Mathematical Modeling, Universidad de Chile, Santiago, Chile.*

‡ *Escuela de Ingeniería Industrial, Universidad Diego Portales, Santiago, Chile.*

 ISSN 2225-6253. Paper received Feb. 2017; revised paper received Jul. 2017.

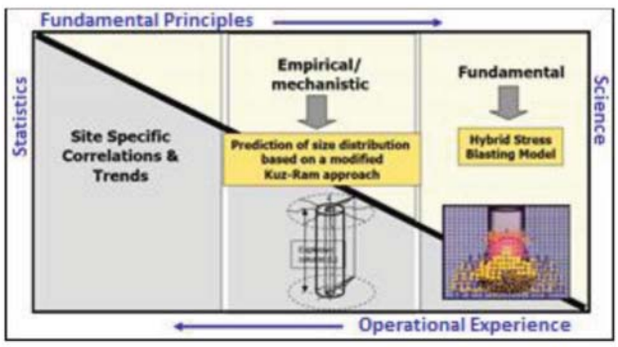

Figure 1—Possible approaches to the problem of modelling fragmentation by blasting (Cunningham, 1983, 1987, 2005)

supports the introduction of different modifications that deal with the limitations contained in its formulation, particularly regarding the correct estimate of the fine fraction of the size distribution, which is consistently underestimated by the original model.

Applied models

Among the main refinements documented in the literature, and without prejudice to the work done by other researchers, are those proposed by Kanchibotla (1999) and Spathis (2005), which correct the fine fraction bias (crushed zone model) and specify the estimation of the parameters described by Weibull and implied in the Rossin-Rammler distribution, respectively. In addition, other authors have proposed alternative three-parameter distributions, such as Ouchterlony (2005) with the Swebrec function, which although also empirical, allows better fits over a wide range of particle sizes when field measurements are available. While there is consensus on the quality of these proposals, they lack mechanical characteristics, thus affecting the correlation with the blasting layout in order to establish causal relationships that respond directly to changes in specifications such as drilling pattern and/or the strength and type of explosive.

The choice between one variant or the other will depend on the nature of the problem (focus only on diggability, or interest in the fine fraction); the quantity and quality of data available, including the chance of running field tests (greenfield project or operating mine); and the experience of those responsible for calibrating the predictive model. In this regard, it is important to point out the ability of the blasting specialists to standardize criteria and develop tools that combine public-domain information with algorithms designed internally, not available in the market, which integrate cross-cutting issues of utmost relevance to the ultimate goal such as blasting characterization and *in situ* block size estimation. All this entails a strong component of stochastic simulation for management of the uncertainty associated with the inherent variability of the rock mass.

The specific case presented in this paper deals with a copper mine located in the north of Chile, with a production over 100 000 t/a, where D&B plays an important role in the fragmentation for heap leaching. The model used to calibrate the fragmentation sampling, obtained as part of the survey of the project baseline, contains elements of the 'site-specific' empirical approach, which has been suitably modified to deal with the fine fraction by utilizing image analysis and size distribution analysis of samples of broken material in the laboratory. Also, representative variables of fragmentation have been included, especially of the rock mass, whose characteristics require a 'site-specific' model due to the presence of fines *in situ* prior to blasting, for the problems are caused not only by the generation, but also by the release of, fines from the rock mass, and the unique characteristics of the rock mass studied in this research. In the case of the mine studied, there is evidence of the presence of fine material (smaller than 150 m) which originates from degradation and the geological alteration characteristic of a porphyry copper deposit, and which affects the ore processing in the plant.

Modelling strategy

Currently, blasting remains as much an art as a science. Although a lot of work has been done in the area of modelling the fracturing process and the propagation of stress waves in an isotropic or anisotropic medium, the natural variability of the rock mass usually distorts the complex blasting layout approaches mentioned above, and consequently much of the engineering conducted ends up relying on relatively simple 'rules of thumb' from global experience, as part of the documentation and dissemination of knowledge typical of the mining industry.

Overall, without considering the dynamic component of blasting (timing), the blasting layout must consider the following parameters (Cunningham, 1983):

- Blast-hole diameter
- Bench height considered in the mining plan
- Burden for blast-holes (B)
- Spacing between blast-holes (S)
- Stemming length (T)
- Deviation and alignment of blast-holes
- Type of drilling pattern (staggered or rectangular)
- Properties of the rock mass and discontinuities
- Properties of the explosive(s) used.

Regardless of the chosen model and its implicit sophistication, the most critical dimension of blasting is none other than the burden, since it represents the rock mass to be fragmented as a result of the detonation of the explosive column in an individual blast-hole. Its value will depend on a combination of variables, including the characteristics of the rock mass and the explosive used.

In this regard, and only for illustrative purposes, it should be noted that within the wide range of empirical references available, one that is appropriate for estimating the effect of the burden is the ratio between this dimension and the hole diameter, a dimensionless ratio typically ranging from 20 to 40. Experience suggests that under average field conditions, satisfactory results can normally be expected for values of 30. While the problem is focused on the fine fraction of the size distribution, this ratio is within the aforementioned range (33 <burden / diameter <37) for both the diameter of interest (10 inches, or 270 mm) and the current blasting layouts. Tables I and II show the drilling and blasting practices applied according to the geological units (GUs) that occur in the mine.

Table I

Drilling and blasting parameters applied for GUs 5 and 6

B (m)	S (m)	GU	GU Density (Ton/m3)	Hole Diameter (Inches)	Bench Height (m)	Overdrilling (m)	Stemming (m)	Explosive Density (ton/m3)	Explosive Quantity (Kg)	Powder Factor (gr/ton]
7,0	8,0	6	2,57	10,625	15	2	7,5	1,22	663	307
8,8	10,2	5	2,48	10,625	15	2	6,0	1,22	768	230
6,0	7,0	6	2,57	10,625	15	2	6,7	1,22	719	444
6,0	7,0	5	2,48	10,625	15	2	6,7	1,22	719	460

Table II

Drilling and blasting parameters applied for GUs 3, 4, and 5

B (m)	S (m)	GU	GU Density (ton/m3)	Hole Diámeter (Inches)	Bench Height (m)	Overdrilling (m)	Stemming (m)	Explosive Density (Ton/m3)	Explosive Quantity (Kg)	Powder Factor (gr/ton)
9,3	10,7	4	2,45	10,625	15	2	6,5	1,30	709	194
9,3	10,7	3	2,35	10,625	15	2	6,5	1,30	709	202
9,3	10,7	3	2,35	10,625	15	2	6,5	1,30	709	202
9,3	10,7	4	2,45	10,625	15	2	6,5	1,30	709	194
8,0	8,0	5	2,48	10,625	14	0	7,0	1,20	436	196
8,8	10,2	4	2,45	10,625	15	2	6,0	1,30	743	225
9,0	12,0	4	2,45	10,625	15	2	6,0	1,30	743	187
9,0	12,0	3	2,35	10,625	15	2	6,0	1,30	743	195
10,0	13,0	4	2,45	10,625	15	2	6,0	1,30	743	155
10,0	13,0	3	2,35	10,625	15	2	6,0	1,30	743	162

It is also important to note that fragmentation by blasting is strongly affected by local geological conditions. For instance, the dip and dip direction of structural sets and their frequency in the rock mass are of great importance, not only because they determine the *in situ* block size, but they also condition the reflection of stress waves produced by the detonation of explosive charges as long as blasting progresses.

Goal of the study

The aim of this study is to generate empirical models based on statistical analyses to predict the values of P_{80}, P_{50}, and P_{20} of the analysed sample for a set of D&B parameters. Predictive statistical models will be tested with actual data from a Chilean mine. Predicting these variables is key to measuring D&B efficiency, but more importantly it is relevant to predicting copper extraction by heap leaching.

Different ore geotechnical units, called GUs, are identified and ranked according to variables of the rock mass such as compressive strength, frequency of fractures, density, *etc.* In this study, the data included pertains to GUs 3 and 4 and GUs 5 and 6. In each of these, different D&B practices are applied by modifying the values for burden (B), spacing (S), and explosive charge per blast-hole (Q), and thus different effects on the blast fragmentation are obtained.

Statistical analysis is then aimed at detecting possible correlations between the variables describing D&B with the variables of interest (P_{80}, P_{50}, and P_{20}). In addition to detecting correlations, the following phases study functional relationships emerging of the phenomenon in order to set mathematical models to predict or anticipate size distribution. Usually, there is an attempt to estimate the resulting size distribution, measured on P_{80} at a sampling line or even a sampling point. However, to fit the D&B layout, an estimate of mean fragmentation is needed, and it is represented by P_{80} on full blasting, and by P_{50} and P_{20} values.

In this article, special emphasis is placed on linear models since nonlinear cases studied did not show significant improvements compared to linear, according to the data available for the study. The whole idea is to derive models aimed at improving the predictive capacity, measured as the relative error between the actual values of the variables and their estimated values. The relative error will be measured as the difference between the estimated value and the actual value divided by the actual value. This relative error is expected to be less than 15% for blast-holes, and with this estimate, the fragmentation prediction measured by the model will be deemed appropriate. This value was considered reasonable given the geological variability of the rock mass and the implementation of the D&B design.

Other non-functional estimation forms can be suggested; for example, the CART method (regression trees), among others. The CART statistical method (for more technical information on these procedures see Breiman, 2001) is descriptive, easy to apply, and often efficient in classifying individuals by proximity of the values of certain variables. In this case, however, as will be shown later, it showed no evidence of improvement over linear regression models.

Blasting modelling

Database and modelling

The project considered sampling a total of 47 data lines divided into two stages. Stage 1 considered sampling 22 lines of post-blasting broken material belonging basically to GUs 3

and 4. The second stage considered sampling 25 lines of post-blasting broken material belonging basically to GUs 5 and 6.

On each sample line, the following variables were measured: layout burden (B), layout spacing (S), bench height (H), stemming (T), predominant geotechnical unit in the blast-hole (GU), hole diameter (D), kilograms of explosives charged (Q), and powder factor (PF). Samples of material broken by blasting were taken for size analysis by sieving to measure P_{80}, P_{50}, and P_{20}.

Tables III and IV show the detail of the database used to construct the models.

With this database we began predictive modelling of the expected fragmentation by blasting. The following paragraphs contain a brief summary of the models that showed the best predictive properties for the observed data.

Table III

Database generated in stage 1

#	B (m)	S (m)	GU	GU Density (ton/m3)	Hole Diámeter (Inches)	Bench Height (m)	Overdrilling (m)	Stemming (m)	Explosive Density (Ton/m3)	Explosive Quantity (Kg)	Powder Factor (gr/ton)	P80 [mm]	P50 [mm]	P20 [mm]
1	9,3	10,7	4	2,45	10,625	15	2	6,5	1,30	709	194	83,4	47,2	12,30
2	9,3	10,7	4	2,45	10,625	15	2	6,5	1,30	709	194	91,8	51,0	12,81
3	9,3	10,7	3	2,35	10,625	15	2	6,5	1,30	709	202	86,3	47,9	9,34
4	9,3	10,7	3	2,35	10,625	15	2	6,5	1,30	709	202	88,3	47,9	9,76
5	9,3	10,7	4	2,45	10,625	15	2	6,5	1,30	709	194	80,5	44,3	7,90
6	8,0	8,0	5	2,48	10,625	14	0	7,0	1,20	436	196	74,1	39,9	4,21
7	8,8	10,2	4	2,45	10,625	15	2	6,0	1,30	743	225	70,3	38,6	7,61
8	8,8	10,2	4	2,45	10,625	15	2	6,0	1,30	743	225	75,6	40,7	8,04
9	9,0	12,0	4	2,45	10,625	15	2	6,0	1,30	743	187	63,4	37,8	6,70
10	9,0	12,0	4	2,45	10,625	15	2	6,0	1,30	743	187	80,6	45,6	8,28
11	9,0	12,0	3	2,35	10,625	15	2	6,0	1,30	743	195	94,4	51,6	14,08
12	9,0	12,0	4	2,45	10,625	15	2	6,0	1,30	743	187	76,6	45,7	11,89
13	9,0	12,0	4	2,45	10,625	15	2	6,0	1,30	743	187	86,0	51,0	13,42
14	9,0	12,0	4	2,45	10,625	15	2	6,0	1,30	743	187	82,3	47,8	11,50
15	9,0	12,0	4	2,45	10,625	15	2	6,0	1,30	743	187	66,2	39,5	8,35
16	9,0	12,0	4	2,45	10,625	15	2	6,0	1,30	743	187	87,3	49,1	7,80
17	9,0	12,0	3	2,35	10,625	15	2	6,0	1,30	743	195	71,6	42,2	5,97
18	9,0	12,0	3	2,35	10,625	15	2	6,0	1,30	743	195	72,3	41,5	4,74
19	10,0	13,0	4	2,45	10,625	15	2	6,0	1,30	743	155	61,9	37,4	7,07
20	10,0	13,0	3	2,35	10,625	15	2	6,0	1,30	743	162	60,9	36,8	6,54
21	10,0	13,0	4	2,45	10,625	15	2	6,0	1,30	743	155	69,5	40,3	5,66
22	10,0	13,0	4	2,45	10,625	15	2	6,0	1,30	743	155	84,0	48,1	8,19

Table IV

Database generated in stage 2

#	B (m)	S (m)	GU	GU Density (Ton/m3)	Hole Diameter (Inches)	Bench Height (m)	Overdrilling (m)	Stemming (m)	Explosive Density (ton/m3)	Explosive Quantity (Kg)	Powder Factor (gr/ton]	P80 [mm]	P50 [mm]	P20 [mm]
1	7,0	8,0	6	2,57	10,625	15	2	7,5	1,22	663	307	260,5	135,9	43,6
2	7,0	8,0	6	2,57	10,625	15	2	7,5	1,22	663	307	225,9	119,8	37,3
3	7,0	8,0	6	2,57	10,625	15	2	7,5	1,22	663	307	237,6	131,6	42,3
4	7,0	8,0	6	2,57	10,625	15	2	7,5	1,22	663	307	222,9	118,1	36,8
5	7,0	8,0	6	2,57	10,625	15	2	7,5	1,22	663	307	232,1	128,8	41,3
6	7,0	8,0	6	2,57	10,625	15	2	7,5	1,22	663	307	216,2	119,0	37,8
7	7,0	8,0	6	2,57	10,625	15	2	7,5	1,22	663	307	236,3	121,3	38,5
8	7,0	8,0	6	2,57	10,625	15	2	7,5	1,22	663	307	161,0	85,1	24,8
9	7,0	8,0	6	2,57	10,625	15	2	7,5	1,22	663	307	218,8	127,6	40,8
10	7,0	8,0	6	2,57	10,625	15	2	7,5	1,22	663	307	218,5	119,5	37,5
11	7,0	8,0	5	2,48	10,625	15	2	7,5	1,22	663	318	184,4	99,8	30,3
12	7,0	8,0	6	2,57	10,625	15	2	7,5	1,22	663	307	180,0	103,2	31,6
13	8,8	10,2	5	2,48	10,625	15	2	6,0	1,22	768	230	276,6	152,6	54,6
14	8,8	10,2	6	2,57	10,625	15	2	6,0	1,22	768	222	234,2	122,9	42,8
15	8,8	10,2	6	2,57	10,625	15	2	6,0	1,22	768	222	178,2	85,2	26,1
16	6,0	7,0	6	2,57	10,625	15	2	6,7	1,22	719	444	194,8	102,7	24,1
17	6,0	7,0	5	2,48	10,625	15	2	6,7	1,22	719	460	140,3	79,8	21,2
18	6,0	7,0	5	2,48	10,625	15	2	6,7	1,22	719	460	272,9	141,7	44,2
19	6,0	7,0	5	2,48	10,625	15	2	6,7	1,22	719	460	192,1	91,8	24,7
20	6,0	7,0	6	2,57	10,625	15	2	6,7	1,22	719	444	314,7	179,3	62,4
21	6,0	7,0	6	2,57	10,625	15	2	6,7	1,22	719	444	348,0	199,0	60,3
22	6,0	7,0	6	2,57	10,625	15	2	6,7	1,22	719	444	322,1	179,2	51,6
23	6,0	7,0	6	2,57	10,625	15	2	6,7	1,22	719	444	220,9	108,7	31,4
24	6,0	7,0	6	2,57	10,625	15	2	6,7	1,22	719	444	288,8	152,1	36,1
25	6,0	7,0	6	2,57	10,625	15	2	6,7	1,22	719	444	241,2	127,6	38,5

In all models, GU variables are binary, that is, they equal unity when there is a lithological unit, and zero in other cases. In addition, they are mutually exclusive, that is, one and only one out of the four equals unity. The best models obtained for P_{80}, P_{50}, and P_{20} are displayed in centimetres. All models are least-squares linear regressions.

Model for P_{80}

The following equation shows the relationship between P_{80} and the type of GU, according to the main variables of blasting.

$$P_{80} = -20.42806\,GU3 - 20.97552\,GU4 - 11.63432\,GU5 - 7.91386\,GU6 - 0.11981\,Area + 0.05485\,Q$$

where
Area = Burden*Spacing= B^*S (m²)
Q: kilograms of explosives per blast-hole.

These variables proved to have the highest statistical significance for the prediction.

The correlation coefficient of the model is 0.92. This model explains a large percentage of the variability in the data (83% fit). Selected variables are statistically significant and GU 6 is the variable that mainly explains the value of P_{80}. Blasting at GUs 5 and 6 results in a P_{80} that is 16 cm larger than for GUs 3 and 4. For GUs 5 and 6 the average is around 25 cm, compared to 9 cm for GUs 3 and 4. The mean error of this model is 15.49% for blast-holes and 2.96% for muckpiles (several blast-holes.)

The graph in Figure 2 shows the relationship between the values observed for P_{80} and the predictions for the 47 blasting lines available in the data obtained from the mine.

Model for P_{50}

The following equation shows the relationship between P_{50} and the type of GU, according to the main blasting variables.

$$P_{50} = 8.83424\,GU3 - 9.06110\,GU4 - 4.47821\,GU5 - 2.46214\,GU6 - 0.05998\,Area + 0.02628\,Q$$

where
Area= Burden*Spacing= (B^*S) (m²)
Q: kilograms of explosives per blast-hole

The correlation coefficient is 0.90.

This model exhibits a large percentage of data variability (77% fit), and the variables selected are statistically significant. In this case, the pattern (B and S) and kilograms of explosives have less explanatory significance than in the P_{80} model, although quite acceptable for this case study. The main variables that affects the P_{50} value are GU 6 and GU 5. Blasting in GU6 and GU 5 results in a P_{50} that is about 6 mm larger than for other GUs. The mean error of this model is 15.71% for blast-holes, and 3.24 for muckpiles.

The graph in Figure 3 shows the quality of predictions using this model. As in the former case (P_{80}), the most relevant variable when estimating is the respective GU, because the model essentially decides based on whether this is GU 3-4 or GU 5-6.

Model for P_{20}

The following equation shows the relation between P_{20} and the type of GU, according to the main variables of blasting.

$$P_{20} = -1.791332\,GU3 - 1.744310\,GU4 + 0.661212\,GU5 + 1.172037\,GU6 - 0.006157\,Area - 0.006157\,Q$$

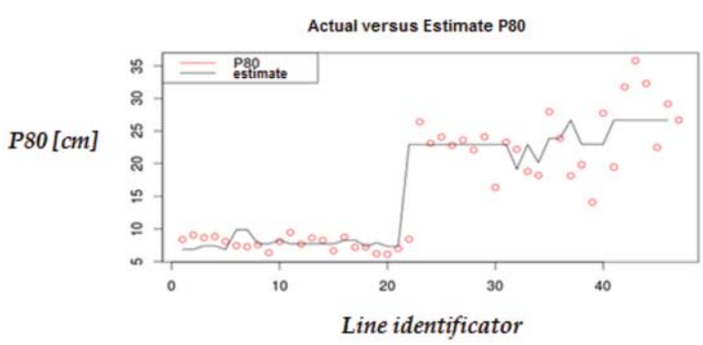

Figure 2—Relationship between actual and estimated P_{80}

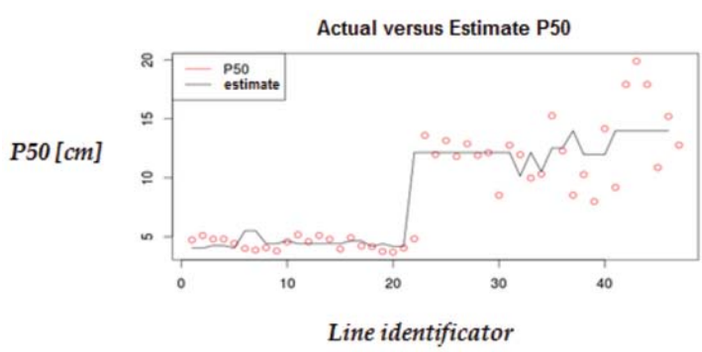

Figure 3—Relationship between actual and estimated P_{50}

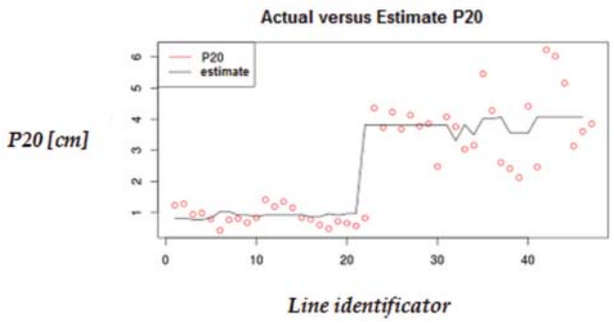

Figure 4—Relationship between actual and estimated P_{20}

where
Area = Burden*Spacing= (B*S) (m²)
Q: kilograms of explosives per blast-hole

The correlation between the actual predicted values is 0.88.

This model exhibits a large percentage of data variability (75% fit.) Since the P_{50} and P_{20} values correlate, so do the sign and magnitude of the coefficients obtained. However, unlike other models, the pattern and kilograms of explosives have neither explanatory significance nor desirable magnitude. The main variables that affect the P_{20} value are GU 6 and GU 5. Blasts in GU 6 result in a P_{20} that is about 3 mm larger than for another GUs. The mean error of this model is 26.34% for blast-holes and 8.52% for muckpiles.

The graph in Figure 4 shows the relationship between actual and estimated P_{20}. It can be seen that the error in the estimation becomes larger as the degree of fragmentation increases.

Conclusions

Although the results of this research have revealed variables with a certain level of significance (stemming, burden, density, explosive), these cannot fully explain the variability of the models. Despite this, the great strength of the models that considered all the available data was their ability to determine in which GU is each line, which has an impact on the values of P_{80}, P_{50}, and P_{20}. While GUs 3 and 4 deliver a P_{80} close to 8 cm, GUs 5 and 6 obtain P_{80} values of about 25 cm. This is a very valuable result because it enabled a typical behaviour to be identified for each GU as a relevant variable to estimate P_{80}, P_{50}, and P_{20} in a given D&B layout for this mining operation.

This research has shown that there is significant correlation between D&B variables, which indicates the possibility of building a predictive tool for fragmentation of blasted material for a particular GU, with reasonable relative errors, close to 15%. This validated hypothesis will enable significant improvements in copper extraction by heap leaching and, in the future, the methodology could be extended to other mining operations in Chile and South America. Our analysis could be replicated in other mines defining appropriated geological units and calibrating new linear models.

In addition to the models shown here, we have tried other classification and prediction techniques such as CART (classification and regression tree), and nonlinear multiplicative models, but these show no evidence of improved predictive power compared with the linear models. This is possibly due to the paucity of data. Such models require further study using more data with greater variability.

Acknowledgment

We would like to thank Geoblast SA for kindly sharing unpublished fragmentation data. Also, the second author thanks FONDECYT Grant 1130816 and BASAL Project CMM-University of Chile. Finally, the third author thanks a CONICYT doctoral grant.

References

Breiman, L. 2001. Random forests. *Machine Learning*, vol. 45. pp. 5–32.

Cunningham, C.V.B. 1983. The Kuz-Ram model for prediction of fragmentation from blasting. *Proceedings of the First International Symposium on Rock Fragmentation by Blasting*, Luleå, Sweden, 23–26 August 1983. Holmberg, R. and Rustan, A. (eds.). Luleå University of Technology. pp. 439–454.

Cunningham, C.V.B. 1987. Fragmentation estimations and the Kuz-Ram model. *Proceedings of the Second International Symposium on Rock Fragmentation by Blasting*, Keystone, CO, 23-26 August 1987. Fourney, W. and Dick, R.D. (eds). Society for Experimental Mechanics, Bethel, CT. pp. 475-487.

Cunningham, C.V.B. 2005. The Kuz-Ram fragmentation model – 20 years on. *Proceedings of the Brighton Conference 2005*. European Federation of Explosives Engineers. pp. 201–210.

Ouchterlony, F. 2005. The Swebrec© function: linking fragmentation by blasting and crushing. *Transactions of the Institution of Mining and Metallurgy*, Section A, vol. 114, no. 1. pp. 29–44

Ouchterlony, F. 2005. What does the fragment size distribution of blasted rock look like? *Proceedings of the Brighton Conference 2005*. European Federation of Explosives Engineers. pp. 189–199.

Ouchterlony, F. Olsson, M., Nyberg, U., Andersson, P., and Gustavsson, L. 2006. Constructing the fragment size distribution of a bench blasting round, using the new Swebrec function. *Fragblast 8. Proceedings of the 8th International Symposium on Rock Fragmentation by Blasting*, Santiago, Chile. Editec, Santiago. pp. 332–344.

Spathis, A.T. 2010 Formulae and techniques for assessing features of blast-induced fragmentation distributions. *Fragblast 9, Proceedings of the 9th International Symposium on Rock Fragmentation by Blasting*, Granada, Spain. CRC Press. pp. 209–219.

Spathis, AT. 2012., A three parameter rock fragmentation distribution. *Measurement and Analysis of Blast Fragmentation*. Sanchidrián, J.A. and Singh, A.K. (eds.). CRC Press. pp. 73–86.

Sanchidrián, J.A. *et al.* 2010. Evaluation of some distribution functions for describing rock fragmentation data. *Fragblast 9, Proceedings of the 9th International Symposium on Rock Fragmentation by Blasting*, Granada, Spain. CRC Press. pp. 239–248.

Sanchidrián, J.A., Segarra, P., López, L. M., and Moser, P. 2012. On the performance of truncated distributions to describe rock fragmentation. *Proceedings of the 10th International Symposium on Rock Fragmentation by Blasting. Workshop on Measurement and Analysis of Blast Fragmentation*, New Delhi, India. Sanchidrián, J., Ouchterlony, F., and Singh, A.K. (eds.). CRS Press. pp. 87–96. ◆

Clarification Summary in response to a reader's quarry: 'Installation of resin-grouted rock bolts in hard rock mining: Challenges and solutions for improved safety'

by T.G. Maepa and T. Zvarivadza

Annulus size

Hagan (2003) stated that the relationship between the diameter of the support hole and the diameter of the rockbolt has a large effect on the efficiency of reinforcement. The difference between the radius of the support hole and the radius of the bolt is known as the annulus size. Since the design diameter of the rockbolt is 25 mm, the design annulus size is 3.5 mm. According to the mine support standard, the required annulus size should not be greater than 5 mm. The design annulus size of 3.5 mm is within the required range as stipulated in the mine's code of practice. The design annulus size is also within the manufacturer's recommended optimal design annulus size of between 3–4 mm. From this observation, the design is anticipated to be highly efficient.

Optimizing the support design

In practice, the support holes require 8% more resin per hole. Possible solutions to this problem would be to increase the sizes of the rockbolts, increase the sizes of the resin capsules, or reduce the sizes of the support holes. Increasing the sizes of the rockbolts and resin capsules will have serious cost implications. Therefore, the size of the support holes should be reduced. Many authors have suggested different optimal ranges of annulus size. The manufacturer of the resin capsules that are used at the mine suggested an optimal design annulus size between 3 mm and 4 mm. While Hagan (2003) suggested an optimal practical annulus size ranging from 4 mm to 6 mm. The specifications from the manufacturer also state that the optimal length of the support holes for the resin bolt installation should be 50–60 mm shorter than the bolt length.

The support holes should be drilled at an optimal length of 2.34 m with a drill bit of 30.5 mm in diameter. This will result in a design annulus size of 3.15 mm [(30.5–24.2)/2], which is within the manufacturer's recommendations of between 3 mm and 4 mm. Taking into account the reaming of the support holes, the final diameter of the support holes will be 32 mm. This results in a practical annulus size of 4 mm, which is also within the optimal practical annulus size ranging from 4 mm to 6 mm.

Summary of the optimal support design:

- Bolt length: 2 400mm
- Bolt diameter: 24.2mm
- Support hole length: 2 340mm
- Final support hole diameter: 32mm (30.5mm diameter drill bit plus 5% reaming)

The authors' recommended support design is presented in Table V. The design will not only enhance safety at the mine but it will also reduce the costs associated with mine support. With such an optimal support system, the mine can save costs by reducing the size of the slow setting resin capsules from 500 mm by 25 m to 400 mm by 24 mm. The system is still efficient in terms of support, with 2% excess resin resulting in a waste of R1.20 per hole. The 2% excess resin will come in handy where there are geological discontinuities and resin may seep into the discontinuities. With the decrease in drill bit diameter and the length of the support hole, the mine will also reduce costs associated with drilling.

Table V

The efficiency of support based on the authors' optimal design of the support system

Andre se Resin anchor calculation

Bolt		Hole		Resin		
Bolt length	2400 mm	Hole Length	2340 mm	Fast Capsule Length	500 mm	
Protruding	130 mm	Hole Diameter	32 mm	Fast Capsule Diameter	25 mm	
Bolt Diameter	24.2 mm			Fast of Green capsules	2 units	
Bolt Volume	1044.11 cm3	Hole Volume	1881.94 cm3	Slow Capsule Length	400 mm	
				Slow Capsule Diameter	24 mm	
				Slow of Yellow capsules	2 units	% resin
Required resin volume	837.83 cm3	GOOD!!		Resin Volume	852.79 cm3	102%
Resin excess	14.96 cm3	You are waisting resin!! R 1.20 per hole!!				

Unit Cost	R/Box	Installation
Bolt Cost		R 50.00
Fast Resin Cost	R 223.00	R 9.29
Slow Resin Cost	R 223.00	R 9.29
Cost		R 68.58

* *School of Mining Engineering, University of the Witwatersrand, Johannesburg, South Africa.*

Economic benefits of the investigation

With the standard mine support design, the Andre Se Resin Anchor calculation indicated that the mine is wasting resin and losing R12.61 per support hole. The optimal design recommended by the authors will provide the mine with an efficient support system with a loss of only R1.20 per support hole, thus saving R11.41 per hole. This is a huge reduction in costs considering that the design is till efficient and providing full security. A total of 5 021 rockbolts were installed in the last quarter of 2015 (Table I in the paper). With a cost reduction of R11.41 per support hole, the mine could have saved R57 289.61, sufficient for the installation of 47 741 more rockbolts.

Figure 8 shows the total amount that could have been saved per month based on Table I and the reduction of R11.41 per support hole, as a result of the optimal design. Furthermore, addressing the design and operational inefficiencies will also result in a decrease in number of rockbolts that are installed incorrectly at the mine. The costs associated with the replacement of incorrectly installed resin-grouted rockbolts will thus be reduced significantly.

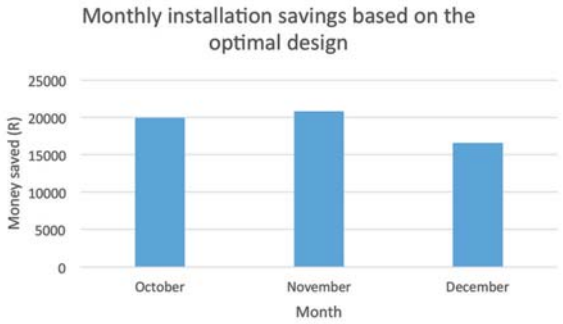

Figure 8—Monthly installation savings based on the proposed optimal support design

Conclusions

Decreasing the design diameter of the support holes from 32 mm to 30.5 mm, supplemented by a decrease in design length from 2.4 m to 2.36 m, result in an optimal support design and a reduction of money wasted per support hole from R12.61 to R1.20.

- The standard mine support design should be optimized by reducing the diameter of the drill bit from 32 mm to 30.5 mm and reducing the length of the support hole from 2.4 m to 2.36 m. These changes will enable the mine to use different combinations of resin capsules to reduce the cost of installation per support hole.

The paper was first published in the April 2017 issue of the SAIMM *Journal* and a reader requested clarification of a particular issue.

Johannesburg and its Holey Mining Heritage

Johannesburg is probably unique in the world, in that it is now a major city that developed on and around the gold reefs discovered in 1886. Today these mined reefs run directly through the CBD and adjacent areas. It is probable that very few residents of the city know that they cross old mine workings on a daily basis, and that there are stopes of these old mine workings that are still open below surface. Surface development was not permitted in the region of the outcrops and shallow mining, and these open areas, close to the city and industry, have resulted in areas on which informal settlements have developed over the past two decades. Although most of the old mine openings were closed when mining ceased, the quality of the closure was often inadequate, and over time many holes into the old mine workings have appeared on surface. These can be a significant hazard to residents of the informal settlements, which prompted a recent investigation of old mine openings in the Johannesburg and Central Witwatersrand area. In this investigation 244 mine openings were located, and 80 of the more hazardous openings were subsequently sealed. This investigation provided a large source of information, which is considered to be of significant historical value. To document this valuable historical information regarding the city of Johannesburg and the Central Witwatersrand area, the Southern African Institute of Mining and Metallurgy is planning a special publication (book). In addition to details of the investigation and sealing project, additional material will be included, describing cases of stabilisation of mine workings that have taken place in past years to facilitate surface development. One such example is the Standard Bank building to the east of Simmonds Street and south of Frederick Street. Details are available of the investigation of the mine workings for this site, and the foundation stabilisation work carried out. This was the first major building to be developed across the mining outcrops, and Standard Bank must take great credit for proceeding with this project 30 years ago. The experience gained from this pioneering project subsequently facilitated the development of adjacent major buildings. It is planned that descriptions of these other developments will also be included in the publication, as well as historical information associated with other cases of instability and sealing of mine openings. The book will preserve some of the unique mining heritage associated with Johannesburg's past, and make a significant contribution regarding this aspect of the history of a holey City.

T.R. Stacey

NATIONAL & INTERNATIONAL ACTIVITIES

2018

25–28 February 2018 — **Infacon XV: International Ferro-Alloys Congress**
Century City Conference Centre and Hotel, Cape Town, South Africa
Contact: Gugu Charlie
Tel: +27 11 834-1273/7
Fax: +27 11 838-5923/833-8156
E-mail: gugu@saimm.co.za
Website: http://www.saimm.co.za

12–14 March 2018 — **Society of Mining Professors 6th Regional Conference 2018**
Overcoming challenges in the Mining Industry through sustainable mining practices
Birchwood Hotel and Conference Centre, Johannesburg, South Africa
Contact: Camielah Jardine
Tel: +27 11 834-1273/7
Fax: +27 11 838-5923/833-8156
E-mail: camielah@saimm.co.za
Website: http://www.saimm.co.za

6–7 June 2018 — **Digitalization in Mining Conference**
'Mining business make-over –Exploiting the digital resolution'
Johannesburg, South Africa
Contact: Camielah Jardine
Tel: +27 11 834-1273/7
Fax: +27 11 838-5923/833-8156
E-mail: camielah@saimm.co.za
Website: http://www.saimm.co.za

11–14 June 2018 — **SAIMM: Diamonds — Source to Use 2018 Conference** *'Thriving in Changing Times'*
Birchwood Conference Centre (Jet Park)
Contact: Camielah Jardine
Tel: +27 11 834-1273/7
Fax: +27 11 838-5923/833-8156
E-mail: camielah@saimm.co.za
Website: http://www.saimm.co.za

9–12 July 2018 — **Copper Cobalt Africa in association with The 9th Southern African Base Metals Conference**
Avani Victoria Falls Resort, Livingstone, Zambia
Contact: Gugu Charlie
Tel: +27 11 834-1273/7
Fax: +27 11 838-5923/833-8156
E-mail: gugu@saimm.co.za
Website: http://www.saimm.co.za

6–8 August 2018—**Geometallurgy Conference 2018**
Johannesburg, South Africa
Contact: Camielah Jardine
Tel: +27 11 834-1273/7
Fax: +27 11 838-5923/833-8156
E-mail: camielah@saimm.co.za
Website: http://www.saimm.co.za

10–11 September 2018 — **ASM Conference 2018**
'Fostering a regional approach to ASM transformation in sub-Saharan Africa'
Nasrec, Johannesburg (Electra Mining)
Contact: Camielah Jardine
Tel: +27 11 834-1273/7
Fax: +27 11 838-5923/833-8156
E-mail: camielah@saimm.co.za
Website: http://www.saimm.co.za

15–17 October 2018 — **Furnace Tapping 2018 Conference**
Nombolo Mdhluli Conference Centre, Kruger National Park, South Africa
Contact: Gugu Charlie
Tel: +27 11 834-1273/7
Fax: +27 11 838-5923/833-8156
E-mail: gugu@saimm.co.za
Website: http://www.saimm.co.za

Company Affiliates

The following organizations have been admitted to the Institute as Company Affiliates

3M South Africa (Pty) Limited
AECOM SA (Pty) Ltd
AEL Mining Services Limited
Air Liquide (Pty) Ltd
AMEC Foster Wheeler
AMIRA International Africa (Pty) Ltd
ANDRITZ Delkor(Pty) Ltd
Anglo Operations Proprietary Limited
Anglogold Ashanti Ltd
Arcus Gibb (Pty) Ltd
Atlas Copco (SA) (Pty) Ltd
Aurecon South Africa (Pty) Ltd
Aveng Engineering
Aveng Mining Shafts and Underground
Axis House (Pty) Ltd
Bafokeng Rasimone Platinum Mine
Barloworld Equipment -Mining
BASF Holdings SA (Pty) Ltd
BCL Limited
Becker Mining (Pty) Ltd
BedRock Mining Support (Pty) Ltd
Bell Equipment Limited
BHP Billiton Energy Coal SA Ltd
Blue Cube Systems (Pty) Ltd
Bluhm Burton Engineering (Pty) Ltd
Bouygues Travaux Publics
CDM Group
CGG Services SA
Chamber of Mines
Concor Opencast Mining
Concor Technicrete
Council for Geoscience Library
CRONIMET Mining Processing SA(Pty) Ltd
CSIR Natural Resources and the Environment (NRE)
Data Mine SA
Department of Water Affairs and Forestry
Digby Wells and Associates
DRA Mineral Projects (Pty) Ltd
Duraset
Elbroc Mining Products (Pty) Ltd
eThekwini Municipality
Expectra 2004 (Pty) Ltd
Exxaro Coal (Pty) Ltd
Exxaro Resources Limited
Filtaquip (Pty) Ltd
FLSmidth Minerals (Pty) Ltd
Fluor Daniel SA (Pty) Ltd
Franki Africa (Pty) Ltd-JHB
Fraser Alexander (Pty) Ltd
Geobrugg Southern Africa (Pty) Ltd
Glencore
Hall Core Drilling (Pty) Ltd
Hatch (Pty) Ltd
Herrenknecht AG
HPE Hydro Power Equipment (Pty) Ltd
Impala Platinum Limited
IMS Engineering (Pty) Ltd
Ivanhoe Mines SA
Joy Global Inc. (Africa)
Kudumane Manganese Resources
Leco Africa (Pty) Limited
Longyear South Africa (Pty) Ltd
Lonmin Plc
Lull Storm Trading (Pty) Ltd
Magnetech (Pty) Ltd
Magotteaux (Pty) Ltd
MBE Minerals SA (Pty) Ltd
MCC Contracts (Pty) Ltd
MD Mineral Technologies SA (Pty) Ltd
MDM Technical Africa (Pty) Ltd
Metalock Engineering RSA (Pty)Ltd
Metorex Limited
Metso Minerals (South Africa) (Pty) Ltd
Minerals Operations Executive (Pty) Ltd
MineRP Holding (Pty) Ltd
Mintek
MIP Process Technologies (Pty) Ltd
Modular Mining Systems Africa (Pty) Ltd
MSA Group (Pty) Ltd
Multotec (Pty) Ltd
Murray and Roberts Cementation
Nalco Africa (Pty) Ltd
Namakwa Sands (Pty) Ltd
Ncamiso Trading (Pty) Ltd
New Concept Mining (Pty) Ltd
Northam Platinum Ltd - Zondereinde
PANalytical (Pty) Ltd
Paterson & Cooke Consulting Engineers (Pty) Ltd
Perkinelmer
Polysius A Division Of Thyssenkrupp Industrial Sol
Precious Metals Refiners
Rand Refinery Limited
Redpath Mining (South Africa) (Pty) Ltd
Rocbolt Technologies
Rosond (Pty) Ltd
Royal Bafokeng Platinum
Roytec Global (Pty) Ltd
Runge Pincock Minarco Limited
Rustenburg Platinum Mines Limited
Salene Mining (Pty) Ltd
Sandvik Mining and Construction Delmas (Pty) Ltd
Sandvik Mining and Construction RSA(Pty) Ltd
SANIRE
Sasol Mining
Sebilo Resources (Pty) Ltd
Sebilo Resources (Pty) Ltd
SENET (Pty) Ltd
Senmin International (Pty) Ltd
Smec South Africa
SMS group Technical Services South Africa (Pty) Ltd
Sound Mining Solution (Pty) Ltd
SRK Consulting SA (Pty) Ltd
Technology Innovation Agency
Time Mining and Processing (Pty) Ltd
Timrite Pty Ltd
Tomra (Pty) Ltd
Ukwazi Mining Solutions (Pty) Ltd
Umgeni Water
Webber Wentzel
Weir Minerals Africa
Worley Parsons RSA (Pty) Ltd

2018 INFACON XV
15TH INTERNATIONAL FERRO-ALLOYS CONGRESS
CAPE TOWN, SOUTH AFRICA

Infacon XV: International Ferro-Alloys Congress

25–28 February 2018

Century City Conference Centre and Hotel, Cape Town, South Africa

The 15th International Ferro-Alloys Congress (Infacon XV) will be held at the Century City Conference Centre in Cape Town, South Africa from 25-28 February 2018.

INFACON (International Ferro-Alloys Congress) was founded in South Africa in 1974 by the SAIMM (Southern African Institute of Mining and Metallurgy), Mintek (then the National Institute for Metallurgy), and the Ferro Alloys Producers' Association (FAPA) when the first INFACON was held in Johannesburg.

The intention of INFACON is to stimulate technical interchange on all aspects of ferro-alloy production.

Topics for discussion:

Topics include but are not limited to

- Operational updates from ferro-alloy producers
- Technical aspects of ferro-alloy production
- Status of the ferro-alloys markets
- FeCr, FeMn, FeNi, FeV, FeSi, SiMn, *etc.*
- Effects of electricity cost and availability
- Energy efficiency and recovery
- Pre-treatment technologies
- New technologies and processes
- Safety
- Environmental issues
- Carbon dioxide emissions and climate change
- Government policies affecting ferro-alloys
- Carbon tax
- Export restrictions or subsidies
- Sustainability
- Use of natural gas
- Sale of ore versus ferro-alloy production
- Market supply and demand
- Future of the ferro-alloys industry in South Africa

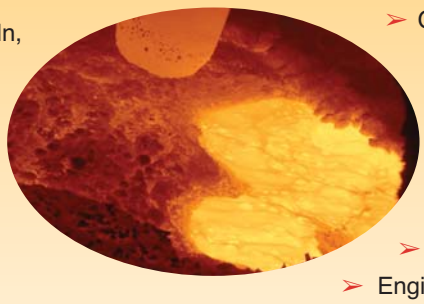

- The impact of UG2 chromite from the PGM industry
- Fines, tailings, and low-grade ores
- Volatility of ore and ferro-alloy prices
- Approach to a circular economy
- How to extract maximum value from resources
- Other topics of relevance to ferro-alloy production

Who should attend?

- Metallurgists
- Ferro-alloy producers
- Steel and stainless steel producers
- Smelter operations managers
- Plant general managers
- Engineers, technicians, and scientists
- Process engineers
- Engineering companies
- Furnace equipment and refractory suppliers
- Researchers / Academics
- Specialists in production, economics, and the environment
- Policy makers
- Investors
- Students

For further information please contact:

Gugu Charlie • Conference Co-ordinator • E-mail: gugu@saimm.co.za
Website: http://infacon15.com

SAIMM
THE SOUTHERN AFRICAN INSTITUTE OF MINING AND METALLURGY

Conference Announcement

New Concept Mining

Support for the World's Deepest Mines

Next Generation Yielding Support

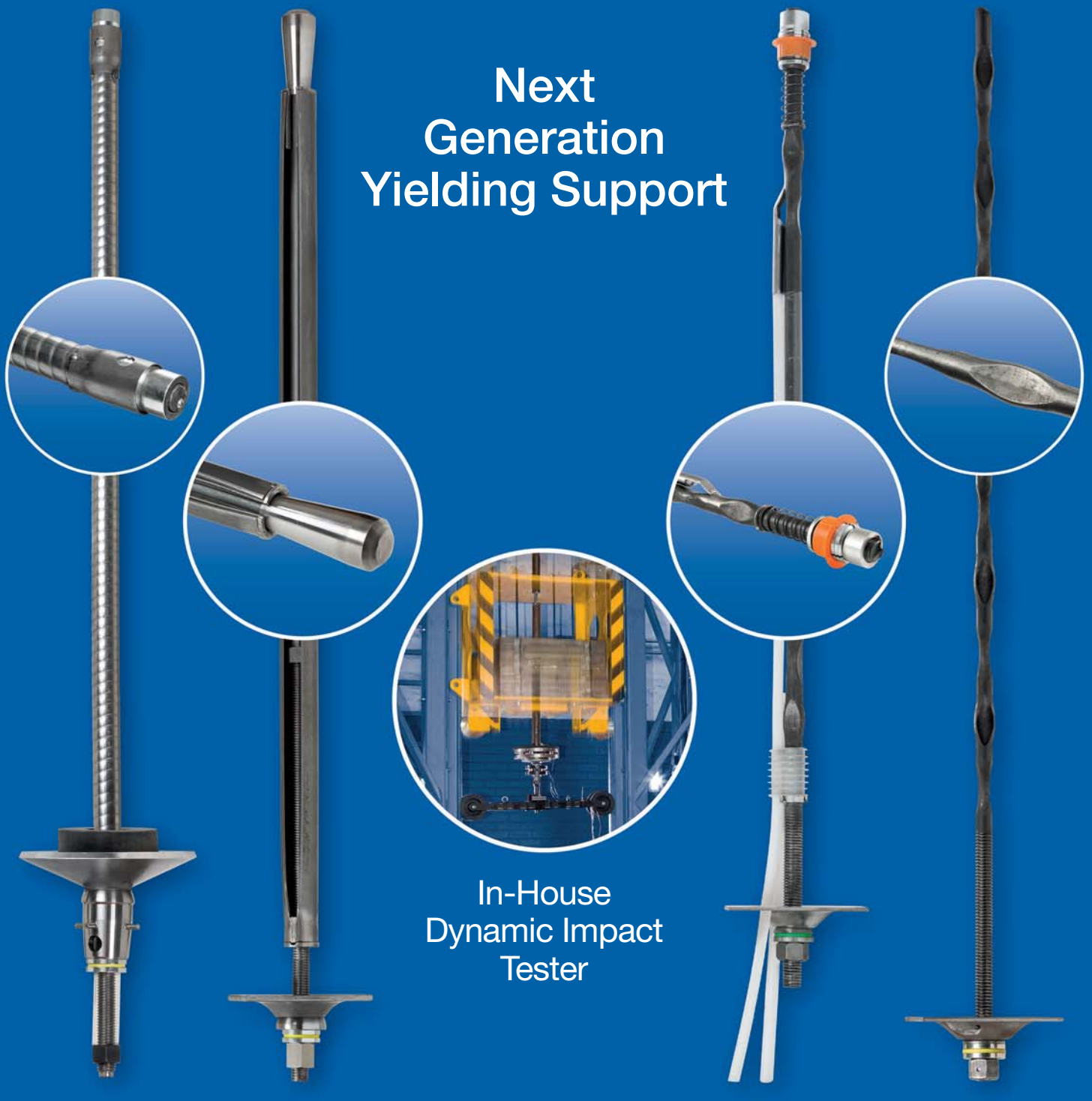

In-House Dynamic Impact Tester

MP1 Bolt. Vulcan Bolt. Par1 Bolt. Par1 Resin Bolt.

+27 11 494 6000 www.ncm.co.za